

水流經挺水性水生植物之阻力研究

研究生:陳宥達

指導教授:葉克家

國立交通大學土木工程研究所

摘要

水流經水生植物所產生之阻力可用以計算水位、流速變化、水流能量消散和滯留時間、輸砂變化、擴散速率等；為水利、生態與其它水相關工程於設計、操作與維護上之重要資訊。為以直接量測法研究水流經臺灣天然挺水性水生植物之瞬時流力阻力，本研究分成以下四個階段進行：挺水性水生植物之實地觀測與選取、建設小型種植區培育選取之水生植物、設計與建造一嵌入水槽式電子阻力量測儀器、及水槽中挺水性水生植物流阻控制試驗與無因次數數據分析。

實驗設計量測並分析水流於五種流速變化下，流經蘆葦、香蒲、大安水蓼與燈心草在四種不同植生密度變化下之阻力。本研究所開發之電子阻力量測儀器可直接量測並記錄水流經一陣列不同生長密度之天然(根系與土壤完整)挺水性水生植物所產生的瞬時(秒)阻力數據。實驗結果發現當流速增加，植物流線型因子(流阻係數與植物投影面積之積)隨之下降，顯示這四種挺水性水生植物具有流線型化的能力，於一定流速範圍內，可降低總體植物阻力。試驗研究進一步發現於固定流速下，挺水性水生植物如蘆葦具有其最低植物流線型因子(最高流線型化)所對應之最佳種植密度。

無因次分析水流經蘆葦的實驗數據，發展出二條以流線型係數及阻力係數之自然對數為應變數之高相關性($R^2=0.94$)無因次方程式[Eq. (3-55)及(3-67)]；並推導出阻力粗糙係數如：達西-威斯巴 f 值、蔡司 C 值及曼寧 n 值。此二式可應用於含有天然挺水性水生植物的明渠流、漫地流、輸砂與海岸淺水波流等控制方程式。

關鍵詞：挺水性水生植物，植生密度，電子阻力量測系統，阻力係數，流線型化因子，流線型係數，無因次分析，摩擦係數

Experimental Study on Drag Force of Emergent Macrophytes in Aquatic Flows

Student: Yo-Ta Chen

Advisor: Keh-Chia Yeh

Institute of Civil Engineering
National Chiao Tung University

Abstract

This research is an experimental study on the drag force of four types of emergent macrophytes: *Phragmites australis*, *Typha orientalis*, *Hygrophila pogonocalyx*, and *Juncus effusus*, in aquatic flows with four varying plant densities under five different flow rates. There are four phases of this experiment: field observation and selection of emergent macrophytes, cultivation of selected emergent macrophytes, design and construction of a direct drag force measurement system to obtain drag force per second of an array of natural emergent macrophytes with roots and soil intact, and execution of controlled flume experiments with dimensional data analysis.

Experimental results revealed a drop of the streamline factor (product of drag coefficient and plant projected frontal area) as flow velocity increases, indicating the streamlining ability of these emergent macrophytes which in a range of velocity, reduces overall drag force. In addition, an optimum plant density is observed corresponding to a lowest streamlined factor (highest streamlining ability) for *Phragmites australis* under each flow velocity. Dimensional analysis on the data sets from flume experiments for *Phragmites australis* arrives at two dimensionless equations [Eq.(3-55) and (3-67)] achieving high correlativeness ($R^2=0.94$), with the natural logarithm of the streamlined coefficient and the drag coefficient as dependent variables. Three friction factors, Darcy-Weisbach f , Chezy's C , and Manning's n are derived from each of these two dimensionless equations, which allow further applications on the governing equations for open-channel flow, overland flow, sediment transport, and coastal shallow water flow through emergent macrophytes.

Keywords: Emergent macrophytes, Plant density, Direct drag force measurement system, Drag coefficient, Streamline factor, Streamline coefficient, Dimensional analysis, Friction factors

Acknowledgement

I would like to express my sincere thanks to my advisor, Professor Yeh K. C., for his encouragement, support, and guidance in this research. Professor Yeh has taught me the professional knowledge, the approach for problem solving, and the attitude of a researcher. I would also like to thank Professor Tsai C. T. and Deputy Director Tsai W. F. for their insightful comments and suggestions on an earlier version of this thesis. My heartfelt appreciation also goes to Professor Chang W. L., who inspires me in the study of ecological engineering.

Furthermore, I would like to give my thanks to all the students of Professor Yeh who are my companions through this study, especially the members of the river sediment transportation laboratory.

Finally my warmest thanks go to my family members whose patience, love, guidance, and tolerance support me through this study. I am also grateful for the servants in the Christian fellowships. In all, I am grateful to my Lord Jesus Christ for leading and accompanying me throughout this journey with grace and mercy, and for guiding me using His words daily to help me to follow Him.

Table of Contents

Abstract.....	I
Acknowledgement.....	III
Content.....	IV
List of Tables.....	VI
List of Figures.....	VIII
List of Symbols.....	XIV
Chapter 1. Introduction.....	1
1.1. Background.....	1
1.2. Literature Review.....	2
1.2.1. Flow resistance of vegetation.....	2
1.2.2. Direct drag force measurement.....	4
1.3. Objective of the study.....	12
Chapter 2. Experimental Methodology.....	14
2.1. Phase 1: Field Studies.....	14
2.2. Phase 2: Plant Cultivation.....	17
2.3. Phase 3: Design of Instrument - Direct Force Measurement System.....	18
2.3.1. Design of depth.....	18
2.3.2 Design to level with channel elevation.....	20
2.3.3. Member force design.....	20
2.3.4 Design for static friction.....	21
2.3.5 Design for reduction of eddy current.....	22
2.3.6 Building of the in-channel drag force measurement system.....	22
2.3.7 The rails and bearings.....	23
2.3.8 Front water stops.....	24
2.3.9 Side channel connections and supports.....	24
2.3.10 Pulleys and strings.....	24
2.4. Phase 4: Flume Experiments.....	24
2.4.1 Preparation of the channel: the embedded level.....	24
2.4.2 Measurement of drag force of emergent macrophytes.....	25
Chapter 3. Results and Data Analysis.....	28
3.1. Preliminary Data Analysis.....	28
3.1.1. The analysis of direct plant drag force system.....	28
3.1.2. Validation of drag force system.....	32
3.1.3. Computation of plant projected frontal area.....	35
3.1.4. Drag force verses flow and density.....	37
3.1.5. Product of drag coefficient and plant projected frontal area.....	38

3.1.6. Drag coefficient (C_d) variation.....	41
3.2 Dimensional Analysis on Drag of Phramites Australis in Aquatic Flows	45
3.2.1. Dependent variables.....	47
3.2.2. Independent variables	48
3.2.3. Dimensional analysis of streamline coefficient: Model 1.....	52
3.2.4 Dimensional analysis of drag coefficient: Model 2	56
Chapter 4. Conclusion and Recommendation.....	63
4.1 Conclusion	63
4.2 Recommendation	68
References.....	73
Tables.....	84
Figures.....	116
Appendix A	159
Appendix B.....	171
Appendix C.....	174



List of Tables

Table 2.1 Probability distribution of length of roots of <i>Typha angustifolia</i> L. growing in aquatic farms.....	84
Table 2.2 List of sites of field studies.....	84
Table 2.3 Macrophytes under different environmental conditions in the Xin-Hai-Qiao Constructed Wetland, Taipei County.....	85
Table 2.4 Field study of wetland ecology and engineering in Dunan Bridge surface flow constructed wetland.....	86
Table 2.5 Field study of wetland ecology and engineering in Dunan Bridge Surface flow constructed wetland phase two.....	87
Table 2.6 Water quality monitor for treatment units in phase one.....	87
Table 3.1 Drag force of movable platform for <i>Phragmites australis</i> and <i>Typha orientalis</i>	88
Table 3.2 Drag force of movable platform for <i>Hygrophila pogonocalyx</i> and <i>Juncus effusus</i>	88
Table 3.3 Water level of <i>Juncus effusus</i> , <i>Hygrophila pogonocalyx</i> , <i>Typha orientalis</i> , and <i>Phragmites australis</i>	89
Table 3.4 Average stream velocity of <i>Juncus effusus</i> , <i>Hygrophila pogonocalyx</i> , <i>Typha orientalis</i> , and <i>Phragmites australis</i>	90
Table 3.5 Drag force of <i>Typha orientalis</i>	91
Table 3.6 Drag force of <i>Phragmites australis</i>	91
Table 3.7 Drag force of <i>Hygrophila pogonocalyx</i>	92
Table 3.8 Drag force of <i>Juncus effusus</i>	92
Table 3.9 Drag coefficient (C_d) of <i>Phragmites australis</i>	93
Table 3.10 Drag coefficient (C_d) of <i>Typha orientalis</i>	93
Table 3.11 Drag coefficient (C_d) of <i>Hygrophila pogonocalyx</i>	94
Table 3.12 Drag coefficient (C_d) of <i>Juncus effusus</i>	94
Table 3.13 Reynolds numbers (Re) of <i>Phragmites australis</i>	95
Table 3.14 Froude number (Fr) of <i>Phragmites australis</i>	96

Table 3.15 Ratio of average plant stem height to water level (h_p/y_n) of <i>Pragmites australis</i>	97
Table 3.16 Ratio of average stem spacing to water level (S_p/y_n) of <i>Pragmites australis</i>	98
Table 3.17 Ratio of plant projected frontal area to vegetated channel bed area (A_p/a) of <i>Pragmites australis</i>	99
Table 3.18 Ratio of fluid drag to plant rigidity ($\rho V^2 h_p^4/(GI)$) of <i>Pragmites australis</i>	100
Table 3.19 Dimensionless streamline coefficient ($C_d A_p h/\nabla$) of <i>Pragmites australis</i>	101
Table 3.20 Streamline factor ($C_d A_p$) of <i>Phragmites australis</i>	102
Table 3.21 Drag coefficient (C_d) of <i>Phragmites australis</i>	103
Table 3.22 Manning's n of <i>Phragmites australis</i>	104
Table 3.23 Manning's n of <i>Typha orientalis</i>	105
Table 3.24 Manning's n of <i>Hygrophila pogonocalyx</i>	106
Table 3.25 Manning's n of <i>Juncus effuses</i>	107
Table 3.26 Standard Manning's n	108
Table 3.27 Results of multiple regression analysis for <i>Phragmites australis</i> and <i>Typha orientalis</i>	109
Table 3.28 Results of multiple regression analysis for <i>Hygrophila pogonocalyx</i> and <i>Juncus effuses</i>	110
Table 3.29 Summary statistics of Model 1.....	111
Table 3.30 Summary statistics of Model 2 Part 1.....	112
Table 3.31 Summary statistics of Model 2 Part 2.....	113
Table 3.32 Summary of R^2 of Model 1.....	114
Table 3.33 Summary of R^2 of Model 2 Part 1.....	114
Table 3.34 Summary of R^2 of Model 2 Part 2.....	115

List of Figures

Figure 1.1 Research conceptual plan.....	116
Figure 2.1 Plant density verses time for three different ratios of plant capacities.....	117
Figure 2.2 Flow paths of the Du Nan Qiao surface flow constructed wetland.....	117
Figure 2.3 Variation of water quality indicators over treatment units.....	118
Figure 2.4 Touchien River surface flow constructed wetland system.....	119
Figure 2.5 Water quality test equipment.....	120
Figure 2.6 Mini roof farm at the top of Engineering Block 1, NCTU.....	121
Figure 2.7 Direct drag force measurement system.....	122
Figure 2.8 Schematic design of the drag force measurement system before amendments.....	123
Figure 2.9 Overall isometric view of the drag force measurement system in the channel.....	123
Figure 2.10 Isometric view of the embedded movable platform in the channel.....	124
Figure 2.11 Zoom in of isometric view of the side support of the movable platform.....	124
Figure 2.12 Isometric view highlighting main frame of structures.....	124
Figure 2.13 Isometric view of the drag force system.....	125
Figure 2.14 Plan view of the drag force measurement system in the channel.....	125
Figure 2.15 Cross sectional view of the drag force measurement system in the channel.....	125
Figure 2.16 Side view of the drag force measurement system in the channel.....	126
Figure 3.1 Photographs of direct drag force measurement system in operation in the flume.....	127
Figure 3.2 Free body diagram of the forces acting on the drag force measurement system.....	128
Figure 3.3 Simplified free body diagram for the drag force measurement system.....	128

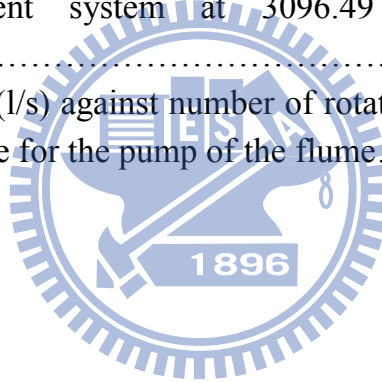
Figure 3.4 Back view of the second design of the movable platform.....	129
Figure 3.5 Original photo of <i>Typha orientalis</i>	129
Figure 3.6 Photograph of <i>Typha orientalis</i> cut according to water level.....	129
Figure 3.7 Photograph cut and turned into grey scale.....	129
Figure 3.8 Successful match of the water level combined to the original photograph of <i>Typha orientalis</i>	129
Figure 3.9 Upper part of photograph set to white.....	130
Figure 3.10 Adjustment by brightness value.....	130
Figure 3.11 Adjustment by contrast value.....	130
Figure 3.12 Adjusted photograph of <i>Typha orientalis</i>	130
Figure 3.13 Patching up the remaining plant area of using black color.....	130
Figure 3.14 Threshold value applied to the color-adjusted photograph.....	130
Figure 3.15 Original photograph of <i>Typha orientalis</i>	131
Figure 3.16 Number of pixels verses lightness values for the original photo of <i>Typha orientalis</i>	131
Figure 3.17 Treated photograph for <i>Typha orientalis</i>	131
Figure 3.18 Number of pixels verses lightness values for the fully adjusted photograph of <i>Typha orientalis</i>	131
Figure 3.19 Summary of average drag force of all four types of <i>Typha orientalis</i> , <i>Juncus effusus</i> , <i>Hygrophila pogonocalyx</i> , and <i>Phragmites australis</i>	132
Figure 3.20 Relationship between averaged streamline factor ($C_d A_p$) in (m^2) and squared stream velocity (V^2) in (m/s) ² for <i>Phragmites australis</i>	132
Figure 3.21 Relationship between averaged streamline factor ($C_d A_p$) in (m^2) and squared stream velocity (V^2) in (m/s) ² for <i>Typha orientalis</i>	133
Figure 3.22 Relationship between averaged streamline factor ($C_d A_p$) in (m^2) and squared stream velocity (V^2) in (m/s) ² for <i>Hygrophila pogonocalyx</i>	133
Figure 3.23 Relationship between averaged streamline factor ($C_d A_p$) in (m^2) and squared stream velocity (V^2) in (m/s) ² for <i>Juncus effusus</i>	134
Figure 3.24 Relationship between averaged streamline factor ($C_d A_p$) in (m^2) and plant density (no. of stems/ m^2) for <i>Phragmites australis</i>	134
Figure 3.25 Relationship between streamline factor ($C_d A_p$) in (m^2) and plant density (no. of stems/ m^2) for <i>Phragmites australis</i>	135
Figure 3.26 Relationship of drag coefficient and Reynolds number for <i>Phragmites australis</i>	135
Figure 3.27 Relationship of drag coefficient and Froude number for <i>Phragmites australis</i>	136
Figure 3.28 Relationship of drag coefficient and the ratio of fluid drag to plant rigidity for <i>Phragmites australis</i>	136
Figure 3.29 Relationship of drag coefficient and the ratio of average stem spacing to water level for <i>Phragmites australis</i>	137
Figure 3.30 Relationship of drag coefficient and the ratio of average plant	

height to water level for <i>Phragmites australis</i>	137
Figure 3.31 Relationship of drag coefficient and the ratio of plant projected frontal area to vegetated bed area for <i>Phragmites australis</i>	138
Figure 3.32 Relationship of drag coefficient and the ratio of average plant diameter to water level for <i>Phragmites australis</i>	138
Figure 3.33 Relationship between drag coefficient (C_d) and plant density (no. of stems/m ²)	139
Figure 3.33.1 Relationship between Manning's n and plant density (no. of stems/m ²)	139
Figure 3.34 Relationship of natural logarithm of streamline coefficient ($C_d A_p h_p / \nabla$) to natural logarithm of Reynolds number (Re).....	140
Figure 3.35 Relationship of natural logarithm of streamline coefficient ($C_d A_p h_p / \nabla$) to natural logarithm of Froude number (Fr)	140
Figure 3.36 Relationship of natural logarithm of streamline coefficient ($C_d A_p h_p / \nabla$) to natural logarithm of the ratio of fluid drag force to plant rigidity $\{ \rho V^2 h_p^4 / (G_s I) \}$	141
Figure 3.37 Relationship of natural logarithm of streamline coefficient ($C_d A_p h_p / \nabla$) to natural logarithm of the ratio of averaged stem spacing to water level (s_p / y_n)	141
Figure 3.38 Relationship of natural logarithm of the streamline coefficient ($C_d A_p h_p / \nabla$) to natural logarithm of the ratio of averaged stem height to water level (h_p / y_n)	142
Figure 3.39 Relationship of natural logarithm of streamline coefficient ($C_d A_p h_p / \nabla$) to natural logarithm of the ratio of plant projected frontal area to area of vegetated bed (A_p / a).....	142
Figure 3.40 Relationship of natural logarithm of streamline coefficient ($C_d A_p h_p / \nabla$) to natural logarithm of the ratio of average stem diameter to water level (d_s / y_n)	143
Figure 3.41 Relationship of natural logarithm of drag coefficient (C_d) to	

natural logarithm of Reynolds number (Re)	143
Figure 3.42 Relationship of natural logarithm of drag coefficient (C_d) to natural logarithm of Froude number (Fr).....	144
Figure 3.43 Relationship of natural logarithm of drag coefficient (C_d) to natural logarithm of the ratio of fluid drag force to plant rigidity: $\rho V^2 h_p^4 / (G_s I)$	144
Figure 3.44 Relationship of natural logarithm of drag coefficient (C_d) to natural logarithm of the ratio of averaged stem spacing to water level (s_p/y_n).....	145
Figure 3.45 Relationship of natural logarithm of drag coefficient (C_d) to natural logarithm of the ratio of averaged stem height to water level (h_p/y_n) .	145
Figure 3.46 Relationship of natural logarithm of drag coefficient (C_d) to natural logarithm of the ratio of plant projected frontal area to area of vegetated bed (A_p/a).....	146
Figure 3.47 Relationship of natural logarithm of drag coefficient (C_d) to natural logarithm of the ratio of average stem diameter to water level (d_s/y_n).....	146
Figure 3.48 An example of drag force of <i>Phragmites australis</i> measured by the direct drag force measurement system at 1522.632 stems/m ² and 0.0209 m ³ /s.....	147
Figure 3.49 An example of drag force of <i>Phragmites australis</i> measured by the direct drag force measurement system at 1522.632 stems/m ² and 0.0121 m ³ /s.....	147
Figure 3.50 An example of drag force of <i>Phragmites australis</i> measured by the direct drag force measurement system at 1522.632 stems/m ² and 0.0158 m ³ /s.....	148
Figure 3.51 An example of drag force of <i>Phragmites australis</i> measured by the direct drag force measurement system at 1522.632 stems/m ² and 0.0177 m ³ /s.....	148
Figure 3.52 An example of drag force of <i>Phragmites australis</i> measured by the direct drag force measurement system at 1522.632 stems/m ² and 0.0209	

m ³ /s.....	149
Figure 3.53 An example of drag force of <i>Phragmites australis</i> measured by the direct drag force measurement system at 1350.88 stems/m ² and 0.0077 m ³ /s.....	149
Figure 3.54 An example of drag force of <i>Phragmites australis</i> measured by the direct drag force measurement system at 1350.88 stems/m ² and 0.0121 m ³ /s.....	150
Figure 3.55 An example of drag force of <i>Phragmites australis</i> measured by the direct drag force measurement system at 1350.88 stems/m ² and 0.0158 m ³ /s.....	150
Figure 3.56 An example of drag force of <i>Phragmites australis</i> measured by the direct drag force measurement system at 1350.88 stems/m ² and 0.0177 m ³ /s.....	151
Figure 3.57 An example of drag force of <i>Phragmites australis</i> measured by the direct drag force measurement system at 1350.88 stems/m ² and 0.0209 m ³ /s.....	151
Figure 3.58 An example of drag force of <i>Phragmites australis</i> measured by the direct drag force measurement system at 1052.63 stems/m ² and 0.0077 m ³ /s.....	152
Figure 3.59 An example of drag force of <i>Phragmites australis</i> measured by the direct drag force measurement system at 1052.63 stems/m ² and 0.0121 m ³ /s.....	152
Figure 3.60 An example of drag force of <i>Phragmites australis</i> measured by the direct drag force measurement system at 1052.63 stems/m ² and 0.0158 m ³ /s.....	153
Figure 3.61 An example of drag force of <i>Phragmites australis</i> measured by the direct drag force measurement system at 1052.63 stems/m ² and 0.0177 m ³ /s.....	153
Figure 3.62 An example of drag force of <i>Phragmites australis</i> measured by the direct drag force measurement system at 1052.63 stems/m ² and 0.0209 m ³ /s.....	154
Figure 3.63 An example of drag force of <i>Phragmites australis</i> measured by the direct drag force measurement system at 719.30 stems/m ² and 0.0077 m ³ /s.....	154
Figure 3.64 An example of drag force of <i>Phragmites australis</i> measured by the direct drag force measurement system at 719.30 stems/m ² and 0.0121 m ³ /s.....	155
Figure 3.65 An example of drag force of <i>Phragmites australis</i> measured by the	

direct drag force measurement system at 719.30 stems/m ² and 0.0158 m ³ /s.....	155
Figure 3.66 An example of drag force of <i>Phragmites australis</i> measured by the direct drag force measurement system at 719.30 stems/m ² and 0.0177 m ³ /s.....	156
Figure 3.67 An example of drag force of <i>Phragmites australis</i> measured by the direct drag force measurement system at 719.30 stems/m ² and 0.0209 m ³ /s.....	156
Figure 3.68 An example of drag force of <i>Typha orientalis</i> measured by the direct drag force measurement system at 2315.79 stems/m ² and 0.0158 m ³ /s.....	157
Figure 3.69 An example of drag force of <i>Hygrophila pogonocalyx</i> measured by the direct drag force measurement system at 131.58 stems/m ² and 0.0158 m ³ /s.....	157
Figure 3.70 An example of drag force of <i>Juncus effusus</i> measured by the direct drag force measurement system at 3096.49 stems/m ² and 0.0158 m ³ /s.....	158
Figure 3.71 Plot of flow (l/s) against number of rotational turns which controls the revolutions per minute for the pump of the flume.....	158



List of Symbols

Symbols and Notations

Symbol	Description	SI unit	Dimension
a	: Area of vegetated channel bed	m^2	L^2
A_p	: Cross sectional area of plant	m^2	L^2
A_i	: Cross sectional area of individual plant	m^2	L^2
A_c	: Cross sectional area of flow	m^2	L^2
C_i	: Inflow concentration	mg/L	M/L^3
C_o	: Effluent concentration	mg/L	M/L^3
$C_d A_p$: Streamline factor	m^2	L^2
d_p	: Plant stem diameter	m	L
D_{hg}	: Distance between surface of water to the center of gravity of the trapezoidal container	m	L
E	: Modulus of elasticity	N/m^2	$M/T^2/L$
E_s	: Stiffness modulus of elasticity	N/m^2	$M/T^2/L$
EP	: Eddy flow pressure force	N	ML/T^2
ET	: Evapotranspiration	cm	L
f_{board_p}	: Static friction of the movable board	N	ML/T^2
F_b	: Drag force of platform (movable board)	N	ML/T^2
F_d	: Total drag force	N	ML/T^2
F_{dp}	: Drag force of vegetation	N	ML/T^2
F_e	: Force of eddy flow	N	ML/T^2
F_f	: Friction force on water conveyance	N	ML/T^2
F_g	: Force of water by gravity	N	ML/T^2
F_p	: Force of pressure	N	ML/T^2
$F_{p_measured}$: Drag force measured by the direct drag force measurement system	N	ML/T^2
F_{R_Total}	: Total hydrostatic pressure force	N	ML/T^2

F_{Rt4} : Hydrostatic pressure force of trapezoidal container	N	ML/T^2
F_{rrec} : Hydrostatic pressure force of rectangular board	N	ML/T^2
F_s : Force applied for a displacement of Δx	N	ML/T^2
$F_{viscous}$: Shear force resulted by viscosity	N	ML/T^2
F_w : Force of wind	N	ML/T^2
g : Earth's gravity = 9.81	m^2/s	L^2/T
G_p : Plant flexural rigidity ($G_s I$)	Nm^2	ML^3/T^2
G_s : Plant shear modulus of elasticity	N/m^2	$M/T^2/L$
h_p : Height of plant	m	L
h_{pd} : Designed height of plant under shear	m	L
H_g : Distance between center of gravity to the bottom of the board	m	L
H_t : Distance between surface of water to the bottom of the trapezoidal container	m	L
H_T : Total water head	cm	L
I : Plant second moment area of inertia	m^4	L^4
J : Product of EI	Nm^2	M/T^2L
K : Capacity climax of plant growth	<i>No. of stems</i>	
K_l : Capacity sub-climax of plant growth	<i>No. of stems</i>	
l : Length coordinate of the control volume	m	L
M : Plant population density	$No./m^2$	L^{-2}
MAA : Moment absorbing area	m^2	L^2
n : Manning's n	$sm^{-1/3}$	$TL^{-1/3}$
N : Capacity (no.) of macrophytes	<i>No. of stems</i>	
N_0 : Initial capacity (no.) of macrophytes	<i>No. of stems</i>	
P : Wetted perimeter	m	L
p : Fluid (water) pressure	N/m^2	$M/T^2/L$

ρ_p : Plant population density	$No./m^2$	L^{-2}
ρ_f : Density of water	kg/m^3	M/L^3
q : Water transported in soil	cm/day	L/T
Q : Flow	m^3/s	L^3/T
r : Growth rate of plant	$No./day$	$1/T$
R : Hydraulic radius (A/P)	m	L
s_p : Spatially averaged plant stem spacing	$No./m^2$	L^{-2}
t : Time	s	T
T : Rate of transpiration	cm/day	L/T
v : Free stream velocity	m/s	L/T
v_1 : Stream velocity at x_1	m/s	L/T
v_2 : Stream velocity at x_2	m/s	L/T
v_x : Stream velocity in x direction (longitudinal)	m/s	L/T
v_y : Stream velocity in y direction (lateral)	m/s	L/T
v_z : Stream velocity in z direction (verticle)	m/s	L/T
v_a : Average stream velocity	m/s	L/T
v^* : Shear velocity	m/s	L/T
∇ : Control volume of the flow regime	m^3	L^3
w : Width of the control volume	m	L
W_x : Self-weight of platform in the x -direction	N	ML/T^2
x_1 : Distance at x_1	m	L
x_2 : Distance at x_2	m	L
Δx : Designed horizontal displacement of plant under shear	m	L
y_1 : Water level at x_1	m	L
y_2 : Water level at x_2	m	L
y_n : Water level	m	L
z : Height of the control volume	m	L
δ : Characteristic length of plant	cm	L

	root		
ω	: Frequency of oscillation of flow	No./s	T^{-1}
ε	: Surface roughness of the plant	cm	L
γ	: Unit weight of water	N/m^3	$M/T^2/L^2$
μ	: Dynamic viscosity of water	Ns/m^2	MT^3/L
σ_x	: Normal stress in the x direction	N/m^2	M/T^2L
τ_0	: Total boundary shear stress	N/m^2	$M/T^2/L$
τ_b	: Channel bed shear stress	N/m^2	$M/T^2/L$
τ_p	: Plant shear stress	N/m^2	$M/T^2/L$
τ_{xx}	: Shear force along the xx plane	N/m^2	$M/T^2/L$
τ_{xy}	: Shear force along the xy plane	N/m^2	M/T^2L
τ_{yz}	: Shear force along the yz plane	N/m^2	$M/T^2/L$
τ_{zz}	: Shear force along the zz plane	N/m^2	M/T^2L
τ_{zx}	: Shear force along the zx plane	N/m^2	$M/T^2/L$

Dimensionless Groups

Symbol

C : Chezy's C

C_d : Drag coefficient

$C_d A_p h_p / \nabla$: Streamline coefficient

dy/dx : Water level variation over distance

dv/dx : Flow velocity variation over distance

d_p/y_n : Ratio of averaged plant diameter to water level variation

ε/d_p : Ratio of surface roughness to averaged plant diameter

f : Darcy-Weisbach friction factor

Fr : Froude Number ($V^2/g/y_n$); Ratio of stream velocity to wave velocity



h_p/y_n : Ratio of averaged plant height to water level variation

K_n : Factor of Manning's n (=1 in SI unit)

K_p : Constant relating plant polutation density to cross sectional density

k_s : Reaction constant for 1st chemical dynamic equation

LHS : Left hand side

ρ_{p_cross} : Plant cross sectional density (A_p/A_c)

$\rho V^2 h_p^4 / G_p$: Ratio of flow drag to plant flexural rigidity

Re : Renolds number ($\rho VR/\mu$) Raito of inertia force to viscous force

RHS : Right hand side

R_{kn} : Ratio of the growth of plant at n^{th} number of sub-climaxes

S_0 : Channel bed slope

S_f : Energy slope of water flow

s_p/y_n : Ratio of averaged stem spacing to water level variation

$\omega y_n / V$: Ratio of inertia (local) force to inertia (convective) force; Stouhal number

Φ : Dimensional analysis

π : Circular constant = 3.14

$\xi, \psi, \eta, \zeta, \phi, \beta$: Parameter estimates (constants) in the multiple linear regression

Chapter 1. Introduction

1.1. Background

Vegetations along river floodplains, wetlands, watersheds, and vegetated channels have been discovered as important controls for the exchange of nutrients, sediments, metals and other contaminants (Odum 1983; Kadlec and Knight 1996; Nepf 1999; Morris 2002; Toet 2005; Akrotos 2007), forming important transition zones that acts as buffers between terrestrial and aquatic regions (Mitsch and Grosselink 2007). Their existences provide shelters for animals and form the basis of the food chain, and therefore the fundamental support of the ecological living environment (Odum 1975; Steytler 1995; Bruggen 2006; Wilosn 2006; Mitsch and Grosselink 2007).

Emergent macrophytes are among these aquatic vegetations which stand at places where land and water meets. Some of these transition and buffer zones (Leopez and Fennessy 2002) are artificially formed for the purpose of bank protection, water purification, land conservation and restoration, and recreational purposes. Surface flow constructed wetlands are one of these features (Toet 2005; Mitsch and Grosselink 2007) which are becoming important as resources for non-point pollution and flood control, where purification of water and storage of storm and surface runoffs are made possible (Office of Water 1993; Crites and Tchobanogous 1998; Bruggen 2006; Guo 2006; Rousseau et al. 2007). Their efficient function largely depends on the careful design and choice of the species and densities of the macrophytes, channel geometry, flow velocity, and water level, which in turn, greatly affects the survival of species of plants and animals in these sensitive areas (Reed et al. 1995; Yen 2002; Jarvela 2003; Carollo et al. 2005; Musleh and Cruise 2006; Chang 2007).

In addition, macrophytes are also crucial for the protection of banks and shores (Morris et al. 2002; Li and Yan 2007; Luong 2008). It is reported that emergent macrophytes such as mangroves effectively dissipated wave energy in Pitchavaram and Muthupet, southeast coast of India, during the 2004 Indian

Ocean Tsunami (Evgeny and Leopold 2005; Sonak et al. 2008; Luong 2008; Paris et al. 2009). In the same way, densely vegetated swamps in the Louisiana Delta (Mitsch and Grosselink 2007; Wilson and Allison 2008) have long absorbed the force of waves and storm surges. With those lands utilized for other purposes or submerged, New Orleans took the heavy impact of Hurricane Katrina (Fritz et al. 2007).

As water flow through these emergent macrophytes, drag force or flow resistance is induced which affects water conveyance and water levels in the flow regime (Yen 2002). Therefore the estimations of drag coefficients and the friction factors are important tasks in both the conservation and restoration of land and the design of hydraulic structures (e.g. dikes) on river banks and bay shores (Kouwen 2000; Jarvela 2003, 2005). These friction factors are also crucial in the calibration and validation of numerical models applied in the river hydraulics (Mason et al. 2003; Wilson 2008).

1.2. Literature Review

1.2.1. Flow resistance of vegetation

Dense and heterogeneous combination of macrophytes and various types of vegetation growing in the natural river floodplains, adjacent wetlands, and vegetated channels, waterways, and linings are essential for the determination of the transport phenomena of water, sediment, nutrient, and pollutant. Effects of vegetation on flow are key factors in the inter-dependent system of flow, sediment transport, and geomorphology in rivers, which are essential in hydraulic design. Generally it has been acknowledged that vegetation increases flow resistance, alters backwater profiles, and results in variation of sediment transport and deposition (Chow 1959; Yen 2002). At certain terrains such as river sections and wetlands with dense emergent or submerged macrophytes, vegetation drag is usually the major source of flow resistance to the surface water flow compared to the friction at the boundaries (Kadlec 1990). These vegetations also result in major variations of flow resistance as a result of change of season, weather, and effects of species succession, which in turn

cause temporal variations of the flow resistance and the effective area of the river cross sectional areas.

The use of reference publications (Chow 1959) has been the conventional approach which greatly assisted hydraulic engineers in the determination of friction factors (roughness coefficients) for the design of channels. In some of these manuals, flow resistances of all sources including vegetation are grouped into Manning's n values. Building on the foundation of these publications, advancements have been made to gain understanding of flow phenomena in floodplain and wetland flows, including the researches on resistance of rigid vegetation (Li and Shen 1973; Petryk and Bosmajian 1975; Huang and Yu 1992; Huang M. H. 1993; Jarvela 2002; Stone and Shen 2002; Musleh and Cruise 2006; Liu 2008; Tanino and Nepf 2008) and flexible vegetation (Kouwen and Unny 1973; Faith-Moghadam and Kouwen 1997; Kouwen and Fathi-Moghadam 2000; Freeman et al. 2000; Lee et al. 2004; Jarvela 2004, 2005; Carollo 2005; Wilson et al. 2008). Recently several researches and experiments have been conducted on the determination of drag, velocity profiles, longitudinal dispersion, shear dispersion, and turbulence characteristics of flow over vegetated areas (Nepf et al. 1996; Nepf and Vivoni 2000; Jarvela 2004; Lightbody and Nepf 2006; Tanino and Nepf 2008; Wilson et al. 2008).

In the above-mentioned studies, rigid vegetations usually consist of artificial rods in various types of materials and densities, while the flexible vegetations include both artificial and natural vegetations. For studies on the drag force of flexible and natural vegetations in aquatic flows, the approaches for obtaining the drag force data can be categorized into the direct and indirect drag force measurement methods. The later usually utilizes information of flow velocities and water elevations followed by the computation of drag force induced, while the direct drag force measurement method usually involves the development of instrumentations capable of accurately recording drag force experienced by the vegetations, which is especially important in distinguishing the effect of the streamlining of plant branches and foliage and their rigidity on

the total drag (Niklas 1992; Fathi-Maghadam and Kouwen 1997; Oplatka 1998; Kowen and Fathi-Moghadam 2000; Freeman et al. 2000; James et al. 2004; Armanini et al. 2005; Wilson et al. 2008).

Kouwen et al. (1969), who proposed the determination of the relationship between vegetation density and flexibility, was one of the first to study the effect of plant flexibility on overall drag. Due to the technical constraints in the design and construction of the direct drag force measurement system, previous related researches are forced to use natural vegetation detached from their roots and the soils. Vegetations in this status behave differently from truly living natural vegetations, which exhibits a wide variety of forms and flexibility. The special characteristics associated with vegetation such as its permeable, heterogeneous nature and its ability to bend and change shape (streamline) under flow action (Niklas 1992) needs to be accounted for when determining the hydraulic resistance of the vegetation. The biomechanical properties of vegetation would be greatly affected if parts of them are dying or dead (Kaack and Schwarz 2001). In searching of the effect of varying living conditions of plant stems on their mechanical properties, Kaack et al. (2003) developed an equation which indicated that the modulus of elasticity of the stem is significantly related to its chemical composition, including the mass of living lignin and cellulose, and its anatomical characteristics, such as the area of the outer ring, the parenchyma, and the vascular bundles (Kaack et al. 2003). Therefore, it is important to consider the natural ecosystem of the vegetation with roots and soils intact during the design of the direct drag force measurement system in order to obtain representative and realistic results.

1.2.2. Direct drag force measurement

Measurement of plant drag force has been long carried out by the use of equations for friction force, the measurement of water level, flow velocity, and the estimation of the drag coefficient C_d (Li and Shen 1973; Wu et al. 1999; Wilson et al. 2003). However, direct measurement of plant drag force involves the obtaining of plant drag force without these procedures. When the term

“direct measurement of drag force” is mentioned in this study, it implies that a system or device has been designed to measure plant drag force directly through a set of transducers, computers, and force balancing components. The plant drag force is measured directly by this device, not by the measurement of the water level, flow velocities, channel slope, and the estimation of the C_d values used for rigid cylinders.

If done in a proper way, this method would greatly reduce the possible inaccuracies in the difficult measurement of the central water elevations along the flow through emergent vegetation and the difficult and expensive task of measuring flow velocity in a non-intrusive way ($F_d = 1/2 \rho C_d A V^2$). The results of direct measurement of plant drag force have been found to match with the drag force derived from the measurement of velocity variation along the stream (Wilson et al. 2008). Recently, studies of direct measurement of plant drag force in aquatic flow have been carried out around the world with different focuses (Fathi-Maghadam and Kouwen 1997; Oplatka 1998; Kowen and Fathi-Moghadam 2000; Freeman et al. 2000; James et al. 2004; Armanini et al. 2005; Wilson et al. 2008).

In Waterloo, Canada and Ahvaz, Iran, Kouwen and Fathi-Moghadam derived a functional relationship between dimensionless parameters for estimation of resistance to flow in non-submerged, tall, densely vegetated channel (Fathi-Moghadam et al. 1997):

$$C_d \left(\frac{A}{\nabla} \right) h = f_4 \left(\frac{\rho V^2 y_n^4}{J} \right) \quad (1-1)$$

where C_d is the drag coefficient; A is the projected area of the plant in the stream-wise direction; V is the flow velocity; ρ is the fluid density; ∇ is the control volume; y_n is the water level; and J is the flexural rigidity which is the product the modulus of elasticity (E) and the second moment of inertia (I). All variables in this equation were measured for the analysis of the resistance to flow in non-submerged densely vegetated zones. The drag force on a single tree (pine and cedar tree models) in non-submerged aquatic flow was measured using a force-balance apparatus holding a model tree mounted in the floor of a

frame.

Fathi-Moghadam's experiments (1997) were conducted in a 13 m long, 600 mm wide Perspex flume with 7/1000 slope and flow depth of 60 and 120 mm. The channel slope is 4/1000 for high flow depth of 180, 240, and 300 mm. This change in slope was carried out to maintain the desired flow depth within the entire range of velocities in the channel. Velocities were measured at upstream of the model using a propeller current meter. A system of load cells was designed to measure the drag force instantaneously. The tree models were attached to the top of the table that was supported by four knife-edge frictionless legs in a Perspex box. The top of the glass mounting cone was set to be at the same level with the channel bed. The load cell measuring drag was installed between the edge of a table and the wall of the Perspex box which contained the entire force-balancing system beneath the flume. To account for the effect of the buoyancy, water was stabilized at desired depth with near-zero velocity and the load cell was set to zero at the beginning of each run.

Experimental results (Fathi-Moghadam et al. 1997) showed strong effect of vegetation flexibility in the reduction of the foliage area (MAA) and reduction of the drag coefficient as velocity increases. The Manning's n value was found to increase proportionally to the square root of flow depth and inversely proportional to the flow velocity for non-submerged conditions. The variation of Manning's n with depth was due to the increased submerged MAA with depth of flow. Therefore, density of vegetation was concluded as a dominant parameter for the non-submerged condition. The authors (Fathi-Moghadam et al. 1997) stated that their equation had been derived from self-similarity, dimensional analysis, and experiments conducted. To calculate the coefficients in the model, repetition of experiments with additional tree specimens and estimation of EI is recommended.

Comparison between the above experiment and this research is made as follows. For experiments conducted in this study, the effect of buoyancy was restricted by the tracks along the sides of the movable platform. Therefore there was no need to fill the channel at the desired depth with near-zero velocity

before the load cell was set to zero. Moreover, the measurements of drag force in this study could not be done by gradually increasing the velocity in the flume since the engineering string used to transfer the drag force to the transducer is lack of elasticity. When a lower velocity is set, water flowing through the channel would place an impact on the plants and therefore the string connecting to the transducer. The string was pulled to the fullest extend and the movable platform would be pulled in the direction of flow. However, after the motor of the pump was turned off, the movable platform of the direct drag force measurement system would lose its ability to move freely back to its original place. Therefore, the effect of an immediate following increase in flow velocity would not place a desired impact on the drag force measured. This problem was solved by turning off the stream after each and every experiment before the next desirable stream velocity was set.

In the United States, direct flow resistance due to shrubs and woody vegetation was determined in a final report presented to the U.S. Army Corps of Engineers (Freeman et al. 2000). Dimensional analysis arrived at the following results:

$$C_{D\text{ or }} \frac{V_*}{V} = f\left(\frac{\rho V^2 A_i}{E_s A_s}, \frac{Y_o}{H}, MA_i, Re\right) \quad (1-2)$$

where V_* is the shear velocity = \sqrt{gRS} in m/s; M is the plant density in no. of stems/m²; A_s is the plant blockage area in m²; Re is the Reynolds number; Y_o is the water level in meters; H is the height of the vegetation in meters; E_s is the stiffness modulus in N/m²; and ρ is the density of water in kg/m³. The experimental results were also used to develop regression equations for non-submerged (emergent) vegetation:

$$\frac{V_*}{V} = \frac{\sqrt{g}}{C} = 3.487 - 05 \left(\frac{E_s A_s}{\rho A_i^* V_*^2} \right)^{0.150} (MA_i^*)^{0.166} \left(\frac{V_* R_h}{\nu} \right)^{0.622} \quad (1-3)$$

$$n = K_n 3.487 - 05 \left(\frac{E_s A_s}{\rho A_i^* V_*^2} \right)^{0.150} (MA_i^*)^{0.166} \left(\frac{V_* R_h}{\nu} \right)^{0.622} \left(\frac{R_h^{2/3} S^{1/2}}{V_*} \right) \quad (1-4)$$

where S is the slope of the channel bed; ν is the kinematics viscosity of water in

m/s^2 ; g is the gravitational constant in m/s^2 ; K_n is a dimensionless factor of Manning's n which is equal to 1.486 in English units and 1 in SI units; R_h is the hydraulic radius in meters; and C is the Chezy's C friction factor. Two flumes were used during the experiments conducted by Freeman et al. (2000). The large flume was 2.44 m in width, 1.82 m in depth, and 152.4 m in length; a single average-sized plant was selected and inserted into a metallic platform at the center of arrays of vegetation in the test section for the direct measurement of plant drag force. Underneath the shallow metallic box, ball bearings were used in the bottom in a small section of the flume bed with a metal plate resting upon the ball bearings. A single plant with roots removed was attached to the plate. A strain indicator was attached to the downstream end of the plate to measure the compression force as the drag force applied to the plant by the moving water column. The platform was covered with a section of drain cloth to prevent soil from interfere the movement of the plate. The platform was also covered with plastic lid to reduce friction drag on the plate.

The small sectional flume was a 0.914 m wide and 0.914m high channel. All roots from al the plants were cut off at the base of the stems in the small flume. The plant stems were inserted through the washer into the grommet used to protect the base of the stem and prevent breakage of the stem. Without this precaution, the plant stems tended to break the stem in contact with the surface of the plywood floor. The plant selected for measurement in this flume was the downstream plant with four plants located upstream.

There were four challenges found in Freeman's study (Freeman et al. 2000), which were overcome in this research.

1. The ball bearings in Freeman's study (Freeman et al. 2000) couldn't direct the movement of the platform. This indicates that the platform was allowed to move in an angle θ to the 'x' direction in the midst of vegetation flow. If drag force of the vegetation is denoted as F_d , this instrument could be measuring the force of $F_d / \cos \theta$. In addition, serious friction force might be resulted at the sides of the platform for this undirected movement. Even if the platform was directed, the friction resulted from this directed movement

was not measured or stated in the report.

2. Although drain cloth could prevent soil from entering into the ball bearings, its existence prevented the smooth movement of the platform in the direction of flow.
3. Most importantly, with roots removed, the plants were dying and therefore losing their mechanical characteristics such as stiffness, modulus of elasticity and even the second area moment of inertia. These are important characteristics allowing the plants to streamline with the flow in their specific way for each and different types of plants. This dying process could be relatively fast (especially for some macrophytes) and therefore causing possibly unrepresentative or inconsistent results over the duration of the experiment.
4. Freeman et al.'s research (2000) were using plants that are detached from soil and roots. The biomechanical properties of the macrophytes would be greatly affected if parts of them are dying or dead. In the research of the effect of varying stem conditions on mechanical properties of plants (*Miscanthus*), Kaack et al. (2003) developed equation (1-5), which indicated that the modulus of elasticity of the stem is significantly ($R^2 = 0.968$, $p < 0.05$) related to the chemical composition, including the mass of living lignin and cellulose, and the anatomical characteristics, such as the area of the outer ring, the parenchyma, and the vascular bundles.

$$E = 0.14 + 0.0107(AOR \cdot \text{lignin}) + 0.00128(AOP \cdot \text{cellulose}) + 0.0212(AOV B \cdot \text{cellulose}) \quad (1-5)$$

where E is the modulus of elasticity; AOR is the area of outer ring; AOP is the area of parenchyma, and $AOVB$ is the area of vascular bundles. Lignin is a chemical compound and an integral part of the secondary cell walls of plants. Cellulose is an organic compound consisting of a linear chain of several hundred to over ten thousand linked glucose units. It is the structural component of the primary cell wall of green plants. It is noted that the product of the modulus of elasticity and the second moment of inertia (I)

would produce the flexural rigidity (J) of the plant, which is an important element in equation (1-1).

5. The installation of the strain indicator under water level could cause serious damage by the moisture and water inundation. Maintenance and repair are much harder under water in a confined below bed channel compared to a device secured above water or in a more convenient place above/outside the flume channel.

Direct measurements of vegetation resistance were also conducted at the Experimental Center for Hydraulic Models of Consorzio Venezia Nuova, in Voltabarozzo, Padova, Italy (Armanini et al., 2005). The hydrodynamic force exerted by water flow on isolated full scale willow of several size and foliage was analyzed. The plants were both fully and partially submerged in the stream. The hydrodynamic resistance was measured by a properly designed force transducer put in a 150 m long, 2 m wide, and 2 m deep flume.

The plants drag coefficient was evaluated. It was found to decrease with the plant's Reynolds number due to the willow's flexibility. Linear relationship between the drag force and the square of velocity was determined. Linear increase of drag force with flow velocity was observed for the flexible plants while linear decrease of the product of the drag coefficient and the momentum absorbing area with increasing square of velocity was found due to the streamlining (bending of trunk and shrinking of branches).

Force transducer was used in the measurement of the drag force. It was made up of two steel plates bounded together by four aluminum foils. The transducer was fixed at the bottom of the channel and was carefully surrounded with sand, grave and concrete in order to avoid discontinuity in the channel bed and the flow field. The plant was secured on the cylinder placed on the plate of the sensor, perfectly integral to the cylinder. The strength that acted on the tree was assumed to be totally transferred to the plate and then to the four aluminum foils. Eight strain gages were placed on the four foils to measure their deformation, and therefore, the force and the bending moment produced by the

force acting along the direction of flow.

Armanini's (2005) experiment extends the view points of Fathi & Kouwen (1997) in the analysis of the product of the drag coefficient and the plant blockage area in the stream. The experimental setup was an example of using partially dead plants for the drag force measurements in the aquatic flows. This again could result in unrealistic bending due to a different modulus of elasticity from the living plant.

Researchers (Wilson et al., 2008) in the United Kingdom used a cantilever technique to measure the contribution of a plant's foliage to the total plant's hydrodynamic drag. Experiments were conducted in a laboratory flume using samples of Branches of pine (*Pinus sylvestris*) and Ivy Stipes (*Glechoma Hederacea*) with different physical forms and biomechanical properties. The drag force was measured directly using a strain gauge technique and determined for a series of velocities for each vegetation species with and without foliage.

The results showed that the drag force exerted by the plant changed as it bended and streamlined with the flow. The frontal projected area of a flexible plant was also a variable dependent on the flow velocity and the plant properties. Since it was technically difficult to determine the variation in frontal projected area for all plant species under all flow conditions, the effective frontal projected area of the vegetation could be determined in still air (not under flow condition) in Wilson's study as in previous studies (Armanini et al., 2005). The experiment revealed a distinct contribution of foliage to the total plant drag. This was observed for both the needles of the pine branches and the foliage of the ivy. The additional drag contribution from the needles of the pine branches was particularly marked at lower velocities, whereas for the ivy plants, the additional drag contribution of the foliage showed little dependence on the velocity. This was because ivy foliage had better streamlining properties than the willow in the flow. Therefore the increase of flow velocity did not have great influence on the drag force experienced by the ivy branches. For the pine branches, the F_d ratio decreased with increasing velocity. For the ivy branches,

the F_d ratio tended towards a constant with increasing velocity. This was likely due to the gradual streamlining of the needles (pine branches) with increasing velocity where the frontal area was continuously compressed as the velocity was increased. For the ivy plants, this may indicate that the foliage was becoming closer to the point of maximum streamlining at lower relative velocities than for the pine plant.

1.3. Objective of the study

The purpose of this research is to directly measure the drag force induced by flow over four selected emergent macrophytes in Taiwan to assist engineers and ecologists in the estimation of drag coefficients and friction factors for natural, emergent (non-submerged), flexible, and living macrophytes in the vegetated zones. As the planet is under the effect of climate change, extreme weather conditions with high precipitation and increasingly intense tropical cyclone activities (I.P.C.C. 2007) are expected in certain areas, which would result in flows with high speed in steep terrains. Therefore drag forces of an array of emergent macrophytes in aquatic flows are to be measured in a steady, non-uniform, majorly transitional and supercritical flow using a self-developed direct drag force measurement system (Please see Figure 1 for the conceptual plan of this research). A backward facing step is located immediately after the vegetated zone to better represent flow over vegetated sand belts on the floodplain, surface flow constructed wetlands, and vegetated fish ladders. The drag force data obtained are then applied in the calculation of the streamline factor ($C_d A_p$), the streamline coefficient ($C_d A_p h_p/\nabla$), the drag coefficient (C_d), and therefore the Darcy-Weisbach f , Chezy C , and Manning's n friction factors. Multiple regressions may be carried out for the drag force and drag force coefficient in varying plant densities and flows. Dimensional Analysis is carried out to build an empirical model for the calculation of for the drag coefficient and the streamlining coefficient, and hence the friction factors of *Phragmites australis*.

A drag force measurement system is developed specially for the purpose of

direct measurement of the drag force induced by flow over an array of four types of emergent macrophytes with varying plant densities and flow velocities. Different from previous studies, this system is the first to directly measure drag force of an array of realistic living emergent macrophytes with roots and soils intact. These living aquatic plants therefore are alive and strong in a mini-ecosystem placed on the drag force measurement device which greatly improves the results of the drag force measured due to the reflection of true flexural rigidity and streamlining function of the emergent macrophytes.



Chapter 2. Experimental Methodology

The experiments were conducted in four phases. The first phase involved data collection and field observation of aquatic plants found in Taiwan. Field trips were made to confirm the status of the macrophyte species and their specific function in the constructed wetlands. Water quality tests were conducted to test the function of the existing constructed wetland systems.

The second phase of the experiment aimed to cultivate these plants on the roof top of Engineering Block 1 in NCTU for further use in the flume experiments. Water quality tests were conducted to monitor phosphorous absorption of *Phragmites australis*, *Juncus effusus*, and *Hygrophila pogonocalyx*. Plant characteristics were recorded right before the flume tests.

The third phase included the design, construction and testing of the direct drag force measurement system. This system was specially designed to measure the drag force of an array of realistic and living emergent macrophyte canopies in aquatic flow with varying stream velocities, types of plants, and plant densities. According to the reviews, it could be the first device to measure fluid drag of an array of living emergent macrophytes with roots and soils intact.

The fourth phase was the actual examination of drag force induced by the four types of macrophytes chosen. Experiments were conducted in a flume located at the river sedimentation laboratory in National Chiao Tung University.

2.1. Phase 1: Field Studies

Field surveys were mainly carried out for the selection of aquatic plants. The purpose was to observe and select macrophytes for the flume tests. Since emergent macrophytes are often found in the wetlands, field trips were directed to the constructed wetlands in northern part of Taiwan. Suitable macrophytes in the constructed wetland had been determined using field data collected by previous researchers in Taiwan (Chang 2007). Since the constructed wetlands are built for stream purification in a natural environment, its ability to purify

polluted water and to stand in physical environmental stresses such as storms, floods and typhoon are required. The growth pattern for macrophytes could be determined by the logistic equation:

$$\frac{dN}{dt} = rN \left(\frac{K - N}{K} \right) \quad (2-1)$$

where N is the number of a chosen macrophyte; t is the time; r is the growth rate; and K is the maximum capacity of number of macrophytes.

This equation is denoted as:

$$\frac{N}{N_0} = e^{rt} - \frac{1}{K} N e^{rt} \quad (2-2)$$

$$N = \frac{K}{1 + \left(\frac{K}{N_0} \right) e^{-rt}} \quad (2-3)$$

since $K > N_0$ and $\frac{K}{N_0} > 1$.

where N_0 is the initial plant density.

In the field studies, it is difficult to measure the values for N_0 . Therefore let:

$$\frac{K}{N_0} = e^a \quad (2-4)$$

where a is a positive number, which gives:

$$N = \frac{K}{1 + e^{a-rt}} \quad (2-5)$$

Although the macrophyte communities could reach to its maximum capacity or the climax, re-succession occurs under the variation of environmental conditions before it reaches the next climax called “*sub-climax*.” The ratio of the capacities of these two climaxes is:

$$R_{k1} = \frac{K_1}{K} \quad (2-6)$$

where K_1 is the number of macrophytes for the sub-climax period. Since variation in environmental conditions occurs from time to time, R_{kn} is denoted as:

$$R_{kn} = \frac{K_n}{K} \quad (2-7)$$

where K_n is the n number of sub-climaxes and R_{kn} is the ratio of the growth of plant at n number of sub-climaxes. Generally the variation of the environment could affect the growth of the plants in three ways as shown in Figure 2.1.

For $R_{kn} < 1$, the natural environment is a 'stress' for the aquatic plants. The number of plants would not be as many as the first maximum capacity. If a species is classified as a community with $R_{kn} = 1$, it is considered to have resistance stability and resilience stability. The former means the chosen macrophyte is able to recover to the original climax capacity under stressful environmental conditions. The later represents a shorter time required for this recovery. Species fall into this category are prioritized for considering the building, management and maintenance of the constructed wetlands.

Plants with $R_{kn} > 1$ fall into the category of superior species, representing an increase in growth under various environmental conditions. They would be the most competitive species occupying a large area in the floodplain or in the constructed wetland. Floods and storms could hardly take them away from their habitats. Ecological management through the application of subsidy-stress gradient is needed to manually decrease the number of inhabitants for habitat control (Thullen J. S. et al. 2002, Knight R. L. et al. 2003, and Nakase Kota et al. 2008).

Table 2.1 is a reference from the Ecological Engineering Research Center at National Taiwan Univeristy (Chang 2007). It can be observed from Table 2.1 that *Hygrophila*, *Eleocharis dulcis*, *Ludwigia octovalvis*, *Schoenoplectus mucronatus*, *Phragmites australis*, and *Typha orientalis* are more stable in the periods of rain storms compared to other plants, especially those who have high r values at the beginning stage.

Under larger environmental disturbances such as typhoons and floods, *Hygrophila pogonocalyx*, *Bacopa monnieri*, *Typha orientalis*, *Eleocharis dulcis*, and *Phragmites australis* demonstrate stability under stress. From Table 2.3, these five macrophytes are the most recommended species. In this research, drag force of *Hygrophila pogonocalyx*, *Typha orientalis*, *Phragmites australis*, and *Juncus effusus* were measured in aquatic flow with varying plant densities

and flow velocities.

Except for a plantation zone located in Changhua County, sites visited in this research mainly located in the northern part of Taiwan, including Taipei County and Hsinchu County. The list of constructed wetlands visited is shown in Table 2.2.

Water quality tests were conducted during and after some of the field trips to confirm of the functionality of the constructed wetlands. A major number of experiments were conducted with the ecological research team from National Taiwan University. An example of field water quality test conducted at Du-Nan-Qiao Constructed Wetland in May 2007 is shown in Table 2.4, Table 2.5, Table 2.6, Figure 2.2, and Figure 2.3. Although water was being purified, the water quality varied (Figure 2.3) due to constant inflow of water along the flow path (unsteady flow).

2.2. Phase 2: Plant Cultivation

A mini-scale roof farm was established on top of Engineering Block 1 in NCTU, Hsinchu, Taiwan, for the cultivation of plants selected for the drag force test in aquatic flows. A total of twenty two boxes each with the size of 61 x 45 x 25 cm containing 10 different aquatic plant species were placed on the roof top with constant maintenance of water levels and debugs. Soil was put around the pot to secure the array of pots in the container. Some filling soil particles tended to float at the surface of the water, which required efforts and patience for their final settlement to the soil bed. When the entire soil stratum was fully saturated with water, the water level was maintained according to the different needs for these types of aquatic plants (Lin 2005, Chang 2007). It is noted that shallow water was the desired water depth for most of the types of aquatic plants chosen.

Water samples were collected to measure the reduction of phosphorus by testing the reduction of phosphate content (PO_4^{-3}). Phosphates in polluted water usually appear in forms of orthophosphates, polyphosphates, and organic phosphates. The orthophosphates are formed by the existence of a balanced relationship in phosphates, hydrogen phosphates, dihydrogen phosphates and

unionized phosphoric acid. However, due to soil conditions (rich in phosphate) and lack of overall water circulation for some containers, some test results showed an increase of phosphorus content over time. Laboratory and field studies such as the ones carried out by Ishigami Tomohide (2008) should be referenced for further measurements of the amount of phosphorus released from sediments in the wetlands and riparian communities.

Two sets of containers were connected together, each with an overflow weir with water circulation ensured by the installation of the submerged pumps and the necessary pipes. Water levels had to be constantly checked for the effect of wind and sun on the roof top which accelerated evaporation. It was also observed that the concrete slab on the roof was extremely hot during sunny days in Hsinchu, when much heat was absorbed by the water body of the mini wetland systems. Meanwhile, orientations of some containers had to be changed to avoid strong wind and massive invasion of bugs which tended to eat up a whole container of *Ludwigia octovalvis* (水丁香) and *Myriophyllum aquaticum* (粉綠狐尾藻).

2.3. Phase 3: Design of Instrument - Direct Force Measurement System

Below is a brief description of the innovation, research and development of the emergent aquatic plant drag force measurement system.

2.3.1. Design of depth

Additional depth of the drag force system and therefore the elevation of the channel were required for the plantation of full-scale living aquatic plants. The minimum required depth of soil for realistic emergent macrophytes is a major concern in designing constructed wetlands. This sensitive area is where the roots of these aquatic plants grow. The characteristics of the top soil determine the evapotranspiration of the plant which is related to the transportation of moisture in this layer of soil. This transportation would in turn affect the rate of water intake of the aquatic plants which sustains the growth of macrophytes and reflects true flexibility to bending and vibration in aquatic flows, which would in turn, affect the accuracy of the measured projected plant area and hence the drag coefficient. In the design of constructed wetlands, the

depth of this surface soil (z) is designed based on the following equation:

$$z = \delta \ln \left(1 + \frac{q_0}{T} \right), \quad q = -k \frac{dH_T}{dz} \quad (2-8)$$

where q is the water transported in the top soil (cm/day); z is the depth of soil (cm); T is the rate of transpiration (cm/day); δ is the characteristic length of plant roots (cm); k is the hydraulic conductivity of soil (m/day); and H_T is the total water head (cm).

Reports from the ecological engineering research center (Chang 2007) indicated that the probability distribution of the length of the roots of Typha is shown in Table 2.1, from which the characteristic length of the roots of Typha was calculated as the sum of the product of each individual length of the root and the probability of its existence ($\delta = 14.97$ cm).

From experiments carried out at the Xin-Hai-Qiao Constructed Wetland in Taipei County, the ratio of evapotranspiration (ET) and evaporation (E) at the beginning stage of plantation was (55cm in height) $ET/E = 1.01$. In its fully grown stage, a chosen Typha with 179 cm had a ET/E ratio of 1.40. Considering the period with the highest amount of evapotranspiration, water consumption for Typha was: $1.4/1.01 = 1.386$ times compared to the normal amount of evaporation.

Average evapotranspiration = 6 mm/day

Daily water consumption (depth) was: 6 mm/day x (1.386) = 8.317 mm/day

Averaged saturated hydraulic conductivity in the constructed wetland = 5 mm/day.

Therefore, the depth of the surface soil in the constructed wetland should be:

$$z = \delta \ln \left(1 + \frac{q_0}{T} \right) = 14.97 \ln \left(1 + \frac{8.317}{5} \right) = 14.67 \text{ cm} \quad (2-9)$$

The average height of Typha in Xin-Hai-Qiao Constructed Wetland could be around the range of: $(55+179)/2 = 117$ cm.

Since the Typha orientalis used right before the flume tests conducted in this research had an average height of 65.77 cm, by assuming a direct proportionality between the depth of soil and the height of plant, the soil depth

in this experiment should be $65.77/117 \times 14.67 = 8.24$ cm

Therefore, the average height of pots containing the emergent macrophytes was designed to be 8.3 cm in this experiment. Following this design consideration, the frame holding these pots on the movable platform was also designed with a height of 8.3 cm. This would increase the total weight carried by the movable platform in the direct drag force measurement system compared to a system without the weight of soils. The design sketches of the direct drag force measurement system are shown in Figures 2.4 to 2.10.

2.3.2 Design to level with channel elevation

This inclusion of the depth of soil required the elevation of the whole flume channel bed in order to embed the drag force measurement system containing the soil and the roots of the aquatic plants to ensure smooth flow transition before the stream contacted with the vegetations. The front part of the channel bed (7.5 m) had been elevated by 10.4 cm using wooden structures. The movable board and its supports had to match this height. Adding up the thickness of the movable board, the wooden cover, the space for free movement, and the thickness of the acrylic base, the height of the in-channel part of the drag force measurement system is brought to a total of 10.4 cm of height underneath the channel bed elevation, which was exactly flushed with the original channel bed elevation.

The entire structure had to be water proofed to ensure steady flow (no loss of water during conveyance). It was also designed to have a uniform surface to ensure a constant friction value. It had to stand for a period of time therefore its durability was a required design task. Constant maintenance, monitor, and inspection were required to ensure its current status.

Soil was held in a confined space where movements were not allowed. At first, incipient mechanism of the soil particle was put into consideration. This problem was completely eliminated later by the covering of the soil in confined containers.

2.3.3. Member force design

Design for sum of forces and moments:

Structural member forces were estimated by setting the summations of forces at the 'x' and 'y' directions to zero. All clockwise and anticlockwise turning moments at one end of the structure were designed and calculated to achieve equilibrium. However, under slight movement of the movable board, the bearings at the last part of the railing would achieve a friction at the top of the railing instead of at the bottom part. Therefore friction force at the top of the railing was also put into consideration when calculating the plant drag force.

2.3.4 Design for static friction

One of the challenges in designing this system was to overcome the friction force provided by the body weight of the system: the saturated soil, the water, the movable board, the railings and wheels, the plant holders and the array of emergent macrophytes; under the drag force induced by the array of the emergent macrophytes. Minimum static friction forces between the wheels and the railings were required for the measurement of the drag force exerted by the fluid on the plants. Static friction must be kept significantly less than the drag force acting on the array of canopies. However, soil added weights to the whole drag force measurement system which increased the static friction and therefore threatened the measurement of the fluid drag on the vegetation. To solve this problem, the relationship between the static friction and the weight of this drag force measurement system was first developed. At the same time, an estimation of the area of the plant and the flow velocity was made in order to estimate the drag forces required to overcome the static friction. ($F_d = 1/2 \rho C_d A V^2 > \text{static friction} = \text{constant} \times \text{weight}$)

The static friction was significantly reduced by the following measures. The system was much lightened after the second PVC structure was constructed to hold the plants instead of the original heavy acrylic structure. In addition, frame structures were used instead of solid wall partitions for the support of the containers. These two methods greatly reduced the weight of the system and therefore the static friction resulted.

Friction force was significantly reduced when stainless steel railing and

reinforced plastic wheels were used in combination to provide smooth movement in only the 'x' direction (the direction of the flow). In addition, lubrication of the wheels and their contacting rails were ensured throughout the test.

Small amount of water leakage was redirected to increase the drag force acting on the system. In the second design of the movable board, as an attempt to mimic natural bed surface, additional roughness of surface at the plant zone was provided. This inclusion further ensured the overcoming of the friction force. This bed shear was also measured under various flow conditions and was deducted by the total drag for the finding of the plant drag.

As the result of these design efforts to overcome the static friction, the induced plant drag is shown much higher than the maximum friction force in the data collected. For example, for *Phragmites australis* at 1522.6 stems/m² under the flow of 20.91 l/s, the average total force measured was 9.18 N and the average static friction measured was only 2.94 N.

2.3.5 Design for reduction of eddy current

Design for reduction of eddy current and pressure at the back of the system when water flows by the drag force system was carried out. These two forces had to be minimized or measured in order to have an accurate measurement of the plant drag. The force resulted by the eddy current was minimized by providing a small stream underneath the movable board to break the eddy structure formed at the back of the drag force measurement system. The structure of the eddy current was assumed to be destroyed and balanced out by the stream underneath the drag force system, therefore leaving the hydrostatic pressure alone for consideration in the force balance equation.

2.3.6 Building of the in-channel drag force measurement system

Structural integrity and stability of the drag force measurement system were ensured by pre-calculating the member forces. The materials used were solid wood, acrylic, and PVC members. The wooden part was double coated with waterproof paint. The joints were strengthened by special waterproof glue which enabled strong bonding and smooth transfer of loading weights to the

channel bed.

Choice of material and waterproof consideration:

Acrylic and wood were the main sources of material chosen for the construction of the drag force measurement system. All wooden working materials were painted with acrylic fiber enhanced waterproof paint that was originally used for roof top surface treatment. The first treatment used paint to water ratio of 2:1, while the second treatment after 24 hours of drying utilized paint without water dilution. Since some neutral silicon sealants were not suitable for total water immersion purposes, the KS Bond GS 30 strong adhesive sealant (KuoSen Enterprise Co. Ltd.) was used for waterproof and shockproof purposes in the construction of the flume bed, the side channel connections, the railings and the wooden part of the movable board. This product was selected for its ability for waterproof, relatively easy workability and its slightly elastic behavior after finishing.

The acrylic base:

Acrylic was chosen to be the construction material for the base of the drag force system. It was designed to bear large loads including its self-weight, the weight of the water, the entire movable platform, the plant holders, the plants, the saturated soil, and the rails with bearings. It was designed to have a double-T shape when looking from the cross-sectional view. The spacings at the two sides of the base (toes) allowed additional resistance of bending of the wall constructed to bear loadings of the plants and soils. This double T-shape was also necessary to prevent damage of the glass-walled channel, so that the whole construction would not place any adhesives, holes, and nails on the flume wall.

2.3.7 The rails and bearings

The rails and bearings were installed to allow movement of the platform in only the 'x' direction for accurate measurement of the drag force. Numerous ideas were tried (wheels at the bottom, wheels at the side, tracks at the bottom, and railings) and rails at the sides were found to be the best option allowing movement only in the 'x' direction, and minimize possible friction caused by

suspended particles.

The movable board and the plant container:

The final version of the movable platform had two railings at the sides of a wooden waterproof painted board. Dimensions were carefully measured to ensure least amount of friction at the two sides of the board. A PVC frame with 12 holders was constructed on top of the movable board where the pots could be tightly secured. This plant container was constructed with much lesser weight due to the material and the frame structure compared to the other plan where solid acrylic partitions were utilized to hold the plants.

2.3.8 Front water stops

The front water stops were formed by three blocks of 'T' shaped wooden blocks in order to passively prevent under bed water leakage entering the system directly. These blocks were also designed so that in case there was a leakage, minimum or non additional force would trust the drag force measurement system directly.

2.3.9 Side channel connections and supports

Since the movable board was designed to slide along the two sides of the acrylic base, there would be one spacing left between the acrylic wall and the flume wall at each side of the flume. Two side channel connections were designed in order to provide smooth surface transition at these junctions where the front, central and the sides of the additional flume bed converged.

2.3.10 Pulleys and strings

Strings were used under water to transfer the drag force of the entire system up to the top of the flume by two 90° turns through two pulleys. A 4mm-thick waterproof painted wooden board was used at the junction of the elevated channel bed and the direct drag force measurement system to provide smooth transition of flow.

2.4. Phase 4: Flume Experiments

2.4.1 Preparation of the channel: the embedded level

The supporting structures of the elevated flume bed in front of the drag force system were reinforced with waterproofing elements that performed well

under shear, pressure, and weight resulted from the flowing water. A uniform surface treatment was applied for a 5-meter length of the channel to provide uniform friction at the flume bed.

Laboratory experiments were conducted in a re-circulating, glass walled flume framed by steel beams and columns. The channel was 0.004 in slope, 80 cm in height, 60 cm wide and 15 m long. The positive x -axis was in the stream-wise direction, y -axis was in the cross-channel direction, and $z = 0$ at the flume bed with positive values in the upward direction. The flume bed was elevated by steel columns 93 cm above the floor followed by two steel beams with 30 cm in height. At the inlet, a still basin was used to reduce turbulence, and a 0.65 m long flow straightener was used to eliminate swirl. The total inlet still length was 7.5 m. Smooth inlet conditions were achieved by a set of straw forming a honeycomb and a styrofoam stilling board. A 20-horsepower motor with 1760 revolutions-per-minute was controlled by a 15kW AC speed motor controller with program/read, stop/reset, forward/reverse, and on/off functions. The digital display on the speed controller could accurately repeat the experiments with the same number of rotational speeds. This number of turns was related to the flow of water in the flume. A set of experiments was conducted to confirm this relationship.

Stream velocities were measured using an electromagnetic flow meter (Model ACM-300, Alec Electronics Co. Ltd) capable of measuring three velocity components (x, y, z) corresponding to stream-wise, lateral, and vertical directions with a range of -250cm/s to + 250 cm/s. Only the stream-wise data was recorded in this experiment since it was the dominant flow velocity in directed channel flow. The functional characteristics of the flume were then determined by measuring the respective flow (product of flow velocity and cross sectional area) under each rotational turns at appropriate intervals (Figure 3.71). The selected turns include: 14 turns ($0.0077\text{m}^3/\text{s}$), 17 turns ($0.0121\text{ m}^3/\text{s}$), 20 turns ($0.0158\text{ m}^3/\text{s}$), 23 turns ($0.0177\text{ m}^3/\text{s}$), and 26 turns ($0.0209\text{ m}^3/\text{s}$).

2.4.2 Measurement of drag force of emergent macrophytes

After deciding on the type of plant for the direct force measurement, the

plants were dug out from the containers located at the roof top. Twelve pots of plants were selected with roughly consistent height. The roots extending outside the pots were cleaned with clear water to avoid unnecessary imbalanced movement when placed in the drag force measurement system. Each pot was dried with clothe, numbered, and tapped at the top of the pot to avoid lost of soil particles during the flume tests. Measurements of plant height, diameter, degree of spread, and number of stems per pot were made as a record of plant characteristics. These statistics were critical for later data analysis in the finding of the ratio of plant height to water level, plant diameter to water level, averaged spacing to water level, and the dimensionless terms in the dimensional analysis.

Four photographs were taken for each individual plant in order to calculate the projected frontal area of the plant, and therefore, the drag coefficients. This set of photographs included one photograph of the plant with a scaled ruler, one with a 10 dollar coin, one with itself, and the last one which includes the full length of the plant. A total of 192 photographs were taken. Another four photographs were also taken for grouped plants in 4 different densities with the same concepts and methods. A total of 80 photographs were taken for the purpose of calculating the grouped projected frontal area of the plant.

Experiments were conducted to obtain the shear modulus of elasticity of *Phragmites australis*. Shear modulus of elasticity was considered as an elastic modulus used for the deformation which took place when force was applied parallel to one face of the object. The shear modulus of elasticity G_p was defined as the ratio of shear stress to shear strain. The shear stress was defined as the magnitude of the force per unit cross-sectional area of the stem (the face) whiles the shear strain was defined as the horizontal displacement per unit height resulted by the force applied. Random samples of *Phragmites australis* were taken to measure the representative cross sectional area of the stem. A force gauge was used to pull the stem at a fixed height horizontally until it reached a desired horizontal length. This force was recorded and used to calculate the shear stress.

When all the preliminary tests were done, the plants were put into the movable platform of the drag force measurement system. This system was specially designed to hold the pots containing the soil and the plants tightly to ensure proper drag force transfer into the movement of the wheels at the railings.

After all the plants were secured and the computer was ready, the drag force measurement gauge was turned on while special care was taken at the two ends of the strings, the pulleys and the wheels in the railings to make sure they were not obstructed. The surface of the channel bed, the valves at the motor (to check for cavitations), the water conveyance structure, the adjustable board and the stilling basin at the back of flume were examined. The drag force measurement gauge was zeroed while the video camera was turned on a little ahead of the speed controller of the motor of the pump. After the motor was turned on by using the speed controller to a speed of 19 rotations, water started to be pumped up to the still basin at the front part of the flume. Once it passed through the straws used to direct the flow, the speed was changed to the designed speed (14, 17, 20, 23, and 26 rotational speed turns). After the water flowed through the electromagnetic flow meter located at upstream of the plant canopies, it was turned on to measure the flow velocities in cm/s when steady stream flow was achieved. Readings of drag forces per second immediately appeared on the drag force measurement system and were recorded and monitored on the computer screen. This file was then transferred into the excel file after the test were completed. Water levels were measured by both the transparent rulers arranged on the flume wall with designed spacing and the pointer gauge mounted and centered on top of the flume. This pointer gauge was used specially for the measurement of water levels along the center of the vegetated flow regime. After each run, the pump was brought to a complete stop by turning the speed control to zero. The drag force measurement gauge was zeroed and the same steps were repeated before the next test run.

Chapter 3. Results and Data Analysis

3.1. Preliminary Data Analysis

After following the experimental procedures mentioned in the previous chapter, raw data were obtained for preliminary data analysis which included: derivation of the plant drag force and its validation, computation of plant projected frontal area, study on the relationships between drag force of plants with varying plant densities under different flow rates, and basic interpretation of the results of drag coefficient.

3.1.1. The analysis of direct plant drag force system

The free body diagram of the longitudinal view of the direct drag force measurement system is shown in Figure 3.1 and Figure 3.2. The following is the force balance equation in the x -direction:

$$F_{p_measured} + EP + F_{R_Total} + f_{board_p} = F_{dp} + F_{viscous} + W_x + F_b \quad (3-1)$$

where

$F_{p_measured}$ = Drag force experienced by the plant and the board as water passes through. It was measured by the direct drag force measurement system.

EP = Eddy flow pressure formed as a result of a drop at the back of the drag force measurement system (a backward facing step).

Static water pressure formed at the back of the system is determined by:

$$F_{R_Total} = \gamma h_c A \quad (3-2)$$

f_{board_p} = Static friction of the movable platform. Static friction is proportional to the weight of the movable platform. Averaged static friction was obtained by setting the force gauge so that only maximum force upon initial movement was recorded.

Shear force resulted by fluid moving along the two parallel plates is determined by:

$$F_{viscous} = 2\mu \frac{du}{dy} A_i \quad (3-3)$$

where

$\frac{du}{dy}$ is the velocity distribution along the y direction between the two parallel planes; μ is the dynamic viscosity of water; and A_i is the total area of the two parallel planes.

In this experiment, half of this force was along the solid boundary at the bottom of the channel, which was canceled out by the supporting frame of the channel. Weight in the x component as a result of the 0.004 slope is shown by:

$$W_x = W \sin \theta = W \frac{0.004}{\sqrt{0.004^2 + 1^2}} \quad (3-4)$$

This force had been included into the setting of the drag force system, thus it would appear to be zero in this equation.

F_{dp} = Actual drag force exerted on the plant

F_b = Drag force resulted from shear and obstruction of the movable board. This force differed for two different arrangements of the drag force measurement system and the flow rates introduced to the channel.

For *Phragmites australis* and *Typha orientalis*, the average maximum drag force of the movable board is shown in Table 3.1. For *Hygrophila pogonocalyx* and *Juncus effusus*, the average maximum drag force of the movable board is shown in Table 3.2. After simplification, Equation (3-1) is written as:

$$F_{p_measured} + F_{R_Total} + f_{board_p} = F_{dp} + F_b \quad (3-5)$$

Figure 3.3 is the plot of the dimensions of the back of the second design of movable platform, which is utilized for the calculation of the total hydraulic pressure.

$$F_{R_Total} = F_{Rt4} + F_{Rrec} \quad (3-5-1)$$

where

F_{R_Total} is the total hydrostatic pressure force.

F_{Rt4} is the hydrostatic pressure force experienced by the four trapezoidal areas.

F_{Rrec} is the hydrostatic pressure force experienced by the rectangular board.

For a trapezoidal figure with the top greater than the bottom ($a > b$), the distance between the center of gravity to the bottom is denoted as:

$$H_g = \frac{H_t(2a+b)}{3(a+b)}$$

where

H_t is the total height of the trapezoidal figure = 3.85 cm.

“ a ” is the top of the trapezoidal figure = 6.6 cm.

“ b ” is the bottom of the trapezoidal figure = 6 cm.

Therefore, the depth of water from the water surface to the center of gravity is:

$$D_{hg} = H_t - HG = H_t - \frac{H_t(2a+b)}{3(a+b)}$$

$$D_{hg} = \frac{H_t 3(a+b) - H_t(2a+b)}{3(a+b)}$$

$$D_{hg} = \frac{H_t(a+2b)}{3(a+b)} \tag{3-6}$$



Hydrostatic force on a trapezoidal figure is:

$$F_{Rt1} = \gamma h_c A = \gamma D_{hg} A$$

where

γ is the unit weight of water = $1000 \times 9.81 = 9810 \text{ N/m}^3$

$$F_{Rt1} = \rho g \left[\frac{H_t(a+2b)}{3(a+b)} \right] \left[\frac{1}{100} \right] \left[\frac{H_t(a+b)}{2} \right] \left[\frac{1}{100^2} \right]; \quad \text{if } a \text{ and } b \text{ are in cm}$$

ρ is the density of water = 1000 kg/m^3 .

g is the gravity of earth = 9.81 m/s^2 .

$$F_{Rt1} = \frac{1}{6} \rho g H_t^2 (a+2b) (10^{-6}) \tag{3-7}$$

$$F_{Rt4} = F_{Rt1} \times 4$$

$$F_{Rt4} = \frac{2}{3} \rho g H_t^2 (a+2b) (10^{-6}) \tag{3-8}$$

The hydrostatic pressure force at the back of the rectangular board is shown as:

$$F_{Rrec} = \gamma_c A = \rho g \left(H_t + \frac{w}{2} \right) \left(\frac{1}{100} \right) (wl) \left(\frac{1}{100^2} \right); \text{ if } a \text{ and } b \text{ are in cm}$$

$$F_{Rrec} = \rho g \left(H_t + \frac{w}{2} \right) (wl) (10^{-6})$$

where (3-9)

w = width of board = 1.35 cm; and

l = length of the board = 45.7 cm.

Hence, from Eq. (3-5-1), we have

$$F_{R_Total} = F_{Rt4} + F_{Rrec} \quad (3-10)$$

$$F_{R_Total} = \frac{2}{3} \rho g H_t^2 (a + 2b) (10^{-6}) + \rho g \left(H_t + \frac{w}{2} \right) (wl) (10^{-6})$$

$$F_{R_Total} = \rho g (10^{-6}) \left[\frac{2}{3} H_t^2 (a + 2b) + (H_t + w/2) wl \right] \quad (3-11)$$

$$= 1000(9.81)(10^{-6}) \left[\frac{2}{3} 3.85^2 (6.6 + 2 \times 6) + (3.85 + 1.35/2)(1.35 \times 45.7) \right]$$

$$\approx 4.54 \text{ N}$$

The static friction force f_{board_p} was calculated as the average of the maximum force required to just move the trailer part of the drag force measurement system. The drag force transducer was pulled by the stream 41 times and maximum force required to move the trailer is recorded by setting the 'max. force' function key. The average of these results showed a static friction value of 2.93 N (Table 1).

$$F_{p_measured} + F_{R_Total} + f_{board_p} = F_{dp} + F_b \quad (3-12)$$

Therefore, the total force measured for the friction drag of board and the form drag of the plants, $F_{p_measured}$ is derived by deducting the static friction ($f_{board_p} = 2.93$ N) and static water pressure ($F_{R_Total} = 4.54$ N) from the force measured by the transducer and recorded by the computer. Equation (3-12) leads to:

$$F_{p_measured} + 2.93 + 4.54 = F_{dp} + F_b$$

$$F_{p_measured} + 7.47 = F_{dp} + F_b \quad (3-13)$$

where F_b is the drag force of the movable board which changes with flow rates and types of measurement system used.

3.1.2. Validation of drag force system

The total boundary shear stress can be expressed as follows:

$$\tau_0 = \tau_p + \tau_b \quad (3-14)$$

$$\tau_p = \frac{F_{dp}}{a} \quad (3-15)$$

$$\tau_b = \frac{F_b}{a} \quad (3-16)$$

$$F_{dp} + F_b = \tau_0 a \quad (3-17)$$

where

τ_0 is the total shear boundary stress at the bottom of the channel resulted from channel roughness and obstruction;

τ_p = vegetation shear stress; and

τ_b = channel bed shear stress.

$$\text{Since } F_{dp} = \frac{1}{2} C_d \rho_f A_p V^2$$

$$\therefore \tau_p = \frac{1}{2} C_d \rho_f \frac{A_p}{a} V^2 \quad (3-18)$$

$$\therefore \tau_p = \frac{1}{2} C_d \rho_f \frac{A_p}{A_c} \frac{l}{y_n} V^2$$

$$\text{Note that the plant vertical density } = \rho_{plant} = \frac{A_p}{A_c}$$

In the open-channel flow, the total boundary shear stress can also be expressed by $\tau_0 = \gamma R S_f$, where R is the hydraulic radius (a ratio of cross sectional area to the wetted perimeter); S_f is the friction or energy slope; and γ is the unit weight of water, which is the product of water density and the

gravitational constant acceleration. Therefore by substituting Equation (3-18) and (3-16) into (3-14), we have:

$$\tau_0 = \frac{1}{2} C_d \rho_f \frac{A_p}{a} V^2 + \frac{F_b}{a}$$

$$\tau_0 = \frac{1}{2} C_d \rho_f \frac{A_p}{a} V^2 + \frac{F_b}{a} = \gamma R S_f \quad (3-19)$$

$$S_f = S_0 - \frac{dy}{dx} - \frac{v}{g} \frac{dv}{dx} \quad (3-20)$$

where v is velocity of flow; y is the water elevation; and S_0 = channel slope. The proof of Equation (3-20) is shown in Appendix A, Method 1 to 2.

$$\therefore \tau_0 = \frac{1}{2} C_d \rho_f \frac{A_p}{a} V^2 + \frac{F_b}{a} = \gamma R \left\{ S_0 - \frac{dy}{dx} - \frac{v}{g} \frac{dv}{dx} \right\} \quad (3-21)$$

$$F_{dp} + F_b = a \gamma R \left\{ S_0 - \frac{dy}{dx} - \frac{v}{g} \frac{dv}{dx} \right\} \quad (3-22)$$

From the force balance Equation (3-1) for the direct drag force measurement system, we have:

$$F_{p_measured} + EP + F_{R_Total} + f_{board_p} = F_{dp} + F_{viscous} + W_x + F_b$$

After simplification:

$$F_{p_measured} + F_{R_Total} + f_{board_p} = F_{dp} + F_b$$

Substitute Equation (3-22):

$$F_{p_measured} + F_{R_Total} + f_{board_p} = F_{dp} + F_b = a \gamma R \left\{ S_0 - \frac{dy}{dx} - \frac{v}{g} \frac{dv}{dx} \right\} \quad (3-23)$$

Equation (3-22) forms the basis for the validation of the drag force system. On the left hand side (*LHS*), it is clear that the shear force is calculated as the summation of the drag force of emergent macrophytes in aquatic flows (F_{dp}) and the shear force over channel bed area (platform drag force: F_b). These two forces are equivalent to the total of force measured by the direct drag force measurement system, the hydrostatic force at the back of the system, and the static friction force along the railings and wheels. On the right hand side (*RHS*), the same shear force could be computed from measured channel slope, channel

width, water elevation, stream velocity at the chosen upstream and downstream locations, and the distance between these two respective locations.

A case study on the experimental results for drag force of *Phragmites australis* at 1522.63 stems/m² in aquatic flow of 0.021 m³/s (20.9 l/s) is shown below:

$$F_{p_measured} + F_{R_Total} + f_{board_p} = a\gamma R \left\{ S_0 - \frac{dy}{dx} - \frac{v}{g} \frac{dv}{dx} \right\} \quad (3-24)$$

LHS:

The averaged measured drag force of the plant and the board = (10.52+10.14+8.68)/3 = 9.18 N. The average hydrostatic force has been shown previously to be 4.54 N. The average static friction was measured as 2.94 N.

Total force at *LHS* = 17.27 N

RHS:

Average flow rate (*Q*) = 0.021 m³/s

Average stream lost at left and right side = 0.00055 m³/s + 0.00044 m³/s
 ≈ 0.99 l/s

Deduction of these two flows gives 0.021 m³/s - 0.00099 m³/s ≈ 19.9 l/s

Distance between upstream and down stream = 50.1 cm

For Upstream:

Upstream water level = 14.5 cm

Area of upstream cross sectional area = (14.5/100) x (60/100) = 0.087 m²

$R = A / P$

$P =$ wetted perimeter = (2x14.5/100+60/100) = 0.89 m

Velocity at upstream = $Q / A = 0.0199 \text{ m}^3/\text{s} / 0.087 \text{ m}^2 = 0.23 \text{ m/s}$

For Downstream:

Downstream water level = 10.6 cm

Area of downstream cross sectional area = (10.6/100) x (60/100) = 0.0636 m²

Velocity at downstream = $Q / A = 0.0199 / 0.0636 = 0.313 \text{ m/s}$

$dy/dx =$ (Downstream water level – upstream water level) / distance

$dy/dx = (10.6 - 14.5) / 5.01 = -0.078$

$dV/dx =$ (Velocity at downstream – Velocity at upstream) / distance

$$dV/dx = (0.31 - 0.23) / 50.1 = 1.68 \times 10^{-3} \text{ m/s/m}$$

$$V/g = 0.229/9.81 = 0.023 \text{ m/s}$$

$$R = A / P = 0.087/0.89 = 0.098 \text{ m/s}$$

$$\gamma = \rho g = 1000 \times 9.81 = 9810 \text{ N/m}^3$$

$$S_o = 0.004$$

$$\begin{aligned} \tau_o &= \gamma R S_f = \gamma R \left\{ S_o - \frac{dy}{dx} - \frac{v}{g} \frac{dv}{dx} \right\} \\ &= (9810) (0.098) \{ 0.004 - (-0.078) - (0.023) (1.68 \times 10^{-3}) \} \\ &\approx 78.447 \text{ N/m}^2 \end{aligned}$$

$$F_{dp} + F_b = \tau_o a = 78.447 \times 0.415 \times 0.51 \approx 16.6 \text{ N}$$

$$LHS = 17.27 \text{ N}$$

$$RHS = 16.60 \text{ N}$$

The differences was 0.66 N

The percentage difference = $0.66/17.27 = 3.82\%$

The percentage difference between the *LHS* results measured by the direct drag force measurement system and the *RHS* total shear force calculated from the measurement of water elevations and flow velocities was 3.82%. This is within the acceptable range of accuracy.

3.1.3. Computation of plant projected frontal area

Typha orientalis of plant density 8 under 26 Rotational turns with water level of 5.05 cm was chosen as an example for the computation of vegetation area in Figures 3.4 to 3.17.

A photo with *Typha orientalis* with plant density of 1771.93 stems/m² was taken with a scaled ruler. The length of the ruler was determined from the picture as 30.1cm with the height of the picture in 1536 pixels. The length of the vertical ruler was 30.5-0.4=30.1 cm. In many cases where the ruler was not vertical, the true vertical was calculated as: $(\cos\theta) \times (\text{top reading} - \text{bottom reading})$.

$$\text{Length ratio} = 30.1:1536 = 1: 1536/30.1 = 1: 51.0299 \text{ (1cm} = 51.03 \text{ pixels)}$$

$$\text{Area ratio} = (\text{length ratio})^2 = 1: 2604.1$$

Another digital photograph without the ruler was cut using this ratio to find area of plant submerged in the water. The height of this picture (H) was computed using the ratio:

$$H = 5.05 \times 51.03 = 257.7 \text{ pixels}$$

An average threshold of 175 was chosen. The threshold dialog box was used to turn the digital photographs into a black-and-white image (Fig. 3.13), while the histogram values (Fig. 3.17) were used to determine whether a pixel became white or black. All pixels with brightness values below the threshold level became black and all pixels with brightness values equal to or greater than the threshold level became white.

When using the threshold dialog box, two preview boxes were utilized to see a before-and-after view of the image. One of the boxes showed the original image while the other updated as settings were adjusted. Proof and auto-proof buttons were later used to view the changes on the original image before applying them.

The final analysis of the total black and white pixels was done by using the histogram feature in Figure 3.15 of the distribution of red, green, blue, grey scale, hue, saturation, and/or lightness values in an image (Fig. 3.15 and Fig. 3.17). The horizontal axis indicated the lightness values of the digital photograph from black to white (0 to 255). The vertical axis represented the number of pixels at each value. For dark images, most of the pixels were grouped at the left side. For this black and white photograph of *Typha orientalis*, the entire black pixel could be found at the extreme left vertical axis while all the white pixels were found at the extreme right axis.

$$\text{Total area} = \text{width} \times \text{height} = 2048 \times 1536 = 3145728$$

$$\text{Total area} = \text{black} + \text{white} = 424626 (13.5\%) + 2721466 (86.5\%) = 3145728$$

$$\text{Plant projected frontal area in number of pixels} = 424626 \text{ pixels}$$

$$\text{Plant projected frontal area in center meter square} = 424626 / 2604.1 = 163.1 \text{ cm}^2$$

For grouped plant canopies, a total of 70 photographs and plant areas were calculated. For individual plants, a total of 840 photographs and plant areas (A_p)

were processed in order to obtain accurate values of drag coefficients ($C_d = 2F_d/(\rho A_p V^2)$).

3.1.4. Drag force verses flow and density

In this section averaged values of drag forces are taken into consideration. Each drag force was the average of three experimental data with consistent controlled experimental conditions. Figure 3.19 shows different characteristics of macrophytes with their respective reactions to flow induced drag force. Drag force of *Phragmites australis* with all densities increased as flow increased till an optimum drag force was reached. After this optimum value was achieved under the flow of 0.015 m³/s, drag force decreased as flow increased. As the flow was increased to 0.021 m³/s, maximum averaged drag force of *Phragmites australis* of 1522.63 stems/m² dropped 22.01% from 11.27N to 8.79N. It was also found that macrophytes with higher population density seemed to experience more drag force than the lower ones.

As shown from Figure 3.19, increasing drag force measured for *Typha orientalis* with densities of 2315.79 stems/m², 2122.81 stems/m², and 1771.93 stems/m² are observed with increasing flow. A 47.21% increase of drag force for *Typha orientalis* with 2315.79 stems/m² was observed with 56.78% increase of flow. Since the variation of flow for *Typha orientalis* was less sufficient compared to the ones for *Phragmites australis*, it was inconclusive whether there would be an optimum drag force for *Typha orientalis*. However, since an optimum drag force at around 0.015 m³/s was found (Figure 3.19) for *Typha orientalis* with the density of 1114.04 stems/m², it could be speculated that by increasing the range of flow, possible optimum drag forces could be found for *Typha orientalis* at different population densities.

On the contrary, data for *Hygrophila pogonocalyx* demonstrated an immediate decrease of drag force when flow was increased. From Figure 3.19 drag force of *Hygrophila pogonocalyx* with densities of 131.58 stems/m² and 114.04 stems/m² drop 15.65% and 10.15% respectively with a 23.42% increase in flow; achieving an minimum drag at the optimum flow of 0.012 m³/s. After

this point, drag forces of these two groups of *Hygrophila pognocalyx* increased 16.13% and 5.17% respectively with a 37.19% increase of flow. For *Hygrophila pogonocalyx* with densities of 87.72 stems/m² and 1114.04 stems/m², drag forces dropped with increasing flow.

For *Juncus effusus* with plant densities of 2035.09 stems/m² and 1500 stems/m², drag forces roughly remained unchanged with increasing flow. At higher plant densities, *Juncus effusus* experienced higher drag force with increasing flow. A maximum drag force was reached for *Juncus effusus* with 3096.42 stems/m² at an optimum flow of 0.012 m³/s.

Since drag force for rigid bodies increases with increasing flow velocities, the plants with decreasing or unchanged drag force with increasing flow velocities are of particular interest in the natural environment. In this experiment, since fluid densities didn't change. According to the equation for drag force, the drag coefficient and the plant projected frontal area were likely to change due to streamlining with increasing flow which resulted in the decrease in drag force.

3.1.5. Product of drag coefficient and plant projected frontal area

The product of the drag coefficient and the plant projected frontal area ($C_d A_p$) was selected for the respective streamlining effect and the deflection of the plants on the reduction of drag force. Since it was difficult to measure the projected frontal area in water flow, it was calculated from the digital photographs taken in still air with a scaled ruler instead. As a result, the combination of C_d and A_p could be used to describe and explain the variation of drag experienced by emergent macrophytes in the stream flow.

In this section, averaged values of the product of drag coefficients and plant projected frontal areas were taken into consideration. Each value of drag coefficient was the average of three experimental data with consistent controlled experimental conditions. Values of $C_d A_p$ were calculated by the following formula:

$$C_d A_p = \frac{2F_d}{\rho V^2} \quad (3-25)$$

where ρ = density of water; A_p is the projected frontal area of the plant; V (Q/A) is flow velocity; and F_d is the measured drag force.

Graphs of $C_d A_p$ versus the square of stream velocity for all four types of emergent macrophytes are plotted in Figure 3.19 to Figure 3.22. Recall that for rigid bodies, drag force increases with increasing flow velocity with a chosen C_d value. However, in Figure 3.19 and Figure 3.21 ($C_d A_p$ v.s. V^2) for *Phragmites australis* and *Hygrophila pogonocalyx*, values of $C_d A_p$ start to drop when stream velocity begins to increase. These graphs show that in the presence of stream velocity of any magnitude, *Phragmites australis* and *Hygrophila* tend to streamline with the flow once they are placed in aquatic flows.

It is observed from Figure 3.19 that a total of 60.14% drop of $C_d A_p$ with 34.83% increase of velocity is observed for *Phragmites australis* with 1552.63 stems/ m^2 . A total of 74.05% drop of $C_d A_p$ with 25.05% increase of velocity is observed for *Phragmites australis* with 719.3 stems/ m^2 . At 1350.88 stems/ m^2 and 1052.63 stems/ m^2 , the ability to streamline (or need to streamline) for *Phragmites australis* seemed to reach to a maximum, when $C_d A_p$ values started to increase at around $V^2 = 0.7 \sim 0.8 \text{ m}^2/\text{s}^2$.

It is noted from Figures 3.19 ~ 3.22 that generally higher densities contribute to higher $C_d A_p$ values. This could indicate that it is harder (or less needed) for plants to streamline with flow at higher plant densities. It could also be further interpreted that in a control volume, plants with higher densities are more rigid, being less able to change shape or having less need to change shape, and therefore harder to streamline with the flow.

In Figure 3.19 of $C_d A_p$ v.s. plant density for *Phragmites australis*, it is found that under all controlled flow conditions, the $C_d A_p$ value drops initially with increasing stream velocity but rises again after an optimum plant density is reached. Before and after this optimum density, it is harder for *Phragmites australis* to streamline with the flow.

From the formula of drag force, a relationship between the drag coefficient C_d and the Darcy-Weisbach friction factor can be developed as below:

$$f = \frac{8\tau_0}{\rho V^2} = \frac{8\left(\frac{F_d}{a}\right)}{\rho V^2} = \frac{8\left(\frac{1/2 C_d \rho A_p V^2}{a}\right)}{\rho V^2} = 4C_d \frac{A_p}{a}$$

Therefore, when the term $C_d A_p$ is multiplied with $4/a$, Darcy-Weisbach friction factor could be determined as:

$$f = C_d A_p \frac{4}{a} \quad (3-26)$$

where f is the Darcy-Weisbach factor and a is the area of the vegetated bed.

Manning's n can be computed as:

$$n = \sqrt{\frac{fR^{1/3}}{8g}} \quad (3-27)$$

Chezy's C is given by the following equation:

$$C = \sqrt{\frac{8g}{f}} \quad (3-28)$$

The ratio of shear velocity to velocity is:

$$\frac{V_*}{V} = \sqrt{\frac{f}{g}} \quad (3-29)$$

Another method which could be used to validate $C_d A_p$ values in future studies is listed below:

$$\text{Since } S_f \approx S_0 - \frac{\partial h}{\partial x} - \frac{v_x}{g} \frac{\partial v_x}{\partial x} - \frac{1}{g} \frac{\partial v_x}{\partial t} \quad (3-30)$$

For steady non-uniform flow, velocity varies with distance, but the initial and other velocities at their respect position do not vary with time. Therefore:

$$S_f \approx S_0 - \frac{\partial h}{\partial x} - \frac{v_x}{g} \frac{\partial v_x}{\partial x} \quad (3-31)$$

$$S_f = S_0 - \frac{dh}{dx} - \frac{v}{g} \frac{dv}{dx} \quad (3-32)$$

$$\tau_0 = \frac{1}{2} C_d \rho_f \frac{A_{c_plant}}{a} V^2 + \frac{F_b}{a} = \gamma R \left\{ S_0 - \frac{dy}{dx} - \frac{v}{g} \frac{dv}{dx} \right\} \quad (3-33)$$

$$\tau_0 = \frac{1}{2} C_d \rho_f \frac{A_{c_plant}}{a} V^2 = \gamma R \left\{ S_0 - \frac{dy}{dx} - \frac{v}{g} \frac{dv}{dx} \right\} - \frac{F_b}{a} \quad (3-34)$$

$$A_{c_plant} = A_p \quad (3-35)$$

$$C_d A_p = \frac{2a}{\rho V^2} \left\{ \gamma R \left(S_0 - \frac{dy}{dx} - \frac{v}{g} \frac{dv}{dx} \right) - \frac{F_b}{a} \right\} \quad (3-36)$$

From Equation (3-27), values of Manning's n for *Phragmites australis*, *Typha orientalis*, *Hygrophila pogonocalyx*, and *Juncus effusus* are computed under different plant densities and flows. The maximum and minimum Manning's n for all of these four emergent macrophyte shown in Table 3.22 to Table 3.25 are within the range of Manning's n proposed by V. T. Chow (Table 3.26, Chow 1959). For example, the maximum and minimum values of the Manning's n for *Phragmites australis* are 0.087 and 0.038, respectively. This further ensured the accuracy of the direct drag force measurement system and its ability to reflect variation of Manning's n in different plant characteristics and flow conditions. The Darcy-Weisbach f ranged from 0.345 to 2.020. However, it could be observed in this experiment that Manning's n varied with plant density and flow. One fixed value of n for a certain type of plant condition may not be suitable. Equations for Darcy-Weisbach f , Chezy C , and Manning's n were developed for *Phragmites australis* at the end of this chapter.

3.1.6. Drag Coefficient (C_d) variation

From this section onwards, only data related to *Phragmites australis* were analyzed for the complex phenomenon of differences in types of vegetation and thus, their different ability and need to streamline under drag force induced in aquatic flows. Averaged values of drag coefficients (C_d) were taken into consideration for *Phragmites australis* in this section. Each value of drag coefficient was the average of three experimental data with consistent

controlled experimental conditions. Values of C_d were calculated by the following formula:

$$C_d = \frac{2F_d}{\rho A_p V^2} \quad (3-37)$$

which can be demonstrated in an summation of stem drag coefficients and projected frontal areas:

$$\sum C_{di-n} = \frac{2F_d}{\rho \sum A_{pi-n} V^2} \quad (3-38)$$

Another method for calculating C_d , which would be of interest in future studies, is shown as:

$$C_d = \frac{2a}{\rho A_p V^2} \left\{ \gamma R \left(S_0 - \frac{dy}{dx} - \frac{v}{g} \frac{dv}{dx} \right) - \frac{F_b}{a} \right\} \quad (3-39)$$

$$C_d = \frac{2}{(A_p / a) \rho V^2} \left\{ \gamma R \left(S_0 - \frac{dy}{dx} - \frac{v}{g} \frac{dv}{dx} \right) - \frac{F_b}{a} \right\} \quad (3-40)$$

Applying a simplified control volume of $y_n w l$ with the bed area of $a = w l$ and the cross-sectional area of $A_c = y_n w$ would give:

$$a = A_c \left(\frac{l}{y_n} \right) \quad (3-41)$$

Substitute Equation (3-41) into Equation (3-40):

$$C_d = \frac{2}{\left(\frac{A_{c_plant}}{A_c} \frac{l}{y_n} \right) \rho V^2} \left\{ \gamma R \left(S_0 - \frac{dy}{dx} - \frac{v}{g} \frac{dv}{dx} \right) - \frac{F_b}{a} \right\} \quad (3-42)$$

where $A_{c_plant} / A_c =$ vertical density of plant, which is directly proportional to the plant population density to a certain extend.

For realistic plants tested in this experiment, the vertical density of plant varies with water level. For some cases in this research, the vertical plant density slightly decreased with rising water level due to the area of obstruction at the root and litter zone of plants in shallow water flow. However, if the water level continued to increase till the level of vast branches and foliages, this vertical plant density would be increased again.

From Figure 3.26 to Figure 3.32, values of C_d for *Phragmites australis* are plotted against physical dimensionless factors that dominate this experiment and the dimensional analysis in the following section. In these figures, characteristics of drag force of *Phragmites australis* in aquatic flows can be clearly shown.

In Figure 3.26, the drag coefficient is found to decrease linearly with increasing Reynolds number with a R^2 of 0.88. For Reynolds numbers less than 500, in the range of 500 to 2000, and greater than 2000, the aquatic flows are classified into laminar, transitional, and turbulent flow respectively. The Reynolds numbers in this experiment ranged from 758.76 to 1968.64, indicating that the drag forces of emergent *Phragmites australis* were measured under a transitional aquatic flow.

From the graph of drag coefficient verses Froude number (C_d v.s. Fr) in Figure 3.27, no apparent linear relationship is observed with a relatively low R^2 value of 0.16. However, it can be observed from Figure 3.26 that almost all Froude numbers (Fr) in this experiment are greater than one. For Froude number > 1 , the flow is termed as the supercritical flow. Froude number of unity, $Fr = 1$, is termed critical flow. A flow with Froude number less than 1 ($Fr < 1$) is termed subcritical. In this experiment, all Froude numbers were greater than 1 with max. $Fr = 3.01$, except for 3 data with Fr roughly equaled to 0.73. Therefore, the majority of the flow conditions in this experiment were classified as supercritical flow.

In the flume tests for *Phragmites australis*, most of the flow conditions were supercritical. Supercritical flows could be found in flows over steep channels, sudden contraction of channel cross sectional areas, junction of channels, high speed flow at extreme weather conditions...etc. Researchers had found that water flows became supercritical at junctions in open-channels when the slope was greater than 1% with the absence of the tailwater submergence (Schwalt and Hager 1994). These junctions occur quite often in hydraulic structures, irrigation, and sewer channels. The perturbation of supercritical open-channel flows could lead to standing waves associated with flow

concentrations. Two scenarios might be resulted: 1. walls of open-channel flow had to be higher according to a 1D design; 2. hydraulic jump upstream of the junction might occur for a free surface flow, where the local waves may cause a transition to pressurized air-water flow. In Taiwan, where altitude change is rapid, supercritical flow could be observed in the watershed areas where steep slopes and rapid flows often exist (Water Resources Agency 1985, 2007, 2008; Yen 2000).

Supercritical flow was also found to occur at some lake inlets during the exchange of flow between wetlands and lakes in the spring, when cold stream returned from the lake dominated this flow (Andradottir and Nepf 2001). This circulation was river-dominated where inertial forces caused the river to behave like a jet, independent of the wind and buoyancy. This supercritical flow at the inlet would take the shortest path across the wetland. As a transitional buffer zone, some wetlands communicate properties from the watershed runoffs to the lake interior. This communication would be altered if these zones are very densely vegetated, with drag force induced by flow over these macrophytes.

From Figure 3.28, the drag coefficient C_d is observed to decrease linearly ($R^2 = 0.81$) with increasing ratio of drag force to plant flexural rigidity $\left(\frac{\rho V^2 h_p^4}{G_p} \right)$ in a range of $8776005 < \left(\frac{\rho V^2 h_p^4}{G_p} \right) < 26353770$.

where G_p is the product of the shear modulus of elasticity (G_s) and the second moment area of inertia (I) of *Phragmites australis*.

The drag coefficient is found to increase linearly in Figure 3.29 with an increase of the ratio of the averaged spacing of stems to the water level (s_p/y_n) with a R^2 of 0.88 in the range of $0.555 < s_p/y_n < 1.496$ for plant densities from 719.3 stems/m² to 1552.63 stems/m². In Figure 3.30, an increase of C_d is noted with an increase of the ratio of averaged plant height to water level, h_p/y_n , in a range of $12.04 < h_p/y_n < 24.97$, indicating shallow water flow with only 4% to 8.31% of the lengths of the stems of *Phragmites australis* under water submergence. A roughly linear decrease of C_d is observed in Figure 3.31 with an increase of the ratio of plant projected frontal area to the area of the

vegetated bed (A_p/a) in the range of $0.012 < A_p/a < 0.047$. An increase of C_d is observed in Figure 3.32 with an increase of the ratio of the averaged plant diameter to the water level (d_p/y_n) in the range of $0.012 < d_p/y_n < 0.069$.

3.2 Dimensional Analysis of Drag of Phragmites Australis in Aquatic Flows

Dimensional analysis is usually used for the following two major applications:

1. It is used to put hypothesis involving a large number of physical parameters in order.
2. It is also used to develop criteria governing similarity between two flow situations with geometrical similarity but different in size.

It is a theory based on the Buckingham π theorem, which states that if there is a functional relationship between ' n ' numbers of physical quantities, which could then be shown in terms of ' k ' numbers of fundamental quantities; then $(n-k)$ dimensionless numbers could be formed. It is formed from the original ' n ' quantities so that there is a functional relationship between them (Henderson 1966, Young 2004, and White 2006).

The ' k ' numbers of fundamental quantities used in this research were: mass, length, and time. The units for these fundamental quantities were kilograms, meters, and seconds, respectively.

In this experiment, the resistance to flow in dense and emergent (non-submerged) vegetation was dominated by drag forces exerted on individual parts of a plant community. In fluid mechanics, drag force coefficient is usually dependent on shape of the obstruction, Reynolds number, compressibility (Mach number), surface roughness of the obstruction, and Froude number. With consideration of the fluid properties, flow fields, and the vegetation properties, the following dominant physical parameters for the estimation of resistance parameter of an array of emergent (non-submerged) macrophytes in aquatic flow could be expressed as:

$$f(C_d, \rho, \mu, V, y_n, g, h_p, s_p, A_p, G_p, d_p, \varepsilon, \omega) = 0 \quad (3-43)$$

where C_d is the average drag coefficient derived from the equation $2F_d/A_p\rho V^2$.

The fluid properties are listed as below:

ρ , the density of the fluid; and

μ , the fluid viscosity (product of fluid density ρ and dynamic viscosity $\nu = \mu/\rho$).

The flow properties include:

V , the average channel velocity;

y_n , the normal flow depth; and

g , the gravitational constant.

The vegetative properties include:

h_p , the average canopy height;

s_p , the spatial average spacing of plants in a canopy;

A_p , the total projected area of submerged biomass in the direction of flow;

$G_p = G_s I$, the shear flexural rigidity of the plant, with G_s as the average shear modulus of elasticity and I as the average cross-sectional moment of inertia of the plant;

d_p , the average diameter of the canopy;

ε , surface roughness of the plant; and

ω , the frequency of oscillation of flow, for flow through vegetated zones with an oscillating motion is often observed.

The assumptions of this equation were (1) soil surface shear was negligible compared to the total plant drag; and (2) the plant stems were randomly and uniformly distributed in a horizontal plane. In realistic vegetation zones, there is a variation of vertical density under change of water levels.

The Buckingham π theorem was applied by assigning ρ , V , and y_n as the repeated variables to represent mass, time, and length scales. There were 13 numbers of physical quantities ($n = 13$). Mass, length, and time were taken as the fundamental quantities ($k = 3$). The numbers of dimensionless numbers were: $13-3 = 10$. These dimensionless numbers are shown in Equation (3-44):

$$f\left(C_d, \frac{A_p}{a}, \frac{h_p}{y_n}, \frac{s_p}{y_n}, \frac{d_p}{y_n}, \frac{\varepsilon}{d_p}, \frac{\rho V^2 h_p^4}{G_p}, \frac{V^2}{g y_n}, \frac{\rho V R}{\mu}, \frac{\omega y_n}{V}\right) = 0 \quad (3-44)$$

3.2.1. Dependent variables

Many researchers had defined the plant projected frontal area, A_p , and the drag coefficient, C_d , in the setting of a control volume (Petryk 1975; Fathi-Moghadam and Kouwen 1997; Nepf 1999; Lee et al. 2000; Kouwen and Faith 2000). One of the most important reasons for this definition was the consideration of the streamlined biomass, which still absorbed momentum while hiding behind the projected area under flow condition. It was called the momentum absorbing area (*MAA*) by Fathi in 1996 who defined *MAA* as the projected area of the leaves and stems in the cross-flow direction of the flow. He also set a variable to account for the random three-dimensional orientation (control volume) of the leaves and stems of a tree. In this research, a similar consideration was carried out by combining the first three dimensionless numbers in Equation (3-2) to form a dimensionless streamline coefficient:

$$\left(C_d \frac{A_p h_p}{a y_n}\right) = \left(\frac{C_d A_p h_p}{\nabla}\right), \text{ where } \nabla \text{ is the control volume} = w \times l \times y_n$$

Note that $\nabla = w \times l \times y_n = a y_n = l A_c$, where l = length of channel and A_c is the cross sectional area.

Therefore, the streamline coefficient could be shown in a various way for different interpretations.

$$\left(\frac{C_d A_p h_p}{\nabla}\right) = \frac{C_d A_p h_p}{w l y_n} = \frac{C_d A_p h_p}{l A_c} = \frac{C_d A_p h_p}{a y_n} \quad (3-45)$$

where h_p/y_n could indicate emergent or submerged condition of the plant and A_p/A_c is the vertical density of the plant. Unlike vegetation models consisted of vertical cylinders, this vertical plant density varies with water level for natural emergent macrophytes. In this study for shallow water flow, the vertical density decreases as water level increases. However, if this water level continues to increase to the levels of the leaves and branches of the plants, the vertical density would start to increase again.

In the streamline coefficient shown in Equation (3-45), the term $C_d A_p / a$ was noted to be 1/4 of Darcy-Weisbach friction factor ($f = 4C_d \frac{A_p}{a}$), which was originally developed to account for energy lost in flow through two different locations by using Bernoulli's equation. Darcy-Weisbach friction factor could also be used to compute Chezy C ($C = \sqrt{8g/f}$), Manning's n ($n = \sqrt{\frac{fR^{1/3}}{8g}}$), and the ratio of flow velocity and shear velocity ($v/v^* = \sqrt{8/f}$); which are all of particular importance in the computation and design of open channels.

Among all the benefits of using this dimensionless term, the expression of $C_d A_p$ was of particular importance. It had been noted that in high stream velocity, C_d tended to drop (Young et al. 2004) while A_p was being changed due to the deflection and streamlining movement of the plants (Kouwen and Faith 2000; Armanini et al. 2005; Wilson 2008). Since it was difficult to measure A_p under this condition, the multiple physical effects of stream velocity on plants could be lump-summed into this $C_d A_p$ term accounting for streamlining, deflection, and reduction of projected plant area in the direction of flow. Therefore, this term was named as the streamline factor with a unit of m^2 in this research.

3.2.2. Independent Variables

The ratio of the average height of the plant to the water level variation was indicated by $\left(\frac{h_p}{y_n}\right)$ in the dimensional analysis. This term is a measure of plant submergence and it could be used to classify the type of velocity profiles along the stream. For values of h_p/y_n less than 1, the plants were completely submerged in the stream, with the flow velocity profile appearing to be a S shape when looking at the longitudinal direction. For values of h_p/y_n greater than 1, the vegetation was emergent (non-submerged) and the flow velocity profile was much more like an uniform distribution along the depth compared

to the ones with h_p/y_n less than one. It was also a measure of types of vegetation tested in the experiment. For this research on drag force of emergent macrophytes in aquatic flows, each h_p/y_n value was greater than one.

The ratio of the average spacing of stems to the water level is expressed using $\left(\frac{s_p}{y_n}\right)$. It was noted that the inverse of plant density represented the average area occupied by each stem. The square root of this value arrived at the average one-side distance between the centers of each stem in a square setting. Average stem diameter was deducted from this distance to give the average spacing (s_p) of the array of the emergent macrophytes, which could be written as:

$$s_p = \sqrt{\frac{1}{M}} - d_p \quad (3-46)$$

where M is the plant population density and d_p is the averaged stem diameter.

Since $\left(\frac{s_p}{y_n}\right)$ included the plant density, the diameter of the stem, and the water depth, it was of particular importance in the description of the flow-vegetation interaction.

The ratio of the flow drag force to the forces resisting plant distortion (plant flexural rigidity) is represented by the term $\left(\frac{\rho V^2 h_p^4}{G_p}\right)$. The plant flexural rigidity G_p is the product of the shear modulus of elasticity (G_s) and the second area moment of inertia (I). The shear modulus G_p is the ratio of shear stress to shear strain. The shear stress is defined as the magnitude of the force per unit cross-sectional area of the face while the shear strain is the horizontal displacement resulted by the force per unit height.

Unlike previous researches using the modulus of elasticity, shear modulus of elasticity was chosen here, since it is concerned with the deformation of a solid when it experiences a force (the cross sectional area of stem located at the center of the water depth) parallel to one of its surfaces while its opposite face experiences an opposing force (such as friction at the roots zone). Moreover, it

is much easier to measure G_s both on site and in the laboratory compared to the modulus of elasticity, where the change of cross sectional area of the stems under a pulling force has to be measured. The shear modulus of elasticity is determined by the following:

$$G_s = \frac{\left(\frac{F_s}{d_p}\right)}{\left(\frac{\Delta x}{h_{pd}}\right)} = \frac{F_s h_{pd}}{\Delta x d_p} \quad (3-47)$$

where F_s is the force applied to cause a displacement of Δx of a stem with a designed partial plant height of h_{pd} and an average plant diameter of d_p , in the direction of flow.

The second area moment of inertia (I) is a property of a shape that can be used to predict the resistance of beams to bending and deflection.

$$I = \frac{(\pi d_p^4)}{64} \quad (3-48)$$

Where π is approximately equal to 3.14, the ratio of any circle's circumference to its diameter.

Since G_p was the product of the shear modulus of elasticity (G_s) in Equation (3-47) and the second area moment of inertia (I) in Equation (4-48), the ratio of

drag to plant flexural rigidity $\left(\frac{\rho V^2 h_p^4}{G_p}\right)$ could be expressed as:

$$\left(\frac{\rho V^2 h_p^4}{G_p}\right) = \left(\frac{\rho V^2 h_p^4}{G_s I}\right) = \left(\frac{\rho V^2 h_p^4}{\frac{F_s h_{pd}}{\Delta x d_p} \frac{\pi d_p^4}{64}}\right) \quad (3-49)$$

$$\left(\frac{\rho V^2 h_p^4}{G_p}\right) = \left(\frac{64 \Delta x \rho V^2 h_p^4}{\pi h_{pd} F_s d_p^3}\right) \quad (3-50)$$

Another dimensionless independent variable is the Froude number (Fr) derived by the ratio of the stream velocity to the wave velocity $\left(\frac{V^2}{g y_n}\right)$. It could

be also taken as the ratio of inertia force on an element of fluid to the weight of

the element (gravitational force), which is important in problems involving flows with free surfaces. The Froude number is analogous to the Mach number in gas flow (ratio of gas velocity to sonic velocity). In open-channel flow cases, the determination of a flow to be supercritical or subcritical is judged by the Froude number. For Froude number > 1 , the flow is supercritical. Froude number of unity, $Fr = 1$, is termed critical flow. Flows with the Froude numbers less than 1 ($Fr < 1$) are termed subcritical. Therefore the Froude number is an important dimensionless term involving gravity flow and a convenient parameter in the calculations in the open-channel flow.

The Reynolds number, $Re = \left(\frac{\rho VR}{\mu} \right)$, was adopted as one of the independent variables in the dimensionless analysis. It is the ratio of inertia force to viscous force. The Reynolds number is generally of importance in all types of fluid dynamics problems when there is substantial velocity gradient (shear). For $Re < 500$, the flow is termed laminar flow with streamlines parallel to each other. Shear stress for laminar flow depends mostly on the viscosity. For $500 < Re < 2000$, the flow is called to be transitional flow where fluid particles moves in spiral direction. For $Re > 2000$, the flow is named as the turbulent flow. Shear stress for turbulent flow is a function of density. According to Prandtl (1904) in describing fluid flow over a flat plate with large Reynolds number, the flow is dominated by inertial effects and the viscous effects are negligible everywhere except in a region very close to the plate and in the thin wake region behind a plate. The drag coefficient is also related to the Reynolds number.

The Strouhal number $\left(\frac{\omega y_n}{V} \right)$ was considered in Equation (3-44) as one of the contributing factor to the streamline coefficient. It is denoted as the ratio of local inertia force to the convective inertia force. The Strouhal number is important if the flow pattern is oscillating through a boundary layer or a control volume. According to Kouwen's research (Kouwen and Fathi 2000), most flow over vegetation have an oscillatory pattern to some degree depending on the

Reynolds number. However, they did not consider this dimensionless parameter for the effect of Strouhal number on energy dissipation was assumed to be much less than the drag coefficient and the frontal area. In this research, it was discovered that stems tended to oscillate in local control volumes. However, the frequency and magnitude of this oscillation were yet to be determined through detail video observation. Therefore it was ignored in this experiment.

The ratio of the surface roughness to the diameter of the stems is represented by the term $\left(\frac{\varepsilon}{d_p}\right)$. This ratio is important at the range of Reynolds number of 4×10^4 to 4×10^5 , where certain degree of variation of drag coefficient might take place (Young et al. 2004). Since surface roughness was of interest but not measured in this experiment, it would not be taken into consideration in this research.

Results of the dimensional analysis were shown in the following section in two categories, namely the Model 1 and the Model 2. The dependent variables for Model 1 and 2 were the combined streamline coefficient, $\frac{C_d A_p h_p}{\nabla}$, and the drag coefficient, C_d , respectively.

3.2.3. Dimensional analysis of combined streamline coefficient: Model 1

The dominant parameters for estimating the resistant parameter for flow through emergent macrophytes in a canopy were assumed in equation (3-44):

$$f\left(C_d, \frac{A_p}{a}, \frac{h_p}{y_n}, \frac{s_p}{y_n}, \frac{d_p}{y_n}, \frac{\varepsilon}{d_p}, \frac{\rho V^2 h_p^4}{G_p}, \frac{V^2}{g y_n}, \frac{\rho V R}{\mu}, \frac{\omega y_n}{V}\right) = 0$$

After simplification:

$$\frac{C_d A_p h_p}{w l y_n} = \frac{C_d A_p h_p}{l A_c} = \frac{C_d A_p h_p}{a y_n} = f\left(\frac{s_p}{y_n}, \frac{d_p}{y_n}, \frac{\rho V^2 h_p^4}{G_p}, \frac{\rho V R}{\mu}\right) \quad (3-51)$$

$$\frac{C_d A_p h_p}{\nabla} = f\left(\frac{s_p}{y_n}, \frac{d_p}{y_n}, \frac{\rho V^2 h_p^4}{G_p}, \frac{\rho V R}{\mu}\right) \quad (3-52)$$

The univariate analysis of the natural logarithm of $\frac{C_d A_p h_p}{\nabla}$ to the natural

logarithm of $\left(\frac{s_p}{y_n}\right)$, $\left(\frac{d_p}{y_n}\right)$, $\left(\frac{\rho V^2 h_p^4}{G_p}\right)$, and $\left(\frac{\rho VR}{\mu}\right)$ were carried out respectively. The graphs of these univariate analyses are shown in Figure 3.35 to Figure 3.41. A general linear increase of $\ln\left(\frac{C_d A_p h_p}{\nabla}\right)$ could be observed with respective increase of $\ln\left(\frac{s_p}{y_n}\right)$ and $\ln\left(\frac{d_p}{y_n}\right)$. On the other hand, general decreases of $\ln\left(\frac{C_d A_p h_p}{\nabla}\right)$ were resulted from the increase of $\ln\left(\frac{\rho V^2 h_p^4}{G_p}\right)$ and $\ln\left(\frac{\rho VR}{\mu}\right)$, respectively.

Therefore:

$$\frac{C_d A_p h_p}{\nabla} = \alpha \left(\frac{s_p}{y_n}\right)^\beta \left(\frac{d_p}{y_n}\right)^\varphi \left(\frac{\rho V^2 h_p^4}{G_p}\right)^\eta \left(\frac{\rho VR}{\mu}\right)^\zeta \quad (3-53)$$

$$\ln\left(\frac{C_d A_p h_p}{\nabla}\right) = \ln \alpha + \beta \ln\left(\frac{s_p}{y_n}\right) + \varphi \ln\left(\frac{d_p}{y_n}\right) + \eta \ln\left(\frac{\rho V^2 h_p^4}{G_p}\right) + \zeta \ln\left(\frac{\rho VR}{\mu}\right) \quad (3-54)$$

where α , β , φ , η , and ζ are constants (Parameter estimates).

Note that in the statistical analysis, this equation is:

$$Y_2 = a + b X_3 + c X_6 + d X_2 + e X_1$$

where a , b , c , d , and e are constants.

A statistical model (Model 1) was built with multiple regression analysis using the Statistical Analysis System (SAS) software. Sixty numbers of observations were read and used in this analysis. From the multiple regression model, these constants, or parameter estimates (a , b , c , d , and e) were determined as:

$$Y_2 = a + b X_3 + c X_6 + d X_2 + e X_1$$

The Intercept, $a = 309.0234$

The parameter estimate for X_3 , $b = -0.840$

The parameter estimate for X_6 , $c = 79.392$

The parameter estimate for X_2 , $d = -43.902$

The parameter estimate for X_1 , $e = 85.203$

All parameter estimates have values of $Pr > |t|$ less than 0.0001, showing that all these parameters (dependent variables) are statistically significant in contributing to the variation of $\ln(C_d A_p h_p / \nabla)$.

Therefore,

$$Y_2 = 309.024 - 0.840 X_3 + 79.392 X_6 - 43.902 X_2 + 85.203 X_1$$

Replacing the constants with the values from the parameter estimates in the regression analysis gave:

$$\begin{aligned} \ln\left(\frac{C_d A_p h_p}{\nabla}\right) &= 309.024 - 0.840 \ln\left(\frac{s_p}{y_n}\right) + 79.392 \ln\left(\frac{d_p}{y_n}\right) - 43.902 \ln\left(\frac{\rho V^2 h_p^4}{G_p}\right) \\ &+ 85.203 \ln\left(\frac{\rho VR}{\mu}\right) \end{aligned} \quad (3-55)$$

$\ln \alpha = 309.024$, $\alpha = 1.611E+134$, therefore:

$$\frac{C_d A_p h_p}{\nabla} = (1.6114E + 134) \left(\frac{s_p}{y_n}\right)^{-0.840} \left(\frac{d_p}{y_n}\right)^{79.392} \left(\frac{\rho V^2 h_p^4}{G_p}\right)^{-43.902} \left(\frac{\rho VR}{\mu}\right)^{85.203} \quad (3-56)$$

This was the final version of the dimensionless equation with R -square and adjusted R squared values of 0.94. R -squared values are used for measuring the strength of association between the dependent variables and the chosen independent variables. In this study, model 1 showed high R -Sq. value of 0.94, which meant that about 94 % of the variance in the natural logarithm of the streamlining coefficient could be explained by all of the independent variables including the natural logarithm of the following dimensionless parameters: the Reynolds number, the ratio of drag to plant rigidity, the average stem spacing to water level, and the average stem diameter to water level. A summary of Model 1 is shown in Table 3.32 with specific information in Table 3.29. Note that based on the above equation, the following equations can be deduced:

From Equation (3-56):

$$\frac{C_d A_p h_p}{\nabla} = (1.6114E + 134) \left(\frac{s_p}{y_n}\right)^{-0.840} \left(\frac{d_p}{y_n}\right)^{79.392} \left(\frac{\rho V^2 h_p^4}{G_p}\right)^{-43.902} \left(\frac{\rho VR}{\mu}\right)^{85.203}$$

$$\frac{C_d A_p h_p}{a y_n} = (1.6114E + 134) \left(\frac{s_p}{y_n} \right)^{-0.840} \left(\frac{d_p}{y_n} \right)^{79.392} \left(\frac{\rho V^2 h_p^4}{G_p} \right)^{-43.902} \left(\frac{\rho VR}{\mu} \right)^{85.203}$$

$$\frac{C_d A_p}{a} = (1.6114E + 134) \left(\frac{y_n}{h_p} \right) \left(\frac{s_p}{y_n} \right)^{-0.840} \left(\frac{d_p}{y_n} \right)^{79.392} \left(\frac{\rho V^2 h_p^4}{G_p} \right)^{-43.902} \left(\frac{\rho VR}{\mu} \right)^{85.203}$$

Substituted into Equation (3-26); Darcy-Weisbach factor $f = 4C_d \frac{A_p}{a}$:

$$f = (6.4456E + 134) \left(\frac{y_n}{h_p} \right) \left(\frac{s_p}{y_n} \right)^{-0.840} \left(\frac{d_p}{y_n} \right)^{79.392} \left(\frac{\rho V^2 h_p^4}{G_p} \right)^{-43.902} \left(\frac{\rho VR}{\mu} \right)^{85.203}$$

(3-57)

$$\ln f = 310.410 + \ln \left(\frac{y_n}{h_p} \right) - 0.84 \ln \left(\frac{s_p}{y_n} \right) + 79.392 \ln \left(\frac{d_p}{y_n} \right) - 43.902 \ln \left(\frac{\rho V^2 h_p^4}{G_p} \right) + 85.203 \ln \left(\frac{\rho VR}{\mu} \right)$$

(3-58)

Equation (3-57) could then be used to derive Chezy's C and Manning's n .

From Equation (3-28) for the determination of Chezy's C :

$$C = \sqrt{\frac{8g}{f}}$$

Substitute Equation (3-57) into Equation (3-28), and take natural logarithm at both sides gave:

$$\ln C = -153.023 - \frac{1}{2} \ln \left(\frac{y_n}{h_p} \right) + 0.42 \ln \left(\frac{s_p}{y_n} \right) - 39.696 \ln \left(\frac{d_p}{y_n} \right) + 21.951 \ln \left(\frac{\rho V^2 h_p^4}{G_p} \right) - 42.602 \ln \left(\frac{\rho VR}{\mu} \right)$$

(3-59)

From Equation (3-27) for the determination of Manning's n :

$$n = \sqrt{\frac{fR^{1/3}}{8g}}$$

Substitute Equation (3-57) into Equation (3-27) gave:

$$n = 2R^{1/6} \left(\frac{y_n}{h_p} \right) \left(\frac{1.611E + 134}{g} \right)^{1/2} \left(\frac{s_p}{y_n} \right)^{-0.840/2} \left(\frac{d_p}{y_n} \right)^{79.392/2} \left(\frac{\rho V^2 h_p^4}{G_p} \right)^{-43.902/2} \left(\frac{\rho VR}{\mu} \right)^{85.203/2}$$

$$n = (8.1058E + 66)R^{1/6} \left(\frac{y_n}{h_p} \right) \left(\frac{s_p}{y_n} \right)^{-0.42} \left(\frac{d_p}{y_n} \right)^{39.696} \left(\frac{\rho V^2 h_p^4}{G_p} \right)^{-21.951} \left(\frac{\rho VR}{\mu} \right)^{42.601} \quad (3-60)$$

Checking for the dimension for Manning's n [$TL^{(-1/3)}$]:

$$L^{1/6} \left(\frac{1}{L/T^2} \right)^{1/2} = TL^{(-1/3)}$$

Take natural logarithm at both sides of Equation (3-60) gave:

$$\begin{aligned} \ln n = & 154.063 + 0.167 \ln R + \ln \left(\frac{y_n}{h_p} \right) - 0.42 \ln \left(\frac{s_p}{y_n} \right) + 39.696 \ln \left(\frac{d_p}{y_n} \right) - 21.951 \ln \left(\frac{\rho V^2 h_p^4}{G_p} \right) \\ & + 42.602 \ln \left(\frac{\rho VR}{\mu} \right) \end{aligned} \quad (3-61)$$

3.2.4 Dimensional analysis of drag coefficient: Model 2

The dominant dimensionless parameters for estimating the drag force coefficient (C_d) for flow through emergent macrophytes in a canopy were listed below. From Equation (3-44), drag coefficient could be found as the following function:

$$C_d = f \left(\frac{A_p}{a}, \frac{h_p}{y_n}, \frac{s_p}{y_n}, \frac{d_p}{y_n}, \frac{\rho V^2 h_p^4}{G_p}, \frac{\rho VR}{\mu} \right) = 0 \quad (3-62)$$

The univariate analysis of the natural logarithm of C_d to the natural logarithm

of $\left(\frac{A_p}{a} \right)$, $\left(\frac{h_p}{y_n} \right)$, $\left(\frac{s_p}{y_n} \right)$, $\left(\frac{d_p}{y_n} \right)$, $\left(\frac{\rho V^2 h_p^4}{G_p} \right)$, and $\left(\frac{\rho VR}{\mu} \right)$ were carried out. The

graphs for these univariate analysis are shown in Figure 3.42 to Figure 3.47. It can be observed from these figures that general linear increases of $\ln C_d$ are

resulted from the increases of $\ln \left(\frac{s_p}{y_n} \right)$, $\ln \left(\frac{h_p}{y_n} \right)$, and $\ln \left(\frac{d_p}{y_n} \right)$, respectively. On

the other hand, general decreases of $\ln C_d$ are observed with increasing

$\ln \left(\frac{A_p}{a} \right)$, $\ln \left(\frac{\rho V^2 h_p^4}{G_p} \right)$, and $\ln \left(\frac{\rho VR}{\mu} \right)$.

Therefore:

$$C_d = \alpha \left(\frac{A_p}{a} \right)^\beta \left(\frac{h_p}{y_n} \right)^\varphi \left(\frac{s_p}{y_n} \right)^\eta \left(\frac{d_p}{y_n} \right)^\zeta \left(\frac{\rho V^2 h_p^4}{G_p} \right)^\psi \left(\frac{\rho VR}{\mu} \right)^\xi$$

$$\ln C_d = \ln \alpha + \beta \ln \left(\frac{A_p}{a} \right) + \varphi \ln \left(\frac{h_p}{y_n} \right) + \eta \ln \left(\frac{s_p}{y_n} \right) + \zeta \ln \left(\frac{d_p}{y_n} \right) + \psi \ln \left(\frac{\rho V^2 h_p^4}{G_p} \right) + \xi \ln \left(\frac{\rho VR}{\mu} \right) \quad (3-63)$$

Note: in the simplified form, this equation is:

$$Y_1 = a + b X_5 + c X_4 + d X_3 + e X_6 + f X_2 + g X_1$$

where $a, b, c, d, e, f,$ and g are constants.

The term d_p/y_n (X_6) was found to be perfectly correlated with the h_p/y_n (X_4) term. Therefore one of these two terms had to be taken out of the analysis. It was decided that d_p/y_n to be taken out since d_p had been already included in the calculation of the average stem spacing (s_p) in Equation (3-46) while h_p/y_n is an essential indicator of the status of the plant, the distribution of force acting on the plant, and the longitudinal velocity profile. Moreover, the term h_p/y_n is also crucial for converting C_d and A_p/a into a form of a control volume ($\frac{C_d A_p h_p}{\nabla}$).

The final version of Model 2 is:

$$\ln C_d = \ln \alpha + \beta \ln \left(\frac{A_p}{a} \right) + \varphi \ln \left(\frac{h_p}{y_n} \right) + \eta \ln \left(\frac{s_p}{y_n} \right) + \psi \ln \left(\frac{\rho V^2 h_p^4}{G_p} \right) + \xi \ln \left(\frac{\rho VR}{\mu} \right) \quad (3-64)$$

where $\alpha, \beta, \varphi, \eta, \psi,$ and ξ are constants. (Parameter estimates)

Note: in the simplified form, this equation is:

$$Y_1 = a + b X_5 + c X_4 + d X_3 + f X_2 + g X_1$$

where $a, b, c, d, f,$ and g are constants.

For the independent variable h_p/y_n , a value of 1 represented the just-submerged macrophytes in aquatic flows. All experimental values of h_p/y_n in this research were greater than 1, indicating that all macrophytes were

emergent and standing in the stream. After developing the basic forms of the model 2, it was then split into two parts (part 1 and part 2) due to statistical consideration.

Model 2 part 1

$$Y_1 = a + b X_5 + c X_4 + d X_3 + f X_2 + g X_1$$

The Intercept $a = -100.97283$

The parameter estimate for $X_5 = -0.343$

The parameter estimate for $X_4 = 79.774$

The parameter estimate for $X_3 = -0.107$

The parameter estimate for $X_2 = -44.711$

The parameter estimate for $X_1 = 86.91$

$$Y_1 = -100.943 - 0.343 X_5 + 79.774 X_4 - 0.107 X_3 - 44.711 X_2 + 86.910 X_1$$

$$\ln C_d = \ln \alpha + \beta \ln \left(\frac{A_p}{a} \right) + \varphi \ln \left(\frac{h_p}{y_n} \right) + \eta \ln \left(\frac{s_p}{y_n} \right) + \psi \ln \left(\frac{\rho V^2 h_p^4}{G_p} \right) + \xi \ln \left(\frac{\rho V R}{\mu} \right)$$

$$\ln \alpha = -100.973, \quad \alpha = 1.406E-44$$

Replacing the constants with the values from the parameter estimates in the regression analysis gives:

$$C_d = (1.406E - 44) \left(\frac{A_p}{a} \right)^{-0.342} \left(\frac{h_p}{y_n} \right)^{79.774} \left(\frac{s_p}{y_n} \right)^{-0.107} \left(\frac{\rho V^2 h_p^4}{G_p} \right)^{-44.711} \left(\frac{\rho V R}{\mu} \right)^{86.91} \quad (3-65)$$

The R -squared and the adjusted R -squared values of this dimensionless equation were 0.940 and 0.945, respectively. Therefore, about 94.5% of the variation of the natural logarithm of the drag coefficient (C_d) could be explained by the independent variables including the natural logarithm of the following dimensionless parameters: the ratio of the projected plant frontal area to the bed area occupied by the plants, the ratio of the average plant height to the water level, the ratio of the average stem spacing to the water level, the ratio of drag force to the plant rigidity, and the Reynolds number.

One problem was noted that the p values of the t tests of X_5 [$\ln(A_p/a)$] and X_3 [$\ln(s_p/y_n)$] were greater than 0.05, indicating their relatively less

contributiveness compared to other independent variables. The t -test was made by dividing the coefficient estimates by their standard errors. A summary of model 2 part 1 is shown in Table 3.33 with specific information in Table 3.30.

Model 2 part 2

X_5 , $[\ln(A_p/a)]$, and X_3 , $[\ln(s_p/y_n)]$, in model 2 part 1 had “ $Pr > |t|$ ” values of 0.1887 and 0.7542, respectively. These two variables had the “ $Pr > |t|$ ” values greater than 0.05, which were statically insignificant in the contribution to the variation of Y_1 (C_d) values. For this reason, X_5 and X_3 were eliminated for this run of multiple regression model (Model 2 part 2):

$$\ln C_d = \ln \alpha + \varphi \ln \left(\frac{h_p}{y_n} \right) + \psi \ln \left(\frac{\rho V^2 h_p^4}{G_p} \right) + \xi \ln \left(\frac{\rho VR}{\mu} \right) \quad (3-66)$$

$$Y_1 = a + c X_4 + f X_2 + g X_1$$

The intercept $a = -99.660$

The parameter estimate for $X_4 = 80.04$

The parameter estimate for $X_2 = -44.857$

The parameter estimate for $X_1 = 80.089$

All the above parameter estimates have values of $Pr > |t|$ less than 0.0001, indicating that all these parameters (dependent variables) are statistically significant in contributing to the variation of $\ln(C_d)$.

Since:

$$\ln C_d = \ln \alpha + \varphi \ln \left(\frac{h_p}{y_n} \right) + \psi \ln \left(\frac{\rho V^2 h_p^4}{G_p} \right) + \xi \ln \left(\frac{\rho VR}{\mu} \right);$$

and $a = \ln \alpha = -99.66$; $\alpha = 5.225E-44$

$$\ln C_d = (5.225E - 44) + 80.04 \ln \left(\frac{h_p}{y_n} \right) - 44.857 \ln \left(\frac{\rho V^2 h_p^4}{G_p} \right) + 87.089 \ln \left(\frac{\rho VR}{\mu} \right) \quad (3-67)$$

$$C_d = (5.225E - 44) \left(\frac{h_p}{y_n} \right)^{80.04} \left(\frac{\rho V^2 h_p^4}{G_p} \right)^{-44.857} \left(\frac{\rho VR}{\mu} \right)^{87.089} \quad (3-68)$$

The R -squared and the adjusted R -squared values of this dimensionless

equation were 0.939 and 0.935 respectively. Therefore 93.5% of the variation of the natural logarithm of the drag coefficient (C_d) could be explained by the independent variables including the natural logarithm of the following dimensionless parameters: the ratio of the averaged plant height to water level, the ratio of drag to plant rigidity, and the Reynolds number. A summary of Model 2 Part 2 is shown in Table 3.34 with specific information in Table 3.31.

In this statistical analysis, the variables left were the ratio of the plant height to the water level, the ratio of the drag force to the plant rigidity, and the Reynolds number, which is the ratio of inertia to viscosity effect. Statistically this was a better model compared to model 2 part 1. However, it is also noted that the two terms eliminated (A_p/a and s_p/y_n) were highly correlated to plant density. A_p/a was the ratio of projected plant frontal blockage area to the bed area covered by vegetation. The projected plant frontal area was roughly directly proportional to plant population density. Moreover, the average stem spacing s_p was calculated from the square root of the inverse of plant density minus the average stem diameter. The univariate analysis of C_d verses plant population density for *Phragmites australis* in Figure 3.34 shows that values of C_d are correlated to plant density for mid-range of flow at levels of 0.0121 m³/s (12.1 l/s), 0.0158 m³/s (15.8 l/s), and 0.0177 m³/s (17.7 l/s); but not much correlated at two extreme levels of flows at 0.00764 m³/s (7.64 l/s) and 0.02091 m³/s (20.91 l/s). In multiple regression model built for the values of C_d of *Phragmites australis* with varying plant densities and flows, plant density was also found to be an significant independent variable with $Pr > |t|$ less than 0.0001. In this model with adjusted R -squared of 0.91, C_d was found to slightly decrease with increasing plant densities under controlled flows.

On the other hand, $C_d A_p$ is found to highly correlate with plant density in Figure 3.22. An optimum plant density was even obtained from the polynomial regression equations. In addition, in the dimensional analysis carried out in model 1, the ratio of the average spacing of an array of vegetation $\left(\frac{s_p}{y_n} \right)$ was

found to have strong correlation to the streamlining coefficient $\frac{C_d A_p h_p}{\nabla}$. From the above observation, it could be discovered that the A_p value, which changed when impacted by the stream flow, was an important factor that still needed to be documented in future studies.

Note that in Equation (3-68), a large number of $\left(\frac{\rho V^2 h_p^4}{G_p}\right)$ to the power of -44.857 is a very small number. This would be balanced by the effect of the Reynolds number to the power of 87.089. A more convenient calculation of the C_d values can be achieved by utilizing Equation (3-67).

From Equation (3-68), (3-26), and (3-27), the following equations for friction factors could be deduced:

Darcy-Weisbach factor f is derived from Equation (3-68) and (3-28):

$$f = (5.225E - 44) \left(\frac{4A_p}{a}\right) \left(\frac{h_p}{y_n}\right)^{80.04} \left(\frac{\rho V^2 h_p^4}{G_p}\right)^{-44.857} \left(\frac{\rho VR}{\mu}\right)^{87.089}$$

$$f = (8.3594E - 43) \left(\frac{A_p}{a}\right) \left(\frac{h_p}{y_n}\right)^{80.040} \left(\frac{\rho V^2 h_p^4}{G_p}\right)^{-44.857} \left(\frac{\rho VR}{\mu}\right)^{87.089}$$

(3-69)

$$\ln f = -96.888 + \ln\left(\frac{A_p}{a}\right) + 80.04 \ln\left(\frac{h_p}{y_n}\right) - 44.857 \ln\left(\frac{\rho V^2 h_p^4}{G_p}\right) + 87.089 \ln\left(\frac{\rho VR}{\mu}\right) \quad (3-70)$$

Chezy's C is determined by Equation (3-28) and Equation (3-69):

$$\ln C = 50.625 - \frac{1}{2} \ln\left(\frac{A_p}{a}\right) - 40.02 \ln\left(\frac{h_p}{y_n}\right) + 22.429 \ln\left(\frac{\rho V^2 h_p^4}{G_p}\right) - 43.545 \ln\left(\frac{\rho VR}{\mu}\right) \quad (3-71)$$

Manning's n is derived from Equation (3-27) and (3-69)::

$$n = 2R^{1/6} \left(\frac{A_p}{a}\right)^{1/2} \left(\frac{5.225E - 44}{g}\right)^{1/2} \left(\frac{h_p}{y_n}\right)^{40.02} \left(\frac{\rho V^2 h_p^4}{G_p}\right)^{-22.428} \left(\frac{\rho VR}{\mu}\right)^{43.544}$$

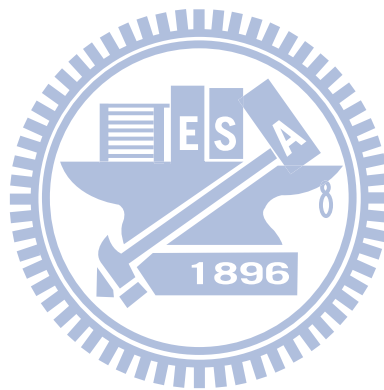
Taking $g = 9.81 \text{ m/s}^2$,

$$n = (1.45956E - 22)R^{1/6} \left(\frac{A_p}{a}\right)^{1/2} \left(\frac{h_p}{y_n}\right)^{40.02} \left(\frac{\rho V^2 h_p^4}{G_p}\right)^{-22.428} \left(\frac{\rho VR}{\mu}\right)^{43.544} \quad (3-72)$$

Checking for the dimension for Manning's n [$TL^{(-1/3)}$]

$$L^{1/6} \left(\frac{1}{L/T^2}\right)^{1/2} = TL^{(-1/3)}$$

$$\begin{aligned} \ln n = & -50.279 + 0.167 \ln R + \frac{1}{2} \ln\left(\frac{A_p}{a}\right) + 40.02 \ln\left(\frac{h_p}{y_n}\right) - 22.429 \ln\left(\frac{\rho V^2 h_p^4}{G_p}\right) \\ & + 43.545 \ln\left(\frac{\rho VR}{\mu}\right) \end{aligned} \quad (3-73)$$



Chapter 4. Conclusion and Recommendation

4.1 Conclusion

In this thesis, the drag forces induced by flow over four selected emergent macrophytes in Taiwan were directly measured to assist engineers and scientists in the determination of the streamline coefficients, the drag coefficients, and the friction factors for emergent (non-submerged), flexible, natural, and living macrophytes with varying plant densities and flow velocities. Drag forces of an array of emergent macrophytes in aquatic flows had been measured in a steady, non-uniform, and mostly transitional and supercritical flow using a self-developed direct drag force measurement system. *Phragmites australis* was set as the focus of this research. The drag force data of *Phragmites australis* were applied in the calculation of the streamline coefficient ($C_d A_p h_p / \nabla$) and the drag coefficient (C_d), and therefore Darcy-Weisbach f , Chezy C , and Manning's n friction factors. Results of the multiple regression analyses on the effect of plant density and flow on drag force have been obtained. Dimensional analysis for *Phragmites australis* was further carried out to build dimensionless models for the derivation of empirical equations for the natural logarithm of the streamline coefficient ($C_d A_p h_p / \nabla$), the drag coefficient (C_d), Darcy Weisbach f , Chezy C , and Manning's n .

A direct drag force measurement system had been developed specially for the purpose of direct measurement of the drag force induced by flow over an array of four types of emergent macrophytes with varying plant densities and flow velocities. Different from previous studies, this system was the first to directly measure drag force of an array of realistic living emergent macrophytes with roots and soils intact, through a set of transducers, computer, and force balancing components. These natural and living aquatic plants, therefore, were alive and strong in a mini-ecosystem placed on the drag force measurement device, which greatly improved the results of the drag force measured due to the reflection of true flexural rigidity and streamlining function of the emergent macrophytes. This true reflection of the natural plant characteristics by the use

of direct drag force measurement system facilitated the discovery of distinctive variation of streamline factor (C_dA_p) with increasing plant population density (ρ_p) and stream velocity (V).

The graphs of the streamline factor (C_dA_p) verses the square of stream velocity (V^2) are useful tools for the design of drag forces experienced by the plants in aquatic flows (Figure 3.20 to 3.23). Drag force could be easily derived from this graph by using the equation: $F_d = 1/2\rho C_dA_pV^2$. From the graph of the streamline factor (C_dA_p) for *Phragmites australis* verses the square of stream velocity (Figure 3.20); it was found that C_dA_p started to drop whenever it was placed in a stream of flow, even at the beginning stage where there was low velocity. Figure 3.20 shows the streamlining ability of *Phragmites australis* once they are placed in aquatic flows with stream velocity of any magnitude. It can be also observed from Figure 3.20 that for *Phragmites australis* with plant population densities of 1052.63 stems/ m² and 1350.88 stems/ m², the ability to streamline (or the need to streamline) seems to reach to a maximum, when C_dA_p values starts to increase after $V^2 > 0.8$ m²/s². It is noted from this graph that higher densities tend to contribute to higher C_dA_p values. This could imply that it was harder (or there was less need) for *Phragmites australis* to streamline with flow at higher plant densities. It could also be further interpreted that in a control volume, plants with higher densities were more rigid, being less able or less needed to change shape, and therefore harder to streamline with the flow.

The above finding is consistent with studies conducted by Fathi-Moghadam and Kouwen on pine and cedar trees (1997), Armanini on tall and small *Salix* (2003), and Wilson on pine and ivy stipes (2008), in which the product of drag coefficient and projected plant frontal area (C_dA_p) was found to decline with increasing square of stream velocities. It is noted that in Fathi-Moghadam and Kouwen's study (1997), decrease of C_dA_p per unit area and per unit control volume over a range of the square of stream velocities was studied. Sand-Jensen (2003) and James et al. (2004) also found a drop of C_d values with increasing flow velocities for a total of seven species of macrophytes. In James' study, data were collected for reeds and bulrushes,

which are emergent macrophytes. Sand-Jensen (2003) also discovered the decline of C_d values of submerged (*Vallisneria natans* and *Egeria densa*) and emergent macrophytes (*Hygrophila corymbosa* and *Limnophila aquatica*) with increasing flow velocities. In addition, since the streamline factor ($C_d A_p$) is directly proportional to Darcy-Weisbach f and Manning's n , its decline will contribute to a decrease in the friction factors, which is consistent with the study conducted by Kouwen and Fathi-Moghadam (2000) in which Darcy-Weisbach f dropped with increasing flow velocity.

The contribution of plant density to the variation of $C_d A_p$ ($C_d A_p$ v.s. plant density) for *Phragmites australis* is shown in Figure 3.24 and Figure 3.25. It is found from Figure 3.24 that under all controlled flow conditions, the $C_d A_p$ value drops initially with increasing stream velocity but rises again after an optimum plant density is reached. After this optimum density, it was harder (or of less need) for *Phragmites australis* to streamline with the flow. Since the $C_d A_p$ value is directly proportional to the Darcy-Weisbach friction factor f and Manning's n in Equation (3-26) and (3-27) respectively, the optimum density which corresponded to the lowest $C_d A_p$ value would contribute to the smallest friction factors chosen for the design of free surface flow in vegetated open channels, river floodplains, and wetlands. This result could be used by hydraulic engineers, scientists, and ecological engineers in the design, control, and management of plant densities for emergent macrophytes standing in river floodplains, wetlands, lakes, vegetated channels and waterways, and vegetated linings.

To determine Darcy-Weisbach friction factors f , Chezy C , or Manning's n for emergent macrophytes in high speed and shallow aquatic flow, equations based on both measurable vegetation characteristics and flow conditions were developed. The advantages of these equations were their ability to estimate flow resistance of an array of natural and living emergent macrophytes in various plant population densities, plant diameters, plant heights, plant shear modulus of elasticity, plant second area moment of inertia, water levels, flow velocities, water densities, water dynamic viscosities, channel cross sectional

areas, and channel wetted perimeters. These equations were developed through dimensional analysis. In Equation (3-55), the streamline coefficient was set as the dependent variable in the dimensional analysis of Model one:

$$\ln\left(\frac{C_d A_p h_p}{\nabla}\right) = 309.024 - 0.840 \ln\left(\frac{s_p}{y_n}\right) + 79.392 \ln\left(\frac{d_p}{y_n}\right) - 43.902 \ln\left(\frac{\rho V^2 h_p^4}{G_p}\right) + 85.203 \ln\left(\frac{\rho V R}{\mu}\right)$$

This model showed high *R*-Squared value of 0.944, which meant that 94.4 % of the variations in the natural logarithm of the streamline coefficient were explained by all of the independent variables including the natural logarithm of the following dimensionless parameters: the ratio of average stem spacing to water level, the ratio of average stem diameter to water level, the ratio of drag to plant flexural rigidity, and the Reynolds number. All of the independent variables had values of $Pr > |t|$ less than 0.0001, indicating their high statistical significance in contributing to the variation of $\ln(C_d A_p h_p / \nabla)$. Based on the above equation (Equation 3-55), the following equations of the friction factors (Equation 3-58 to 3-61) could be derived.

The natural logarithm of Darcy-Weisbach friction factor *f* was given in equation (3-58):

$$\ln f = 310.410 + \ln\left(\frac{y_n}{h_p}\right) - 0.84 \ln\left(\frac{s_p}{y_n}\right) + 79.392 \ln\left(\frac{d_p}{y_n}\right) - 43.902 \ln\left(\frac{\rho V^2 h_p^4}{G_p}\right) + 85.203 \ln\left(\frac{\rho V R}{\mu}\right)$$

The natural logarithm of Chezy *C* was given in equation (3-59):

$$\ln C = -153.023 - \frac{1}{2} \ln\left(\frac{y_n}{h_p}\right) + 0.42 \ln\left(\frac{s_p}{y_n}\right) - 39.696 \ln\left(\frac{d_p}{y_n}\right) + 21.951 \ln\left(\frac{\rho V^2 h_p^4}{G_p}\right) - 42.602 \ln\left(\frac{\rho V R}{\mu}\right)$$

The natural logarithm of Manning's *n* is given in (3-61):

$$\ln n = 154.063 + 0.167 \ln R + \ln\left(\frac{y_n}{h_p}\right) - 0.42 \ln\left(\frac{s_p}{y_n}\right) + 39.696 \ln\left(\frac{d_p}{y_n}\right) - 21.951 \ln\left(\frac{\rho V^2 h_p^4}{G_p}\right) + 42.602 \ln\left(\frac{\rho V R}{\mu}\right)$$

In model two, the drag coefficient was chosen as the dependent variable. Results of Model two part two were found to be more representative than part one for its exclusion of two relatively insignificant independent variables: $\ln(A_p/a)$ and $\ln(s_p/y_n)$. Dimensional analysis and multiple regression analysis for *Phragmites australis* in Model two part two arrived at Equation (3-67):

$$\ln C_d = (5.225E - 44) + 80.04 \ln \left(\frac{h_p}{y_n} \right) - 44.857 \ln \left(\frac{\rho V^2 h_p^4}{G_p} \right) + 87.089 \ln \left(\frac{\rho V R}{\mu} \right)$$

The adjusted *R*-squared value of 0.935 indicated that 93.5% of the variations of the natural logarithm of the drag coefficient (C_d) were explained by the independent variables including the natural logarithm of the following dimensionless parameters: the ratio of the average plant height to water level, the ratio of drag to plant flexural rigidity, and the Reynolds number. All parameter estimates had values of $Pr > |t|$ less than 0.0001, indicating their high statistical significance in contributing to the variation of $\ln C_d$.

Based on the above equation, the following equations were determined.

The natural logarithm of Darcy-Weisbach friction factor f was given in equation (3-70):

$$\ln f = -96.888 + \ln \left(\frac{A_p}{a} \right) + 80.04 \ln \left(\frac{h_p}{y_n} \right) - 44.857 \ln \left(\frac{\rho V^2 h_p^4}{G_p} \right) + 87.089 \left(\frac{\rho V R}{\mu} \right)$$

The natural logarithm of Chezy C was given in equation (3-71):

$$\ln C = 50.625 - \frac{1}{2} \ln \left(\frac{A_p}{a} \right) - 40.02 \ln \left(\frac{h_p}{y_n} \right) + 22.429 \ln \left(\frac{\rho V^2 h_p^4}{G_p} \right) - 43.545 \left(\frac{\rho V R}{\mu} \right)$$

The natural logarithm of Manning's n is given in (3-73):

$$\ln n = -50.279 + 0.167 \ln R + \frac{1}{2} \ln \left(\frac{A_p}{a} \right) + 40.02 \ln \left(\frac{h_p}{y_n} \right) - 22.429 \ln \left(\frac{\rho V^2 h_p^4}{G_p} \right) + 43.545 \left(\frac{\rho V R}{\mu} \right)$$

Since the estimations of the streamline coefficients, the drag coefficients, and the friction factors are important tasks in the conservation and restoration

of land and hydraulic structures on banks and bay shores (Kouwen 2000), these equations could be used for engineers and scientists in the design, control, and management of emergent macrophytes in floodplains, wetlands, lakes, vegetated channels and waterways, and vegetated linings. In this study, there is a more realistic reflection of these friction factors based on plant characteristics: i.e. the plant population density, stem diameter, plant height, stem shear modulus of elasticity, and second area moment of inertia for stem cross sectional area. In addition, these friction factors also incorporate flow conditions including the flow velocity, water level, density, dynamic viscosity, channel cross sectional area, and channel wetted perimeter. Therefore these equations could be applied in the calibration and validation of numerical models adopted in the river hydraulics.

4.2 Recommendation

The maximum and minimum values of Manning's n for the four selected emergent macrophytes derived from the data in this experiment were within the range in the standard manuals (Chow 1959). This further ensured the accuracy of the direct drag force measurement system and its ability to reflect variation of Manning's n in different plant characteristics and flow conditions (Section 3.1.5). Further validations of the values of C_d or $C_d A_p$ could also be done by using the following equations:

$$C_d = \frac{2}{(A_p / a) \rho V^2} \left\{ \gamma R \left(S_0 - \frac{dy}{dx} - \frac{v}{g} \frac{dv}{dx} \right) - \frac{F_b}{a} \right\}$$

$$C_d A_p = \frac{2a}{\rho V^2} \left\{ \gamma R \left(S_0 - \frac{dy}{dx} - \frac{v}{g} \frac{dv}{dx} \right) - \frac{F_b}{a} \right\}$$

In addition to *Phragmites australis*, further analysis of data collected for *Typha orientalis*, *Hygrophila pogonocalyx*, and *Juncus effusus* is suggested be carried out. Statistical models and dimensional analysis for these three species are important for further researches on between-species comparison. However, the number of experiments conducted for *Juncus effusus* is not sufficient for building a model for statistical and dimensional analysis. Further test runs will

make a more accurate result for *Juncus effusus*. In addition, the flow variation for *Hygrophila pogonocalyx* has not been completely extended to the twenty third and twenty sixth rotational turns, which reduces the results of the analysis with nine missing data. Drag force induced by other chosen emergent macrophytes cultivated in the roof farm on campus may also be conducted for future research.

During the experiment, it was discovered that the projected plant frontal area (A_p) varied when impacted by the stream flow. Since it is an important factor in determining drag coefficients, techniques to observe this change of area under submergence of water, is suggested to be developed. In addition, the determination of the following dimensionless terms by experimental means may be carried out to further describe the friction factors.

The ratio of the average surface roughness to the diameter of the stems $\left(\frac{\varepsilon}{d_p}\right)$ may be important for the Reynolds number in the range of 4×10^4 to 4×10^5 , where certain degree of variation of drag coefficient may take place (Young 2004). This average roughness of the stem skin should be measured and analyzed in more detail for future consideration in the dimensional analysis.

The Strouhal number $\left(\frac{\omega y_n}{V}\right)$ is the ratio of local inertia force to the convective inertia force. In this research, it was discovered that stems tended to oscillate in a local control volume. This frequency of oscillation can be determined through detail observations recorded by high speed video camera in future studies.

In this experiment, the shear modulus of elasticity was measured with a relatively simple method which would allow engineers and scientists to measure and estimate the plant rigidity conveniently on site. In order to capture more accurate mechanical properties of emergent macrophytes, more data for shear modulus of elasticity of all four species both in the laboratory and in the field need to be conducted in different seasons to obtain more accurate results

of the ratio of drag to plant flexural rigidity $\left(\frac{\rho V^2 h_p^4}{G_p} \right)$. Comparisons may also be made between the results of friction factors computed by using the shear modulus elasticity and the modulus of elasticity.

At the beginning of each run of the flume test, water level was found to rise rapidly over time before the stream was stabilized. The rate of water level rising when water contacts with the vegetation zone can be found by a relationship of water level verses time. Theoretically this relationship is directly proportional to the relationship of drag forces verses time measured by the direct drag force measurement system, which can be observed from Figure 3.48 to Figure 3.70, presenting change of drag force over time. These drag force data, when divided by the mass of the movable platform, gives the equation of the instant longitudinal acceleration of the system over time. Double integration of this equation may give us a relationship of displacement over time, which should be theoretically directly proportional to water level changes over time. It would be of future research interest to develop and validate the relationship between drag and water level variation over time.

For natural and living plants, the vertical plant density varies with water level. For natural and living emergent macrophytes tested in this research, this ratio decreased slightly with rising water level. However, if the water level continues to increase till the level of vast branches and foliages, this vertical plant density would be increased again. For future study, it is suggested to measure the drag force of emergent macrophytes in aquatic flow with higher water levels to cover the effect of foliages on drag. Previous researchers' studies (Wilson et al. 2008) on the impact of foliage on drag force of pine and ivy stipes could be referenced for future study. Since shallow water is required for the natural habitat of emergent macrophytes, this future study may be only applicable to events of extreme floods.

Improvement for on the drag force measurement system can be done in the following areas. Efforts are still required to solve the problem of back water effect on the direct drag force measurement system when an extension of a

damping platform is installed at the back of this system. This platform would serve to ensure continuous flow (to eliminate spatial varied flow) and the reduction of hydrostatic force at the back of the system. Precautions should be taken to avoid and eliminate the back water force formed in between this extension and the drag force measurement system. Precise tests may be conducted to measure the influence of this addition using the existing drag force measurement system.

In addition, a more advanced engineering solution may be developed upon the two existing types of the movable platforms. One of the existing frame structures is lighter but with minimum water proof mechanism, while the other one is heavily armed with acrylic compartments designed to minimize water leakage, which could possibly increase the static friction and the deformation of the platform and the wheels. Structural analysis of the whole direct drag force measurement system can also be presented using the finite element method.

The approach of this experiment using the momentum principle is appropriate for 1D modeling methods for reach-scale prediction of flood inundation. On the other hand, prediction of flow dynamics and geomorphology using 2D or 3D approaches could enable engineers and researchers to present the normal stress induced by bed roughness and vegetation obstructions separately and in different ways. This would therefore allow the velocity field to be characterized within a water depth or within a river cross-section. Velocity field can also be obtained by utilizing non-intrusive flow field measurement methods such as the particle image velocimetry (PIV) method, which allows more accurate measurement and quantification of this flow field (Ikeda and Kanazawa 1996; Bennett et al. 2002; Yang 2001; Huang 2005; Lin 2006; Liu 2008). This method could also improve the accuracy of measurement of the upstream and downstream velocities, the visualization of flow fields within the canopies, and the quantification of shear and pressure distribution fields. The knowledge of flow field, water levels, shear stress, normal stress, and pressure are crucial criteria in the design,

construction, restoration, and monitoring of the natural habitat for various species within an ecosystem (Odum 1975; Niklas 1992; Kadlec and Knight 1996; Odum 2003; Mitsch and Jorgensen 2004; Tatyana et al. 2005; Mitsch and Grosselink 2007; Wu and Chang 2008).

The variation of flow velocity over the vegetated zones would in turn affect the hydraulic retention time (*HRT*) within a control volume. It has been found that *HRT* is a vital factor for the efficiency of self-purification of natural streams and wetlands (Kadlec and Knight 1996; Crites and Tchobanogous. 1998; Office of Water 1999; Toet et al. 2005; Akkratos and Tsihrintzis 2007; Chang 2007). Therefore, water quality tests, particularly the reduction of pollutants (e.g. phosphorous) under the effect of these emergent macrophytes and the soils should be conducted to measure the ability of this mini ecosystem to purify water under controlled flow velocities and drag forces induced. Water quality models may be utilized to bridge the effect of water quality improvement and drag force induced in various plant densities and flow velocities (Appendix B).

In this study, since a more realistic reflection of the friction factors was presented based on the plant characteristics and the flow conditions, application of these findings in the calibration and validation of numerical models adopted in the river hydraulics may be recommended. For example, by incorporating the logistic function in Equations (2-1) to (2-5), the change of plant density over time (e.g. seasons) could be determined and therefore the seasonal variation of friction factors. The variation of friction factors due to the change of the following plant characteristics and flow conditions: plant population density, stem diameter, stem height, shear modulus of elasticity, second area moment of inertia, stream flow velocity, water level, density, dynamic viscosity, channel cross sectional area, and channel wetted perimeter; may be used to compute the water level variation in realistic river cross sections (Chow 1959; Henderson 1966; Mason et al. 2003). These friction factors (e.g. Manning's *n*) could be further applied in the governing equations for open-channel flow, sediment transport, and coastal flow through emergent macrophytes.

References

1. Andradottir, H. O. and Nepf, H. M. "Impact of exchange flows on wetland flushing." *Water Resources Research*, Vol. 37, No. 12, 3265 – 3273.
2. Akrotos, C. S. and Tsihrintzis, V. A. (2007). "Effect of temperature, HRT, vegetation and porous media on removal efficiency of pilot-scale horizontal subsurface flow constructed wetlands." *Ecological Engineering*, 29(1):173-191.
3. Armanini, A., Righetti, M., and Grisenti, P. (2005). "Direct measurement of vegetation resistance in prototype scale." *Journal of Hydraulic Research*, Vol. 43, No. 5, 481-487.
4. Burggen, Van J.J.A. (2006). "The importance of wetland ecosystems in ecological engineering." *International Symposium on Ecological Engineering*, Public Construction Commission, Executive Yuan, Taiwan R.O.C., 125-134.
5. Carollo, F. G., Ferro, V., and Termini, D. (2005). "Flow resistance in channels with flexible submerged vegetation." *Journal of Hydraulic Engineering*, Vol. 131, No. 7, 554-564.
6. Cazanacli D., Paola C., and Parker G. (2002). "Experimental steep, braided flow: application on flooding risk on fans." *Journal of Hydraulic Engineering*, Vol. 128, No. 3.
7. Chang, W. L. (2006). "A brief review of the development of road construction and river restoration in Taiwan." *International Symposium on Ecological Engineering*, Public Construction Commission, Executive Yuan, Taiwan R.O.C. 149-165.
8. Chow, V. T. (1959). *Open-channel hydraulics*, MacGraw-Hill, New York.
9. Chow, V. T., Maidment, D. R. and Mays, L. W. (1988). *Applied hydrology*, (International Edition), McGraw-Hill, New York.
10. Crites, W. R., Gunther, C. D., Kruzic, P. A., Pelz, D. J., and Tchobanoglous, G. (1988). *Design Manual Constructed Wetlands and Aquatic Plant Systems for Municipal wastewater treatment*, U.S. Environmental Protection Agency Office of Research and Development, Center for Environmental Research Information Cincinnati, OH 45268.
11. Crites, W. R. and Tchobanogous, G. (1998). *Small and decentralized wastewater management systems*, McGraw-Hill, Boston.

12. Currie, I. G. (1994). *Fundamental mechanics of fluids* 3rd ed., Marcel Dekker, Inc., New York.
13. Evgeny, A. K. and Leopold, L. L. (2005). "The Southeast Asia tsunami disaster aftermath: development of new approaches to coastal zone hazard observation and warning systems." *Taiwan-Russia Bilateral Symposium on Water and Environmental Technology*, Water Resource Agency, Ministry of Economic Affairs, Taiwan, R.O.C.
14. Fathi-Maghadam, M. and Kouwen, N. (1997). "Nonrigid, nonsubmerged, vegetative roughness on floodplains." *Journal of Hydraulic Engineering*, Vol. 123, No. 1, 51-57.
15. Fetter, C. W. (1994) *Applied hydrogeology* 3rd ed., Macmillan College Publishing Co., Inc., New York.
16. Fiener, P. and Auerswald, K. (2003). "Effectiveness of grassed waterways in reducing runoff and sediment delivery from agricultural watersheds." *Journal of Environmental Quality*, Vol. 32, 927-936.
17. Freeman, G. E., Raymeyer, W. J., and Copland, R. R. (2000). "Determination of resistance due to shrubs and woody vegetation." *Rep. No. ERDC/CHL TR-00-25*, Engineering Research and Development Center, U.S. Army Corps of Engineers.
18. Fritz, H. M., Blount, C., Sokoloski, R., Singleton, J., Fuggle, A., McAdoo, B. G., Moore, A., Grass, C., and Banks, T. (2007). "Hurricane Katrina storm surge distribution and field observations on the Mississippi Barrier Islands." *Estuarine, Coastal and Shelf Science*, Vol. 74, 12-20.
19. Guo, J. C. Y. "Capture volume for storm water quality control systems." *International Symposium on Ecological Engineering*, Public Construction Commission, Executive Yuan, Taiwan R.O.C., 137-147.
20. Hallam, T. G. (1986). *Mathematical ecology: an introduction*, Springer-Verlag, Berlin.
21. Henderson, F. M. (1966) *Open channel flow*, Macmillan Publishing Co., Inc., New York, NY.
22. Hsiao, Y. W. and John, B. H. (1997). *Guidebook to dragonflies of Taiwan (Part I)*, Shih Pei Ni, Taiwan.
23. Ikeda, S., and Kanazawa, M. (1996). "Three-dimensional organized vortices above flexible water plants." *Journal of Hydraulic Engineering*, 122(1): 634-640.

24. Ishigami, T., Kawabata, M., Shinohara, Y., Nakazono, A., Ryu, E., Yamaguchi, T., Tanaka, M., and Iyobe, T. (2008). "Phosphorous release from the sediment in the riparian community and its effect on the primary productivity of the estuary ecosystem." *The First Asian Wetland Convention*, 166-170.
25. I.P.C.C. core writing group (2007). *I.P.C.C. Fourth assessment report: climate change 2007 synthesis report (AR4)*. Technical Paper of the Intergovernmental Panel on Climate Change, I.P.C.C. Secretariat, Geneva, Switzerland.
26. Jain, S. C. (2001). *Open-channel flow*. John Wiley & Sons, Inc., New York.
27. James, C. S., Birkhead, A. L., Jordanova, A. A., and O'Sullivan, J. J. (2004). "Flow resistance of emergent vegetation." *Journal of Hydraulic Research*, Vol. 42, No. 4, 390-398.
28. Jarvela, J. (2002). "Flow resistance on flexible and stiff vegetation: a flume study with natural plants." *Journal of Hydrology*, Vol. 269, 44-54.
29. Jarvela, J. (2003). "Influence of vegetation on flow structure in floodplains and wetlands." *Proceedings of the 3rd IAHR Symposium on River, Coastal and Estuarine Morphodynamics*, Madrid, International Association of Hydraulic Engineering and Research (IAHR), 845-856.
30. Jarvela, J. (2004). "Determination of flow resistance caused by non-submerged woody vegetation." *International Journal of River Basin Management*, Vol. 2, No. 1, 61-70.
31. Jarvela, J. (2005). "Effects of submerged flexible vegetation on flow structure and resistance." *Journal of Hydrology*, Vol. 307, 233-241.
32. Julien, P. Y. (2002). *River mechanics*, Cambridge University Press, Cambridge, New York.
33. Kaack, K. and Schwarz, K. U. (2001). "Morphological and mechanical properties of Miscanthus in relation to harvesting, lodging, and growth conditions." *Industrial Crops and Products*, Volume 14, Issue 2, Pages 145-154.
34. Kaack, K., Schwarz, K. U., and Brandera, P. E. (2003). "Variation in morphology, anatomy and chemistry of stems of Miscanthus genotypes differing in mechanical properties." *Industrial Crops and Products*, Volume 17, Issue 2, 131-142.

35. Kadlec, R. H. (1990). "Overland flow in wetlands: vegetation resistance." *Journal of Hydraulic Engineering*, Vol. 116, 691–706.
36. Kadlec, R. H. and Knight, R. L. (1996). *Treatment wetlands*, CRC Press Inc., Boca Raton. Florida.
37. Knight, R. L., Walton W. E., O'Meara, G. F., Reisen, W. K., and Wass, R. (2003). "Strategies for effective mosquito control in constructed treatment wetlands." *Ecological Engineering*, 21, 211-232.
38. Kouwen, N. and Fathi-Moghadam, M. (2000). "Friction factors for coniferous trees along rivers." *Journal of Hydraulic Engineering*, Vol. 126, No. 10, 732-740.
39. Kouwen, N., and Li, R. M. (1980). "Biomechanics of vegetative channel linings." *Journal of the Hydraulics Division*, 106: 1085–1103.
40. Kouwen, N., Unny, A. M., and Hill, H. M. (1969). "Flow retardance in vegetated channels." *Journal of Irrigation and Drainage Division*, 95: 329–343.
41. Kouwen, N., and Unny, A. M. (1973). "Flexible roughness in open channels." *Journal of Hydraulics Division*, 33 (5): 713–727.
42. Lee, J. K., Roig, L. C., Jenter, H. L., and Visser, H. M. (2004). "Drag coefficients for modeling flow through emergent vegetation in the Florida Everglades." *Ecological Engineering*, 22, 237-248.
43. Lee, H.Y. et al. (2005). *International symposium on ecological engineering and hydro science*, Water Resources Planning Institute, Water Resources Agency, MOEA; Taiwan International Institute for Water Education.
44. Li, W. C. and Yan, K. (2007) "Numerical investigation of wave-current-vegetation interaction." *Journal of Hydraulic Engineering*, Vol. 133, No. 7, 794 – 803.
45. Li, R. M. and Shen, H. W. (1973). "Effect of tall vegetations on flow and sediment." *Journal of Hydraulics Division*, 99 (HY5), 793-814.
46. Lightbody, A. F. and Nepf, H. M. (2006). "Prediction of velocity profiles and longitudinal dispersion in emergent salt marsh vegetation." *Limnology Oceanography*, 51(1), 2006, 218-228.
47. Luong, H. P. V. (2008). "The role of hydrodynamics in the development of mangroves in coastal Cangio, southern Vietnam." *The First Asian Wetland Convention* 274-278

48. Mason, D. C., Cobby, D. M., Horritt, M. S., and Bates, P. D. (2003). "Floodplain friction parameterization in two-dimensional river flood models using vegetation heights derived from airborne scanning laser altimetry." *Hydrological Processes*, Vol. 17, 1711-1732.
49. Mitsch, W. J. and Grosselink, J. (2007). *G. Wetlands 4th ed.*, John Wiley & Sons, Inc., Hoboken, New Jersey.
50. Mitsch, W. J. and Jorgensen, S. (2004). *Ecological engineering and ecosystem restoration*, John Wiley & Sons, Inc., Hoboken, New Jersey.
51. Morris, J. T., Sundareshwar, P. V., Nietch, C. T., Kjerfve, B., Cahoon D. R. (2002). "Responses of coastal wetlands to rising sea level." *Ecology*, 83 (10): 2869-2877.
52. Musleh, F. A. and Cruise, J. F. (2006). "Functional relationships of resistance in wide flood plains with rigid unsubmerged vegetation." *Journal of Hydraulic Engineering*, Volume 132, Issue 2, 163-171.
53. Nakase, K., Yagi, Y., and Chiba, H. (2008). "Management and wise-use of constructed tidal flat on reclaimed land in the Tokyo Bay area." *The First Asian Wetland Convention*, 269-273.
54. Nepf, H. M. (1999). "Drag, turbulence, and diffusion in flow through emergent vegetation." *Water Resources Research*, Vol. 35, No. 2, 479-489.
55. Nepf, H. M. and Vivoni, E. R. (2000). "Flow structure in depth limited, vegetated flow." *Journal of Geophysical Research*, Vol. 105, No. C12, 547-557.
56. Niklas, K. J. (1992). *Plant biomechanics: an engineering approach to plant form and function*, University of Chicago Press, Chicago.
57. Odum, E. P. (1975). *Ecology: the link between the nature and social sciences 2nd ed.*, Holt, Rinehart and Winston, New York.
58. Odum, E. P. (1983). *Basic ecology.*, CBS College Publishing.
59. Odum, H. T. (2003). "Concepts and methods in ecological engineering." *Ecological Engineering*, Vol. 20, 339-361.
60. Office of Water (July 1993). *EPA Subsurface flow constructed wetlands for wastewater treatment: a technology assessment*, United States Environmental Protection Agency.

61. Office of Water (September 1993). *Constructed wetlands for wastewater treatment and wildlife habitat: 17 case studies*, United States Environmental Protection Agency.
62. Office of Water (June 1999). *EPA Free water surface wetlands for wastewater treatment*, United States Environmental Protection Agency.
63. Office of Research and Development Cincinnati, Ohio (September 2000). *EPA Manual: constructed wetlands treatment of municipal wastewaters*, United States Environmental Protection Agency.
64. Oplatka, M. (1998). "Stability and failure of willow-stabilized river banks using soil bioengineering solutions (in German)." *Stabilität von Weidenverbauungen an Flussufern*, Mitteilungen der Versuchsanstalt fuer Wasserbau, *Hydrologie and Glaziologie*, No. 156, ETH Zurich.
65. Petryk, S. and Bosmajian, G. (1975). "Analysis of flow through vegetation." *Journal of Hydraulics Division*, 101: 871–884.
66. Primack, R., Kobori, H., and Mori, S. (2000). "Diversity: dragonfly pond restoration promotes conservation awareness in Japan." *Conservation Biology*, 14(5): 1553-1554.
67. Reed, S. C., Crites, R. W., and Middlebrooks, E. J. (1995). *Natural systems for waste management and treatment*, McGraw-Hill, New York.
68. Rouse, H. (1965). "Critical analysis of open-channel resistance." *Journal of the Hydraulics Division*, 91(4): 1–26.
69. Rousseau, D., Burggen, Van J.J.A., Toet, S., Kansime, F., Azza, N., Pokorny, J., Vymazal, J., Denny, P., Filho, E. S. (2007). *Constructed wetlands for wastewater treatment*, Course Notes from United Nations Educational, Scientific and Cultural Organization; International Institute for Hydraulic and Environmental Engineering (UNESCO-IHE).
70. Sand-Jensen, K. (2003). "Drag and reconfiguration of freshwater macrophytes." *Freshwater Biology*, Vol. 48, 271-283.
71. Sawyer, C. N., McCarty, P. L., and Parkin, G. F. (2003). *Chemistry for environmental engineering and science 5/e, Vol. II.*, McGraw-Hill, Inc.
72. Schwalt, M. and Hager, W. H. (1994). "Experiments to supercritical junction flow." *Experiments in fluids*, Vol. 18, 429 – 437.
73. Sonak, S., Pangam, P., and Giriyan, A. (2008). "Green reconstruction of the tsunami-affected areas in India using the integrated costal zone management

- concept.” *Journal of Environmental Management*, Vol. 89, Issue 1, 14 -23.
74. State of Arizona Department of Water Resources Engineering Division (1994). *State standard for supercritical flow*. State Standard Attachment SSA 3-94.
75. Stone, B. M., and Shen, H. T. (2002). “Hydraulic resistance of flow in Channels with cylindrical roughness.” *Journal of Hydraulic Engineering*, 128(5): 500-506.
76. Steytler, N. S., and Samways, M. J. (1995). “Biotope selection by adult male dragonflies (Odonata) at an artificial lake created for insect conservation in South Africa.” *Biological Conservation*, 72 (3): 381-386.
77. Stephan, U. and Gutknecht, D. (2002). “Hydraulic resistance of submerged flexible vegetation.” *Journal of Hydrology*, Vol. 269, 27-43.
78. Tanino, Y. and Nepf, H. M. (2008). “Laboratory investigation of mean drag in a random array of rigid, emergent cylinders.” *Journal of Hydraulic Engineering*, Vol. 134, No.1, 34 – 41.
79. The Interstate Technology and Regulatory Council Wetlands Team (2003). *Technical and regulatory guidance document for constructed treatment wetlands*, The Interstate Technology & Regulatory Council.
80. Thom, A. S. (1971). “Momentum absorption by vegetation.” *Quarterly Journal of the Royal Meteorological Society*, Vol. 97, Issue 414, 414-428.
81. Toet, S., Van Logtestijn, R.S.P., Kampf, R., Schreijer, M., Verhoeven, J.T.A. (2005). “The effect of hydraulic retention time on the removal of pollutants from sewage treatment plant effluent in a surface-flow wetland system.” *Wetlands*, Vol. 25, no. 2, pp. 375-391.
82. Tsihrintzis, V. A. and Madiedo, E. E. (2000). “Hydraulic resistance determination in marsh wetlands.” *Water Resource Management*, Vol.14, 285-309.
83. Tsujimoto, T., Shimizu, Y., Kitamura, T., and Okada, T. (1992). “Turbulent open-channel flow over bed covered by rigid vegetation.” *Journal of Hydrology and Hydraulic Engineering*, 10: 13-25.
84. Thullen, J. S., Sartoris, J. J., and Walton, W. E. (2002). “Effects of vegetation management in constructed wetland treatment cells on water quality and mosquito production.” *Ecological Engineering*, Vol. 18, Issue 4, 441 – 457.

85. United States Department of Agriculture, Natural Resources Conservation Service (2003). *Global distribution of wetlands map*, USDA-NRCS, Soil Survey Division, World Soil Resources, Washington D.C.
86. USDA-NRCS PLANTS Database / USDA NRCS. *Wetland flora: field office illustrated guide to plant species*. USDA Natural Resources Conservation Service.
87. USDA-NRCS PLANTS Database / Britton, N.L., and A. Brown. (1913). *An illustrated flora of the northern United States, Canada and the British Possessions*. Vol. 1: 232, 467.
88. USDA-NRCS PLANTS Database / Hitchcock, A.S. (rev. A. Chase). (1950). *Manual of the grasses of the United States*. USDA Miscellaneous Publication No. 200. Washington, DC.
89. Vierssen, van W., Burggen, Van J.J.A., Wetzel, V., Christian, W., Chen, C. L., Guo, J. C. Y., Jiang, S., Nakagoshi, N., Maita, H., Okubo, S., Yang, S. L., Chang, W. L. (2006). *Essays collections on the international symposium on ecological engineering*, Public Construction Commission, Executive Yuan, Taiwan R.O.C.
90. Virginia Department of Conservation and Recreation (1999). *Virginia stormwater handbook: minimum standard 3.03 vegetated emergency spillway* Division of Soil and Water Conservation and National Oceanic and Atmospheric Administration.
91. White, F. M. (2006). *Viscous fluid flow* 3rd ed., McGraw-Hill, Inc., New York.
92. Willosn, J. D., Winne, C. T., Dorcas, M. E., and Gibbons, J. W. (2006). "Post-drought responses of semi-aquatic snakes inhabiting an isolated wetland: insights on different strategies for persistence in a dynamic habitat." *Wetlands*, 26(4): 1071-1078.
93. Wilson, C. A. and Allison, M. A. (2008). "An equilibrium profile model for retreating marsh shorelines in southeast Louisiana." *Estuarine, Coastal and Shelf Science*, Vol. 80, 483 – 494.
94. Wilson, C.A.M.E., Stoesser, T., Bates, P. D., and Batemann, P. A. (2003). "Open channel flow through different forms of submerged flexible vegetation." *Journal of Hydraulic Engineering*, Vol. 129, No. 11, 847-853
95. Wilson, C.A.M.E., Hoyt, J., and Schnauder, I. (2008). "Impact of foliage on the drag force of vegetation in aquatic flows." *Journal of Hydraulic Engineering*, Vol. 134, 885-891.
96. Wu, F. C., Shen, H. W., and Chou, Y. J. (1999). "Variation of roughness

coefficients for unsumberged and submerged vegetation.” *Journal of Hydraulic Engineering*, Vol. 125, No.9, 934 -942.

97. Yang, S. Y., Lin, B. S., and Chang, W. L. (2007). “The analysis and application of biological hydrodynamics on the freshwater snails *Sinotaia quadrata* and *Thiara granifera*.” *Journal of Chinese Soil and Water Conservation*, 38(1):65-76.
98. Yen, B. C. (2002). “Open channel resistance.” *Journal of Hydraulic Engineering*, Vol. 128, No.1, 20-38.
99. Yen, C. L. (2000). *Hydraulic design for high velocity flow report*, Hydrotech Research Institute, National Taiwan University.
100. Young, D. F., Munson, R. B., and Okiishi, H. T. (2004). *A brief introduction to fluid mechanics 3rd ed.*, John Wiley & Sons Inc., New York.
101. 王之佑 (2006), 『藻床淨水技術應用於水中磷之去除研究』, 國立臺灣大學生物環境系統工程學系碩士論文。
102. 本橋 敬之助 (2005), 『水質淨化技術應用在河川以及湖泊沼澤之實例—技術與課題』, 臺日河川水質淨化工法設計及操作維護研討會論文集, 行政院環境保護署與國立臺灣大學生物環境系統工程系。
103. 行政院環境保護署(2005), 『河川水質淨化工法設計研究計畫』, 行政院環境保護署委託國立臺灣大學生物環境系統工程系研究計畫報告。
104. 行政院環境保護署 (2007), 『建立河川水質淨化工法指導原則暨評鑑計畫』, 行政院環境保護署委託國立臺灣大學生物環境系統工程系研究計畫報告。
105. 江恩慧、劉燕 (2007), 『河道整治工程效用及黃河下游遊蕩性河道』, 第九屆海峽兩岸多沙河川整治管理研討會。
106. 尾崎 保夫 (2005), 『利用植物與生物濾床在水路處理家庭污水並循環使用之技術』, 臺日河川水質淨化工法設計及操作維護研討會論文集。
107. 林秉石(2003), 『淡水螺類在不同流速之機械反應作為生態工程之設計』, 國立臺灣大學生物環境系統工程學系碩士論文。
108. 林宣汝(2006), 『彩色質點影像測速法於浸沒植生渠道流場之試驗研究』, 國立交通大學土木工程系所碩士論文。

- 109.林春吉(2005)，『台灣的水生與濕地植物』，綠世界出版社，宜蘭壯圍鄉。
- 110.前臺灣省水利局(1985)，『八掌溪治理規劃報告(上游段)』。
- 111.前臺灣省水利局(1985)，『急水溪治理規劃檢討報告』。
- 112.徐劭涵(2008)，『部分植生渠道之未浸沒植生水理分析』，國立成功大學水利及海洋工程學系碩士論文。
- 113.張乃薇(2006)，『植生渠床之定量緩變速流研究』，國立成功大學水利及海洋工程學系碩士論文。
- 114.張文亮(2007)，『近代河川污水現地處理與在臺灣之落實—以日本現地處理為例』，河川水質淨化工法現地處理生態工程規劃設計講習會，國立臺灣大學生態工程研究中心。
- 115.張文亮(2007)，『濕地生態與工程講義』，國立臺灣大學生物環境系統工程所濕地生態與工程課程。
- 116.許立志、李建堂(2008)，『關渡自然保護區1998—2006年植群變遷之研究』，國際濕地科學家學會第一屆亞洲濕地大會中文論文集，內政部營建署與國際濕地科學家學會127-137。
- 117.陳健志(2002)，『流體動力影響川蝕與石田螺環境適應與吸附行為』，國立臺灣大學生物環境系統工程學系碩士論文。
- 118.陳國誠(2002)，『廢水生物處理學』，國立編譯館，茂昌圖書有限公司。
- 119.陶天麟(2006)，『台灣淡水魚圖鑑』，人人出版股份有限公司，台北縣新店市。
- 120.黃于軒(2005)，『彩色質點影像測速法於植生渠道流場之試驗研究』，國立交通大學土木工程系所碩士論文。
- 121.黃宏斌、游新福(1992)，『植生渠道阻力係數之研究』，台灣水利，第40卷，第4期，50-59。
- 122.黃明興(1993)，『植生倒伏對水流阻力影響之研究』，國立台灣大學

農業工程學研究所碩士論文。

- 123.黃鈞鎰(2008)，『部分植生渠道之浸沒植生水理分析』，國立成功大學水利及海洋工程學系碩士論文。
- 124.楊昇學(2001)，『彩色質點影像測速法於瞬間潰壩流場之試驗研究』，國立交通大學土木工程系所碩士論文。
- 125.楊松岳(2006)，『石田螺、川蜷與瘤蜷的生物力學分析應用於渠道生態工法設計』，國立臺灣大學生物環境系統工程學系博士論文。
- 126.楊遠波、顏聖紘、林仲剛(2001)，『台灣水生植物圖誌』，行政院農業委員會。
- 127.經濟部水利署(2005)，『頭前溪河系情勢調查—第一年期末報告』。
- 128.經濟部水利署(2007)，『八掌溪治理規劃檢討水文分析報告』。
- 129.經濟部水利署(2008)，『中央管河川警戒水位檢訂及訂定(2/2)』。
- 130.經濟部水利署(2007)，『中南東區中央管河川警戒水位檢訂及訂定(2/2)』。
- 131.經濟部水利署(2007)，『東港河流域整體治理規劃檢討』。
- 132.臺北市政府環境保護局(2003)，『影響關渡自然公園生態環境之舊貴子坑溪、水磨坑溪污染整治計畫-期末報告』，財團法人台灣水利環境科技研究發展教育基金會。
- 133.劉治平(2007)，『美國自然水域水質淨化工程之實務案例—水力學與生物系統』，河川水質淨化工法現地處理生態工程規劃設計講習會，國立臺灣大學生態工程研究中心。
- 134.劉誠達(2008)，『水流流經植被區域之阻力研究』，國立交通大學土木工程系所碩士論文。
- 135.環署檢字第 0920061770 號公告(2003)，『水中磷檢測方法—分光光度計/維生素丙法』，NIEA W427.52B，行政院環境保護署環境檢驗所。

Table 2.1 Probability Distribution of length of roots of *Typha angustifolia* L. growing in aquatic farms

Length of Root (cm)	Probability (%)	Product (cm)
1	2.79	0.03
5	13.36	0.67
10	25.36	2.54
15	23.17	3.48
20	17.73	3.55
25	11.17	2.79
30	6.42	1.93
Sum	100.00	<u>14.97</u>

Note: Extracted from notes of wetland ecology and engineering (Chang 2007).

Table 2.2 List of sites of field studies

關渡水磨坑溪人工濕地系統	Guandu Shuimokeng River Constructed Wetland System
關渡貴子坑溪垂直流礫間接觸人工濕地	Guandu Guizikeng River Vertical flow Contact Bed Subsurface Constructed Wetland
枋林北勢溪渡南橋表面流人工濕地	Pinglin Beishi Creek Dunan Bridge Surface Flow Constructed Wetland
金瓜寮溪螢火蟲保護區	Chingualiao Creek Firefly Conservation Zone
南湖地下流人工濕地	Nanhu Subsurface Constructed Wetland
頭前溪表面流人工濕地第一期	Hsinchu Touchien River Surface Flow Constructed Wetland Phase 1
頭前溪表面流人工濕地第二期	Hsinchu Touchien River Surface Flow Constructed Wetland Phase 2
頭前溪表面流人工濕地第三期	Hsinchu Touchien River Surface Flow Constructed Wetland Phase 3
頭前溪表面流人工濕地第五期	Hsinchu Touchien River Surface Flow Constructed Wetland Phase 5
南門溪地下流人工濕地五	Hsinchu Nanmen River Subsurface Flow Constructed Wetland

Table 2.3 Macrophytes under different environmental conditions in the Xin-Hai-Qiao Constructed Wetland, Taipei County

Name of the macrophytes	Rate of growth, r (1/day)	Initial Climax density (stems/m ²)	Period of Rain Strom	R_1	Period of Typhoon	R_2
			sub-climax density 1 (stems/m ²)		sub-climax density 2 (stems/m ²)	
<i>Ludwigia adscendens</i> 水龍	<u>1.67</u>	802	156	0.20	115	0.14
<i>Cyperus imbricatus</i> 覆瓦狀莎草	1.15	831	344	0.41	42	0.05
高野黍	0.60	810	458	0.57	42	0.05
<i>Eleocharis dulcis</i> 荸薺	0.32	825	1688	<u>2.05</u>	146	0.18
<i>Hygrophila pogonocalyx</i> 大安水蓼衣	1.10	128	438	<u>3.42</u>	83	<u>0.65</u>
馬藻	<u>1.54</u>	310	21	0.07	0	0
<i>Torulinium odoratum</i> 斷節莎	0.77	550	229	0.41	0	0
<i>Bacopa monnieri</i> 過長沙	0.79	896	406	0.45	0	0
田字草	1.14	323	188	0.58	208	0.64
<i>Schoenoplectus mucronatus</i> 水毛花	1.35	1741	1406	<u>0.81</u>	229	0.13
<i>Phragmites australis</i> 蘆葦	0.74	382	302	<u>0.79</u>	52	<u>0.14</u>
<i>Cyperus difformis</i> 異花莎草	0.84	906	0	0	0	0
<i>Ludwigia octovalvis</i> 水丁香	1.31	191	313	<u>1.64</u>	0	0
<i>Typha orientalis</i> 香蒲	0.73	168	125	<u>0.74</u>	52	<u>0.31</u>

Note:

1. R_1 is the ratio of plant density after the rainstorm in May and June, to the plant density at the climax in April.
2. R_2 is the ratio of plant density after the Typhoon from July to September, to the plant density at the climax in April.
3. The annual rainfall at the Xing Hai Bridge constructed wetland in 2005 is 3027.8mm

The words in italic represent emergent macrophytes chosen in this research.

Table 2.4 Field study for wetland ecology and engineering in Dunan Bridge surface flow constructed wetland

No.	Title	水溫 water temperature (°C)	pH	導電度 (EC, μS/cm)	溶氧 (DO, mg/L)	濁度 (NTU)
1	尚未完工水池 Pond under construction	22.8	7.00	149.7	5.2	5.49
2	第一期入流水 Phase 1 inflow	25.2	7.04	219.0	8.4	34.60
3	第一期滯留區 Phase 1 detention zone	--	--	--	--	--
4	第一期密植區 Phase 1 densely vegetated zone	25.9	6.87	104.3	6.3	23.80
5	第一期開放水域 Phase 1 open water	--	--	--	--	--
6	第一期植栽濾床 Phase 1 vegetated zone	--	--	--	--	--
7.1	第二期滯留區 I (入流) Phase 2 detention zone one (inflow)	25.4	6.72	128.9	5.2	10.10
7.2	第二期滯留區 I (出流) Phase 2 detention zone one (outflow)	25.4	6.90	106.3	6.9	8.62
8	第二期滯留區 II Phase two detention zone two	25.5	6.86	108.8	4.5	16.60
9	第二期生態池前量水堰 Phase 2 ecological pond measuring weir	25.6	6.68	109.5	4.6	6.96
10.1	第二期生態池 (入流) Phase 2 ecological pond inflow	25.3	6.75	109.6	5.2	7.42
10.2	第二期生態池 (中段) Phase 2 ecological pond mid section	25.5	6.73	109.0	4.7	14.20
10.3	第二期生態池 (出流) Phase 2 ecological pond outflow	25.7	6.70	112.2	5.7	8.86
11	第二期石灰石濾床 Phase 2 limestone zone	--	--	--	--	--
12	第二期礫石濾床 Phase 2 rock bed zone	25.4	7.03	156.8	3.7	3.58
13	第二期出流水 Phase 2 outflow	25.5	6.63	104.2	2.9	6.99
14	地下水溢流口 Groundwater overflow	25.7	6.94	156.2	4.8	8.68

Note: Tests were conducted on 2007/05/17.

Table 2.5 Field study of wetland ecology and engineering in Dunan Bridge
Surface flow constructed wetland: phase two

Flow sequence	No.	Title	水溫 water temperature (°C)	pH	導電度 (EC, μS/cm)	溶氧 (DO, mg/L)	濁度 (NTU)
1	1	尚未完工水池	22.8	7.00	149.7	5.2	5.49
2	7.1	第二期滯留區 I(入流)	25.4	6.72	128.9	5.2	10.10
3	7.2	第二期滯留區 I(出流)	25.4	6.90	106.3	6.9	8.62
4	8	第二期滯留區 II	25.5	6.86	108.8	4.5	16.60
5	9	第二期生態池前量水堰	25.6	6.68	109.5	4.6	6.96
6	10.1	第二期生態池 (入流)	25.3	6.75	109.6	5.2	7.42
7	10.2	第二期生態池 (中段)	25.5	6.73	109.0	4.7	14.20
8	10.3	第二期生態池 (出流)	25.7	6.70	112.2	5.7	8.86
9	12	第二期礫石濾床	25.4	7.03	156.8	3.7	3.58
10	13	第二期出流水	25.5	6.63	104.2	2.9	6.99

Table 2.6 Water quality monitor for treatment units in phase one

Flow sequence	No.	Title	水溫 water temperature (°C)	pH	導電度 (EC, μS/cm)	溶氧 (DO, mg/L)	濁度 (NTU)
1	2	第一期入流水	25.2	7.04	219.0	8.4	34.6
2	4	第一期密植區	25.9	6.87	104.3	6.3	23.8

Table 3.1 Drag force of movable platform for *Phragmites australis* and *Typha orientalis*

Turns	Max Drag (N)
26	9.024
23	7.347
20	4.870
17	3.928
14	1.910

Table 3.2 Drag force of movable platform for *Hygrophila pogonocalyx* and *Juncus effusus*

Turns	Max Drag (N)
20	12.210
17	7.820
14	1.907

Table 3.3 Water level of *Juncus effusus*, *Hygrophila pogonocalyx*, *Typha orientalis*, and *Phragmites australis*

	No. stem/m ²	0.0209 m ³ /s	0.0177 m ³ /s	0.0158 m ³ /s	0.0121 m ³ /s	0.0077 m ³ /s
Juncus effusus	3096.49	4	4.9	<u>3.8</u>	<u>3.4</u>	<u>2.6</u>
	2649.12	4.5	4	<u>3.5</u>	<u>3.15</u>	<u>3</u>
	2035.09	4.4	4.15	<u>4.15</u>	<u>3.3</u>	<u>2.6</u>
	1500	4.25	4.15	<u>3.95</u>	<u>3.3</u>	<u>2.4</u>
Hygrophila pogonocalyx	131.58	4.45	3.85	<u>3.6</u>	<u>3.15</u>	<u>2.45</u>
	114.04	~	~	<u>3.55</u>	<u>3.1</u>	<u>2.3</u>
	87.72	~	~	<u>3.85</u>	<u>3.05</u>	<u>2.4</u>
	70.18	~	~	<u>4</u>	<u>2.65</u>	<u>2.25</u>
Typha orientalis	2315.79	<u>5.05</u>	<u>4.35</u>	<u>4.1</u>	<u>3.6</u>	<u>2.5</u>
	2122.81	<u>4.5</u>	<u>4.35</u>	<u>3.8</u>	<u>3.5</u>	<u>2.5</u>
	1771.93	<u>4.05</u>	<u>3.85</u>	<u>3.6</u>	<u>3.5</u>	<u>2.5</u>
	1114.04	<u>3.95</u>	<u>4.05</u>	<u>3.7</u>	<u>3.3</u>	<u>2.5</u>
Phragmites australis	1552.63	<u>4.1</u>	<u>3.575</u>	<u>3.325</u>	<u>2.75</u>	<u>2.3</u>
	1350.88	<u>4.1</u>	<u>3.3</u>	<u>3.35</u>	<u>2.4</u>	<u>2</u>
	1052.63	<u>4.05</u>	<u>3.25</u>	<u>3.3</u>	<u>2.6</u>	<u>2.15</u>
	719.30	<u>4.15</u>	<u>4.1</u>	<u>4</u>	<u>3.85</u>	<u>2.3</u>

Table 3.4 Average stream velocity of *Juncus effusus*, *Hygrohila pogonocalyx*, *Typha orientalis*, and *Phragmites australis*

	No. stem/m ²	0.0209 m ³ /s	0.0177 m ³ /s	0.0158 m ³ /s	0.0121 m ³ /s	0.0077 m ³ /s
Juncus effusus	3096.49	~	~	0.692	0.594	0.490
	2649.12	~	~	0.751	0.642	0.425
	2035.09	~	~	0.633	0.612	0.490
	1500	~	~	0.665	0.612	0.531
Hygrohila pogonocalyx	131.58	~	~	0.730	0.642	0.520
	114.04	~	~	0.740	0.652	0.554
	87.72	-	~	0.683	0.663	0.531
	70.18	~	~	0.657	0.763	0.566
Typha orientalis	2315.79	~	0.680	0.641	0.561	0.510
	2122.81	~	0.680	0.692	0.577	0.510
	1771.93	~	0.768	0.730	0.577	0.510
	1114.04	~	0.730	0.710	0.612	0.510
Phragmites australis	1552.63	0.850	0.827	0.791	0.735	0.554
	1350.88	0.850	0.896	0.785	0.842	0.637
	1052.63	0.861	0.910	0.797	0.777	0.593
	719.30	0.840	0.721	0.657	0.525	0.554

Table 3.5 Drag force of *Typha orientalis*

	0.0177 m³/s	0.0158 m³/s	0.0121 m³/s	0.0077 m³/s
2315.79 stems/m²	17.15	18.22	13.86	9.75
	20.00	16.00	13.12	9.65
	18.31	15.88	12.63	9.89
2122.81 stems/m²	15.08	13.71	12.28	9.25
	16.72	14.04	12.38	8.62
	16.77	13.95	12.06	8.86
1771.93 stems/m²	12.54	12.13	11.98	8.19
	14.92	13.14	10.73	8.44
	13.79	12.79	11.02	8.51
1114.04 stems/m²	8.51	9.41	8.95	7.71
	8.34	9.06	8.34	7.71
	8.08	9.00	7.93	7.41

Table 3.6 Drag force of *Pragmites australis*

	0.0209 m³/s	0.0177 m³/s	0.0158 m³/s	0.0121 m³/s	0.0077 m³/s
1522.63 stems/ m²	8.963	9.39	11.437	10.86	8.777
	8.583	10.3	11.437	10.62	8.837
	7.123	9.73	10.937	10.7	8.737
1350.88 stems/ m²	6.043	8.72	9.997	9.3	7.877
	5.923	8.96	9.927	9.26	7.877
	5.793	8.41	9.937	9.16	7.757
1052.63 stems/ m²	5.273	7.97	9.267	9.05	7.597
	3.643	7.14	9.157	9.19	8.037
	3.793	6.85	8.787	8.92	8.127
719.30 stems/ m²	4.793	6.07	7.977	7.25	7.277
	4.043	5.85	7.827	6.74	7.187
	4.153	5.72	7.907	6.91	7.377

Table 3.7 Drag force of *Hygrophila pogonocalyx*

	0.0177 m³/s	0.0158 m³/s	0.0121 m³/s	0.0077 m³/s
131.58 stems/ m²	4.61	10.71	9.23	10.67
	3.07	10.45	8.29	10.86
	2.30	10.45	9.16	10.27
114.04 stems/ m²	2.84	10.49	8.48	7.99
	2.77	6.91	7.59	8.49
	~	8.92	7.58	8.46
87.72 stems/ m²	2.20	5.71	6.78	7.96
	~	5.43	7.38	7.61
	~	5.16	7.12	7.77
70.18 stems/ m²	-0.44	2.38	3.13	7.49
	~	4.34	3.70	7.34
	~	0.59	2.96	7.46

Table 3.8 Drag force of *Juncus effusus*

	0.0158 m³/s	0.0121 m³/s	0.0077 m³/s
3096.49 stems/ m²	13.43	15.77	8.87
2649.12 stems/ m²	12.95	11.48	10.45
2035.09 stems/ m²	10.51	10.58	10.44
1500.00 stems/ m²	7.94	8.15	7.85

Table 3.9 Drag coefficient (C_d) of *Phragmites australis*

	0.0209 m³/s	0.0177 m³/s	0.0158 m³/s	0.0121 m³/s	0.0077 m³/s
1522.63 stems/ m²	1.759	2.347	3.059	4.409	7.541
	1.685	2.575	3.059	4.312	7.593
	1.398	2.432	2.925	4.344	7.507
1350.88 stems/ m²	1.613	2.371	3.910	3.616	5.774
	1.580	2.436	3.883	3.601	5.774
	1.546	2.286	3.887	3.562	5.686
1052.63 stems/ m²	1.498	2.408	3.953	4.519	7.948
	1.035	2.158	3.906	4.589	8.409
	1.078	2.070	3.748	4.454	8.503
719.30 stems/ m²	1.693	2.914	4.609	6.730	8.913
	1.428	2.808	4.522	6.256	8.803
	1.467	2.746	4.568	6.414	9.035

Table 3.10 Drag coefficient (C_d) of *Typha orientalis*

	0.0177 m³/s	0.0158 m³/s	0.0121 m³/s	0.0077 m³/s
2315.79 stems/ m²	4.554	6.210	6.463	6.174
	5.311	15.454	6.118	6.111
	4.862	5.413	5.889	6.263
2122.81 stems/ m²	4.110	3.725	5.355	5.604
	4.556	3.815	5.398	5.222
	4.570	3.791	5.259	5.368
1771.93 stems/ m²	2.609	3.421	5.815	5.527
	3.104	3.706	5.209	5.696
	2.869	3.607	5.349	5.743
1114.04 stems/ m²	2.413	4.082	5.562	7.082
	2.365	3.930	5.183	7.082
	2.291	3.904	4.928	6.807

Table 3.11 Drag coefficient (C_d) of *Hygrophila pogonocalyx*

	0.0177 m³/s	0.0158 m³/s	0.0121 m³/s	0.0077 m³/s
131.58 stems/ m²	2.682	7.519	9.352	21.257
	1.786	7.337	8.399	21.636
	1.337	7.337	9.281	20.460
114.04 stems/ m²	~	8.325	10.326	16.907
	~	5.483	9.242	17.965
	~	7.079	9.230	17.902
87.72 stems/ m²	~	7.622	10.523	22.946
	~	7.248	11.455	21.937
	~	6.887	11.051	22.398
70.18 stems/ m²	~	3.772	5.340	28.821
	~	6.882	6.313	28.243
	~	0.931	5.049	28.705

Table 3.12 Drag coefficient (C_d) of *Juncus effusus*

	0.0158 m³/s	0.0121 m³/s	0.0077 m³/s
3096.49 stems/ m²	4.922	8.823	9.388
2649.12 stems/ m²	4.723	6.069	13.752
2035.09 stems/ m²	5.266	7.034	13.546
1500.00 stems/ m²	4.251	6.088	10.599

Table 3.13 Reynolds numbers (Re) of *Pragmites australis*

	0.0209 m³/s	0.0177 m³/s	0.0158 m³/s	0.0121 m³/s	0.0077 m³/s
1522.63 stems/ m²	1965.749	1693.262	1516.802	1186.679	758.764
	1965.749	1693.262	1516.802	1186.679	758.764
	1965.749	1693.262	1516.802	1186.679	758.764
1350.88 stems/ m²	1965.749	1707.246	1515.665	1199.498	765.877
	1965.749	1707.246	1515.665	1199.498	765.877
	1965.749	1707.246	1515.665	1199.498	765.877
1052.63 stems/ m²	1968.636	1709.813	1517.941	1192.140	762.304
	1968.636	1709.813	1517.941	1192.140	762.304
	1968.636	1709.813	1517.941	1192.140	762.304
719.30 stems/ m²	1962.871	1667.193	1486.689	1148.117	758.764
	1962.871	1667.193	1486.689	1148.117	758.764
	1962.871	1667.193	1486.689	1148.117	758.764

Table 3.14 Froude number (Fr) of *Pragmites australis*

	0.0209 m³/s	0.0177 m³/s	0.0158 m³/s	0.0121 m³/s	0.0077 m³/s
1522.63 stems/ m²	0.018	0.019	0.019	0.020	0.014
	0.018	0.019	0.019	0.020	0.014
	0.018	0.019	0.019	0.020	0.014
1350.88 stems/ m²	0.018	0.025	0.019	0.030	0.021
	0.018	0.025	0.019	0.030	0.021
	0.018	0.025	0.019	0.030	0.021
1052.63 stems/ m²	0.019	0.026	0.020	0.024	0.017
	0.019	0.026	0.020	0.024	0.017
	0.019	0.026	0.020	0.024	0.017
719.30 stems/ m²	0.017	0.013	0.011	0.007	0.014
	0.017	0.013	0.011	0.007	0.014
	0.017	0.013	0.011	0.007	0.014

Table 3.15 Ratio of average plant stem height to water level (h_p/y_n) of *Pragmites australis*

	0.0209 m³/s	0.0177 m³/s	0.0158 m³/s	0.0121 m³/s	0.0077 m³/s
1522.63 stems/ m²	0.122	0.140	0.150	0.182	0.217
	0.122	0.140	0.150	0.182	0.217
	0.122	0.140	0.150	0.182	0.217
1350.88 stems/ m²	0.122	0.151	0.149	0.208	0.250
	0.122	0.151	0.149	0.208	0.250
	0.122	0.151	0.149	0.208	0.250
1052.63 stems/ m²	0.123	0.154	0.151	0.192	0.232
	0.123	0.154	0.151	0.192	0.232
	0.123	0.154	0.151	0.192	0.232
719.30 stems/ m²	0.120	0.122	0.125	0.130	0.217
	0.120	0.122	0.125	0.130	0.217
	0.120	0.122	0.125	0.130	0.217

Table 3.16 Ratio of average stem spacing to water level (S_p/y_n) of *Pragmites australis*

	0.0209 m³/s	0.0177 m³/s	0.0158 m³/s	0.0121 m³/s	0.0077 m³/s
1522.63 stems/ m²	0.006	0.006	0.007	0.008	0.010
	0.006	0.006	0.007	0.008	0.010
	0.006	0.006	0.007	0.008	0.010
1350.88 stems/ m²	0.006	0.007	0.007	0.010	0.012
	0.006	0.007	0.007	0.010	0.012
	0.006	0.007	0.007	0.010	0.012
1052.63 stems/ m²	0.007	0.009	0.008	0.011	0.013
	0.007	0.009	0.008	0.011	0.013
	0.007	0.009	0.008	0.011	0.013
719.30 stems/ m²	0.008	0.008	0.009	0.009	0.015
	0.008	0.008	0.009	0.009	0.015
	0.008	0.008	0.009	0.009	0.015

Table 3.17 Ratio of plant projected frontal area to vegetated channel bed area (A_p/a) of *Pragmites australis*

	0.0209 m³/s	0.0177 m³/s	0.0158 m³/s	0.0121 m³/s	0.0077 m³/s
1522.63 stems/ m²	0.124	0.103	0.105	0.080	0.067
	0.124	0.103	0.105	0.080	0.067
	0.124	0.103	0.105	0.080	0.067
1350.88 stems/ m²	0.091	0.080	0.073	0.064	0.059
	0.091	0.080	0.073	0.064	0.059
	0.091	0.080	0.073	0.064	0.059
1052.63 stems/ m²	0.083	0.070	0.065	0.058	0.048
	0.083	0.070	0.065	0.058	0.048
	0.083	0.070	0.065	0.058	0.048
719.30 stems/ m²	0.070	0.070	0.070	0.069	0.047
	0.070	0.070	0.070	0.069	0.047
	0.070	0.070	0.070	0.069	0.047

Table 3.18 Ratio of fluid drag to plant rigidity ($\rho V^2 h_p^4 / (GI)$) of *Pragmites australis*

	0.0209 m³/s	0.0177 m³/s	0.0158 m³/s	0.0121 m³/s	0.0077 m³/s
1522.63 stems/ m²	23021095.810	21779975.649	19904162.901	17200971.498	9778939.378
	23021095.810	21779975.649	19904162.901	17200971.498	9778939.378
	23021095.810	21779975.649	19904162.901	17200971.498	9778939.378
1350.88 stems/ m²	23021095.810	25561221.421	19608194.340	22583740.790	12932647.328
	23021095.810	25561221.421	19608194.340	22583740.790	12932647.328
	23021095.810	25561221.421	19608194.340	22583740.790	12932647.328
1052.63 stems/ m²	23593043.160	26353770.535	20206883.469	19242950.732	11191041.495
	23593043.160	26353770.535	20206883.469	19242950.732	11191041.495
	23593043.160	26353770.535	20206883.469	19242950.732	11191041.495
719.30 stems/ m²	22469724.169	16559292.164	13753310.061	8776005.866	9778939.378
	22469724.169	16559292.164	13753310.061	8776005.866	9778939.378
	22469724.169	16559292.164	13753310.061	8776005.866	9778939.378

Table 3.19 Dimensionless streamline coefficient ($C_d A_p h / \nabla$) of *Pragmites australis*

	0.0209 m³/s	0.0177 m³/s	0.0158 m³/s	0.0121 m³/s	0.0077 m³/s
1522.63 stems/ m²	0.027	0.034	0.048	0.064	0.109
	0.025	0.037	0.048	0.063	0.110
	0.021	0.035	0.046	0.063	0.108
1350.88 stems/ m²	0.018	0.029	0.042	0.048	0.085
	0.018	0.030	0.042	0.048	0.085
	0.017	0.028	0.042	0.047	0.084
1052.63 stems/ m²	0.015	0.026	0.039	0.050	0.088
	0.011	0.023	0.038	0.051	0.093
	0.011	0.022	0.037	0.050	0.094
719.30 stems/ m²	0.014	0.025	0.040	0.060	0.090
	0.012	0.024	0.040	0.056	0.089
	0.012	0.024	0.040	0.057	0.092

Table 3.20 Streamline factor ($C_d A_p$) of *Phragmites australis*

	0.0209 m³/s	0.0177 m³/s	0.0158 m³/s	0.0121 m³/s	0.0077 m³/s
1522.63 stems/ m²	0.025	0.027	0.037	0.040	0.057
	0.024	0.030	0.037	0.039	0.058
	0.020	0.028	0.035	0.040	0.057
1350.88 stems/ m²	0.017	0.022	0.032	0.026	0.039
	0.016	0.022	0.032	0.026	0.039
	0.016	0.021	0.032	0.026	0.038
1052.63 stems/ m²	0.014	0.019	0.029	0.030	0.043
	0.010	0.017	0.029	0.030	0.046
	0.010	0.017	0.028	0.030	0.046
719.30 stems/ m²	0.014	0.023	0.037	0.053	0.047
	0.011	0.023	0.036	0.049	0.047
	0.012	0.022	0.037	0.050	0.048

Table 3.21 Drag coefficient (C_d) of *Phragmites australis*

	0.0209 m³/s	0.0177 m³/s	0.0158 m³/s	0.0121 m³/s	0.0077 m³/s
1522.63 stems/ m²	1.759	2.347	3.059	4.409	7.541
	1.685	2.575	3.059	4.312	7.593
	1.398	2.432	2.925	4.344	7.507
1350.88 stems/ m²	1.613	2.371	3.910	3.616	5.774
	1.580	2.436	3.883	3.601	5.774
	1.546	2.286	3.887	3.562	5.686
1052.63 stems/ m²	1.498	2.408	3.953	4.519	7.948
	1.035	2.158	3.906	4.589	8.409
	1.078	2.070	3.748	4.454	8.503
719.30 stems/ m²	1.693	2.914	4.609	6.730	8.913
	1.428	2.808	4.522	6.256	8.803
	1.467	2.746	4.568	6.414	9.035

Table 3.22 Manning's n of Phragmites australis

	0.0209 m³/s	0.0177 m³/s	0.0158 m³/s	0.0121 m³/s	0.0077 m³/s	~
1522.63 stems/ m²	0.061	0.062	0.071	0.073	0.084	~
	0.059	0.065	0.071	0.072	0.085	~
	0.054	0.064	0.070	0.072	0.084	~
1350.88 stems/ m²	0.050	0.055	0.067	0.057	0.068	~
	0.049	0.056	0.067	0.057	0.068	~
	0.049	0.054	0.067	0.057	0.067	~
1052.63 stems/ m²	0.046	0.052	0.064	0.062	0.073	~
	<u>0.038</u>	0.049	0.063	0.063	0.075	~
	0.039	0.048	0.062	0.062	0.075	~
719.30 stems/m²	0.045	0.059	0.074	<u>0.087</u>	0.077	~
	0.041	0.058	0.073	0.084	0.076	~
	0.042	0.057	0.073	0.085	0.077	~
Max.	0.061	0.065	0.074	<u>0.087</u>	0.085	<u>0.087</u>
Min.	<u>0.038</u>	0.048	0.062	0.057	0.067	<u>0.038</u>

Table 3.23 Manning's n of *Typha orientalis*

	0.0177 m³/s	0.0158 m³/s	0.0121 m³/s	0.0077 m³/s	~
2315.79 stems/m²	0.099	<u>0.112</u>	0.106	0.065	~
	0.107	0.105	0.103	0.065	~
	0.102	0.104	0.101	0.066	~
2122.81 stems/m²	0.098	0.086	0.098	0.082	~
	0.103	0.087	0.098	0.079	~
	0.103	0.087	0.097	0.080	~
1771.93 stems/m²	0.071	0.078	0.097	0.081	~
	0.077	0.081	0.092	0.082	~
	0.074	0.080	0.093	0.082	~
1114.04 stems/m²	0.057	0.071	0.080	0.076	~
	0.056	0.070	0.078	0.076	~
	<u>0.056</u>	0.069	0.076	0.074	~
Max.	0.107	<u>0.112</u>	0.106	0.082	<u>0.112</u>
Min.	<u>0.056</u>	0.069	0.076	0.065	<u>0.056</u>

Table 3.24 Manning's n of *Hygrophila pogonocalyx*

	0.0177 m³/s	0.0158 m³/s	0.0121 m³/s	0.0077 m³/s	~
131.58 stems/m²	0.048	0.076	0.078	0.100	~
	0.039	0.075	0.074	<u>0.101</u>	~
	0.034	0.075	0.078	0.098	~
114.04 stems/m²	~	0.074	0.074	0.080	~
	~	0.060	0.070	0.083	~
	~	0.068	0.070	0.083	~
87.72 stems/m²	~	0.060	0.065	0.084	~
	~	0.058	0.067	0.082	~
	~	0.057	0.066	0.083	~
70.18 stems/m²	~	0.040	0.037	0.076	~
	~	0.054	0.041	0.075	~
	~	<u>0.020</u>	0.036	0.076	~
Max.	0.048	0.076	0.078	<u>0.101</u>	<u>0.101</u>
Min.	0.034	<u>0.020</u>	0.036	0.075	<u>0.020</u>

Table 3.25 Manning's n of *Juncus effusus*

	0.0158 m³/s	0.0121 m³/s	0.0077 m³/s	~
3096.49 stems/m²	0.090	0.112	0.098	~
2649.12 stems/m²	0.080	0.087	0.125	~
2035.09 stems/m²	0.088	0.088	0.106	~
1500.00 stems/m²	0.072	0.078	0.084	~
Max.	<u>0.125</u>	0.090	0.112	<u>0.125</u>
Min.	<u>0.084</u>	0.072	0.078	<u>0.084</u>

Table 3.26 Standard Manning's n

		Min. Manning's n	Max. Manning's n
Vegetation	Low	0.005	0.010
	Medium	0.010	0.025
	High	0.025	0.050
	Very high	0.050	0.100
Flood Plains	Pastures, no brush	~	~
	short grass	0.025	0.035
	High grass	0.030	0.050
	Cultivated areas	~	~
	No crop	0.020	0.040
	Mature row crops	0.025	0.045
	Mature field crops	0.030	0.050
	Brush	~	~
	Scattered brush, heavy weeds	0.035	0.070
	Light brush and trees in winter	0.035	0.060
	Light brush and trees in summer	0.040	0.080
	Medium to dense brush in summer	0.045	0.110
	Medium to dense brush in winter	0.070	0.160

Note: Extracted from Open-channel hydraulics (Chow 1959)

Table 3.27 Results of multiple regression analysis for Phragmites australis and Typha orientalis

	Drag Force (F_d)				Drag Coefficient (C_d)			
	Regression Model	R^2	Adj. R^2	$Pr > t $	Regression Model	R^2	Adj. R^2	$Pr > t $
Phragmites australis	$F_d=5.73890+0.00382(\rho_p)-145.01688(Q)$	0.5108	0.4936	1~2	$C_d=14.47464-0.00151(\rho_p)-761.94007(Q)+10815(Q)^2$	0.9110	0.9062	2~3
	$F_d=-4.76239+0.00382(\rho_p)+1516.25102(Q)-58654(Q)^2$	0.8523	0.8444	3~3		~	~	~
	$F_d=-1.16651-0.00316(\rho_p)+0.00000313(\rho_p)^2+1516.25102(Q)-58654(Q)^2$	0.8652	0.8554	2~4		~	~	~
Typha orientalis	$F_d=-4.39144+0.00489(\rho_p)+543.74662(Q)$	0.8476	0.8409	2~2	$C_d=8.13945-245.26068(Q)$	0.5699	0.5606	1~1
	$F_d=-5.13669+0.00489(\rho_p)+674.44624(Q)-5180.16571(Q)^2$	0.8479	0.8376	1~3	$C_d=4.00926+0.00068687(\rho_p)+258.49709(Q)-19966(Q)^2$	0.6628	0.6398	0~3
	$\log F_d =1.05492+0.00042284(\rho_p)+45.12694(Q)$	0.8861	0.881	2~2	$C_d =10.76273-0.00798(\rho_p) + 0.00000256(\rho_p)^2 + 258.49709(Q)-19966(Q)^2$	0.7552	0.7324	0~4
	~	~	~	~	$\log C_d=2.41531-0.00156(\rho_p)+5.186166E-7(\rho_p)^2+97.95428(Q)-6048.24286(Q)^2$	0.737	0.7125	0~4

Note: Drag force (F_d) and drag coefficient (C_d) as dependent variables; plant density (ρ_p) and flow (Q) as independent variables.

Table 3.28 Results of multiple regression analysis for *Hygrophila pogonocalyx* and *Juncus effusus*

	Drag Force (F_d)				Drag Coefficient (C_d)			
	Regression Model	R^2	Adj. R^2	$Pr > t $	Regression Model	R^2	Adj. R^2	$Pr > t $
Hygrophila pogonocalyx	$F_d=5.19690+0.06996(\rho_p)-448.32120(Q)$	0.5887	0.5676	2~2	$C_d=36.88943-0.00971(\rho_p)-1964.91560(Q)$	0.8024	0.7915	1~2
	$\log F_d=1.62287+0.01287(\rho_p)-92.97447(Q)$	0.5037	0.4782	3~3	$C_d=61.45588-6593.43142(Q)+191297(Q)^2$	0.8571	0.8492	1~2
	$F_d=-4.56314+0.07479(\rho_p)+1210.31651(Q)-67457(Q)^2$	0.6493	0.6216	1~3	$\log C_d=4.40447+0.00167(\rho_p)-193.61089(Q)$	0.7241	0.7088	1~2
	$F_d=-11.93063+0.21702(\rho_p)-0.00069169(\rho_p)^2+1297.56535(Q)-71410(Q)^2$	0.6993	0.6676	0~4	$\log C_d=4.01926-94.52917(Q)-4033.68563(Q)^2$	0.7241	0.7087	0~2
Juncus effusus	$F_d=1.41136+0.00282(\rho_p)+231.37319(Q)$	0.6518	0.5744	0~2	$C_d=17.43088+0.00033940(\rho_p)-873.31641(Q)$	0.825	0.7861	0~2
	$F_d=-6.95302+0.00282(\rho_p)+1796.46241(Q)-67225(Q)^2$	0.7013	0.5893	0~3	$C_d=7.08412+0.00033940(\rho_p)$	0.0041	-0.0955	0~1
	$F_d=-12.72821+0.00823(\rho_p)-0.00000118(\rho_p)^2+1796.46241(Q)-67225(Q)^2$	0.7203	0.5604	0~4	$C_d=24.61039+0.00033940(\rho_p)-2216.70163(Q)+57702(Q)^2$	0.8442	0.7858	0~3
	$\log F_d=1.49700+0.00026110(\rho_p)+20.68311(Q)$	0.6680	0.5943	0~2	$C_d=14.95599+0.00938(\rho_p)-0.00000197(\rho_p)^2-2216.70163(Q)+57702(Q)^2$	0.872	0.7988	0~4
	$F_d=4.15259+0.00282(\rho_p)$	0.5420	0.4962	0~2	$\log C_d=3.15606+0.00005798(\rho_p)-110.20316(Q)$	0.8852	0.8597	1~2

Note: Drag force (F_d) and drag coefficient (C_d) as dependent variables; plant density (ρ_p) and flow (Q) as independent variables.

Table 3.29 Summary statistics of Model 1

Statistical analysis for Model 1

The REG Procedure	
Model: MODEL1	
Dependent Variable: y2	
Number of Observations Read	60
Number of Observations Used	60

Analysis of Variance					
Source	<i>DF</i> *	Sum of Squares	Mean Square	<i>F</i> Value	<i>Pr</i> > <i>F</i>
Model	4	21.89	5.473	248.55	<.0001
Error	55	1.21	0.022	~	~
Corrected Total	59	23.10	~	~	~

Root MSE	0.148	<i>R</i> -Square	0.948
Dependent Mean	1.370	Adj. <i>R</i> -Sq	0.944
Coeff. Var.	10.832	~	~

Parameter Estimates					
Variable	<i>DF</i> *	Parameter Estimate	Standard Error	<i>t</i> Value	<i>Pr</i> > <i>t</i>
Intercept	1	309.02	37.82	8.17	<.0001
<i>X</i> 3	1	-0.84	0.15	-5.57	<.0001
<i>X</i> 6	1	79.39	10.30	7.71	<.0001
<i>X</i> 2	1	-43.90	5.70	-7.70	<.0001
<i>X</i> 1	1	85.20	11.37	7.49	<.0001

* *DF* stands for degree of freedom.

Table 3.30 Summary statistics of Model 2 Part 1

Dependent Variable: Y1	
Number of Observations Read	61
Number of Observations Used	61

Analysis of Variance					
Source	<i>DF</i> *	Sum of Squares	Mean Square	<i>F</i> Value	<i>Pr</i> > <i>F</i>
Model	5	19.52	3.905	188.35	<.0001
Error	55	1.14	0.021	~	~
Corrected Total	60	20.66	~	~	~

Root MSE	0.144	<i>R</i> -Square	0.945
Dependent Mean	1.221	Adj <i>R</i> -Sq	0.940
Coeff. Var.	11.791	~	~

Parameter Estimates					
Variable	<i>DF</i> *	Parameter Estimate	Standard Error	<i>t</i> Value	<i>Pr</i> > <i>t</i>
Intercept	1	-100.97	14.81	-6.82	<.0001
<i>X</i> 5	1	-0.34	0.26	-1.33	0.1887
<i>X</i> 4	1	79.77	9.99	7.98	<.0001
<i>X</i> 3	1	-0.11	0.34	-0.31	0.7542
<i>X</i> 2	1	-44.71	5.54	-8.07	<.0001
<i>X</i> 1	1	86.91	11.05	7.87	<.0001

* *DF* stands for degree of freedom.

Table 3.31 Summary statistics of Model 2 Part 2

Model: MODEL1	
Dependent Variable: <i>YI</i>	
Number of Observations Read	61
Number of Observations Used	61

Analysis of Variance					
Source	<i>DF</i> *	Sum of Squares	Mean Square	<i>F</i> Value	<i>Pr</i> > <i>F</i>
Model	3	19.39	6.465	290.44	<.0001
Error	57	1.27	0.022	~	~
Corrected Total	60	20.66	~	~	~

Root MSE	0.149	<i>R</i> -Square	0.939
Dependent Mean	1.221	Adj. <i>R</i> -Sq	0.935
Coeff. Var.	12.218	~	~

Parameter Estimates					
Variable	<i>DF</i> *	Parameter Estimate	Standard Error	<i>t</i> Value	<i>Pr</i> > <i>t</i>
Intercept	1	-99.66	15.07	-6.61	<.0001
<i>X4</i>	1	80.04	10.16	7.88	<.0001
<i>X2</i>	1	-44.86	5.63	-7.97	<.0001
<i>X1</i>	1	87.09	11.20	7.77	<.0001

* *DF* stands for degree of freedom.

Table 3.32 Summary of R^2 of Model 1

Model 1 Dependent Variable: $\ln(C_d A_p h_p / \nabla)$			
R^2	0.948	Adj. R^2	0.944
Variables	<i>U.L.R.*</i>	<i>M.L.R.**</i>	
	R^2	Coefficients	$Pr > t $
Intercept	~	309.02	<.0001
$\ln(s_p/y_n)$	0.473	-0.84	<.0001
$\ln(d_s/y_n)$	0.671	79.39	<.0001
$\ln(\rho V^2 h_p / G_p)$	0.569	-43.90	<.0001
$\ln(\rho VR/\mu) = \ln(Re)$	0.850	85.20	<.0001

**U.L.R.* = Univariate Linear Regression

***M.L.R.* = Multiple Linear Regression

Table 3.33 Summary of R^2 of Model 2 Part 1

Model 2 Part 1 Dependent Variable: $\ln(C_d)$			
R^2	0.948	Adj. R^2	0.944
Variables	<i>U.L.R.*</i>	<i>M.L.R.**</i>	
	R^2	Coefficients	R^2
Intercept	~	-100.97	<.0001
$\ln(A_p/a)$	0.497	-0.34	0.1887
$\ln(h_p/y_n)$	0.533	79.77	<.0001
$\ln(s_p/y_n)$	0.628	-0.11	0.7542
$\ln(\rho V^2 h_p / G_p)$	0.725	-44.71	<.0001
$\ln(\rho VR/\mu) = \ln(Re)$	0.834	86.91	<.0001

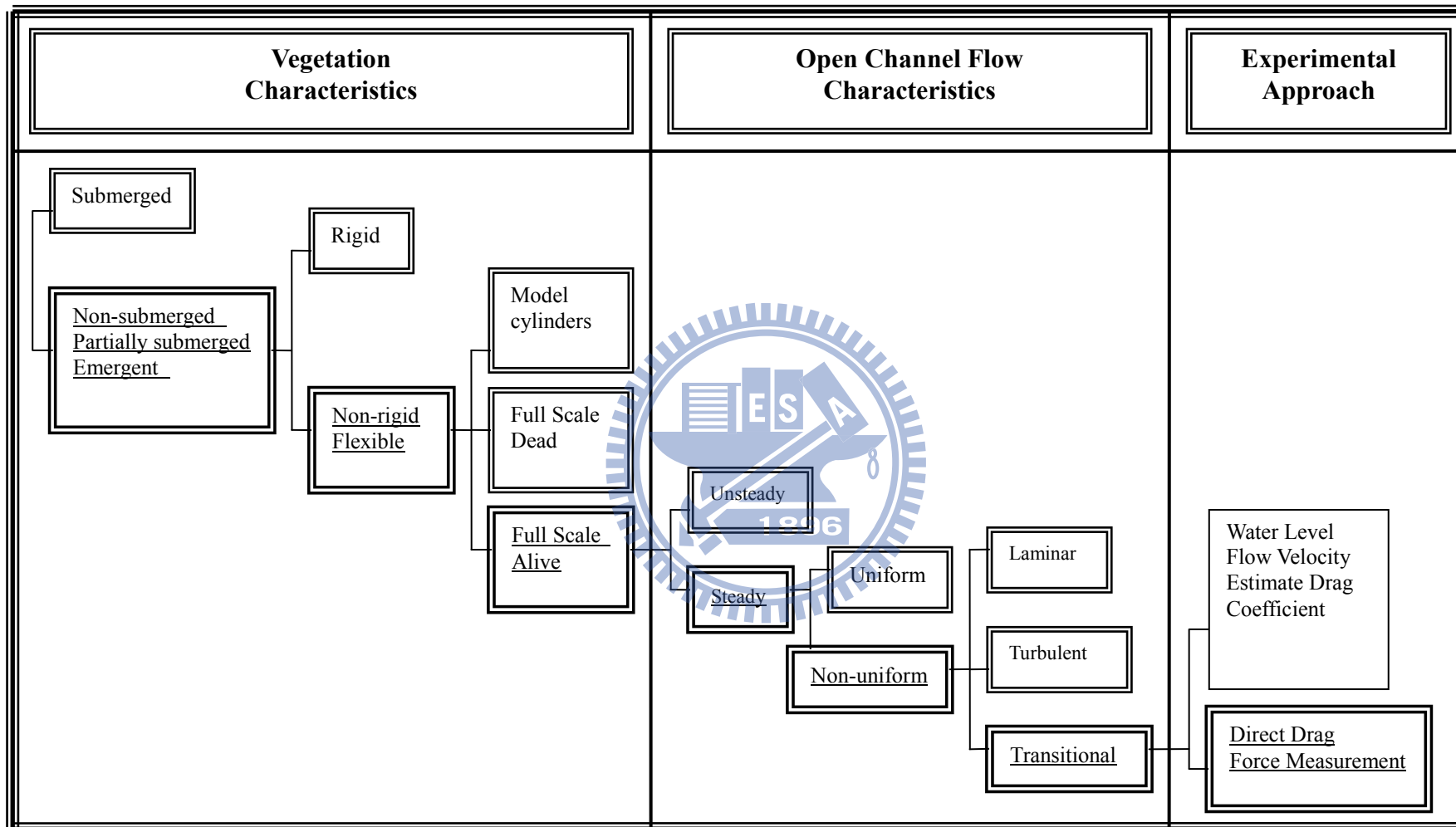
Table 3.34 Summary of R^2 of Model 2 Part 2

Model 1 Part 2 Dependent Variable: $\ln(C_d)$			
R^2	0.948	Adj. R^2	0.944
Variables	<i>U.L.R.*</i>	<i>M.L.R.**</i>	
	R^2	Coefficients	R^2
Intercept	~	-99.66	<.0001
$\ln(h_p/y_n)$	0.533	80.04	<.0001
$\ln(\rho V^2 h_p / G_p)$	0.725	-44.86	<.0001
$\ln(\rho VR / \mu) = \ln(Re)$	0.834	87.09	<.0001

* *U.L.R.* = Univariate Linear Regression

** *M.L.R.* = Multiple Linear Regression





Note: The underlined words are the design considerations for the experiments carried out in this research for *Phragmites australis*.
 Figure 1.1 Research conceptual plan

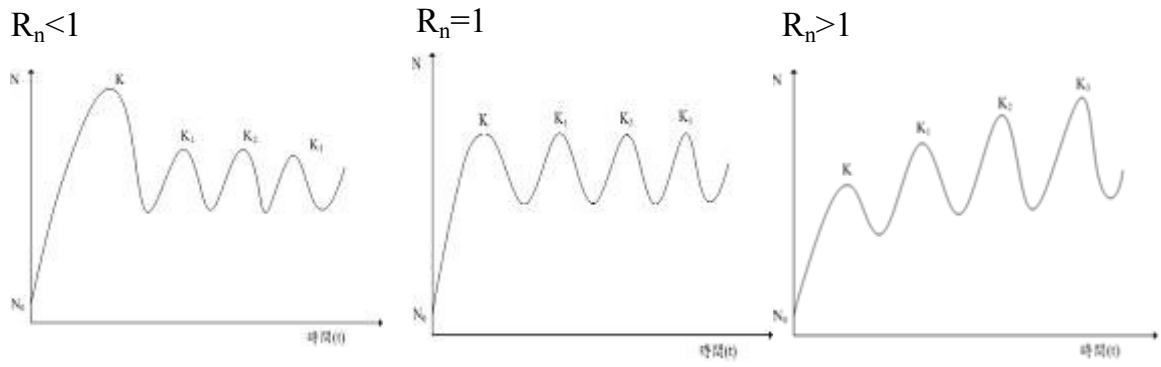


Figure 2.1 Plant density versus Time for three different ratios of plant capacities

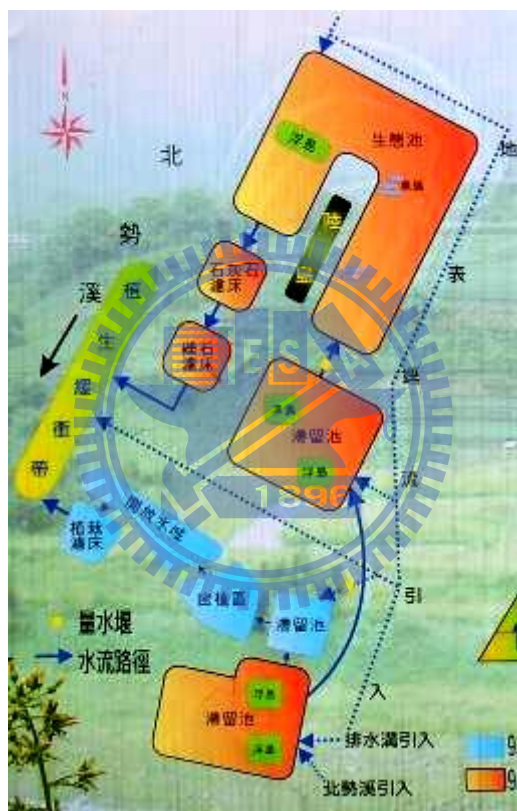


Figure 2.2 Flow paths of the Du Nan Qiao surface flow constructed wetland

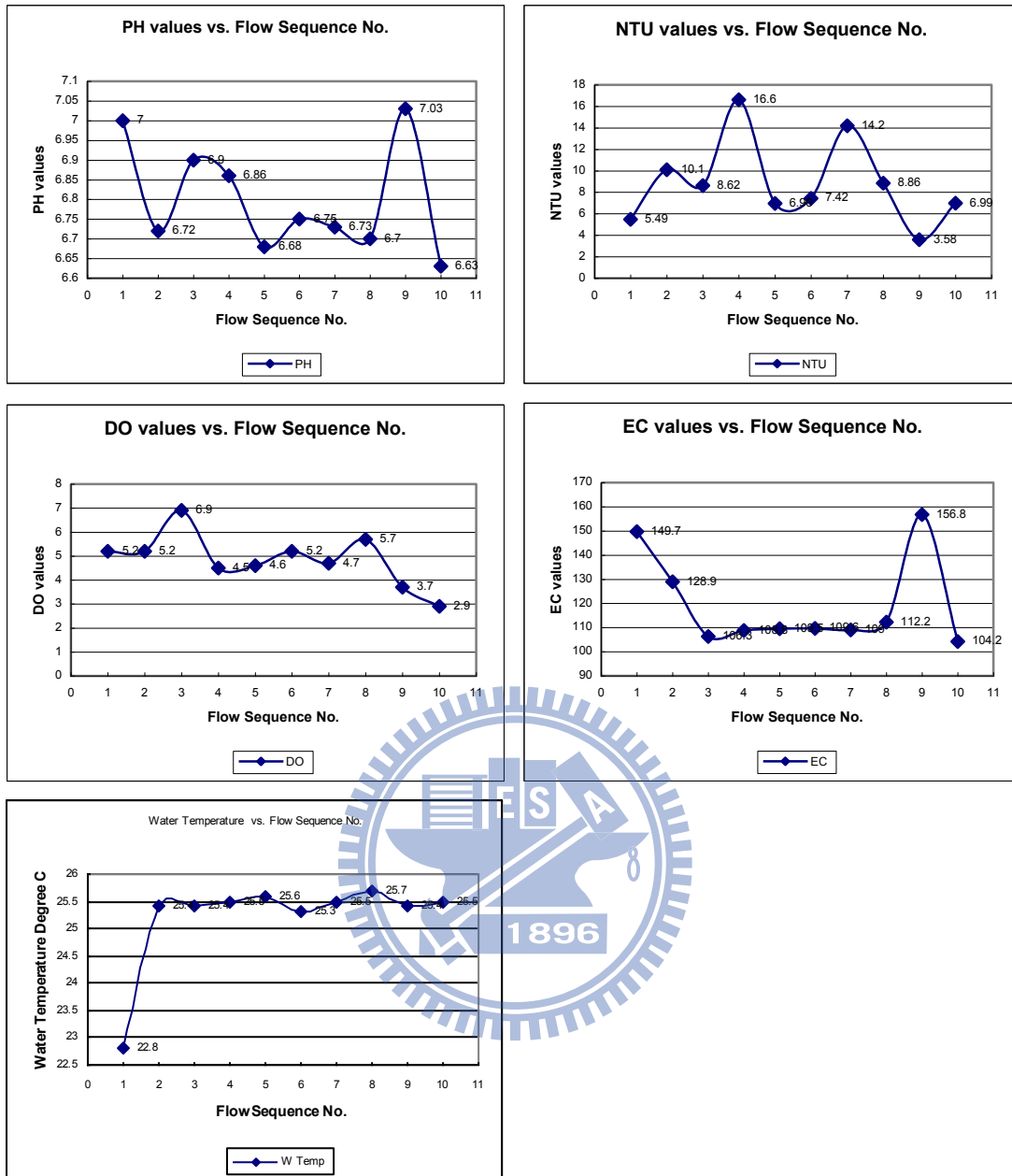


Figure 2.3 Variation of water quality indicators over treatment units

	
<p>Dense emergent macrophytes standing in Touchien river surface flow constructed wetland Phase 2</p>	<p>A vegetated channel in Touchien river surface flow constructed wetland Phase 1</p>
	
<p>A vegetated channel in Touchien River surface flow constructed wetland Phase 1</p>	<p>A vegetated channel with artificial floating islands in Touchien River surface flow constructed wetland</p>
	
<p>A densely vegetated channel in Touchien River surface flow constructed wetland</p>	<p>Densely vegetated floodplain with emergent macrophytes in Touchien River</p>

Figure 2.4 Touchien River surface flow constructed wetland system

	
<p>Apparatus for testing the electrical conductivity (EC), temperature, pH of water quality during field trips (photo taken at Du Nan Bridge surface flow constructed wetland)</p>	<p>Turbidity measured using a portable nephelometer which reads turbidity in Nephelometric Turbidity Units (NTU).</p>
	
<p>Phosphorus Test Equipment – a mini spectrophotometer</p>	<p>Test tube used for spectrophotometer and the nephelometry method</p>
	
<p>Sulphuric Acid as the Phosphate HR Reagent A</p>	<p>Sodium Metabisulfite as the Phosphate HR Reagent B (HI 93717B-0)</p>

Figure 2.5 Water quality test equipment


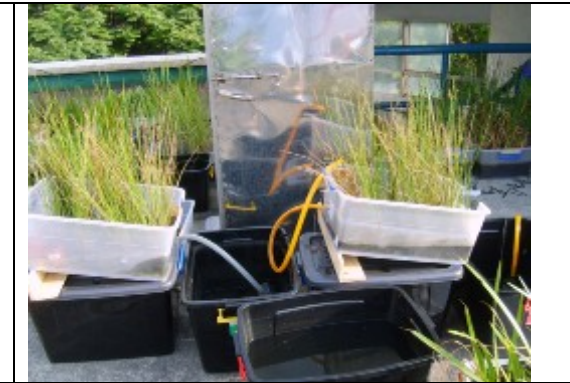




	
<p>Mini roof farm at the top of Engineering Block 1, NCTU (open space)</p>	<p>The circulating system to test phosphorus removal of <i>Juncus effusus</i></p>
	
<p>From left to right: <i>Phragmites australis</i>, <i>Typha orientalis</i>, and <i>Hygrophila pogonocalyx</i> in a semi-open space</p>	<p>From left to right: <i>Phragmites australis</i>, and <i>Typha orientalis</i> in a semi-open space</p>
	
<p>Close up of <i>Typha orientalis</i> in open space after rainfall</p>	<p>Close up of <i>Hygrophila pogonocalyx</i> in open space after rainfall</p>

Figure 2.6 Mini roof farm at the top of Engineering Block 1, NCTU

	
<p>Part of the drag force measurement system being embedded in the channel</p>	<p>Elevated channel surface extension to embed the movable platform</p>
	
<p>Side supports and the acrylic base of the movable platform</p>	<p>The wooden platform with KS bond strong waterproof adhesive</p>
	
<p>Built in transducer force gauge with extension RS232 for data output</p>	<p>Computer monitoring drag force of macrophytes in aquatic flow</p>

Figure 2.7 Direct drag force measurement system

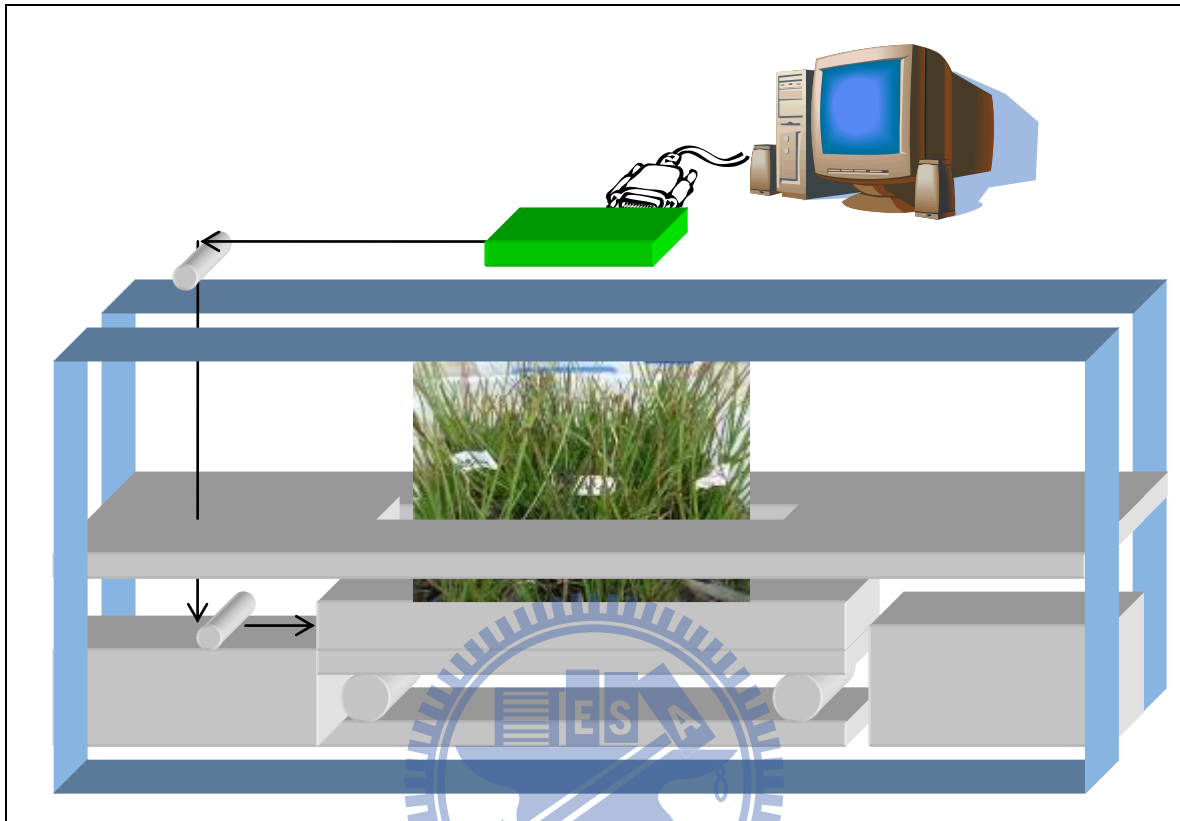


Figure 2.8 Schematic Design of the drag force measurement system before amendments

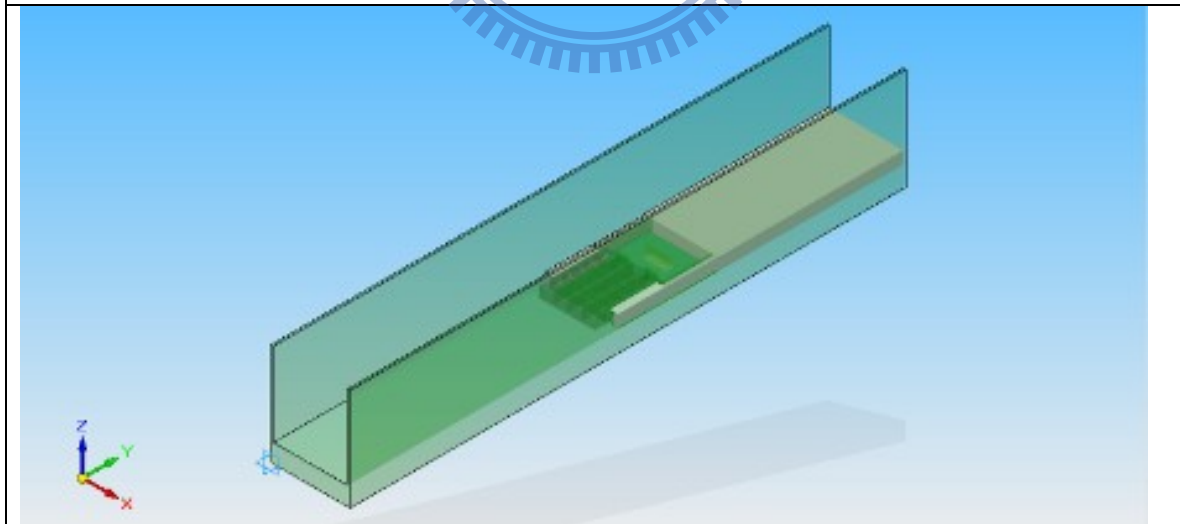


Figure 2.9 Overall isometric view of the drag force measurement system in the channel

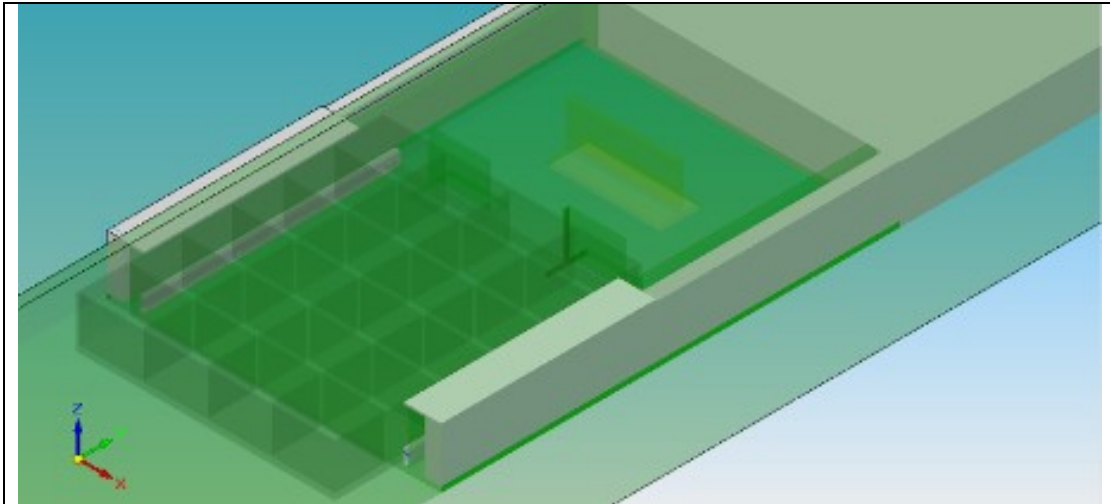


Figure 2.10 Isometric view of the embedded movable platform in the channel

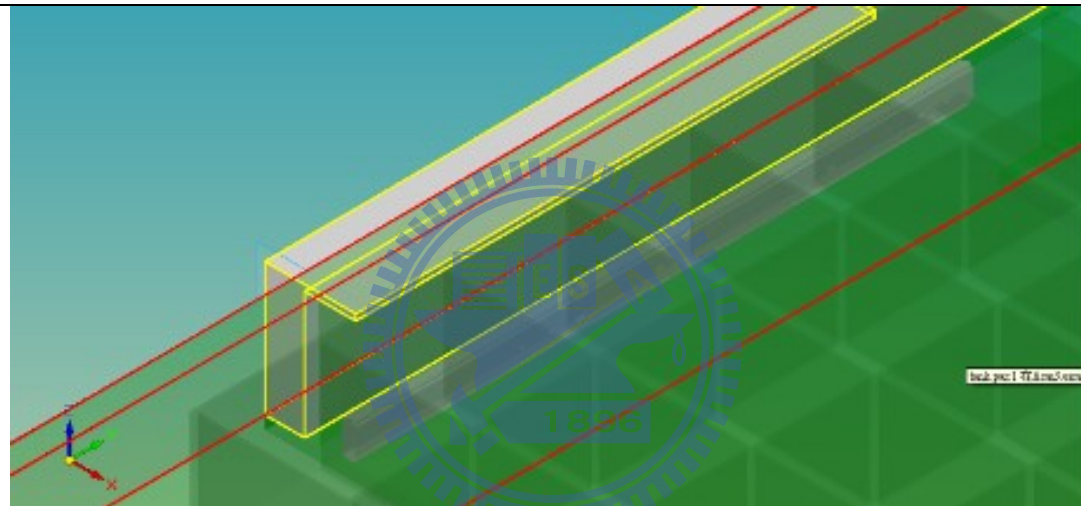


Figure 2.11 Zoom in of isometric view of the side support of the movable platform

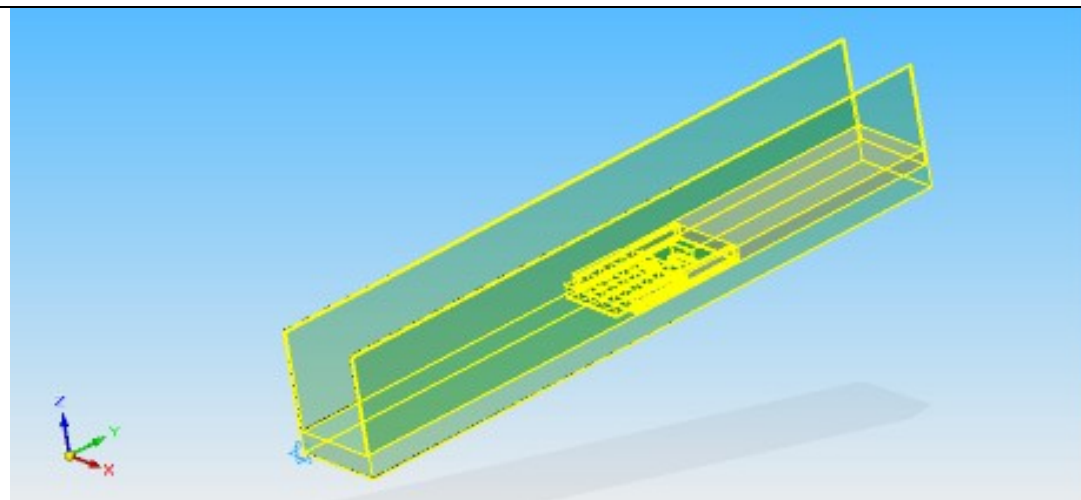


Figure 2.12 Isometric view highlighting main frame of structures

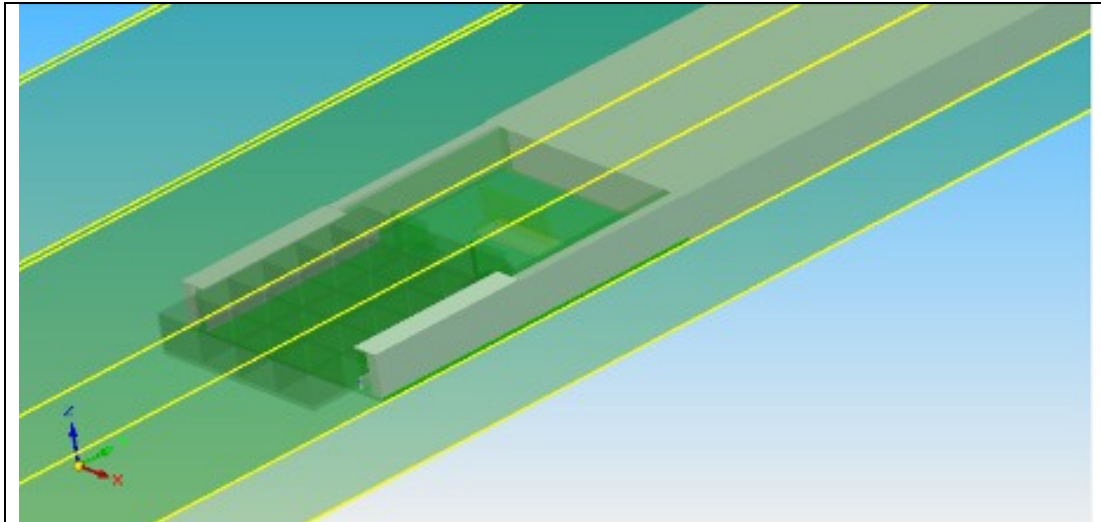


Figure 2.13 Isometric view of the drag force system

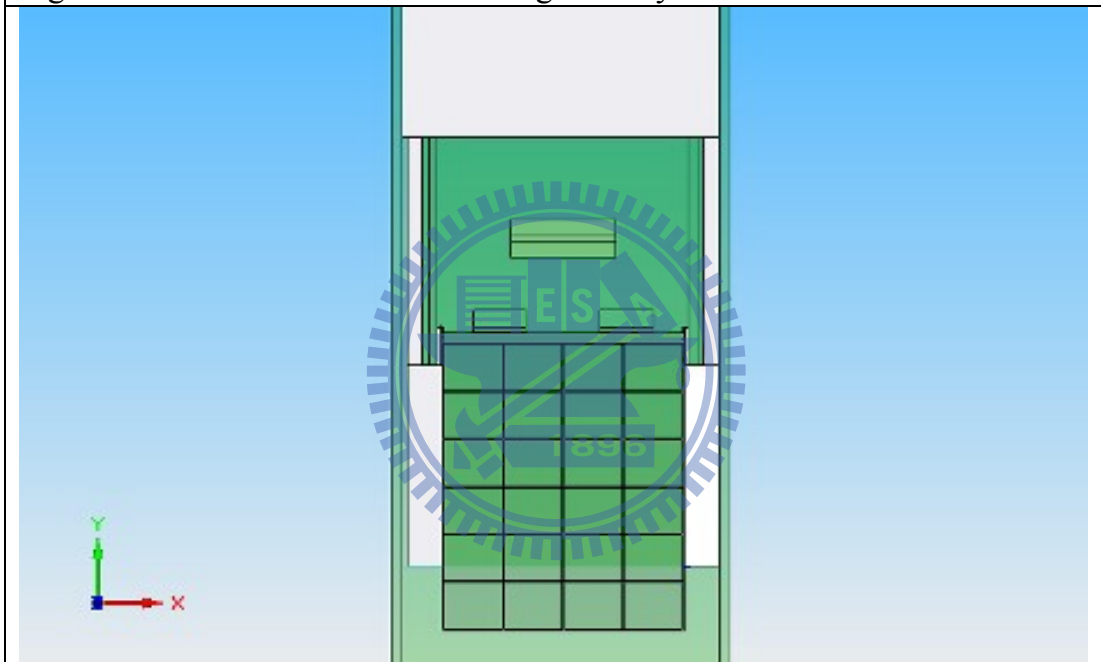


Figure 2.14 Plan view of the drag force measurement system in the channel

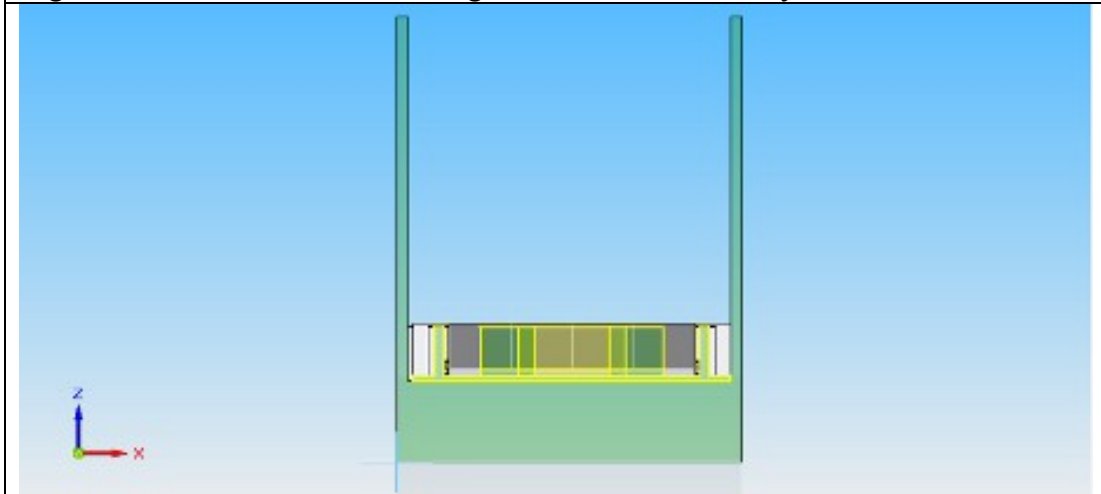


Figure 2.15 Cross sectional view of the drag force measurement system in the channel

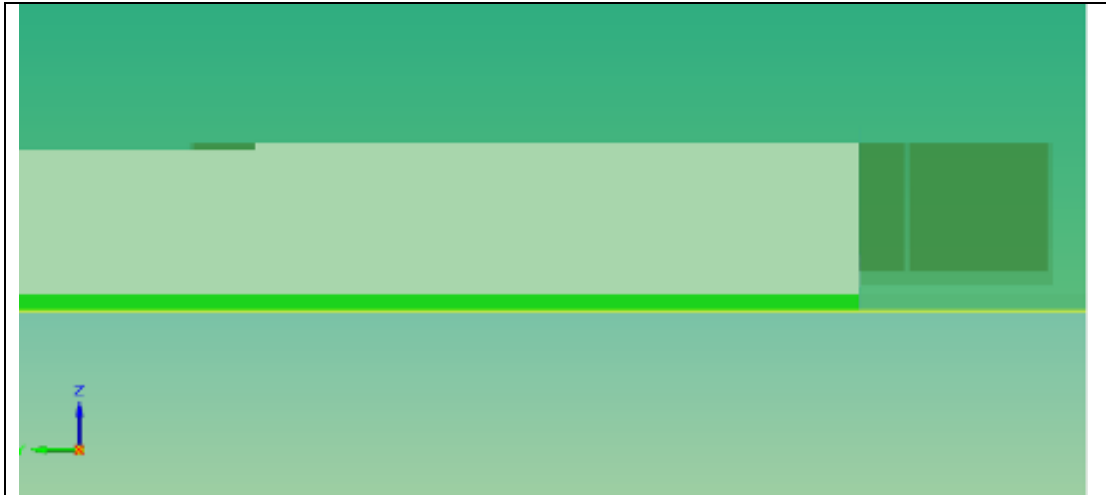
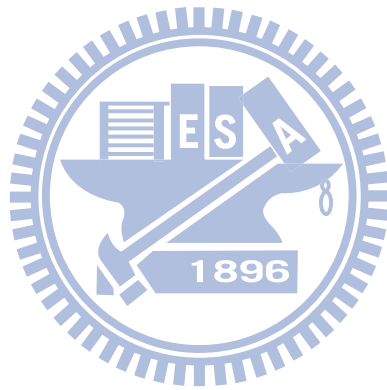


Figure 2.16 Side view of the drag force measurement system in the channel









	
<p>Flume test for <i>Juncus effusus</i> with high flow</p>	<p>Flume Test for <i>Juncus effusus</i> with low flow</p>
	
<p>Upper section of <i>Phragmites australis</i> in the flume</p>	<p>Lower section of <i>Phragmites australis</i> in the flume</p>
	
<p>Flow over emergent macrophytes in aquatic flow</p>	<p>Speed control for the motor</p>

Figure 3.1 Photographs of direct drag force measurement system in operation in the flume

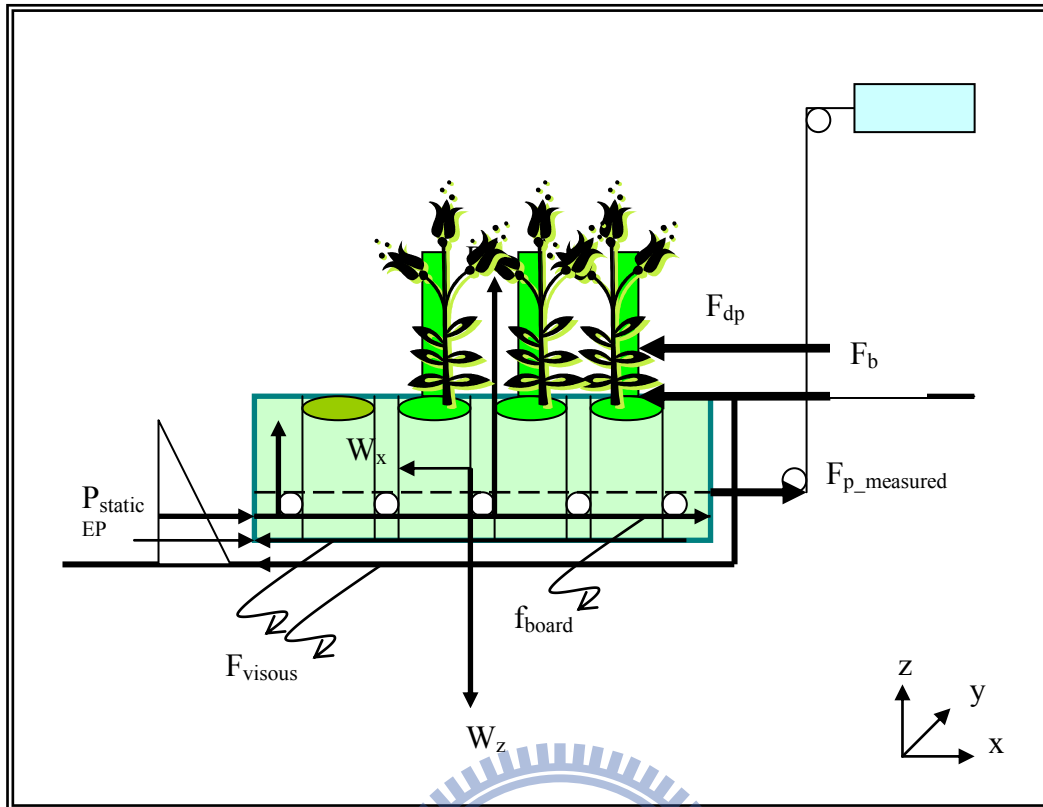


Figure 3.2 Free body diagram of the forces acting on the drag force measurement system

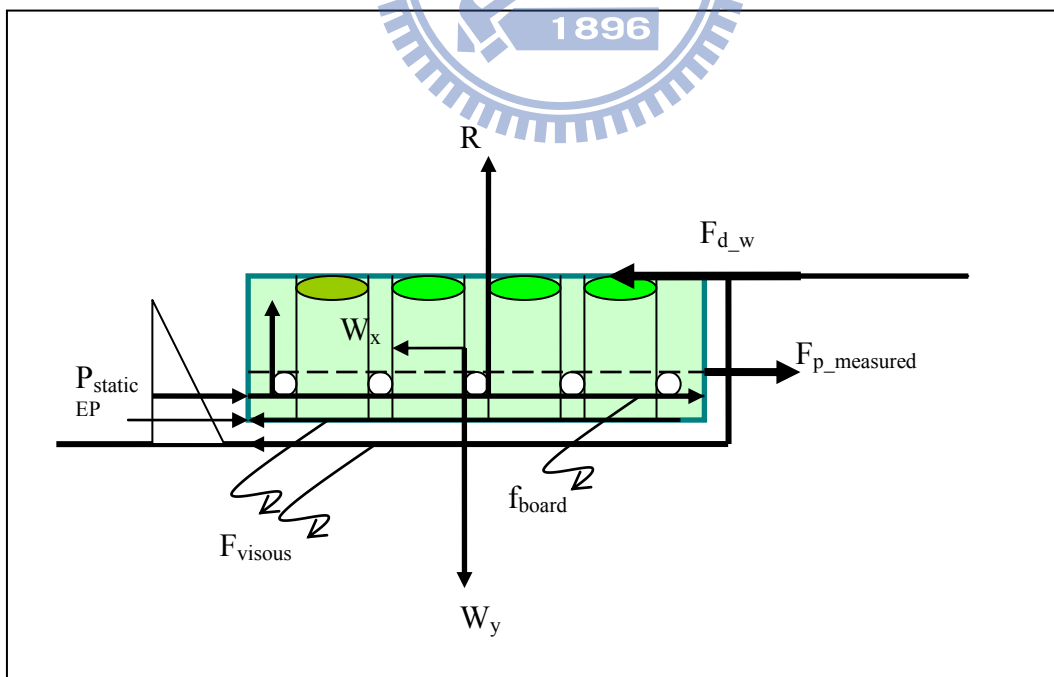


Figure 3.3 Simplified free body diagram for the drag force measurement system

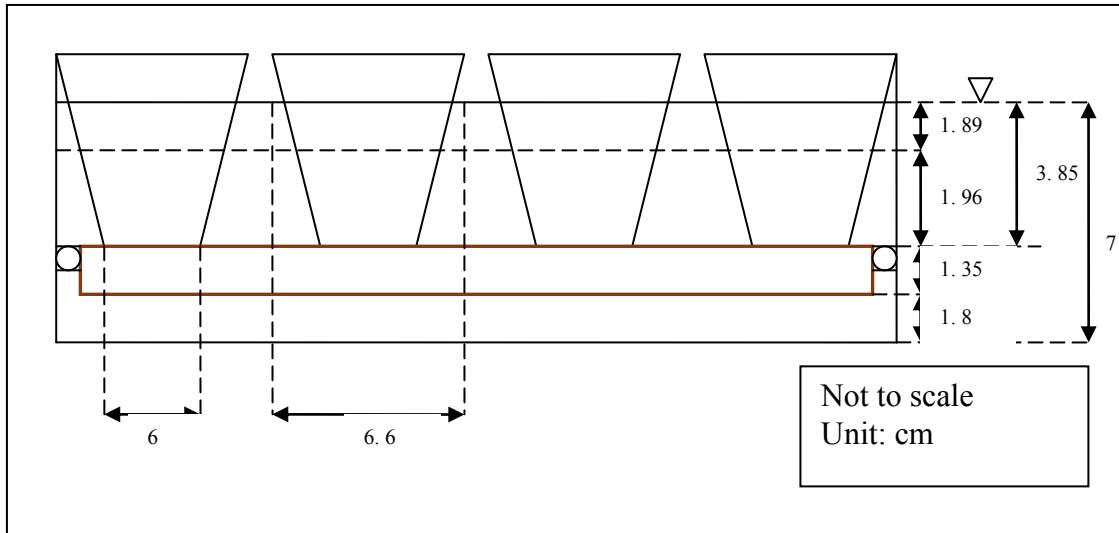
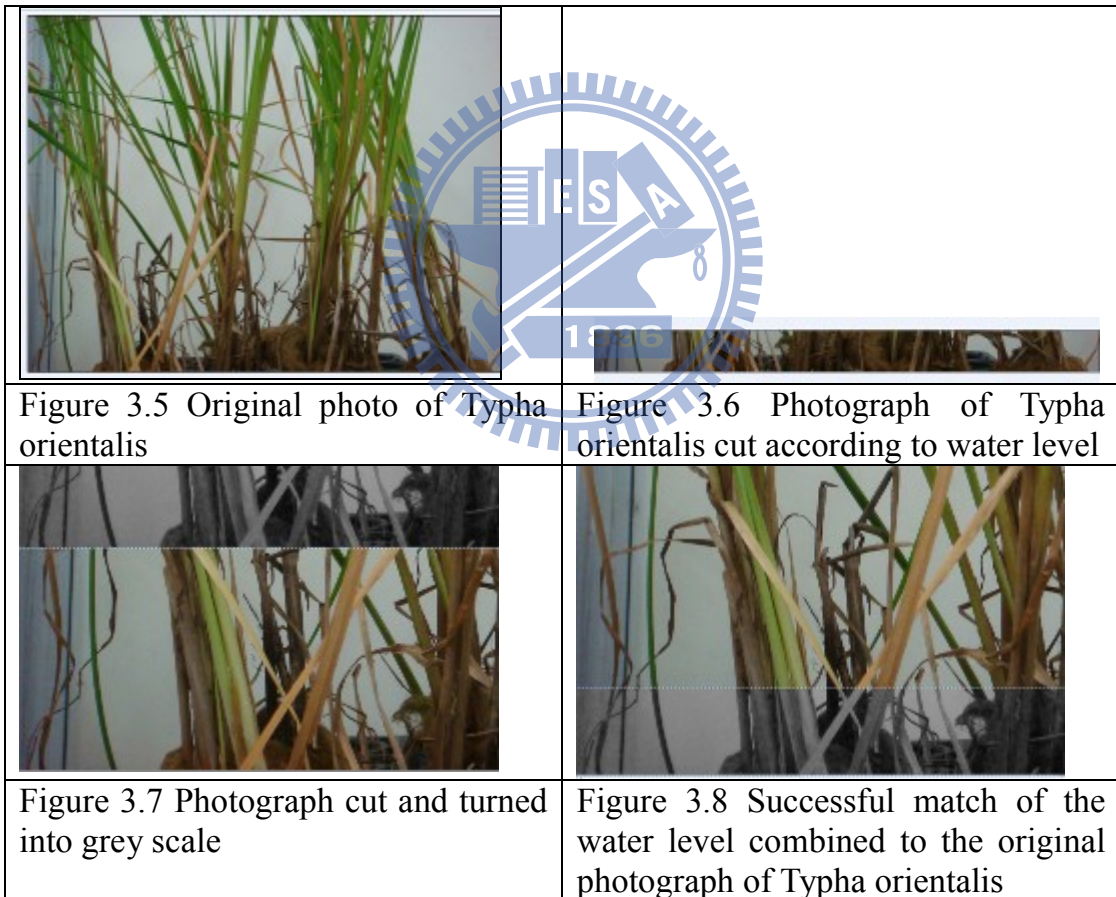








Figure 3.4 Back view of the second design of the movable platform



	
<p>Figure 3.9 Upper part of photograph set to white</p>	<p>Figure 3.10 Adjustment by brightness value</p>
	
<p>Figure 3.11 Adjustment by contrast value</p>	<p>Figure 3.12 Adjusted photograph of <i>Typha orientalis</i></p>
	
<p>Figure 3.13 Patching up the remaining plant area of using black color</p>	<p>Figure 3.14 Threshold value applied to the color-adjusted photograph</p>

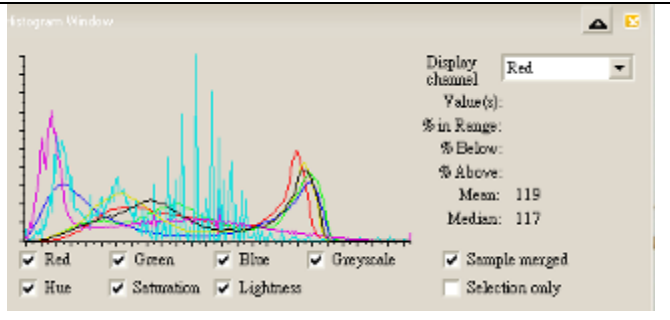


Figure 3.15 Original photograph of *Typha orientalis*

Figure 3.16 Number of pixels versus lightness values for the original photo of *Typha orientalis*

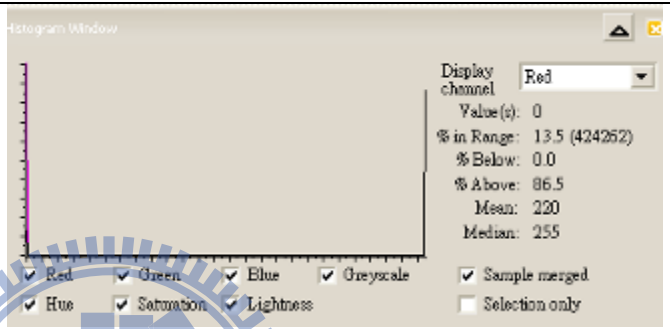
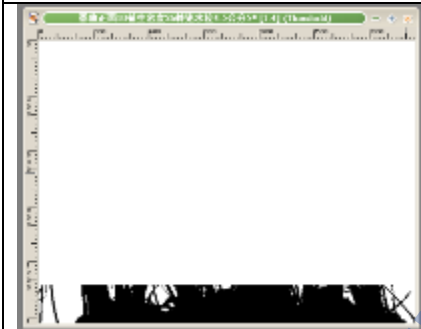
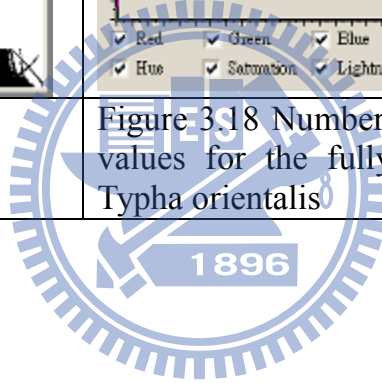


Figure 3.17 Treated photograph for *Typha orientalis*

Figure 3.18 Number of pixels versus lightness values for the fully adjusted photograph of *Typha orientalis*



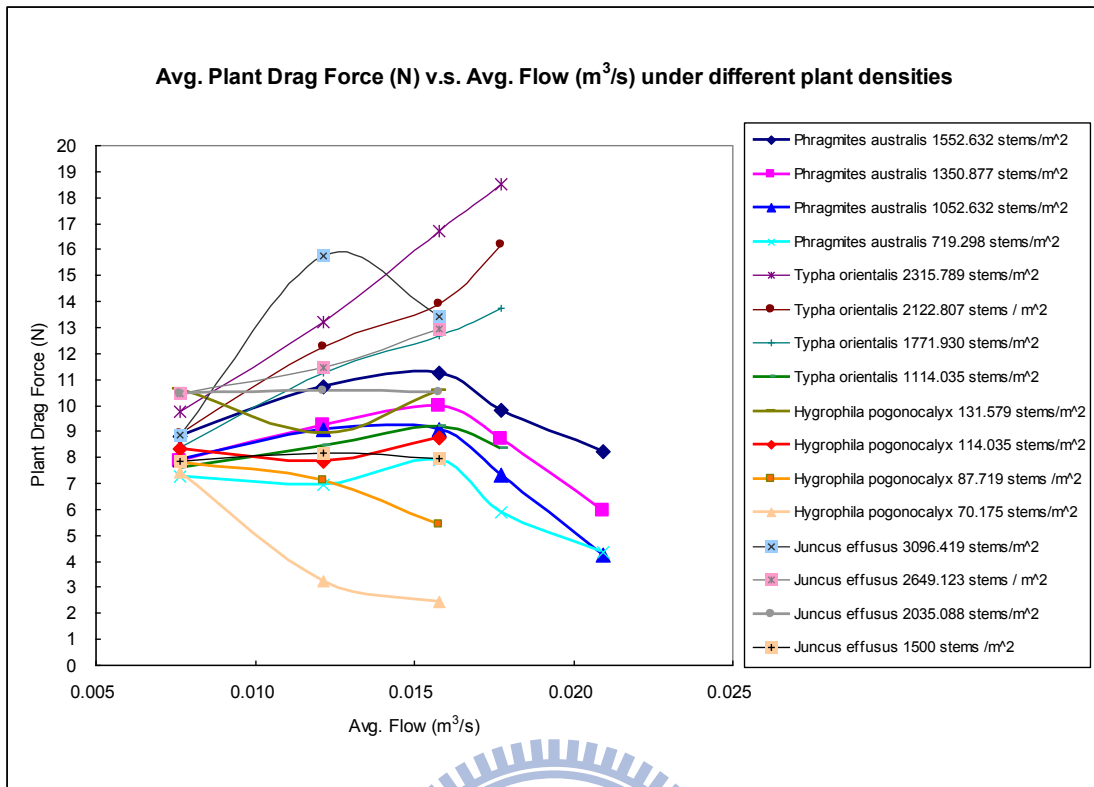


Figure 3.19 Summary of average drag force of all four types of *Typha orientalis*, *Juncus effusus*, *Hygrophila pogonocalyx*, and *Phragmites australis*

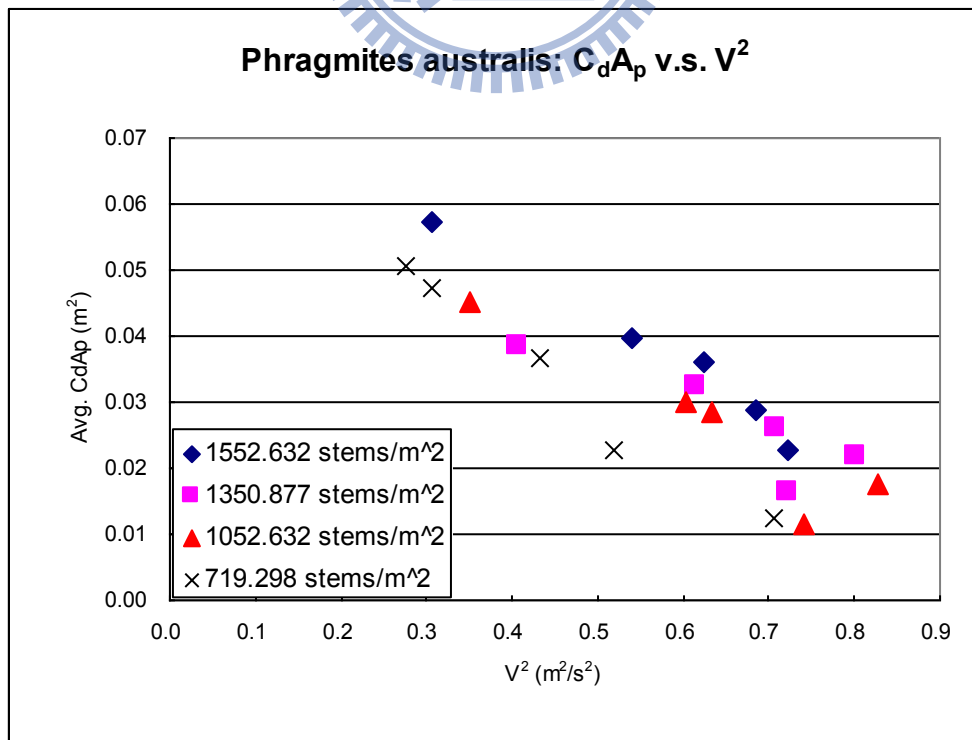


Figure 3.20 Relationship between averaged $C_d A_p$ (m²) and V^2 (m/s)² for *Phragmites australis*

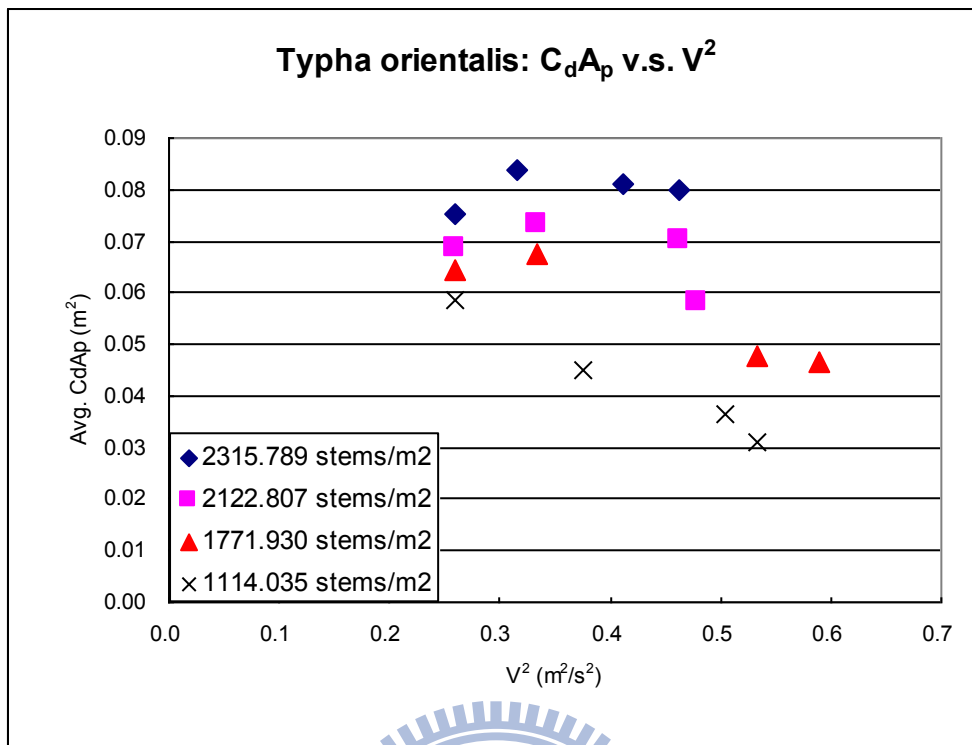


Figure 3.21 Relationship between averaged $C_d A_p$ (m^2) and V^2 (m/s)² for Typha orientalis

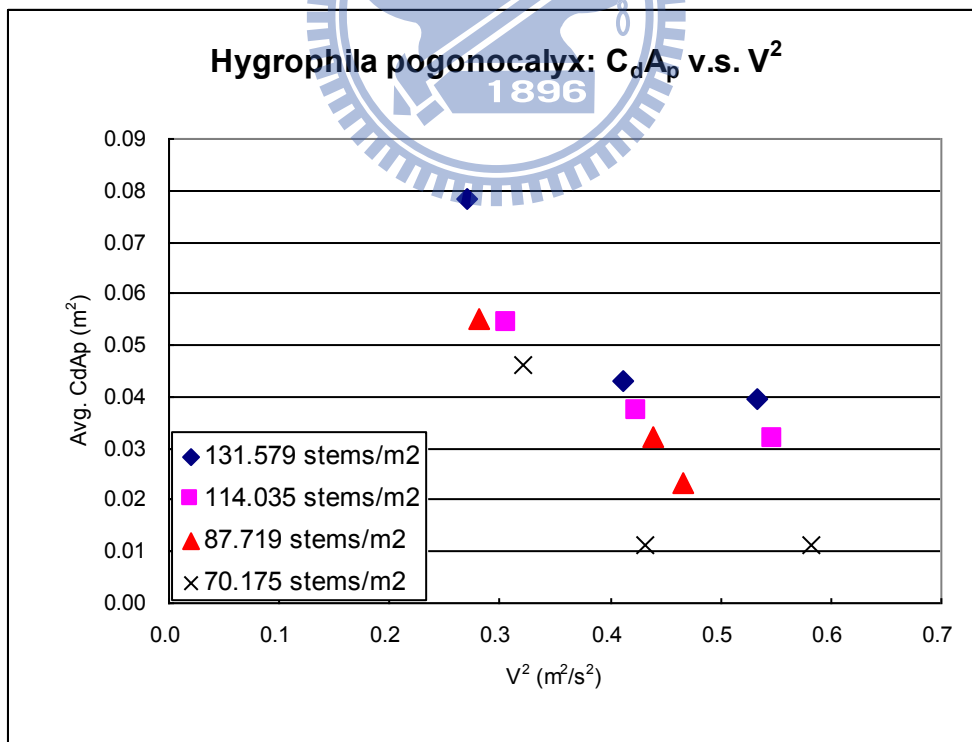


Figure 3.22 Relationship between averaged $C_d A_p$ (m^2) and V^2 (m/s)² for Hygrophila pogonocalyx

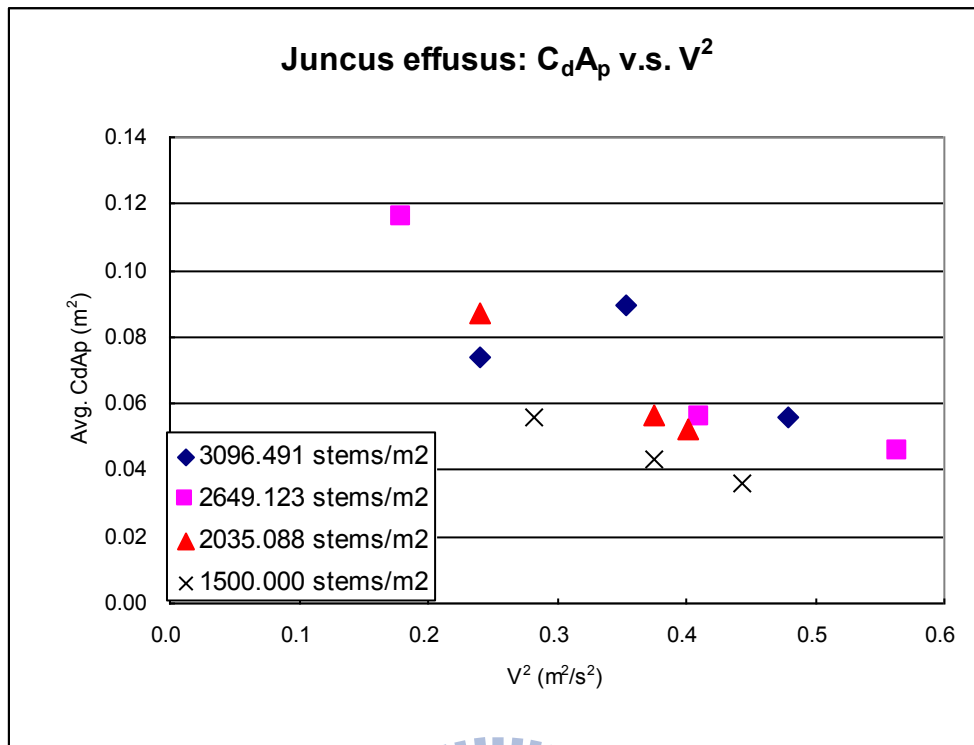


Figure 3.23 Relationship between averaged C_dA_p (m²) and V^2 (m/s)² for Juncus effusus

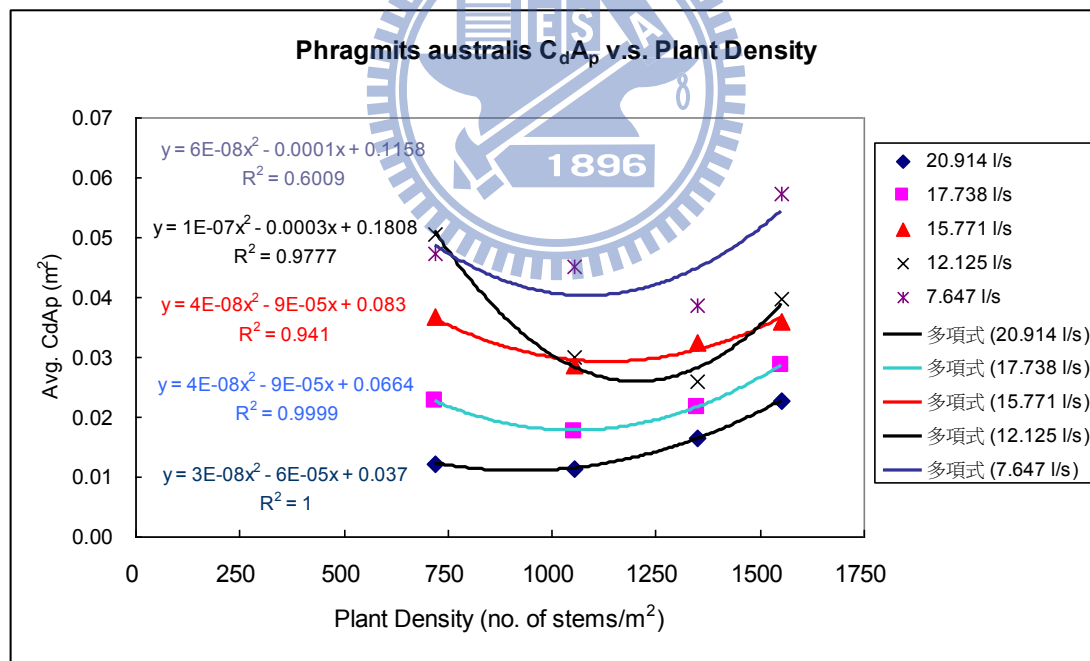


Figure 3.24 Relationship between averaged C_dA_p (m²) and plant density (stems/m²) for Phragmites australis

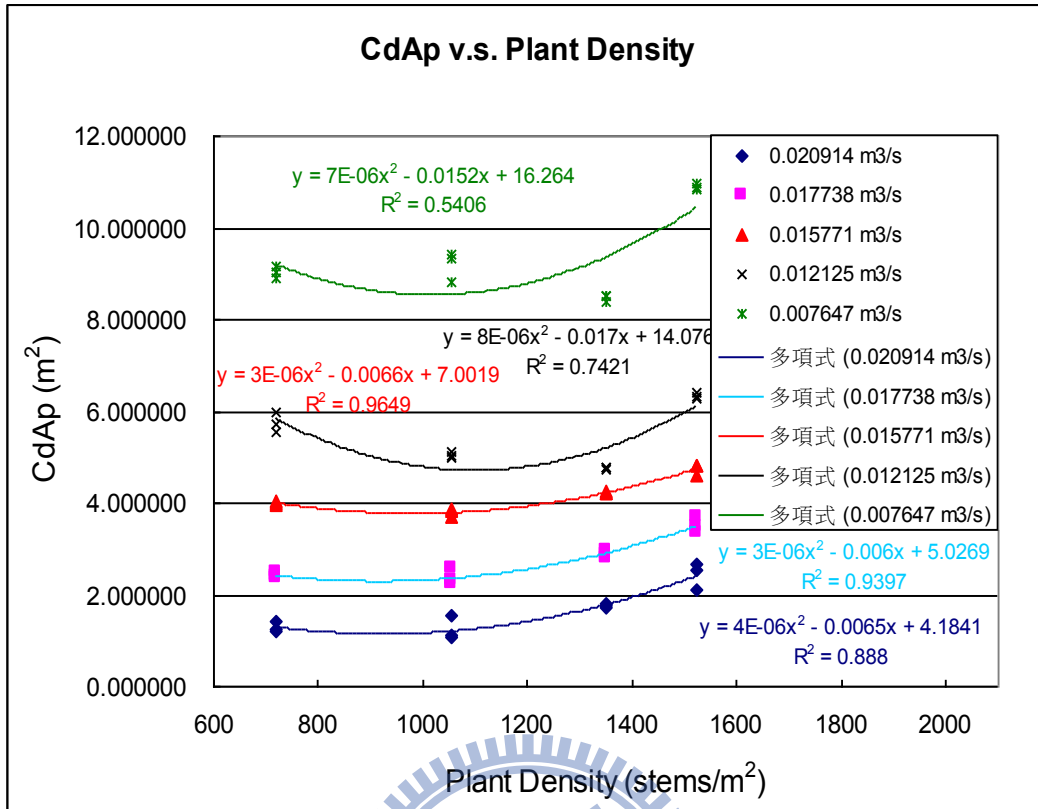


Figure 3.25 Relationship between C_{dAp} (m²) and plant density (No. of stems/m²) for *Phragmites australis*

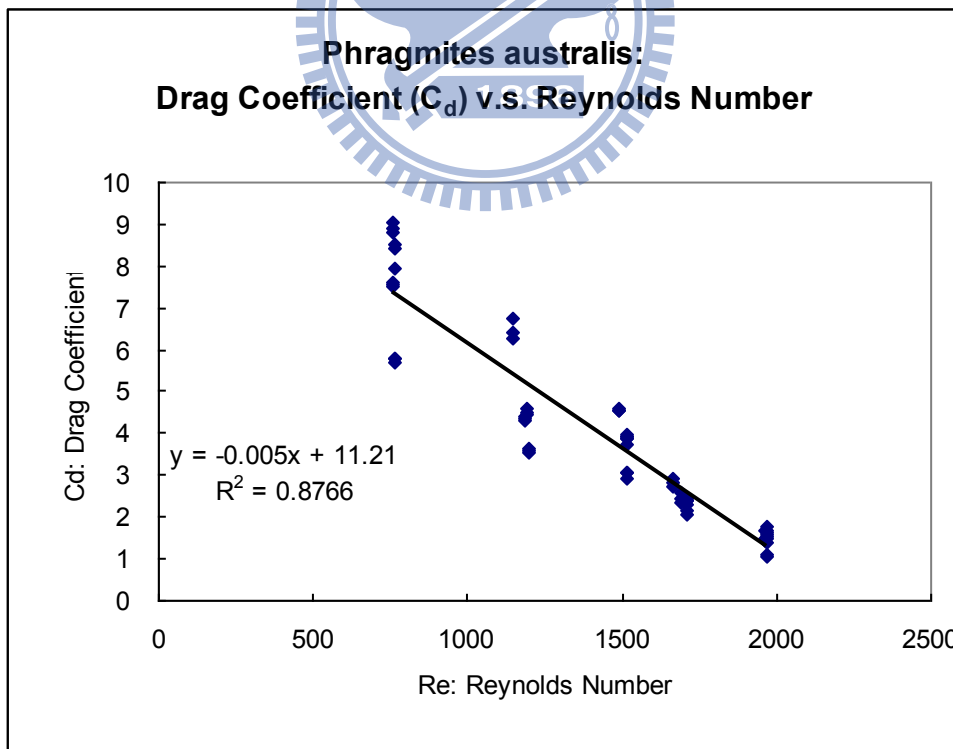


Figure 3.26 Relationship of drag coefficient and Reynolds number for *Phragmites australis*

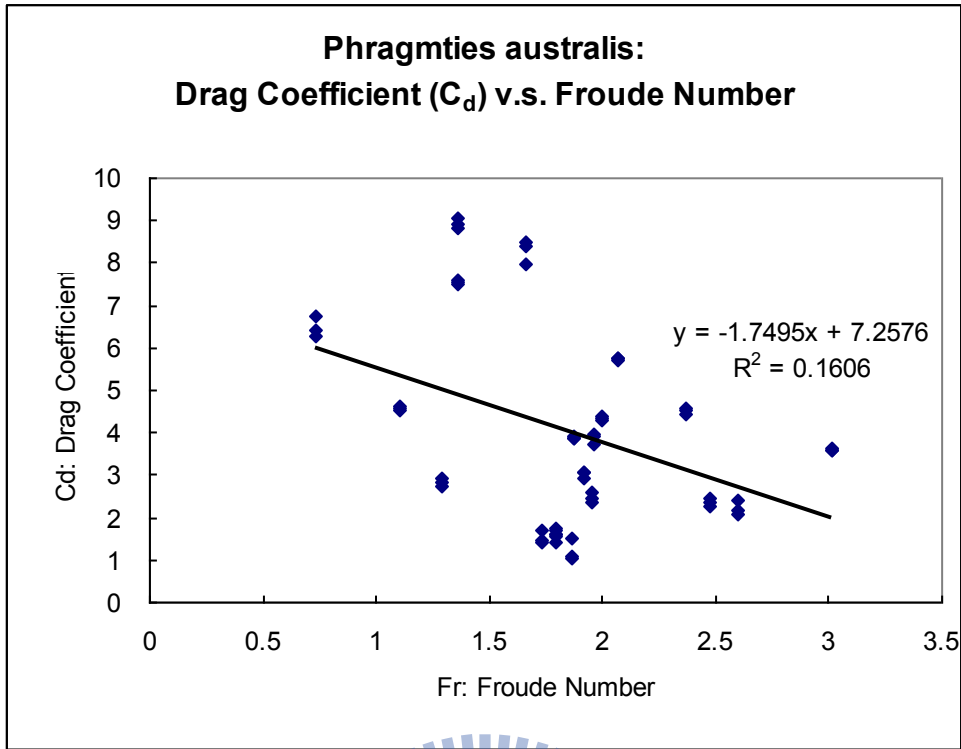


Figure 3.27 Relationship of drag coefficient and Froude number for Phragmites australis

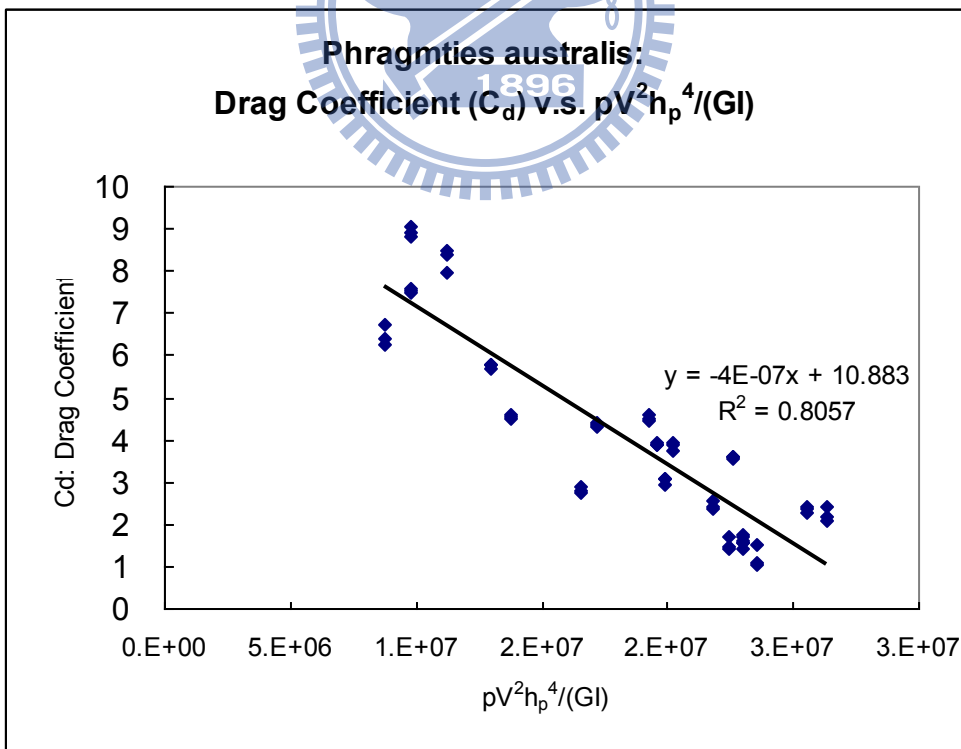


Figure 3.28 Relationship of drag coefficient and the ratio of fluid drag to plant rigidity for Phragmites australis

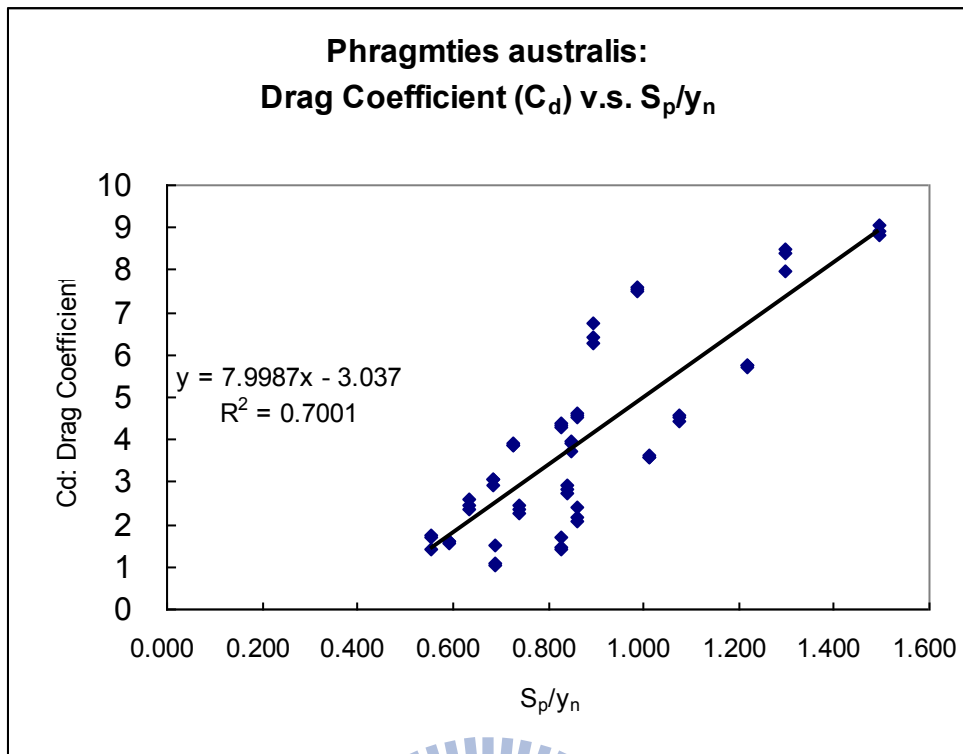


Figure 3.29 Relationship of drag coefficient and the ratio of average stem spacing to water level for *Phragmites australis*

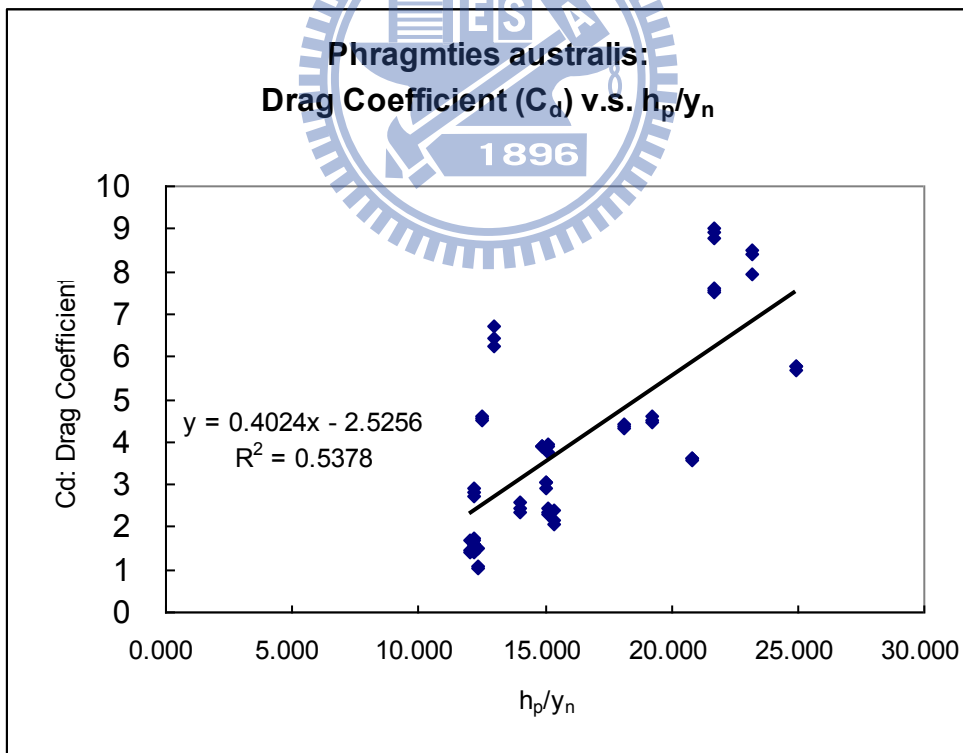


Figure 3.30 Relationship of drag coefficient and the ratio of average plant height to water level for *Phragmites australis*

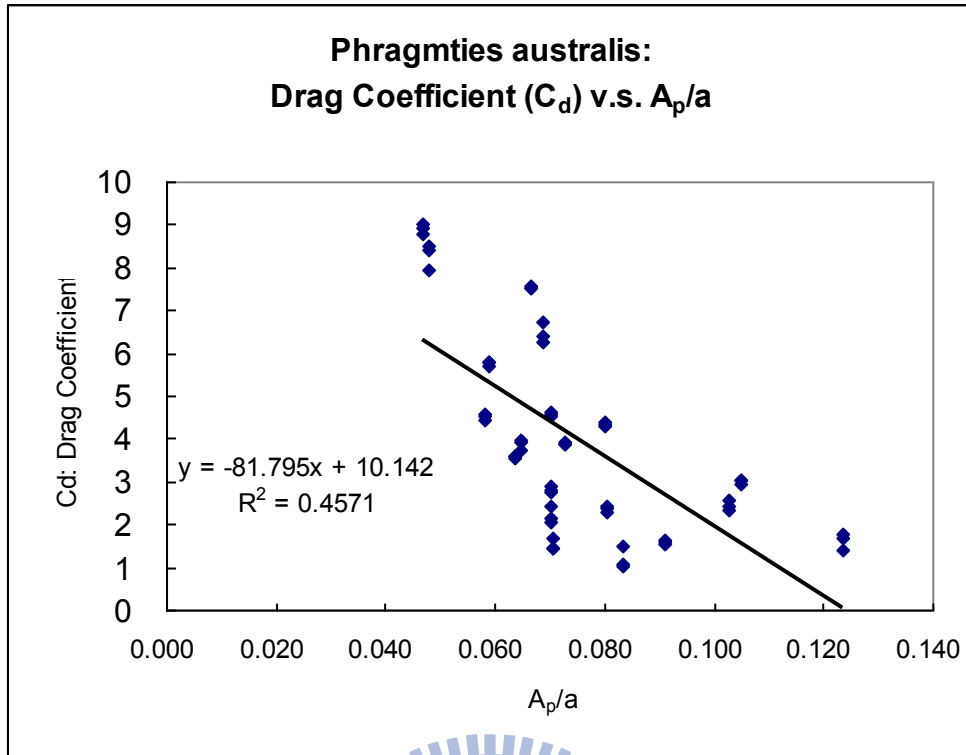


Figure 3.31 Relationship of drag coefficient and the ratio of plant projected frontal area to vegetated bed area for *Phragmites australis*

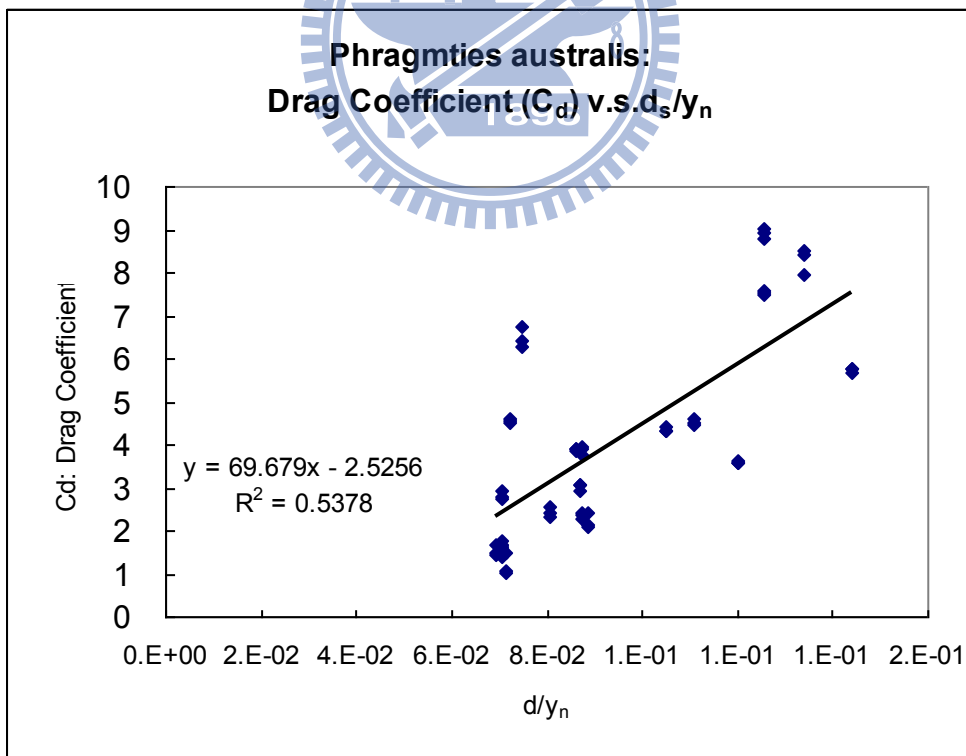


Figure 3.32 Relationship of Drag coefficient and the ratio of average plant diameter to water level for *Phragmites australis*

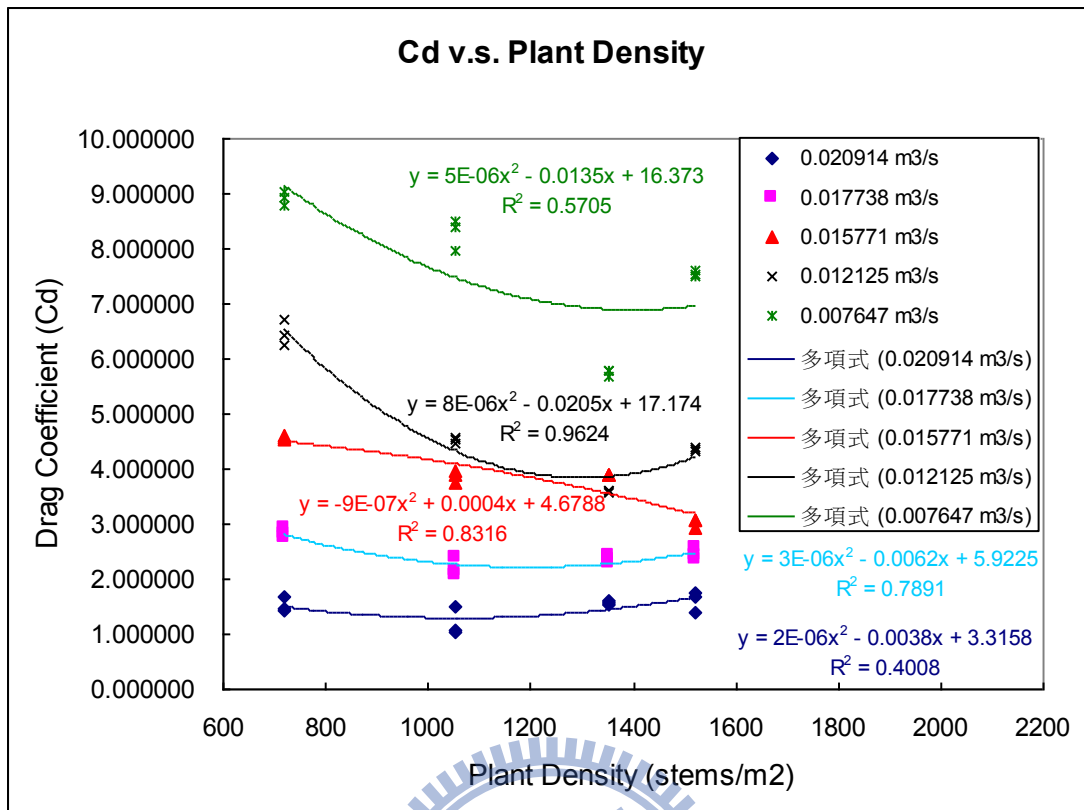


Figure 3.33 Relationship between C_d and plant density (No. of stems/m²)

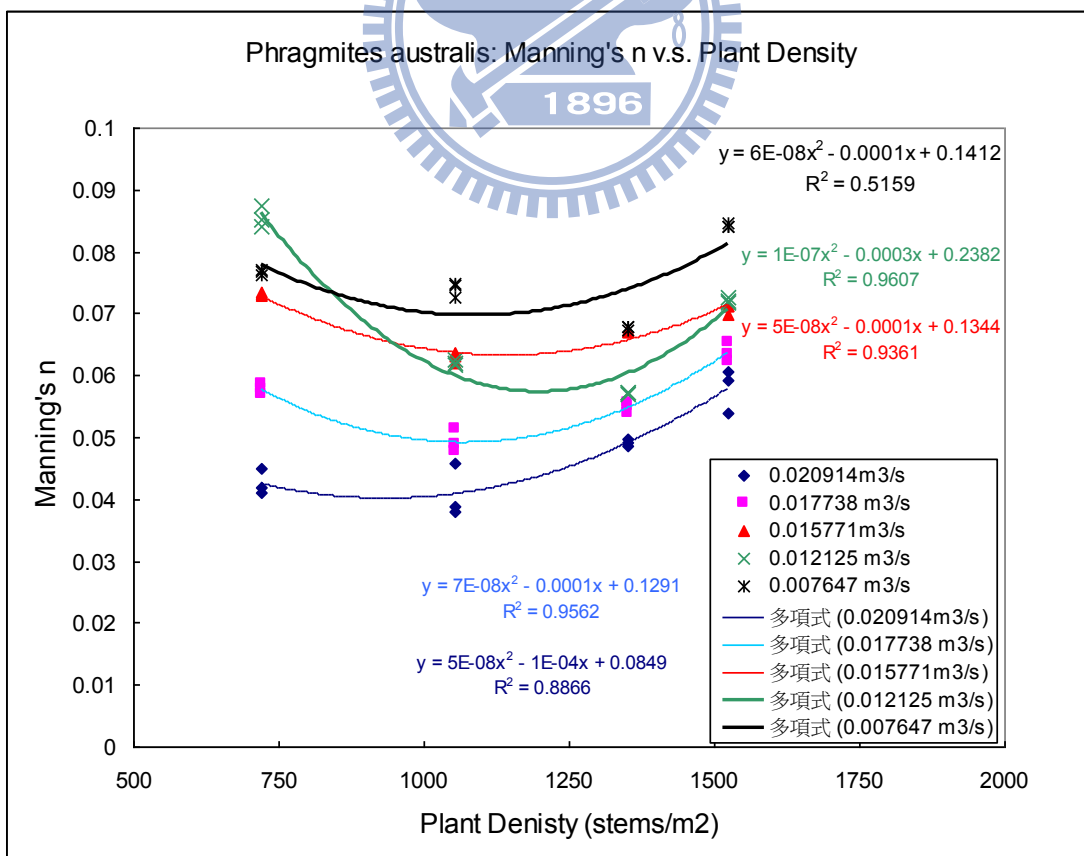


Figure 3.33.1 Relationship between average C_d and plant density (No. of stems/m²)

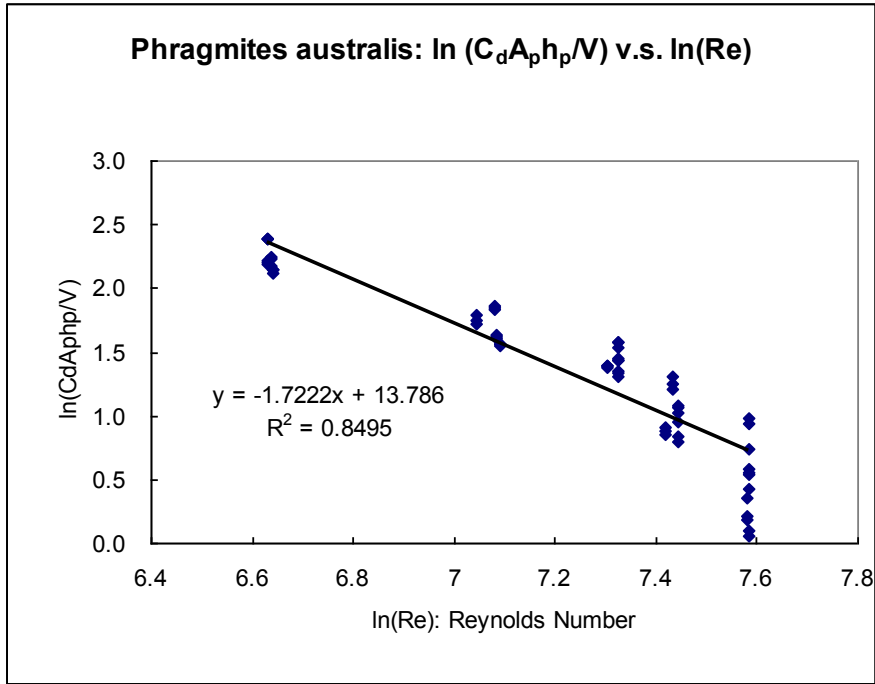


Figure 3.34 Relationship of natural logarithm of streamline coefficient ($C_d A_p h_p / V$) to natural logarithm of Reynolds number

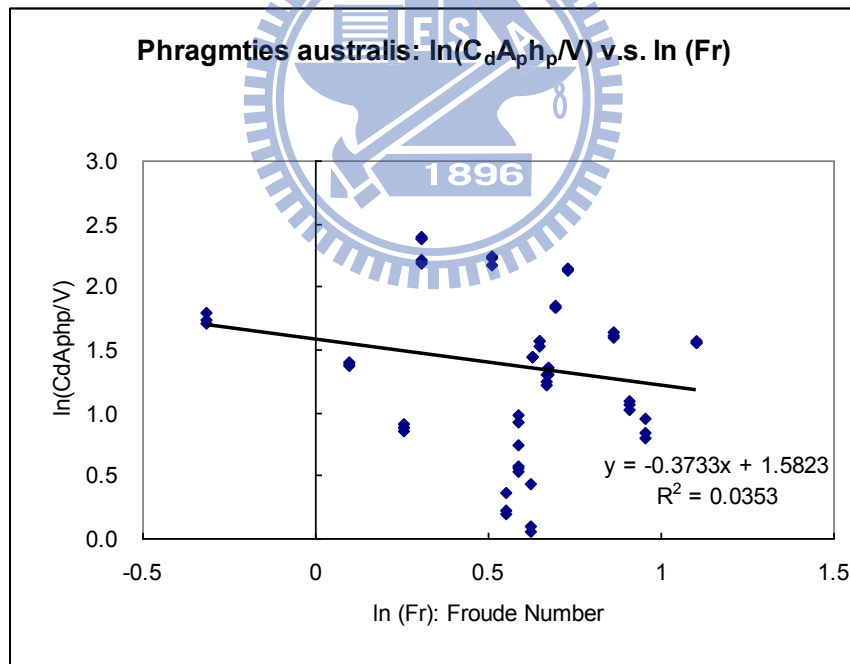


Figure 3.35 Relationship of natural logarithm of streamline coefficient ($C_d A_p h_p / V$) to natural logarithm of Froude number (Fr)

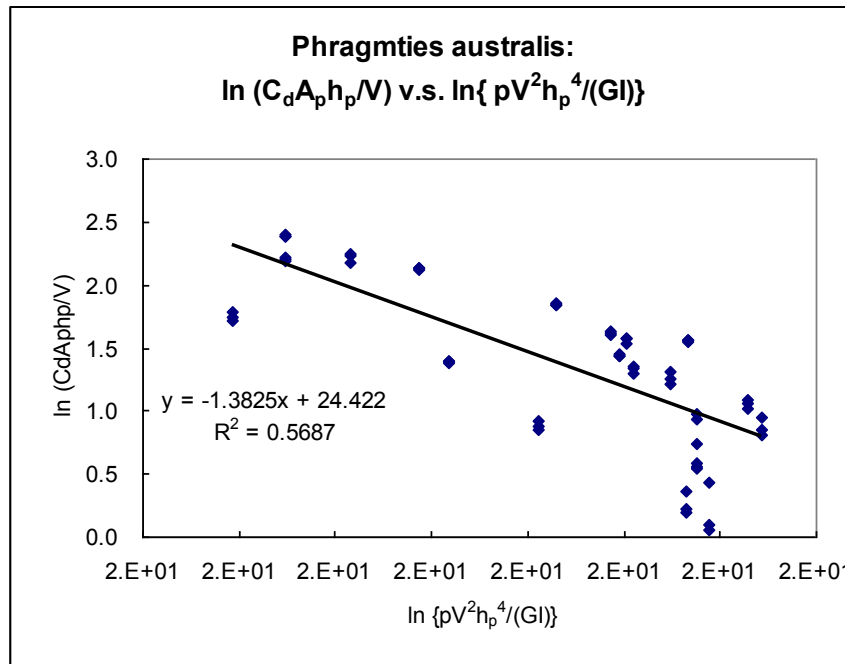


Figure 3.36 Relationship of natural logarithm of streamline coefficient ($C_d A_p h_p / V$) to natural logarithm of the ratio of fluid drag force to plant rigidity: $\rho V^2 h_p^4 / (G_s I)$

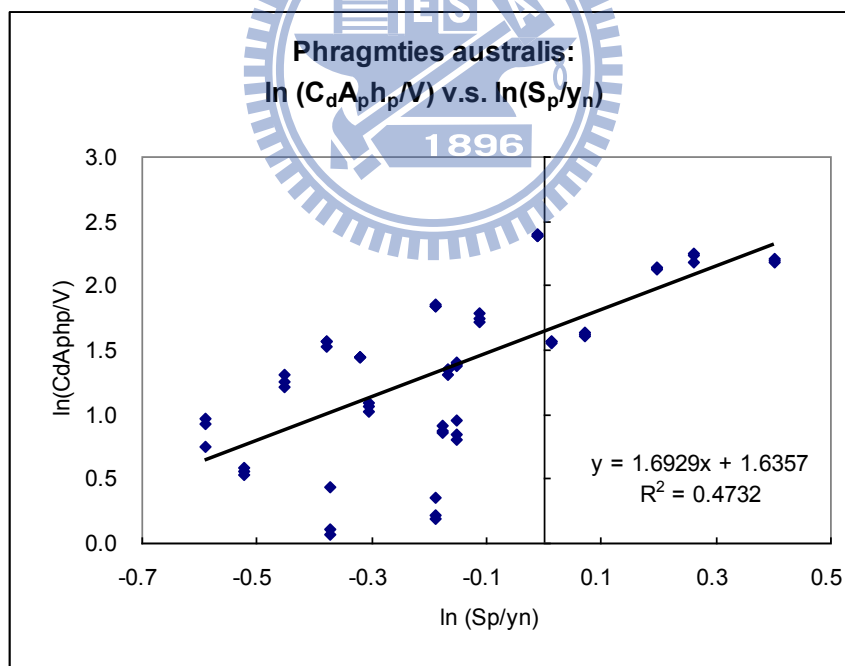


Figure 3.37 Relationship of natural logarithm of streamline coefficient ($C_d A_p h_p / V$) to natural logarithm of the ratio of averaged stem spacing to water level (s_p / y_n)

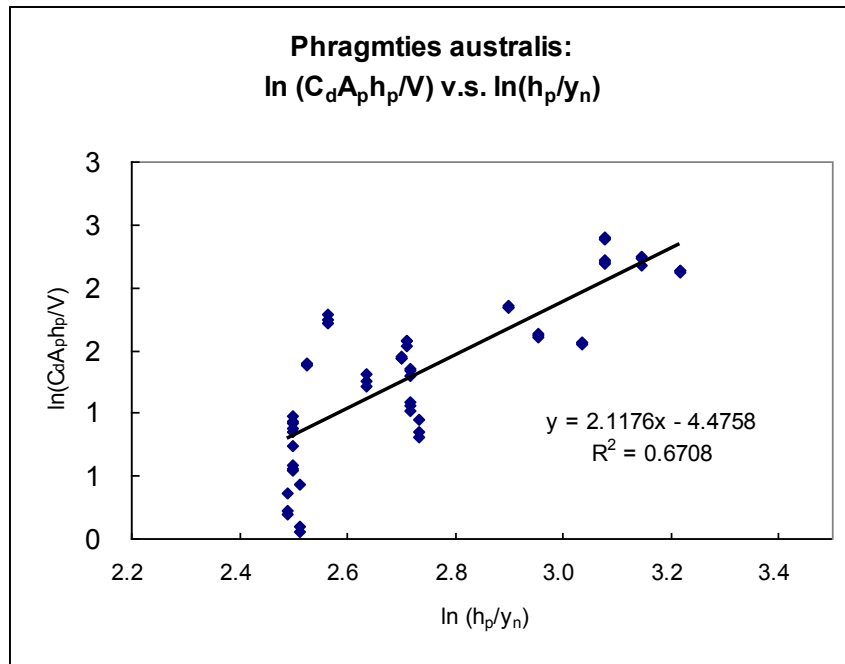


Figure 3.38 Relationship of natural logarithm of the streamline coefficient ($C_d A_p h_p / V$) to natural logarithm of the ratio of averaged stem height to water level (h_p / y_n)

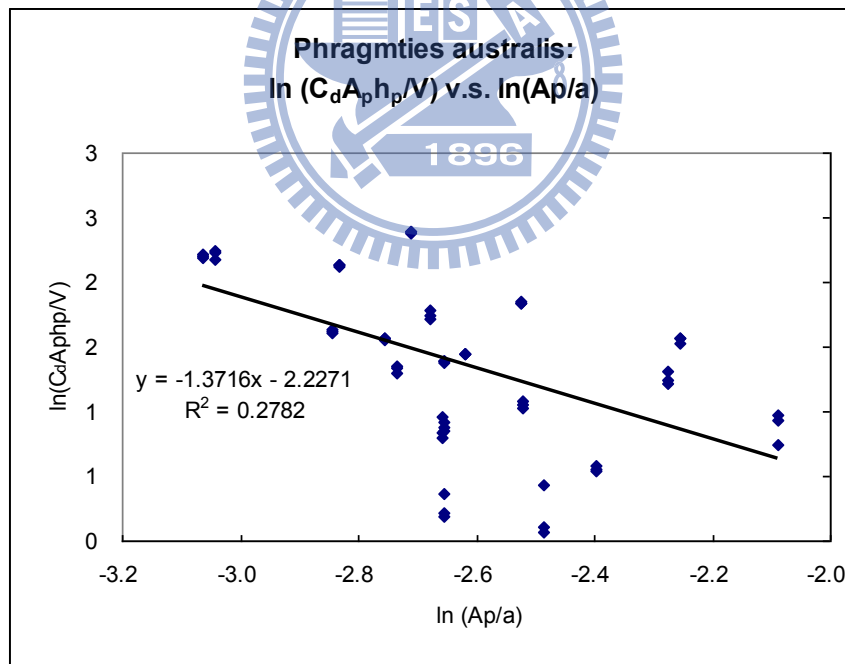


Figure 3.39 Relationship of natural logarithm of streamline coefficient ($C_d A_p h_p / V$) to natural logarithm of the ratio of plant projected frontal area to area of vegetated bed (A_p / a)

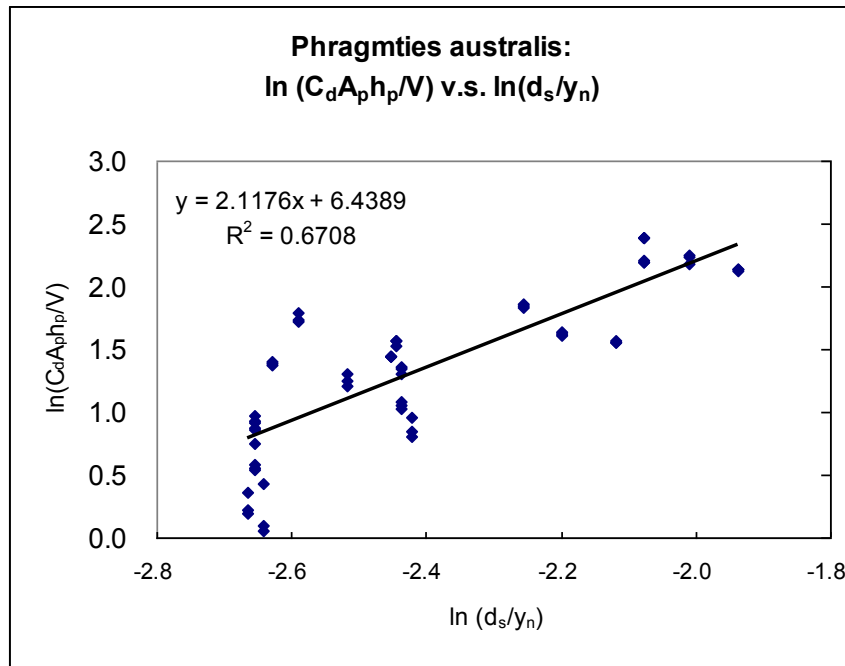


Figure 3.40 Relationship of natural logarithm of streamline coefficient ($C_d A_p h_p / V$) to natural logarithm of the ratio of average stem diameter to water level (d_s / y_n)

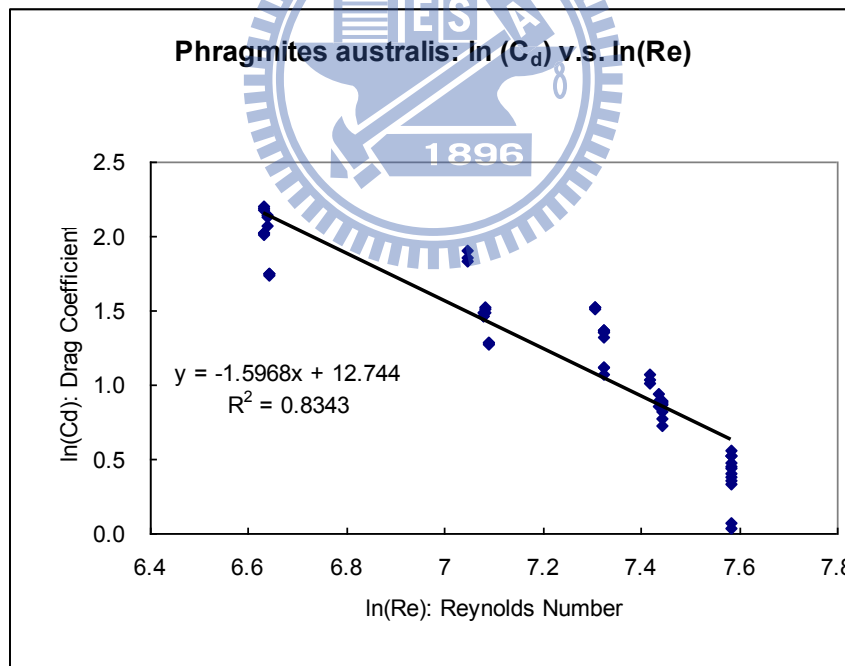


Figure 3.41 Relationship of natural logarithm of drag coefficient C_d to natural logarithm of Reynolds number (Re)

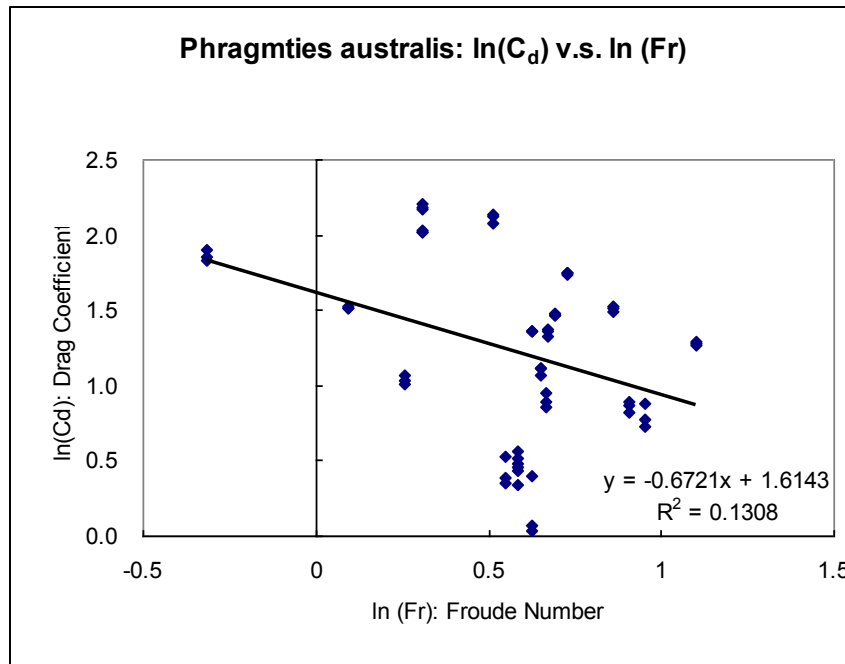


Figure 3.42 Relationship of natural logarithm of drag coefficient C_d to natural logarithm of Froude number (Fr)

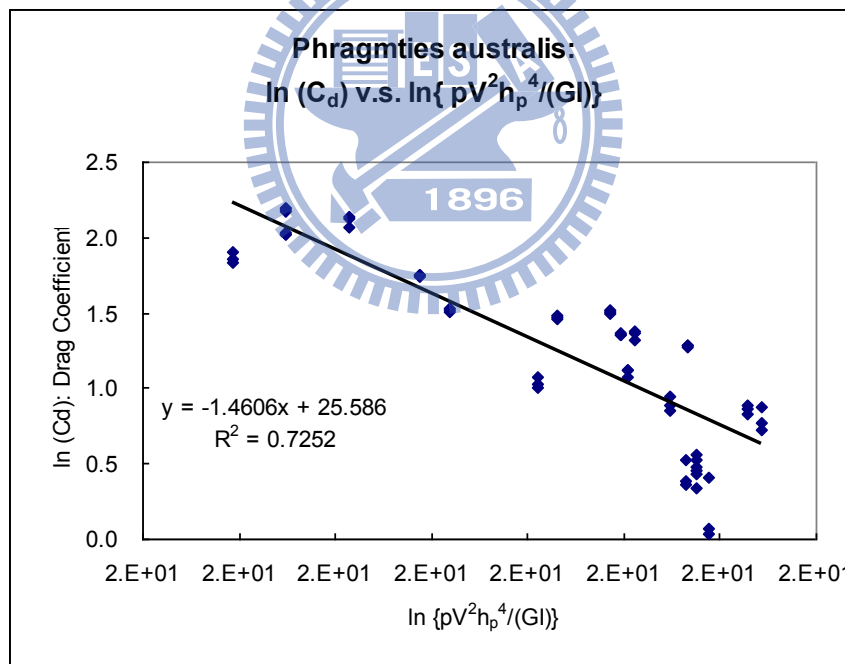


Figure 3.43 Relationship of natural logarithm of drag coefficient C_d to natural logarithm of the ratio of fluid drag force to plant rigidity: $\rho V^2 h_p^4 / (G_s I)$

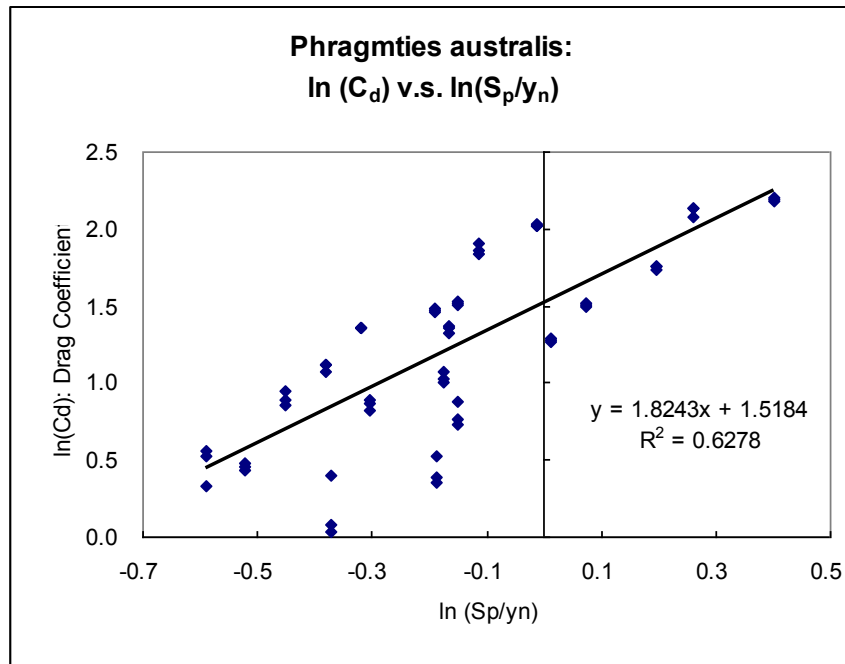


Figure 3.44 Relationship of natural logarithm of drag coefficient C_d to natural logarithm of the ratio of averaged stem spacing to water level (s_p/y_n)

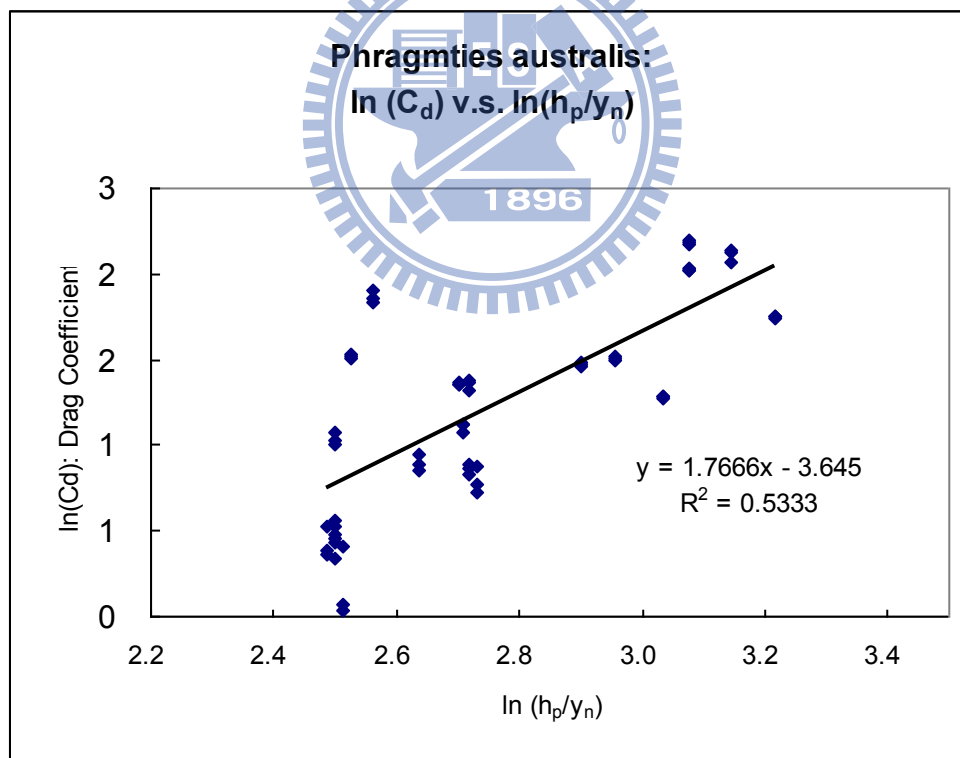


Figure 3.45 Relationship of natural logarithm of drag coefficient C_d to natural logarithm of the ratio of averaged stem height to water level (h_p/y_n)

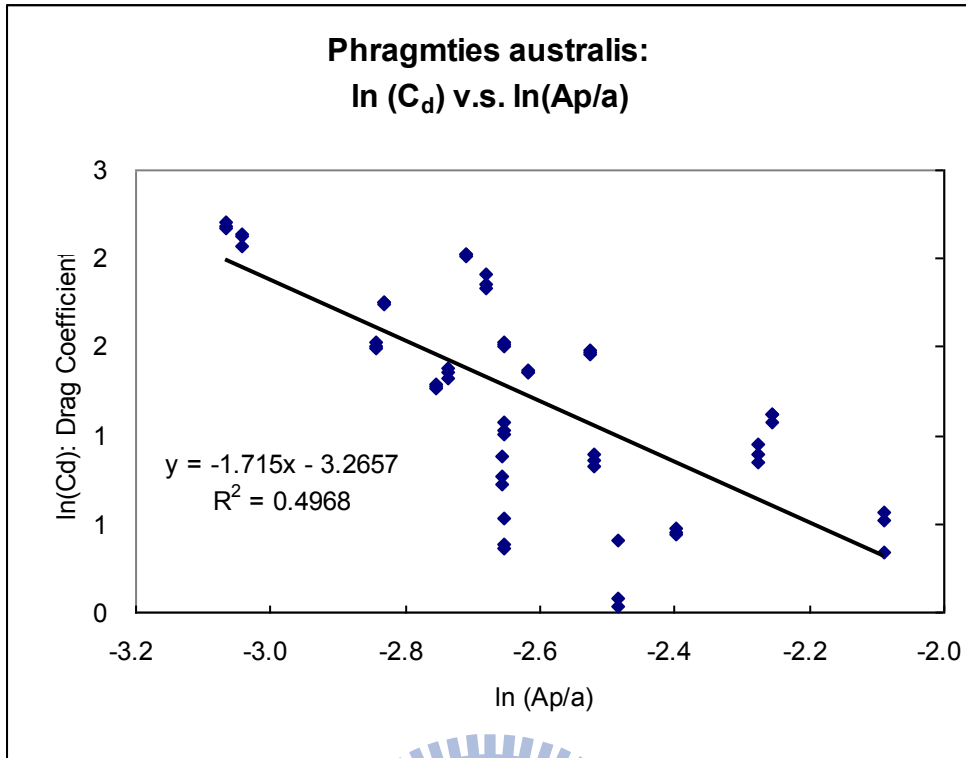


Figure 3.46 Relationship of natural logarithm of drag coefficient C_d to natural logarithm of the ratio of plant projected frontal area to area of vegetated bed (A_p/a)

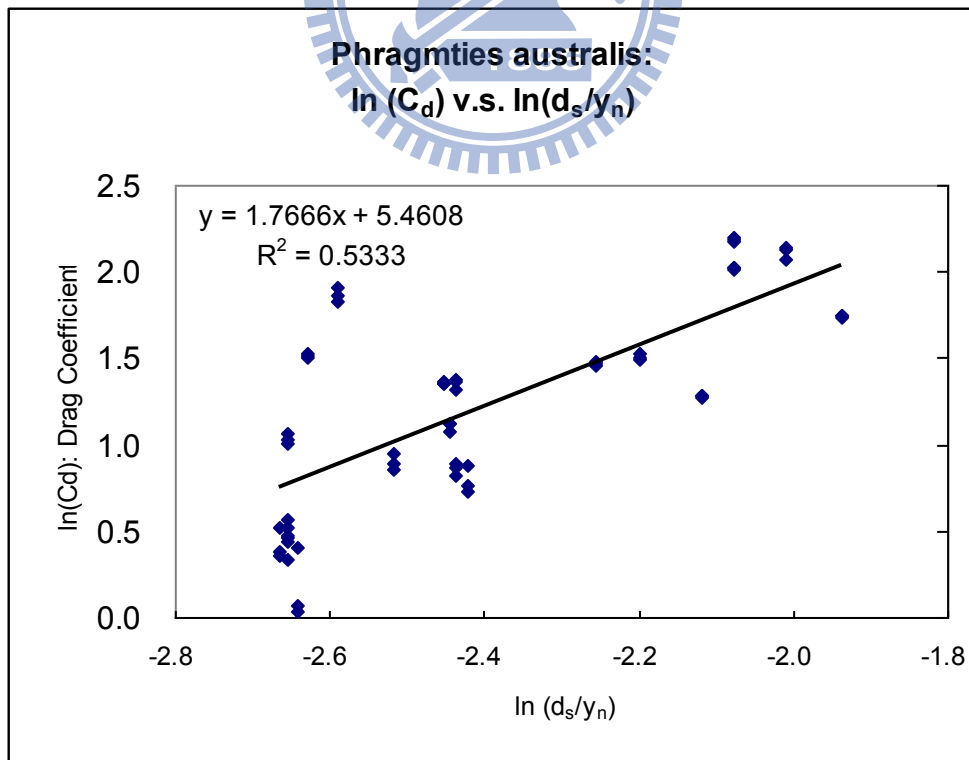


Figure 3.47 Relationship of natural logarithm of drag coefficient C_d to natural logarithm of the ratio of average stem diameter to water level (d_s/y_n)

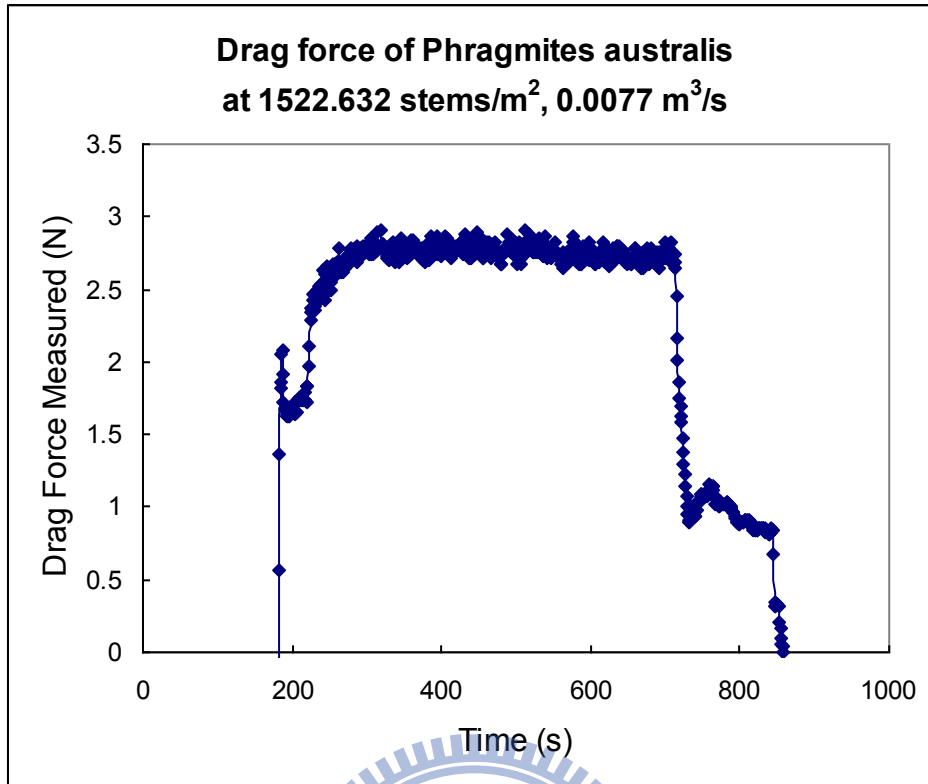


Figure 3.48 An example of drag force of Phragmites australis measured by the direct drag force measurement system at 1522.632 stems/m² and 0.0077 m³/s

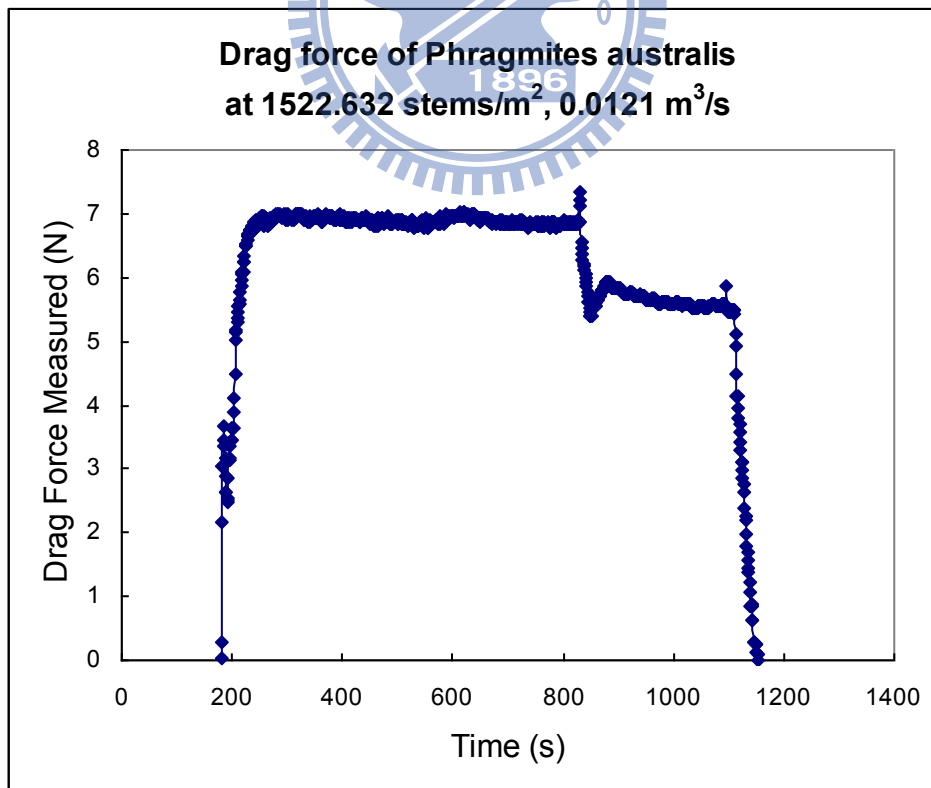


Figure 3.49 An example of drag force of Phragmites australis measured by the direct drag force measurement system at 1522.632 stems/m² and 0.0121 m³/s

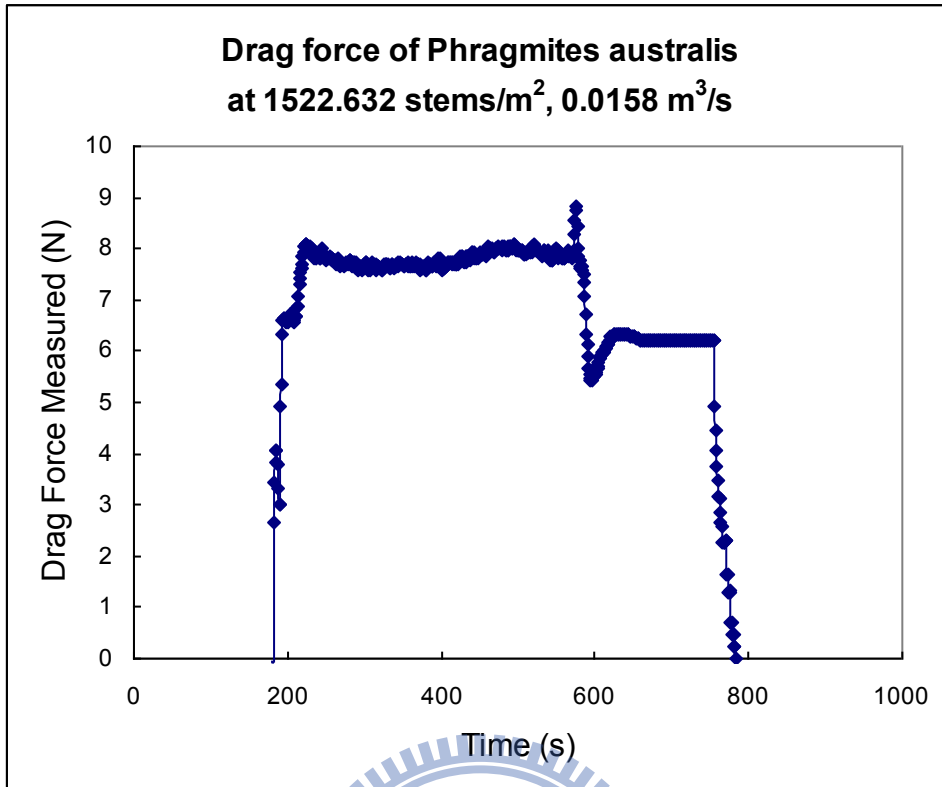


Figure 3.50 An example of drag force of Phragmites australis measured by the direct drag force measurement system at 1522.632 stems/m² and 0.0158 m³/s

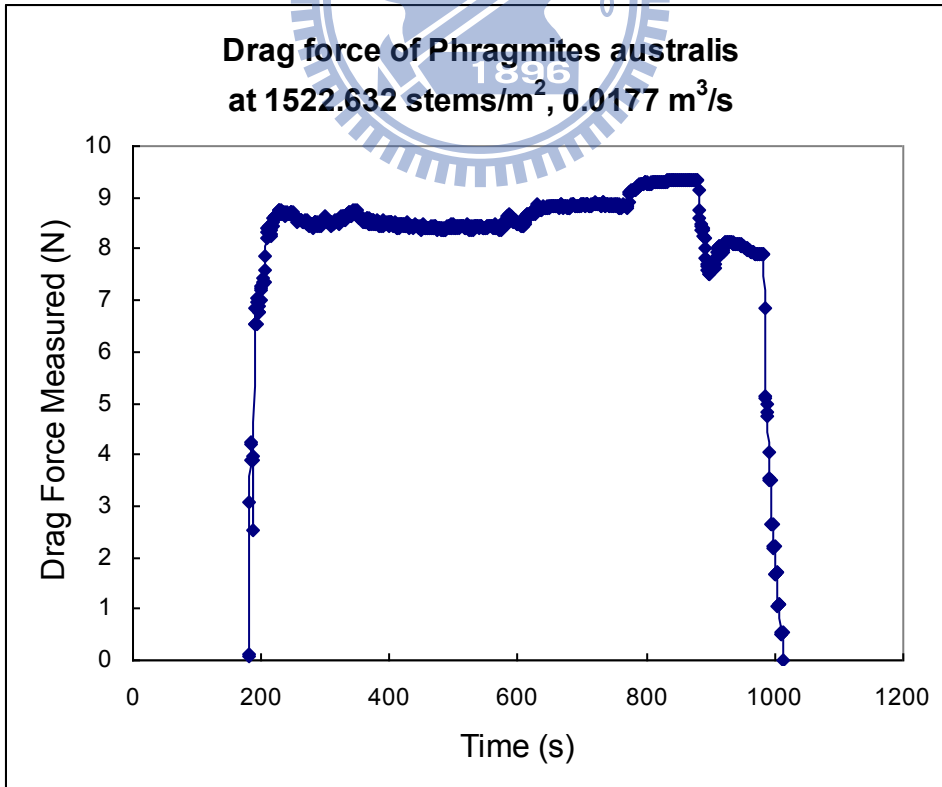


Figure 3.51 An example of drag force of Phragmites australis measured by the direct drag force measurement system at 1522.632 stems/m² and 0.0177 m³/s

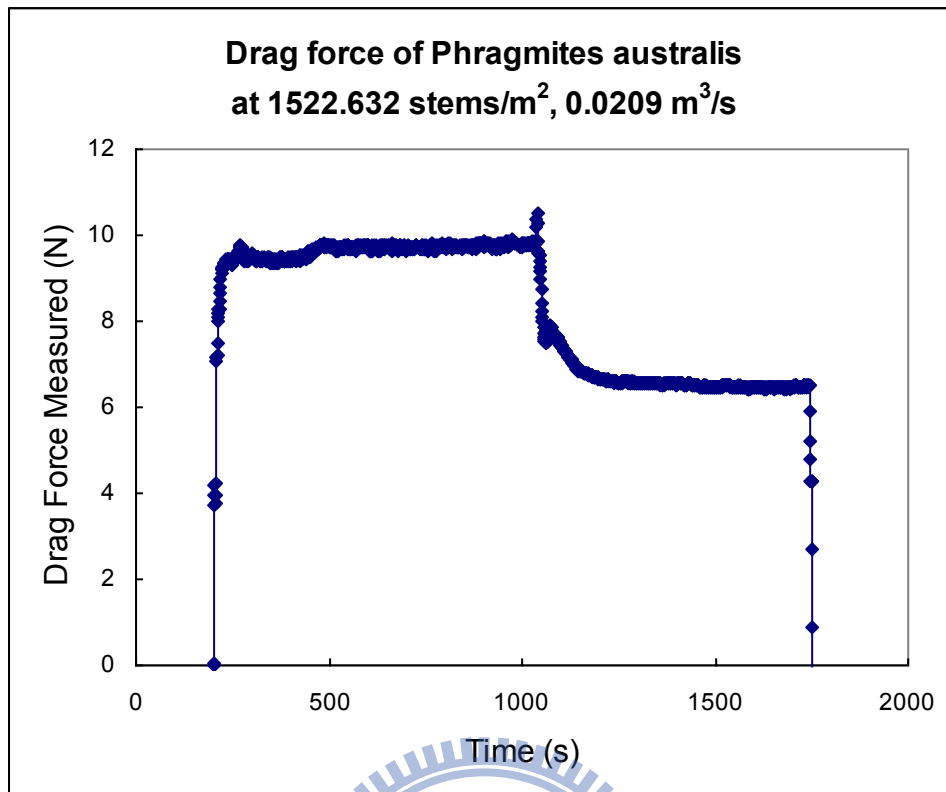


Figure 3.52 An example of drag force of Phragmites australis measured by the direct drag force measurement system at 1522.632 stems/m² and 0.0209 m³/s

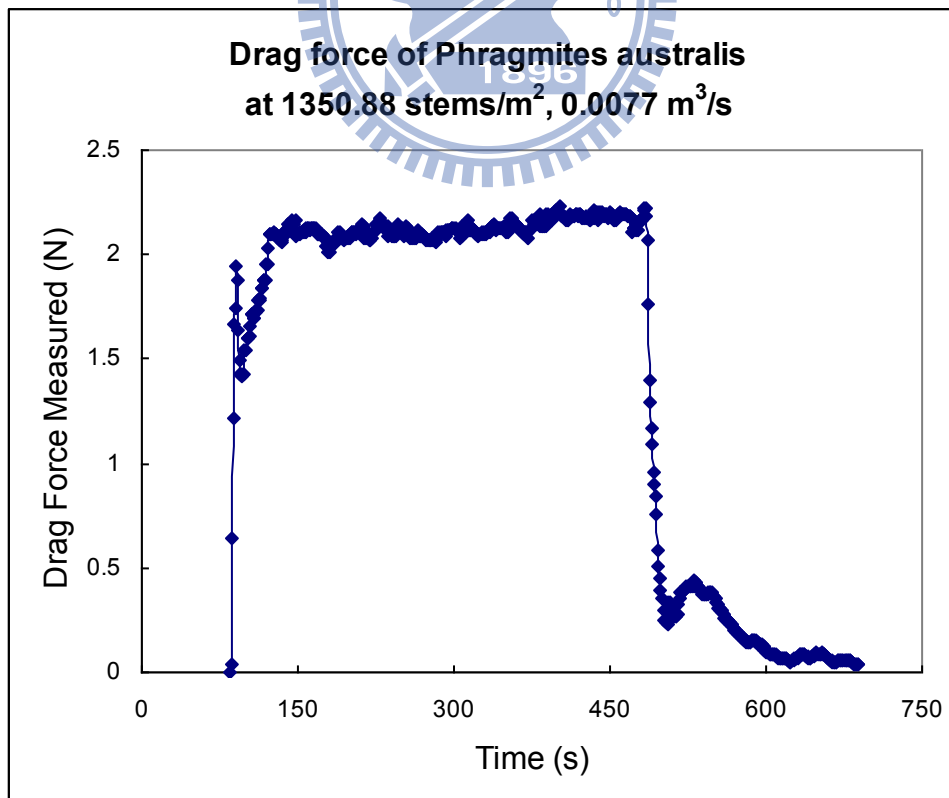


Figure 3.53 An example of drag force of Phragmites australis measured by the direct drag force measurement system at 1350.88 stems/m² and 0.0077 m³/s

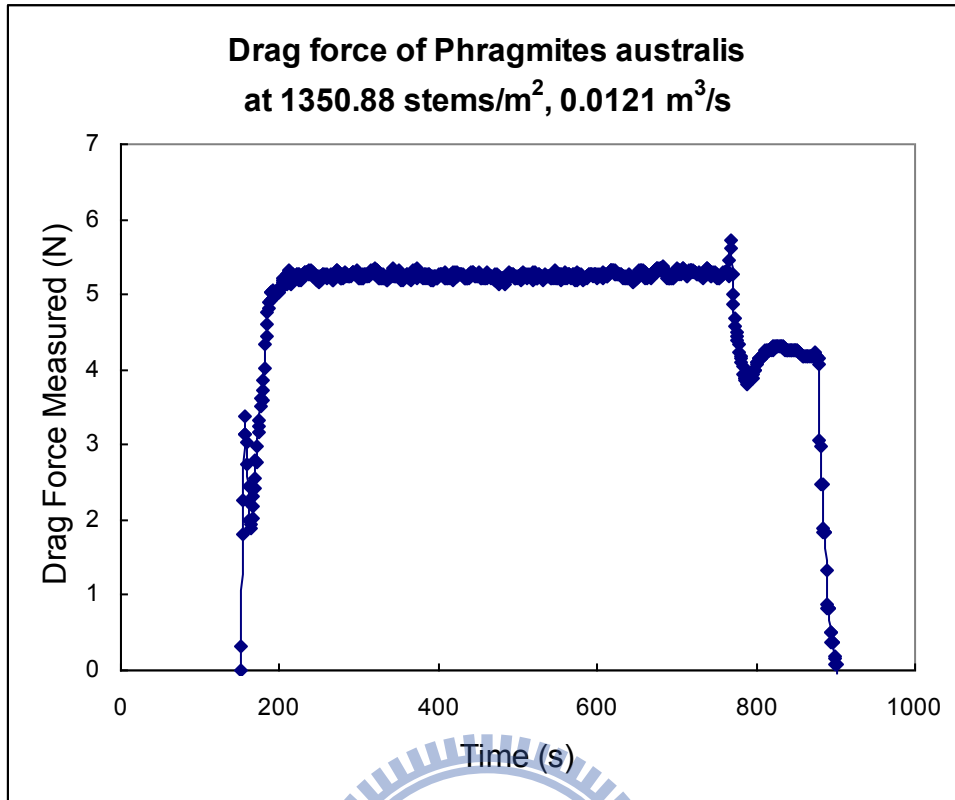


Figure 3.54 An example of drag force of Phragmites australis measured by the direct drag force measurement system at 1350.88 stems/m² and 0.0121 m³/s

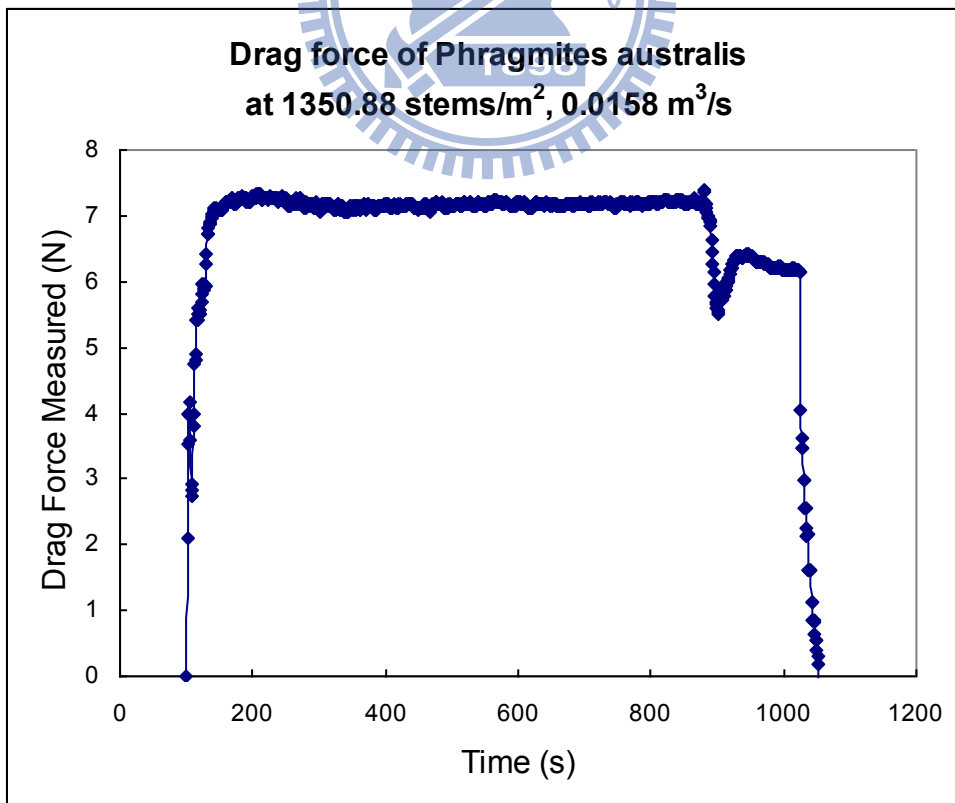


Figure 3.55 An example of drag force of Phragmites australis measured by the direct drag force measurement system at 1350.88 stems/m² and 0.0158 m³/s

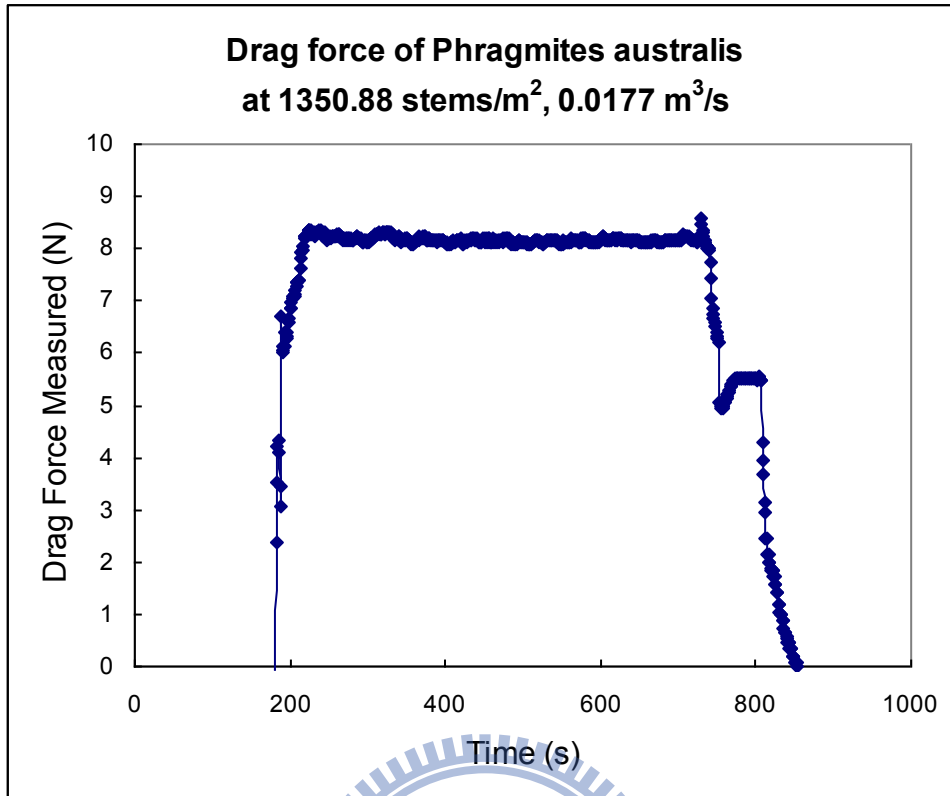


Figure 3.56 An example of drag force of Phragmites australis measured by the direct drag force measurement system at 1350.88 stems/m² and 0.0177 m³/s

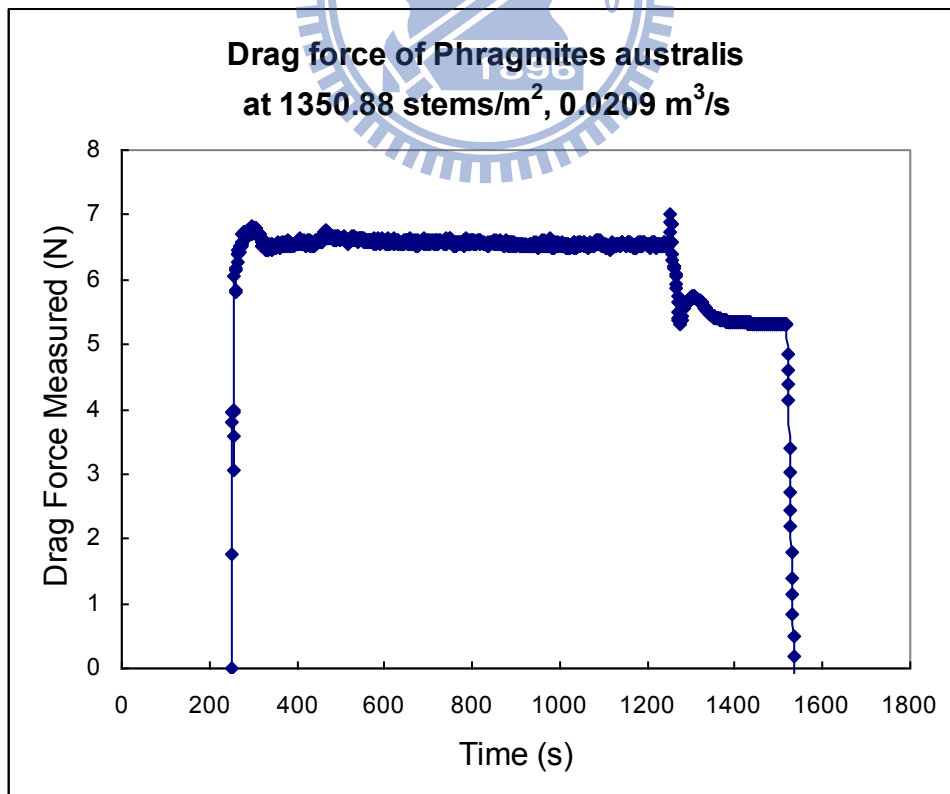


Figure 3.57 An example of drag force of Phragmites australis measured by the direct drag force measurement system at 1350.88 stems/m² and 0.0209 m³/s

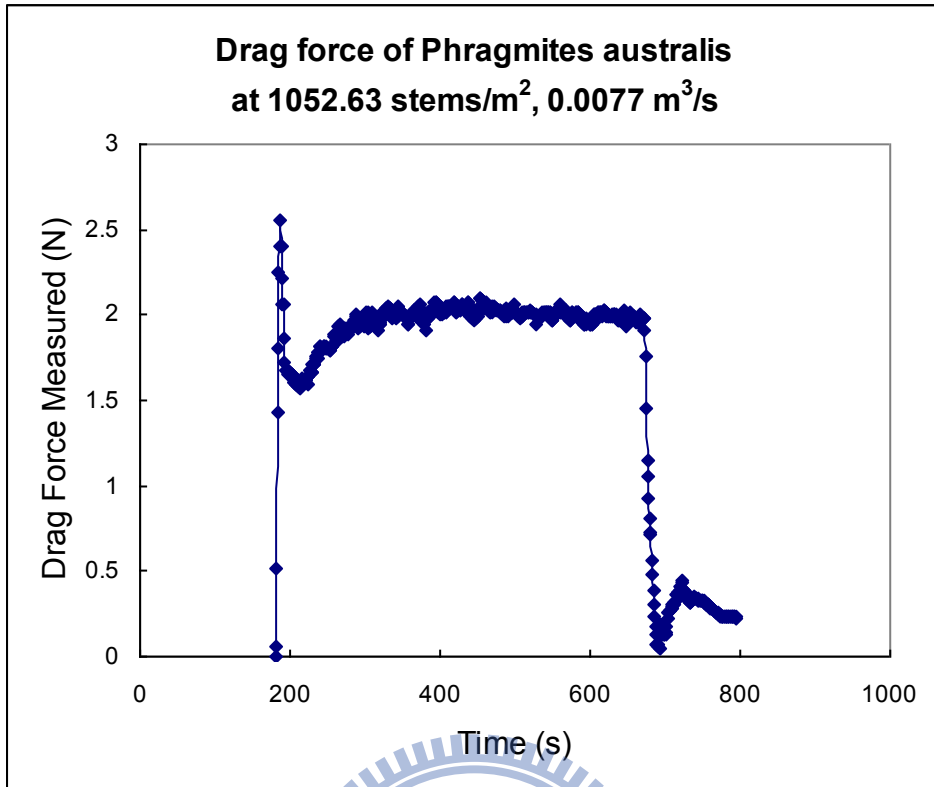


Figure 3.58 An example of drag force of Phragmites australis measured by the direct drag force measurement system at 1052.63 stems/m² and 0.0077 m³/s

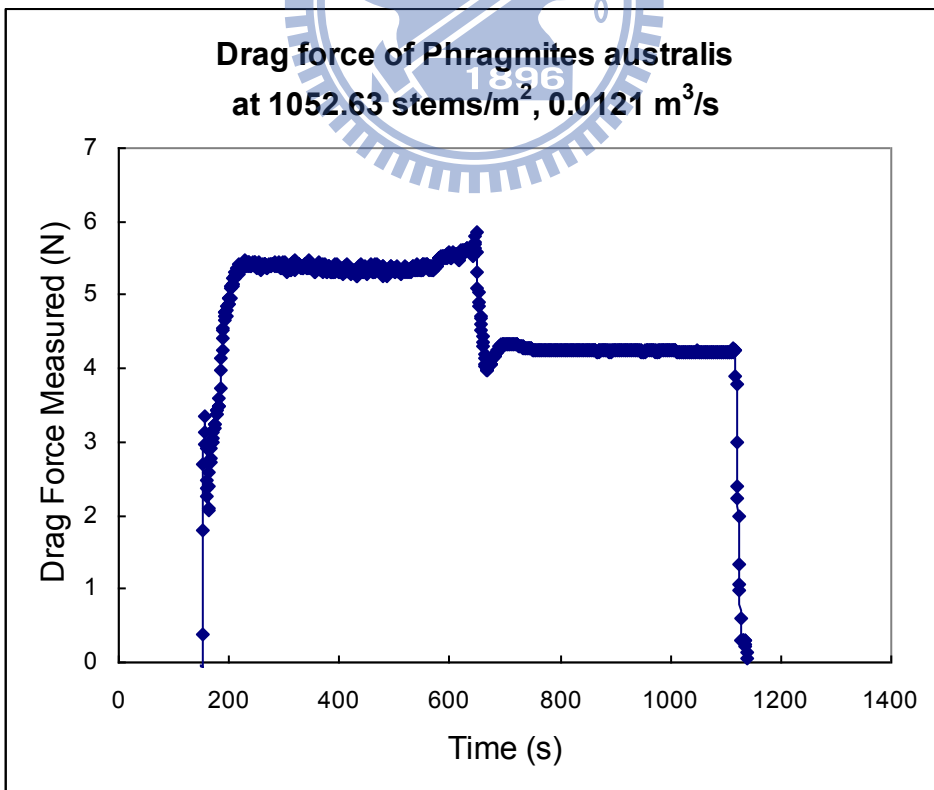


Figure 3.59 An example of drag force of Phragmites australis measured by the direct drag force measurement system at 1052.63 stems/m² and 0.0121 m³/s

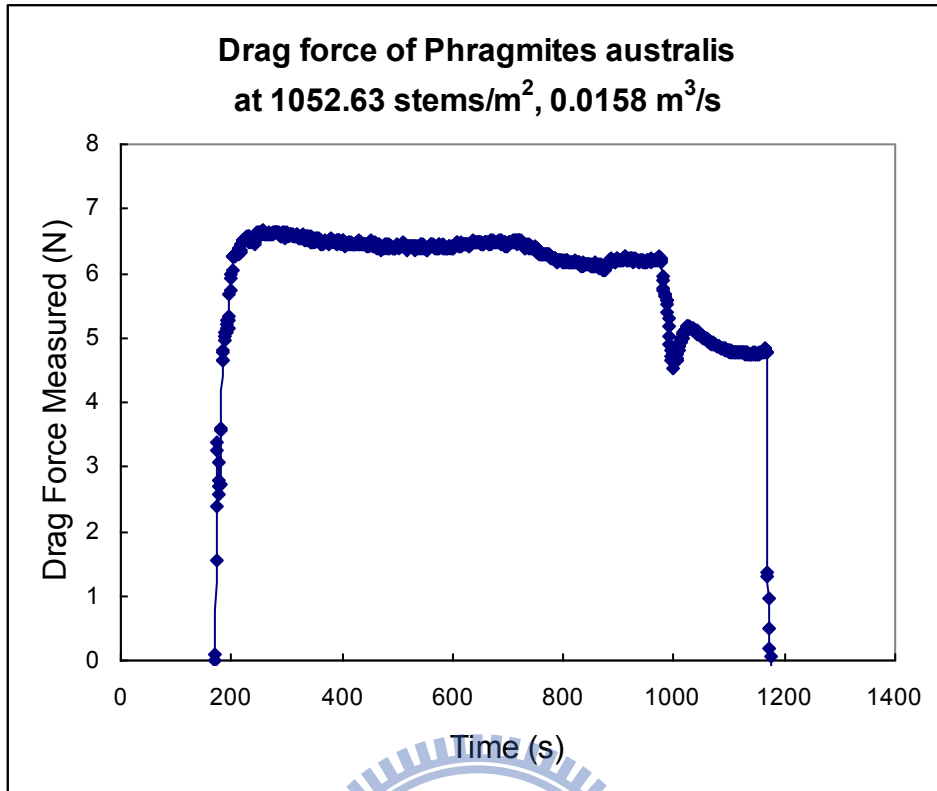


Figure 3.60 An example of drag force of Phragmites australis measured by the direct drag force measurement system at 1052.63 stems/m² and 0.0158 m³/s

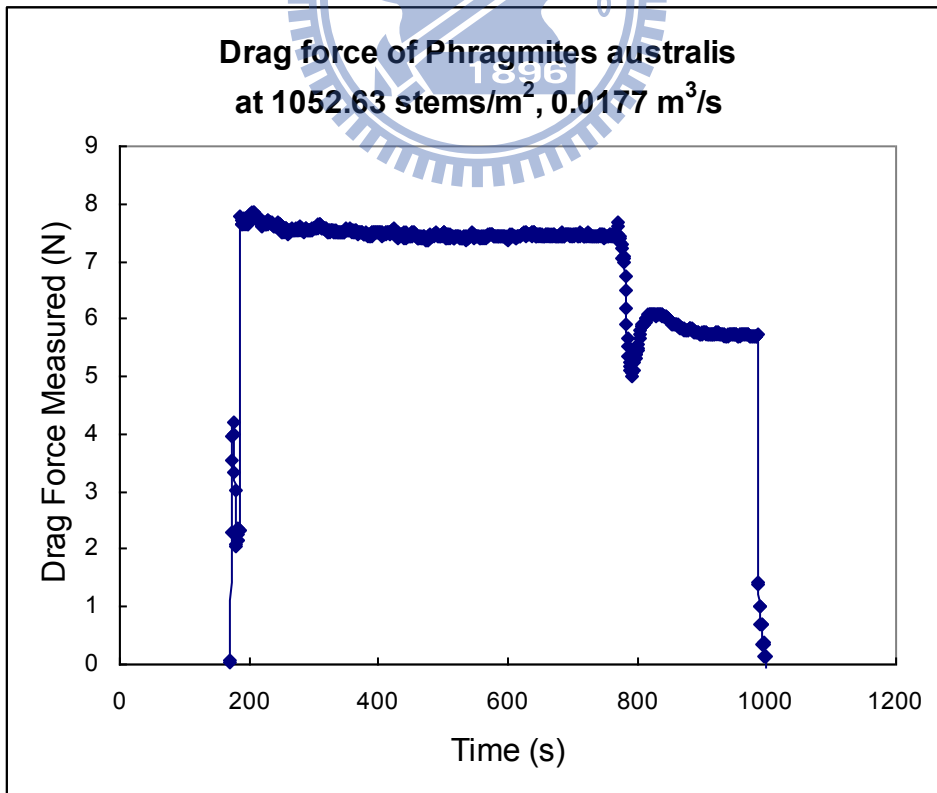


Figure 3.61 An example of drag force of Phragmites australis measured by the direct drag force measurement system at 1052.63 stems/m² and 0.0177 m³/s

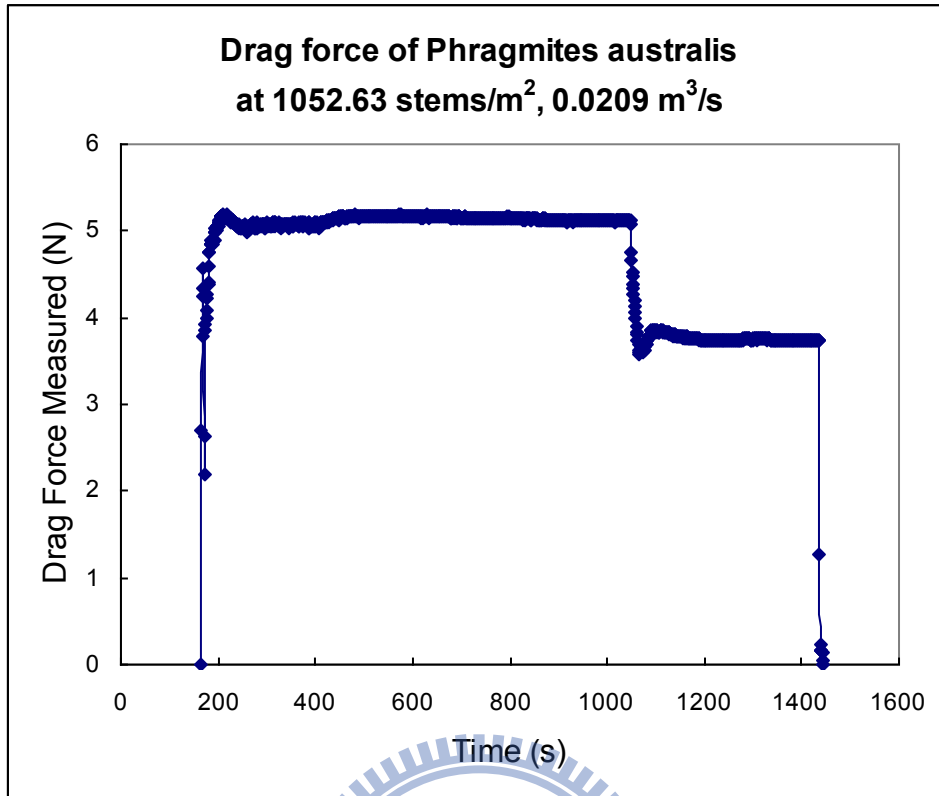


Figure 3.62 An example of drag force of Phragmites australis measured by the direct drag force measurement system at 1052.63 stems/m² and 0.0209 m³/s

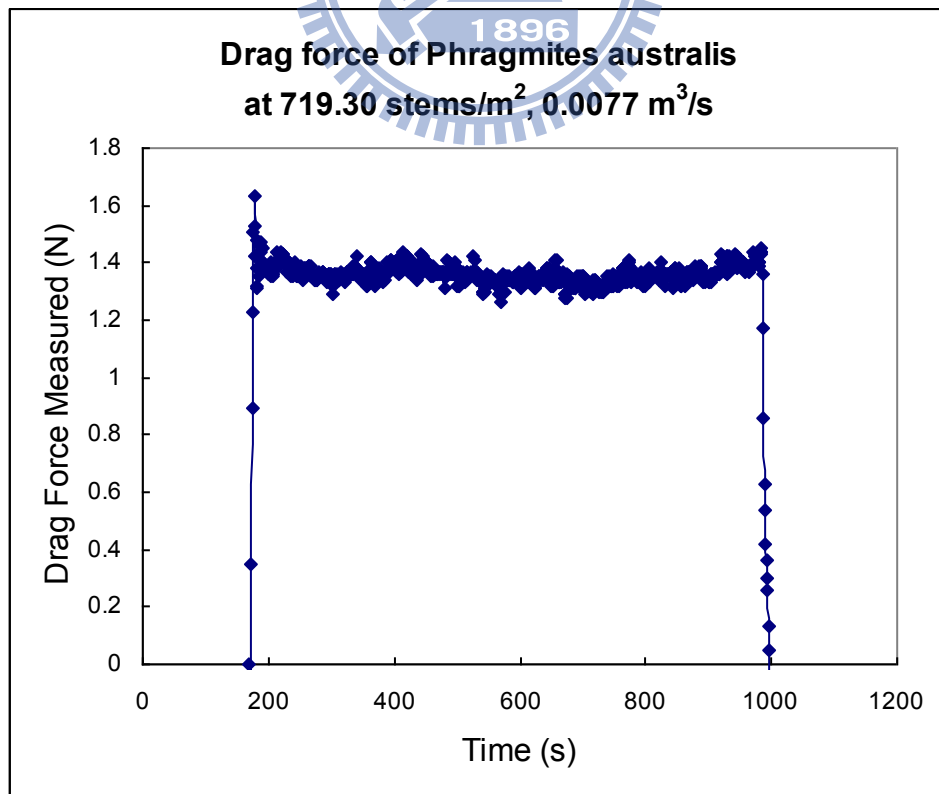


Figure 3.63 An example of drag force of Phragmites australis measured by the direct drag force measurement system at 719.30 stems/m² and 0.0077 m³/s

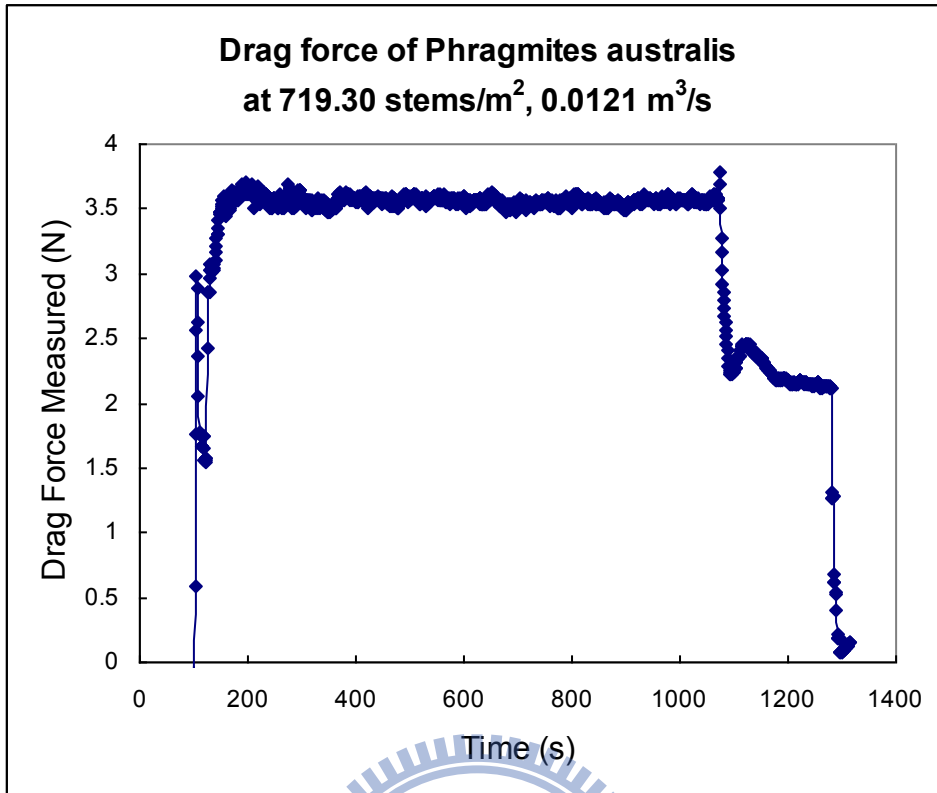


Figure 3.64 An example of drag force of Phragmites australis measured by the direct drag force measurement system at 719.30 stems/m² and 0.0121 m³/s

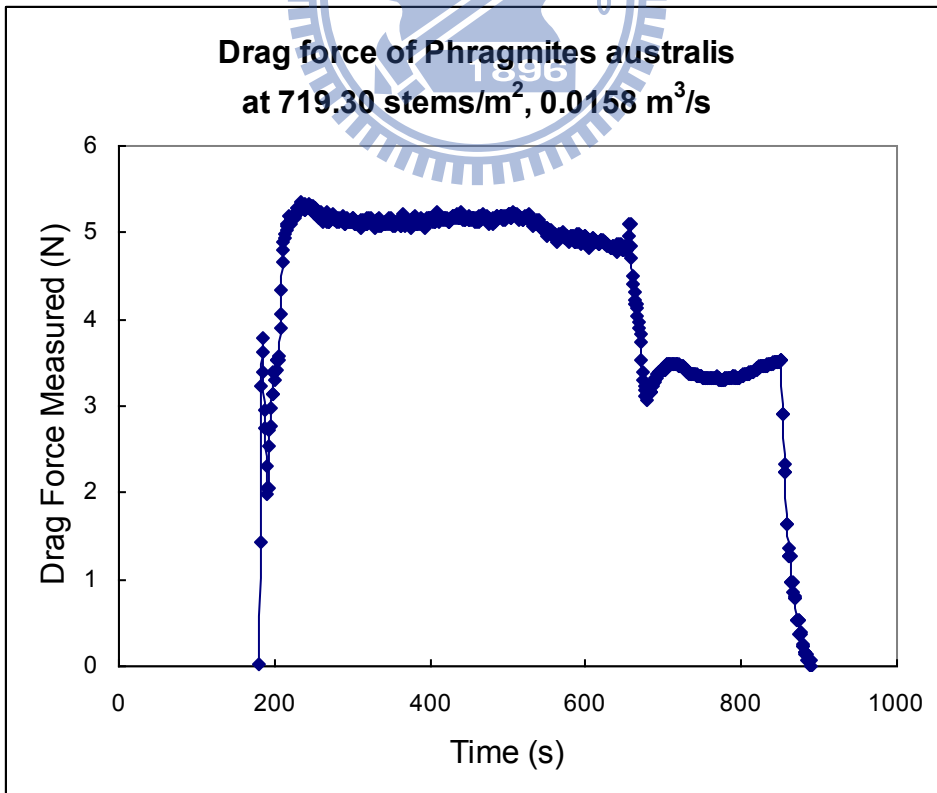


Figure 3.65 An example of drag force of Phragmites australis measured by the direct drag force measurement system at 719.30 stems/m² and 0.0158 m³/s

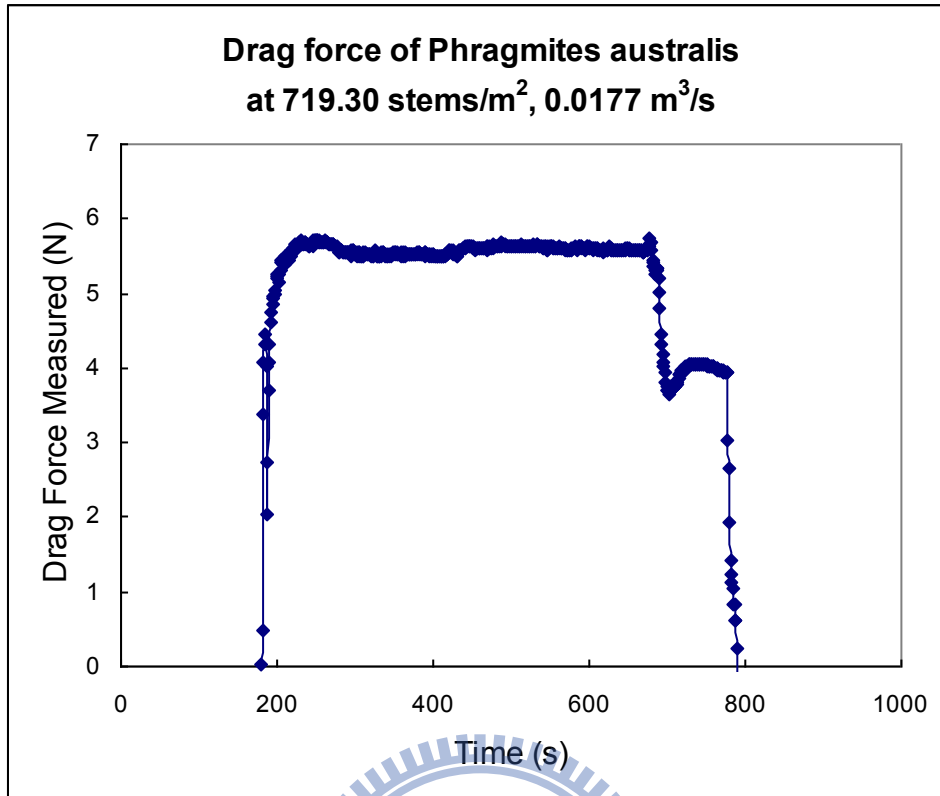


Figure 3.66 An example of drag force of Phragmites australis measured by the direct drag force measurement system at 719.30 stems/m² and 0.0177 m³/s

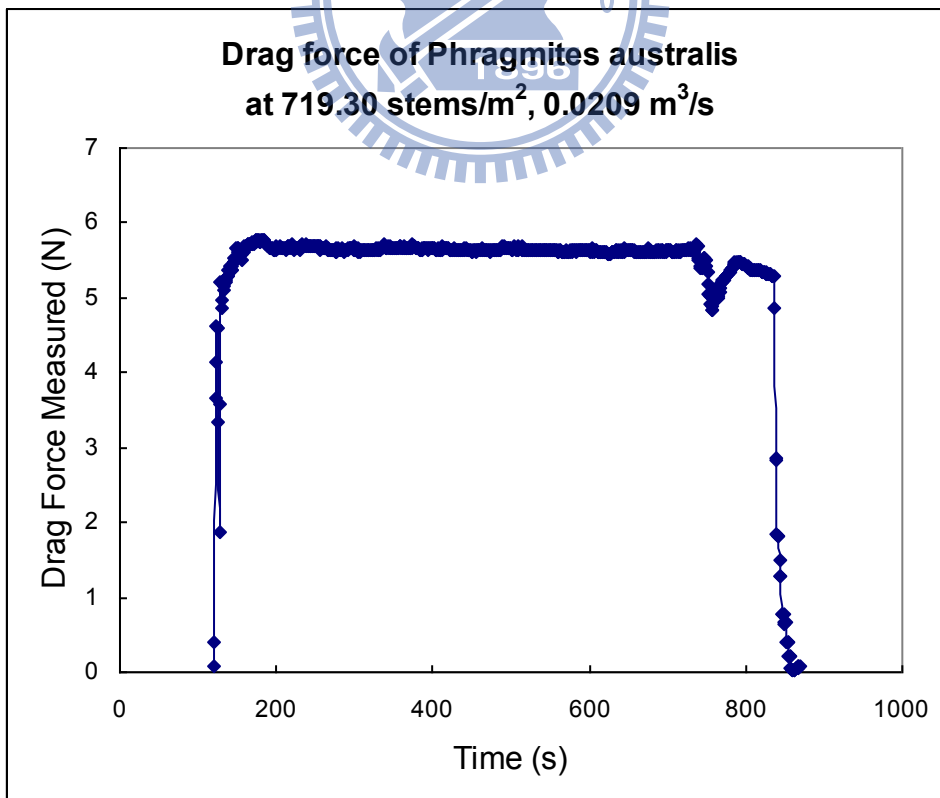


Figure 3.67 An example of drag force of Phragmites australis measured by the direct drag force measurement system at 719.30 stems/m² and 0.0209 m³/s

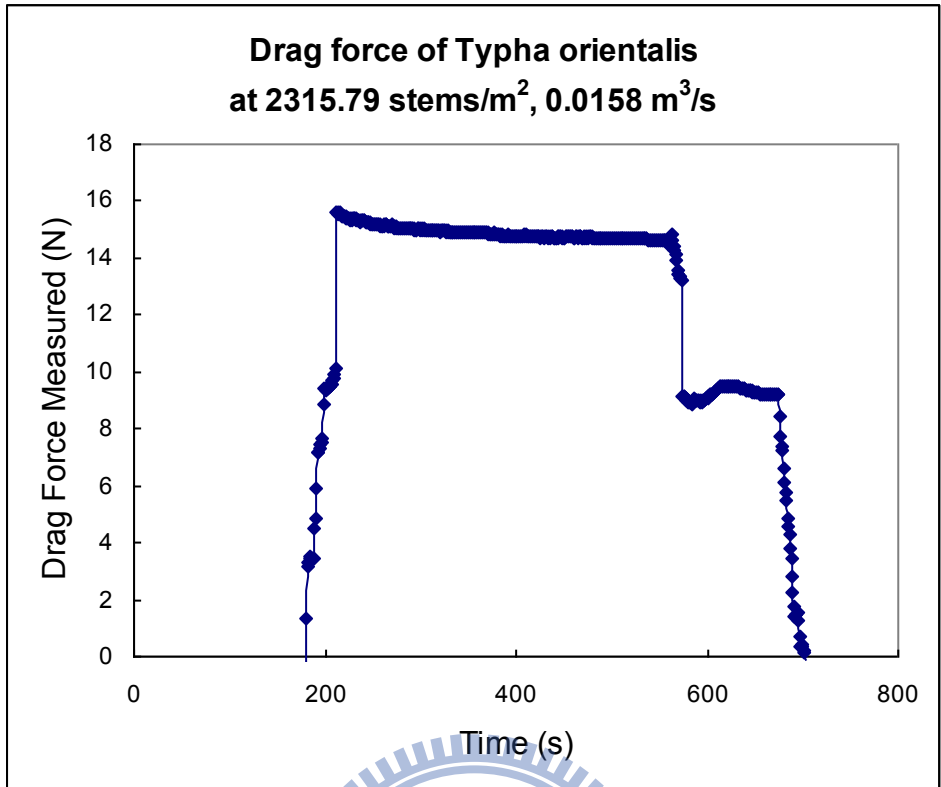


Figure 3.68 An example of drag force of *Typha orientalis* measured by the direct drag force measurement system at 2315.79 stems/m² and 0.0158 m³/s

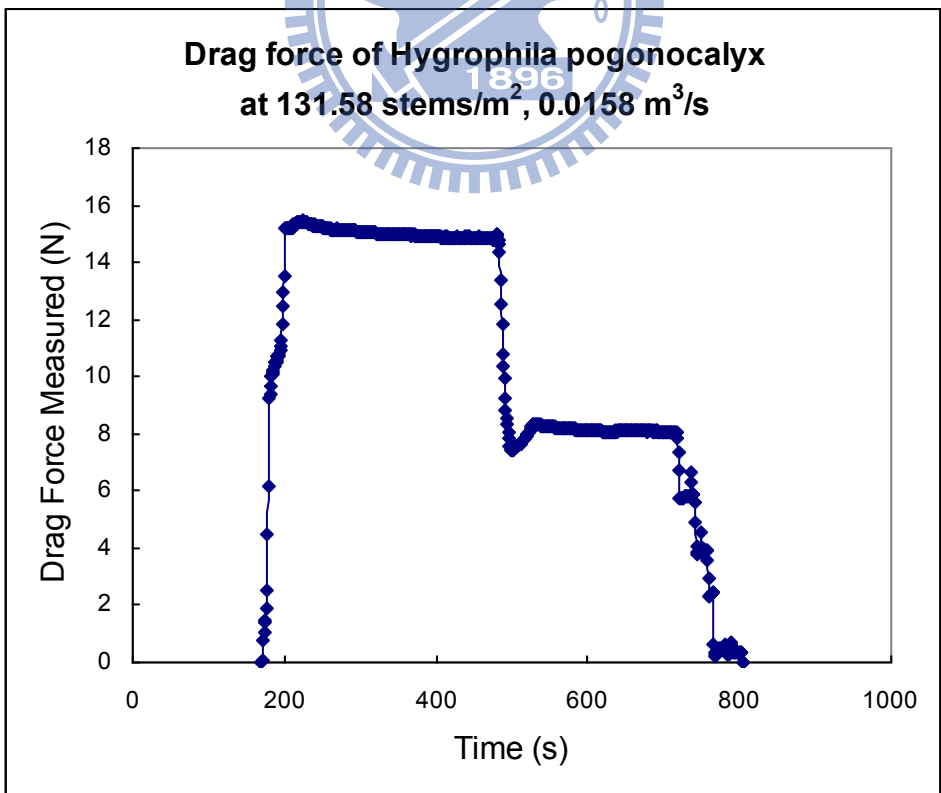


Figure 3.69 An example of drag force of *Hygrophila pogonocalyx* measured by the direct drag force measurement system at 131.58 stems/m² and 0.0158 m³/s

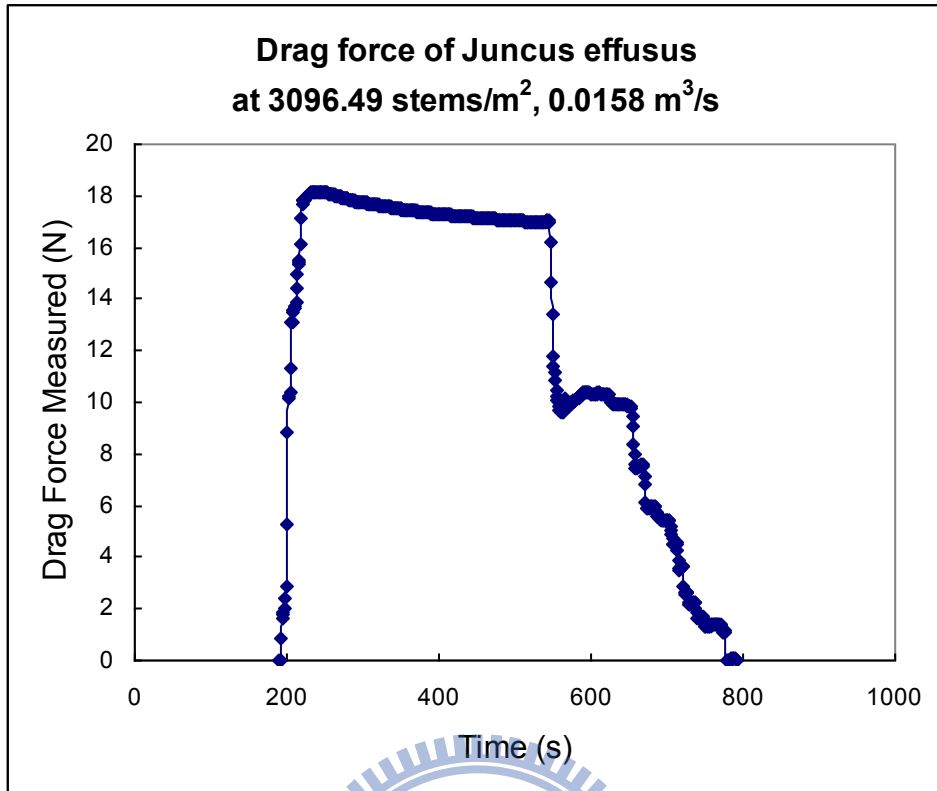


Figure 3.70 An example of drag force of *Juncus effusus* measured by the direct drag force measurement system at 3096.49 stems/m² and 0.0158 m³/s

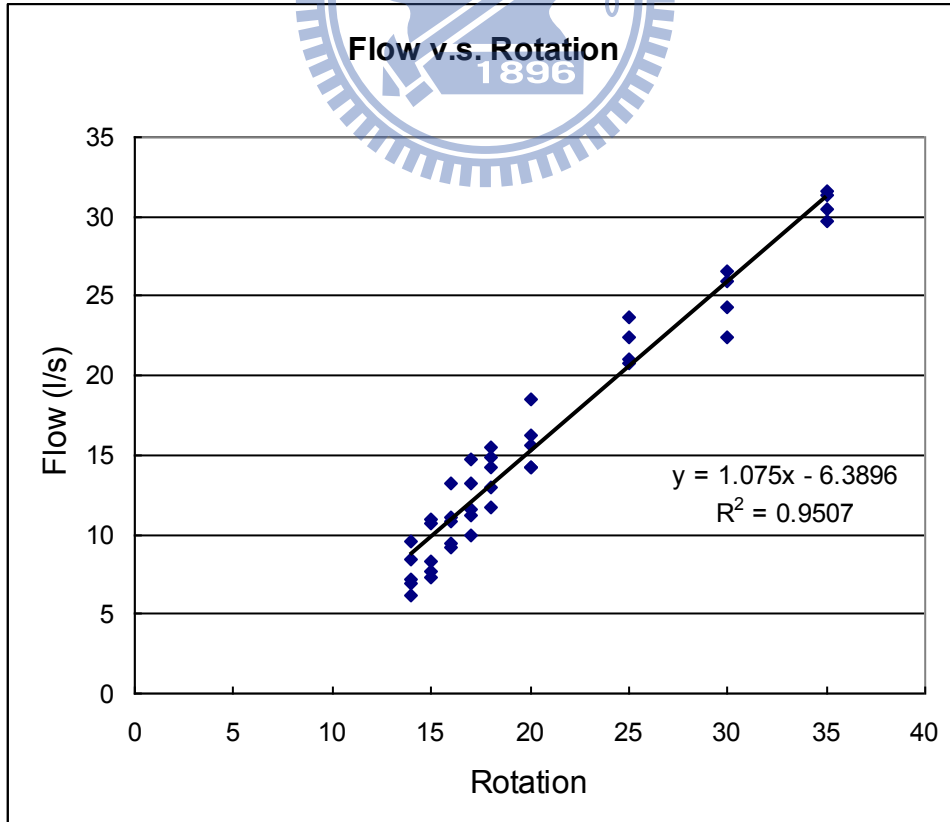


Figure 3.71 Plot of flow (l/s) against number of rotational turns which controls the revolutions per minute for the pump of the flume

Appendix A

Proof for Equation (3-20) – Method 1 (Julien Pierre Y., 2002)

A.1. Fluid flow kinematics

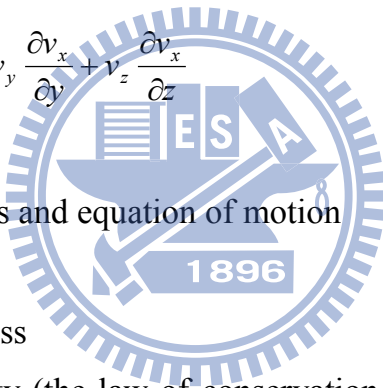
$$v = \sqrt{v_x^2 + v_y^2 + v_z^2}$$

$$v_x = \frac{dx}{dt} \quad ; \quad v_y = \frac{dy}{dt} \quad ; \quad v_z = \frac{dz}{dt} \tag{A-1}$$

Differential velocity over an infinitesimal distance ds (dx, dy, dz) and time increment dt at a point (x,y,z) are:

$$dv_x = \frac{\partial v_x}{\partial t} dt + \frac{\partial v_x}{\partial x} dx + \frac{\partial v_x}{\partial y} dy + \frac{\partial v_x}{\partial z} dz$$

$$a_x = \frac{dv_x}{dt} = \frac{\partial v_x}{\partial t} + v_x \frac{\partial v_x}{\partial x} + v_y \frac{\partial v_x}{\partial y} + v_z \frac{\partial v_x}{\partial z} \tag{A-1.1}$$



A.2. Conservation of mass and equation of motion

A.2.1 Conservation of mass

The equation of continuity (the law of conservation of mass) states that mass cannot be destroyed or created. The equation of continuity is written in differential form here, considering the infinitesimal control volume filled with a fluid particle with homogeneous concentration.

The difference between the mass fluxes entering and leaving the differential control volume equals to the rate of increase of internal mass.

In the ‘x’ direction, the net mass flux leaving the control volume is:

$$\left\{ \left[\frac{(\partial \rho_m v_x)}{\partial x} \right] dx \right\} (dydz)$$

Therefore the change in internal mass is:

$$\left(\frac{\partial \rho_m}{\partial t} \right) dx dy dz$$

In Cartesian coordinates (x, y, z) :

$$\frac{\partial \rho_m}{\partial t} + \frac{\partial}{\partial x}(\rho_m v_x) + \frac{\partial}{\partial y}(\rho_m v_y) + \frac{\partial}{\partial z}(\rho_m v_z) = 0$$

$$\frac{\partial v_x}{\partial t} + \frac{\partial v_y}{\partial x} + \frac{\partial v_z}{\partial y} = 0$$

For homogeneous incompressible suspensions without settling, the mass density is independent of space and time ($\rho_m = \text{constant}$) and $\partial \rho_m / \partial t = 0$.

A.2.2. Equation of motion

$$a_x = g_x + \frac{1}{\rho_m} \frac{\partial \sigma_x}{\partial t} + v_x \frac{\partial v_x}{\partial x} + v_y \frac{\partial v_x}{\partial y} + v_z \frac{\partial v_x}{\partial z}$$

$$a_x = g_x + \frac{1}{\rho_m} \frac{\partial \sigma_x}{\partial x} + \frac{1}{\rho_m} \frac{\partial \tau_{yx}}{\partial y} + \frac{1}{\rho_m} \frac{\partial \tau_{zx}}{\partial z}$$

$$\sigma_x = -p + \tau_{xx}$$

$$a_x = g_x + \frac{1}{\rho_m} \frac{\partial(-p + \tau_{xx})}{\partial x} + \frac{1}{\rho_m} \frac{\partial \tau_{yx}}{\partial y} + \frac{1}{\rho_m} \frac{\partial \tau_{zx}}{\partial z}$$

$$a_x = g_x + \frac{-1}{\rho_m} \frac{\partial p}{\partial x} + \frac{1}{\rho_m} \frac{\partial \tau_{xx}}{\partial x} + \frac{1}{\rho_m} \frac{\partial \tau_{yx}}{\partial y} + \frac{1}{\rho_m} \frac{\partial \tau_{zx}}{\partial z}$$

$$a_x = g_x - \frac{1}{\rho_m} \frac{\partial p}{\partial x} + \frac{1}{\rho_m} \left(\frac{\partial \tau_{xx}}{\partial x} + \frac{\partial \tau_{yx}}{\partial y} + \frac{\partial \tau_{zx}}{\partial z} \right) \quad (\text{A-2})$$

Since Equation (A-1.1) equals to Equation (A-2):

$$a_x = \frac{dv_x}{dt} = \frac{\partial v_x}{\partial t} + v_x \frac{\partial v_x}{\partial x} + v_y \frac{\partial v_x}{\partial y} + v_z \frac{\partial v_x}{\partial z} = g_x - \frac{1}{\rho_m} \frac{\partial p}{\partial x} + \frac{1}{\rho_m} \left(\frac{\partial \tau_{xx}}{\partial x} + \frac{\partial \tau_{yx}}{\partial y} + \frac{\partial \tau_{zx}}{\partial z} \right)$$

If the following assumptions are considered:

- a. The flow is one dimensional
 - i. $v = v_x$
 - ii. $v_y = v_z = 0$
- b. Shear stress due to element stretching and deformation = 0
 - i. $\tau_{xx} = 0$
- c. Bank shear at the sides of the flume = 0
 - i. $\tau_{yx} = 0$

- ii. But the bed shear is significant $\tau_{zx} \neq 0$
- d. At small bed-slope angles, $\sin\theta \approx \tan\theta$.
- i. $g_x = g\sin\theta \approx gS_0$

$$\frac{\partial v_x}{\partial t} + v_x \frac{\partial v_x}{\partial x} \approx gS_0 - \frac{1}{\rho} \frac{\partial p}{\partial x} + \frac{1}{\rho} \left(\frac{\partial \tau_{zx}}{\partial z} \right) \quad (\text{A-3})$$

Equation (A-2) in the z direction is written as:

$$a_z = g_z - \frac{1}{\rho_m} \frac{\partial p}{\partial z} + \frac{1}{\rho_m} \left(\frac{\partial \tau_{xz}}{\partial x} + \frac{\partial \tau_{yz}}{\partial y} + \frac{\partial \tau_{zz}}{\partial z} \right)$$

Given that $a_z = 0$, shear stress variation are small, and $g_z = g\cos\theta \approx -g$

$$g_z = \frac{1}{\rho} \frac{\partial p}{\partial z}$$

$$-g = \frac{1}{\rho} \frac{\partial p}{\partial z}$$

$$-\rho g = \frac{\partial p}{\partial z}$$

$$-\rho g dz = dp$$

$$\rho \int_z^h -g dz = \int_p^0 dp$$

$$\rho g(h-z) = p$$

$$p = \rho g(h-z) \quad (\text{A3.1})$$

At bed level, $z = 0$; $p = \rho g(h)$; at free surface, $h = z$, $p = 0$

At channel bed, the shear stress is expressed as:

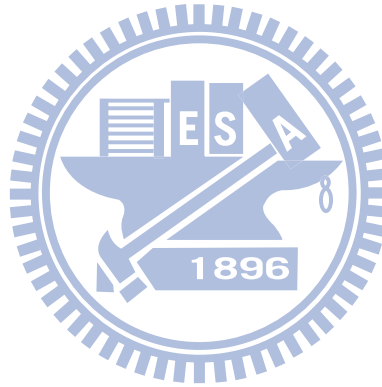
$$\tau_0 = \rho g h S_f$$

Similar to the pressure distribution, shear stress vanishes at the free surface and varies linearly over the depth. Therefore the shear stress distribution is:

$$\tau_{zx} = \rho g(h-z) S_f \quad (\text{A 3.2})$$

Substitute Equation (A.3.1) and (A.3.2) into (A-4):

$$\frac{\partial v_x}{\partial t} + v_x \frac{\partial v_x}{\partial x} \approx gS_0 - \frac{1}{\rho} \frac{\partial p}{\partial x} + \frac{1}{\rho} \left(\frac{\partial \tau_{zx}}{\partial z} \right) \quad (\text{A-4})$$



$$\frac{\partial v_x}{\partial t} + v_x \frac{\partial v_x}{\partial x} \approx gS_0 - \frac{1}{\rho} \left[\frac{\partial (\rho g(h-z))}{\partial x} \right] + \frac{1}{\rho} \left\{ \frac{\partial (\rho g(h-z)S_f)}{\partial z} \right\}$$

$$\frac{\partial v_x}{\partial t} + v_x \frac{\partial v_x}{\partial x} \approx gS_0 - g \frac{\partial h}{\partial x} + g \frac{\partial z}{\partial x} + gS_f \frac{\partial h}{\partial z} - gS_f \frac{\partial z}{\partial z}$$

$$dz/dx = 0, dS_f/dz = dh/dz = 0$$

$$\frac{\partial v_x}{\partial t} + v_x \frac{\partial v_x}{\partial x} \approx gS_0 - g \frac{\partial h}{\partial x} + gS_f$$

$$S_f \approx S_0 - \frac{\partial h}{\partial x} - \frac{v_x}{g} \frac{\partial v_x}{\partial x} - \frac{1}{g} \frac{\partial v_x}{\partial t} \quad (\text{A-5})$$

For steady non uniform flow, velocity varies with distance, but the initial and other velocities at their respect position do not vary with time.

Therefore:

$$S_f \approx S_0 - \frac{\partial h}{\partial x} - \frac{v_x}{g} \frac{\partial v_x}{\partial x}$$

$$S_f = S_0 - \frac{dh}{dx} - \frac{v}{g} \frac{dv}{dx}$$



(A-6)

Proof for Equation (3-20) – Method 2 (Chow V. T. et al., 1988)

Drag force induced from flow over vegetated area is usually considered as an important term in the momentum equation. Below is a demonstration of the channel bed friction force as part of the momentum equation, and the derivation of the validation for drag force used in this thesis.

For any extensive property B , a corresponding intensive property β can be defined as the quantity of B per unit mass m of fluid, that is $\beta = dB/dm$. The Reynolds transport theorem relates the change of an extensive property per unit time in the fluid $[dB/dt]$ to the external causes producing this change. Therefore the Reynolds transport theorem takes physical laws that are normally applied to a discrete mass of a substance and applies these laws to a fluid flowing continuously through a control volume. The governing equation of the Reynolds transport theorem is:

$$\frac{dB}{dt} = \frac{d}{dt} \iiint_{c.v.} \beta \rho d\forall + \iint_{c.s.} \beta \rho V dA \quad (A-7)$$

where ρ is the fluid density, dA is the control surface, and $d\forall$ is the volume of the element. The Reynolds transport theorem states that the total rate of change of an extensive property of a fluid is equal to the rate of change of extensive property stored in the control volume ($d/dt \iiint \beta \rho d\forall$) plus the net outflow of extensive property through the control surface ($\iint \beta \rho V dA$). When the Reynolds transport theorem is applied to fluid momentum, the extensive property is $B = mV$, and $\beta = d(mV)/dm = V$, where V is the fluid velocity. From Newton's second law, the time rate of change of momentum is equal to the net force applied in a given direction. Therefore $dB/dt = d(mV)/dt = \sum F$. Substituting into Equation A-7.1 gives:

$$\sum F = \frac{d}{dt} \iiint_{c.v.} V \rho d\forall + \iint_{c.s.} V \rho V \cdot dA \quad (A-8)$$

= momentum storage + net momentum outflow

For the Momentum Storage:

The time rate of change of momentum stored in the control volume is

found by the product of the volume of the elemental channel ($A dx$), the fluid density (ρ), and the fluid velocity (V), which could be expressed by $\rho A dx V$, or $\rho Q dx$:

$$\frac{d}{dt} \iiint_{c.v.} V \rho dV = \rho \frac{\partial Q}{\partial t} dx \quad (\text{A-9})$$

For the Net Momentum Outflow:

The net momentum outflow is equal to the sum of inflow and the outflow in two different directional signs.

$$\iint_{c.s.} V \rho V dA = \iint_{inlet} V \rho V dA + \iint_{outlet} V \rho V dA \quad (\text{A-10})$$

The mass inflow rate to the control volume is $-\rho(Q + q dx)$, representing both stream flow and lateral inflow. The corresponding momentum is computed by multiplying the two mass inflow rates by their respective velocities and a momentum correction factor β :

$$\iint_{inlet} V \rho V dA = -\rho(\beta V Q + \beta v_x q dx) \quad (\text{A-11})$$

where $\rho \beta V Q$ is the momentum entering from the upstream end of the channel and $\rho \beta v_x q dx$ is the momentum entering the main channel with the lateral inflow having a velocity v_x in the x direction. The term β is known as the momentum coefficient or Boussinesq coefficient that accounts for the nonuniform distribution of velocity at a channel cross section in computing the momentum.

The momentum outlet can be expressed by:

$$\iint_{outlet} V \rho V dA = \rho \left[\beta V Q + \frac{\partial(\beta V Q)}{\partial x} dx \right] \quad (\text{A-12})$$

Substituting Equation (A-12) and (A-11) into (A-10) gives:

$$\iint_{c.s.} V \rho V dA = -\rho(\beta V Q + \beta v_x q dx) + \rho \left[\beta V Q + \frac{\partial(\beta V Q)}{\partial x} dx \right] \quad (\text{A-13})$$

$$\iint_{c.s.} V \rho V dA = -\rho \left[\beta v_x q - \frac{\partial(\beta V Q)}{\partial x} dx \right] \quad (\text{A-14})$$

Therefore,

$$\sum F = \frac{d}{dt} \iiint_{c.v.} V \rho dV + \iint_{c.s.} V \rho V \cdot dA = \rho g \frac{\partial Q}{\partial t} dx - \rho \left[\beta v_x q - \frac{\partial(\beta V Q)}{\partial x} dx \right]$$

$$\sum F = \rho g \frac{\partial Q}{\partial t} dx - \rho \left[\beta v_x q - \frac{\partial(\beta V Q)}{\partial x} dx \right] \quad (\text{A-15})$$

There are five forces acting on the control volume:

$$\sum F = F_g + F_f + F_e + F_w + F_p \quad (\text{A-16})$$

where F_g is the gravity force, F_f is the friction force along the bottom and the side of the control volume, F_e is the contraction/expansion force induced by the change of channel cross section, F_w is the wind shear force on the water surface, and F_p is the pressure force.

The gravity force for a volume of fluid in the control volume is:

$$F_g = \rho g A dx \sin \theta \approx \rho g A S_0 dx \quad (\text{A-17})$$

where the channel bottom slope is $S_0 = -\partial z / \partial x$

The friction force resulted from the shear stress along the bottom and the sides of the control volume are given by $-\tau P dx$ where τ is the bottom shear stress and P is the wetted perimeter. Since τ is given by $\tau = \gamma R S_f$ hence the friction force is expressed as:

$$F_f = -\rho g A S_f dx \quad (\text{A-18})$$

The abrupt contraction or expansion of a channel causes energy loss through eddy motion. The drag forces creating these eddy losses are given by:

$$F_e = -\rho g A S_e dx \quad (\text{A-19})$$

where S_e is the eddy loss slop given by:

$$S_e = \frac{K_e}{2g} \frac{\partial \left(\frac{Q}{A} \right)^2}{\partial x} \quad (\text{A-20})$$

where K_e is the nondimensional expansion (negative) or contraction (positive) coefficient.

The wind shear force is resulted from frictional resistance of wind against the free surface of the water which is given by:

$$F_w = \tau_w B dx \quad (\text{A-21})$$

where τ_w is the wind shear stress written as:

$$\tau_w = \frac{-\rho C_f |V_r| V_r}{2} \quad (\text{A-22})$$

where V_r is the velocity of the fluid relative to the boundary and C_f is the shear stress coefficient.

$$V_r = \frac{Q}{A} - V_w \cos \omega \quad (\text{A-23})$$

where Q/A gives the average velocity, V_w is the wind velocity in a direction at angle ω to the water velocity.

From the above, wind shear is expressed as:

$$F_w = -W_f B \rho dx \quad (\text{A-24})$$

The pressure force is resulted from the unbalanced pressure force of the hydrostatic force on the left side of the control volume, the right side of the control volume, and the pressure force exerted by the banks on the control volume. After simplifying, the pressure force is given by:

$$F_p = -\rho g A \frac{\partial y}{\partial x} dx \quad (\text{A-25})$$

Combining Equation (A-17), (A-18), (A-19), (A-24), and (A-25), the total sum of the five forces is expressed as:

$$\sum F = \rho g A S_0 dx - \rho g A S_f dx - \rho g A S_e dx - W_f B \rho dx - \rho g A \frac{\partial y}{\partial x} dx \quad (\text{A-26})$$

Since Equation (A-26) equals to Equation (A-15), the equation becomes:

$$\sum F = \rho g A S_0 dx - \rho g A S_f dx - \rho g A S_e dx - W_f B \rho dx - \rho g A \frac{\partial y}{\partial x} dx = \rho g \frac{\partial Q}{\partial t} dx$$

$$- \rho \left[\beta v_x q - \frac{\partial(\beta V Q)}{\partial x} dx \right]$$

$$\rho g A S_0 dx - \rho g A S_f dx - \rho g A S_e dx - W_f B \rho dx - \rho g A \frac{\partial y}{\partial x} dx = \rho g \frac{\partial Q}{\partial t} dx$$

$$- \rho \left[\beta v_x q - \frac{\partial(\beta V Q)}{\partial x} dx \right]$$

$$\frac{\partial Q}{\partial t} + \frac{\partial \left(\frac{\beta Q^2}{A} \right)}{\partial x} + g A \left(\frac{\partial y}{\partial x} - S_0 + S_f + S_e \right) - \beta q v_x + W_f B = 0$$

$$h = y + z$$

$$\frac{\partial h}{\partial x} = \frac{\partial y}{\partial x} - \frac{\partial z}{\partial x} ; \quad \frac{\partial z}{\partial x} = -S_0$$

$$\frac{\partial Q}{\partial t} + \frac{\partial \left(\frac{\beta Q^2}{A} \right)}{\partial x} + gA \left(\frac{\partial h}{\partial x} + S_f + S_e \right) - \beta q v_x + W_f B = 0 \quad (\text{A-27})$$

Neglecting eddy losses, wind shear effect, and lateral inflow, the non-conservation form of the momentum equation for a unit width of flow is:

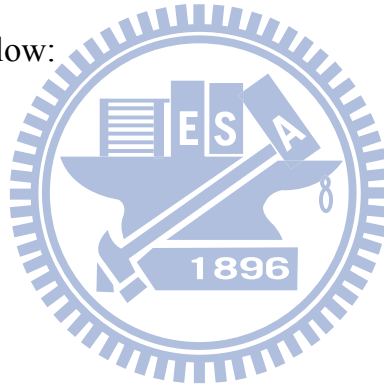
$$\frac{\partial V}{\partial t} + V \frac{\partial V}{\partial x} + g \left(\frac{\partial y}{\partial x} - S_0 + S_f \right) = 0$$

$$\frac{1}{g} \frac{\partial V}{\partial t} + \frac{V}{g} \frac{\partial V}{\partial x} + \left(\frac{\partial y}{\partial x} - S_0 + S_f \right) = 0$$

$$S_f = S_0 - \frac{\partial y}{\partial x} - \frac{V}{g} \frac{\partial V}{\partial x} - \frac{1}{g} \frac{\partial V}{\partial t} \quad (\text{A-28})$$

For steady non-uniform flow:

$$S_f = S_0 - \frac{\partial y}{\partial x} - \frac{V}{g} \frac{\partial V}{\partial x} \quad (\text{A-29})$$



Proof for Equation (3-20) – Method 3 (Henderson, 1966)

Consider a small element in a river channel section with depth of y , longitudinal differences of Δx , and cross sectional width of Δb . Assume that the slope is small and the pressure distribution is hydrostatic, the pressure difference along any horizontal line drawn longitudinally through this element is $\gamma \Delta h$, where Δh is the differences between the water surfaces at the upstream and the downstream face of the element. Taking the downstream direction as the positive direction for vectors, the total horizontal hydrostatic thrust on the small element is equal to $-\gamma y \Delta b \Delta h$, if $\Delta h/y$ and $\Delta z /y$ are small, where Δz is the differences in datum between the upstream level and the downstream level. Therefore the force in the direction of the downstream channel is $-\gamma A \Delta h$, where A is the cross-sectional area ($y \Delta b$).

The shear force resulted by water flowing through its boundary could be denoted as $\tau_0 P \Delta x$, where P is the wetted perimeter of the section and τ_0 is the mean longitudinal shear stress acting over this perimeter. The two forces mentioned here are in opposite directions. Therefore the net force in the direction of flow is:

$$-\gamma A \Delta h - \tau_0 P \Delta x \quad (\text{A-30})$$

In uniform flow, $\tau_0 = \gamma R S_0$ (A-31)

Where $R=A/P$, termed as the hydraulic mean radius, and S_0 is the bed slope, $-dz/dx$, which is equal to $-dh/dx$ in the case of uniform flow. If the flow is nonuniform and the velocity is changing in the downstream direction, the force in Eq. A-13 is not zero since the flow is accelerating. This acceleration could be termed as $v(dv/dx)$ in the case of steady flow. The force in Equation (A-30) when applied to a mass of $\rho A \Delta x$, changed Equation (A-30) into the following:

$$\begin{aligned} -\gamma A \Delta h - \tau_0 P \Delta x &= \text{net force} = ma \\ -\gamma A \Delta h - \tau_0 P \Delta x &= (\rho A \Delta x)[v(dv/dx)] \\ -\gamma A \Delta h - \tau_0 P \Delta x &= \rho A v (dv/dx) \Delta x \end{aligned} \quad (\text{A-32})$$

From Chezy's equation:

$$v = C\sqrt{RS}$$

When the flow is steady, the gradient (dH/dx) of the total energy line is equal in magnitude and opposite in sign to the friction slope $S_f = v^2/(C^2R)$. Here under the present context, two independent definitions are recognized:

$$S_f = \frac{v^2}{C^2R} = \frac{\tau_0}{\gamma R} \quad (\text{A-33})$$

$$\frac{\partial H}{\partial x} = \frac{\partial}{\partial x} \left(h + \frac{v^2}{2g} \right) \quad (\text{A-34})$$

The partial derivatives are introduced because the quantities involved may now vary with time as well as with x . To allow for variation with time, the acceleration term in Equation (A-32) is rewritten as:

$$a_x = \frac{dv}{dt} = v \frac{\partial v}{\partial x} + \frac{\partial v}{\partial t} \quad (\text{A-35})$$

The equation of motion (A-32) becomes:

$$-\gamma A \Delta h - \tau_0 P \Delta x = \rho A \Delta x \left(v \frac{\partial v}{\partial x} + \frac{\partial v}{\partial t} \right) \quad (\text{A-36})$$

$$\tau_0 = -\gamma R \left(\frac{\partial h}{\partial x} + \frac{v}{g} \frac{\partial v}{\partial x} + \frac{1}{g} \frac{\partial v}{\partial t} \right)$$

Substitute Equation (A-34) into (A-36) gives:

$$\tau_0 = -\gamma R \left(\frac{\partial H}{\partial x} + \frac{1}{g} \frac{\partial v}{\partial t} \right) \quad (\text{A-37})$$

Substitute Equation (A-33) into (A-36) gives:

$$\frac{\partial H}{\partial x} + \frac{1}{g} \frac{\partial v}{\partial t} + \frac{v^2}{C^2R} = 0 \quad (\text{A-38})$$

which can be rewritten as:

$$S_e + S_a + S_f = 0 \quad (\text{A-39})$$

Therefore the three terms in Equation (A-38) are namely the energy slope, the acceleration slope, and the friction slope respectively. When substitute Equation (A-34) into Equation (A-38), using the bed slope $S_0 = -\partial z/\partial x$ and $h=z+y$, we have:

$$\frac{\partial H}{\partial x} = \frac{\partial z}{\partial x} + \frac{\partial y}{\partial x} + \frac{v}{g} \frac{\partial v}{\partial x}$$

$$\frac{\partial H}{\partial x} = -S_0 + \frac{\partial y}{\partial x} + \frac{v}{g} \frac{\partial v}{\partial x} \quad (\text{A-40})$$

Substitute Equation (A-21) and (A-22) gives:

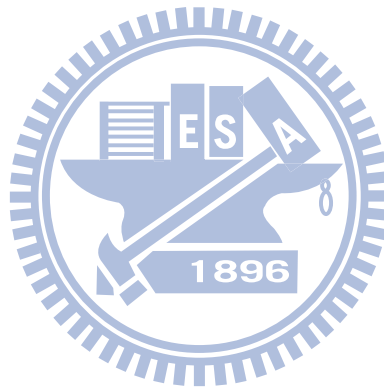
$$\frac{\partial H}{\partial x} = -\frac{1}{g} \frac{\partial v}{\partial t} - S_f \quad (\text{A-41})$$

Since Equation (A-40) is equal to Equation (A-41),

$$S_f = S_0 - \frac{\partial y}{\partial x} - \frac{v}{g} \frac{\partial v}{\partial x} - \frac{1}{g} \frac{\partial v}{\partial t} = \frac{v^2}{C^2 R} \quad (\text{A-42})$$

For steady and non-uniform flow:

$$S_f = S_0 - \frac{\partial y}{\partial x} - \frac{v}{g} \frac{\partial v}{\partial x} \quad (\text{A-43})$$



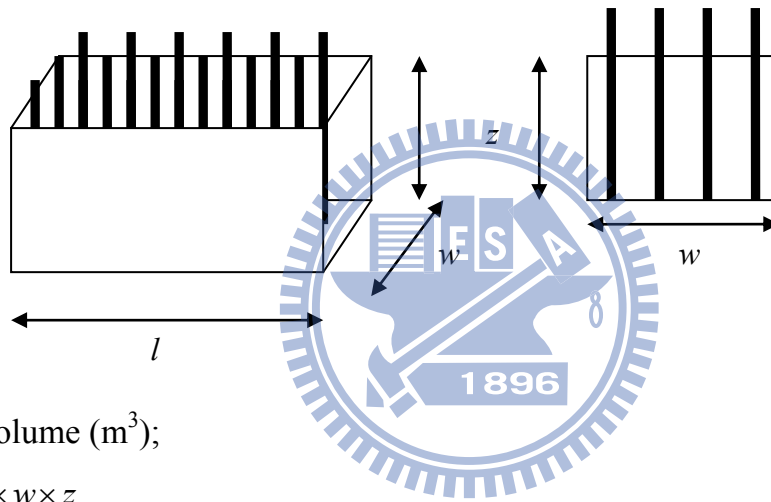
Appendix B

Theoretical relationship between projected frontal area and population density of an array of emergent (non-submerged) cylinders

1 · A_p : Area of plant looking in the direction of the cross sectional area.

2 · ρ_p : No. of Plant per unit area (m^2)

Assumption: in this calculation, plants are thought to be cylinders contained in a rectangular water body



$\forall =$ Volume (m^3);

$$\forall = l \times w \times z$$

$n_w =$ Number of plant in the width

$n_l =$ Number of plant in the length

$$A_p = d \times z \times n_w \tag{B-1}$$

$$\text{Total number of plant} = \rho_p \times l \times w = n_w \times n_l \tag{B-2}$$

$$n_w = \frac{\rho_p l w}{n_l} \tag{B-3}$$

Subst 2 into 1

$$A_p = \frac{d \forall \rho_p}{n_l} \tag{B-4}$$

$$\text{Vertical Plant Density} = \rho_{p_cross} = \frac{A_p}{A_c} = \frac{d \forall \rho_p}{n_l A_c} = \frac{d l \rho_p}{n_l} \tag{B-5}$$

$$\rho_{p_cross} = \frac{dl}{n_l} \rho_p$$

$$\rho_p = \rho_{p_cross} \frac{n_l}{dl} \quad (B-5.1)$$

In the calculation of retention time for 1st order chemical dynamic equation:

$$HRT = \frac{\forall}{Q} \quad (B-6)$$

HRT = Hydraulic Retention Time (s); \forall = Volume (m³); Q = Flow Rate (m³/s)

However, since \forall is occupied with plants, the actual volume is less than the total volume.

From equation (1.1), the total number of plants = $\rho_p \times l \times w = n_w \times n_l$

$$\text{Total volume of plant} = \forall_p = \rho_p \times l \times w \times \frac{\pi d^2}{4} \times z = n_w \times n_l \times \frac{\pi d^2}{4} \times z$$

$$\forall_p = \frac{\rho_p \forall \pi d^2}{4} \quad (B-7)$$

d = average plant diameter (m)

$$\text{There volume of water, } \forall_w = \forall - \forall_p \quad (B-8)$$

$$\forall_w = \forall - \frac{\rho_p \forall \pi d^2}{4}$$

$$\forall_w = \forall \left(1 - \frac{\rho_p \pi d^2}{4} \right) \quad (B-9)$$

$$\text{Subst. Equation (5) } \rho_p = \rho_{p_cross} \frac{n_l}{dl} \text{ into (9) } \forall_w = \forall \left(1 - \frac{\rho_{p_cross} \pi d^2}{4} \right);$$

From experiment, $\rho_p = K \rho_{p_cross}$ can be derived.

$$\forall_w = \forall \left(1 - \frac{\rho_{p_cross} n_l \pi d^2}{4 dl} \right) \quad (B-10)$$

$$V_w = V \left(1 - \frac{K\rho_{p_cross}\pi d^2}{4} \right) \quad (\text{B-10.1})$$

which is the Experimental version.

Now about water quality

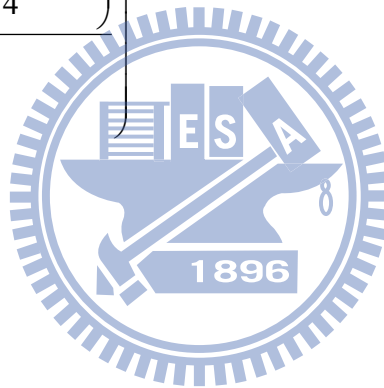
Assume first order chemical dynamic equation

$$\frac{C_o}{C_i} = e^{-kHRT}$$

$$\frac{C_o}{C_i} = \text{EXP}(-kHRT)$$

$$\frac{C_o}{C_i} = \text{EXP}\left(k \frac{V_w}{Q}\right)$$

$$\frac{C_o}{C_i} = \text{EXP}\left(-k \frac{V \left(1 - \frac{K\rho_{p_cross}\pi d^2}{4} \right)}{Q}\right) \quad (\text{B-10.2})$$



Appendix C

Examples of possible applications of the derived friction factors

C-1: Open-Channel Flow

Drag force and energy dissipation are expected in the case of free surface water flow over emergent macrophytes in open-channels. The continuity and dynamic equations of the two-dimensional flow could be presented by:

$$\frac{\partial h}{\partial t} + h \left(\frac{\partial u}{\partial x} + \frac{\partial v}{\partial y} \right) + u \frac{\partial h}{\partial x} + v \frac{\partial h}{\partial y} = 0 \quad (C-1)$$

$$\frac{\partial u}{\partial t} + u \frac{\partial u}{\partial x} + v \frac{\partial u}{\partial y} - \frac{1}{\rho} \left(\varepsilon_{xx} \frac{\partial^2 u}{\partial x^2} + \varepsilon_{xy} \frac{\partial^2 u}{\partial y^2} \right) + g \left(\frac{\partial z}{\partial x} + \frac{\partial h}{\partial x} \right) + \frac{\tau_x}{\rho h} = 0 \quad (C-2)$$

$$\frac{\partial v}{\partial t} + u \frac{\partial v}{\partial x} + v \frac{\partial v}{\partial y} - \frac{1}{\rho} \left(\varepsilon_{yx} \frac{\partial^2 v}{\partial x^2} + \varepsilon_{yy} \frac{\partial^2 v}{\partial y^2} \right) + g \left(\frac{\partial z}{\partial y} + \frac{\partial h}{\partial y} \right) + \frac{\tau_y}{\rho h} = 0 \quad (C-3)$$

where u and v are flow velocity in x and y direction; x and y represent the two directions on the horizontal plane in Cartesian coordinates; t is the time; ρ is the density of water, g is the gravitational acceleration; z is the datum of channel bed; h is the depth of water; ε_{xx} , ε_{xy} , ε_{yx} , and ε_{yy} are eddy viscosity coefficients; τ_x and τ_y are external drags including the friction force at the channel bed, the wind shear force, and Coriolis force.

$$\tau_x = \frac{\rho g u}{\left(\frac{kh^{1/6}}{n} \right)^2} (u^2 + v^2)^{1/2} - \xi v_a^2 \cos \psi + 2\rho h \omega v \sin \phi \quad (C-4)$$

$$\tau_y = \frac{\rho g v}{\left(\frac{kh^{1/6}}{n} \right)^2} (u^2 + v^2)^{1/2} - \xi v_a^2 \cos \psi + 2\rho h \omega u \sin \phi \quad (C-5)$$

where n is Manning's coefficient; ξ is the empirical wind shear coefficient; v_a is the wind velocity with direction ψ ; ω is the angular rotating velocity; and ϕ is the local latitude. The Manning's n derived from this research could be substituted into these equations for the determination of the continuity and

dynamic equations of open-channel flow over emergent macrophytes.

If the wind shear force and Coriolis force are neglected, the friction force in the x direction could be represented by:

$$\tau_x = \frac{\rho g u}{\left(\frac{kh^{1/6}}{n}\right)^2} (u^2 + v^2)^{1/2} = \frac{F_d}{A_p} \quad (\text{C-6})$$

where F_d is the total drag force measured by the direct drag force measurement system and A_p is the area of vegetated channel bed.

C-2: Overland Flow

The governing equations for overland flow could be simplified to the following:

$$\frac{\partial d}{\partial t} + \frac{\partial(ud)}{\partial x} + \frac{\partial(vd)}{\partial y} = q \quad (\text{C-7})$$

$$-\frac{\partial h}{\partial x} = u \left[\frac{n_x^2 |u|}{d^{4/3}} + \frac{q}{dg} \right] \quad (\text{C-8})$$

$$-\frac{\partial h}{\partial y} = v \left[\frac{n_y^2 |v|}{d^{4/3}} + \frac{q}{dg} \right] \quad (\text{C-9})$$



where x and y represent the two directions on horizontal plane in Cartesian coordinates (at the simulated zone); t is the time; d is the depth of water at ground level in the simulated zone; u and v are flow velocities at x and y direction; n_x and n_y are Manning's coefficients along the x and y direction, $h = d + z$ is the water level; z is the datum of channel bed; g is the gravitational acceleration; q is the inflow at unit surface area which is the effective rainfall intensity.

C-3: Coastal Current Flow

Emergent macrophytes such as *Phragmites australis* could be often seen at the coastal regions. For shallow water at far-field and deep water region, where the wave height is usually smaller than 1 m (smaller than the water depth), the advection terms can be neglected and the linear shallow water wave equation read:

$$\frac{\partial h}{\partial t} + \frac{\partial P}{\partial x} + \frac{\partial Q}{\partial y} = 0 \quad (C-10)$$

$$\frac{\partial P}{\partial t} + gH \frac{\partial h}{\partial x} - f \left(\frac{Q}{H} \right) = 0 \quad (C-11)$$

$$\frac{\partial Q}{\partial t} + gH \frac{\partial h}{\partial x} + f \left(\frac{Q}{H} \right) = 0 \quad (C-12)$$

where x, y are the horizontal coordinates;

h is the free-surface displacement;

$H = h + hl$ is the total water depth;

hl is the still water depth;

$P = Hu, Q = Hv$ are the horizontal volume discharges;

g is the gravity acceleration;

t is the time;

f is the Coriolis coefficient.

When a wave or a tsunami travels to the near shore region, the water depth reduces and the wave amplitude increases. The non-linear advection and bottom friction terms become considerable. These are included in the governing equations. The nonlinear shallow water wave equations are written as:

$$\frac{\partial h}{\partial t} + \frac{\partial P}{\partial x} + \frac{\partial Q}{\partial y} = 0 \quad (C-13)$$

$$\frac{\partial P}{\partial t} + \frac{\partial}{\partial x} \left(\frac{P^2}{H} \right) + \frac{\partial}{\partial y} \left(\frac{PQ}{H} \right) + gH \frac{\partial h}{\partial x} + \tau_x = 0 \quad (C-14)$$

where τ_x and τ_y are the bottom frictions.

The bottom friction comes from Manning's formula and is expressed as:

$$\tau_x = \frac{gn^2}{H^{7/3}} P(P^2 + Q^2)^{1/2} \quad (\text{C-15})$$

$$\tau_y = \frac{gn^2}{H^{7/3}} Q(P^2 + Q^2)^{1/2} \quad (\text{C-16})$$

where n is Manning's coefficient.

